The cover image displays the cryo-EM structure of the apo-state MRGPRD-Gi complex (PDB: 7Y15; Suzuki et al., 2022) and the X-ray crystallographic structure of Cathepsin S (PDB: 1NPZ; Pauly et al., 2003). The figure was generated using Adobe Stock and BioRender.com.

ISBN: 978-9-05-728826-5
Royal Library of Belgium Deposit Number: D/2023/12.293/45

Faculty of Pharmaceutical, Biomedical and Veterinary Sciences
Department of Veterinary Sciences

Mas-related G protein-coupled receptors: activations, interactions, and their role in inflammation

Mas-gerelateerde G proteïne-gekoppelde receptoren: activeringen, interacties en hun rol bij ontstekingen

Thesis submitted for the degree of doctor in Veterinary Sciences at University of Antwerp to be defended by

Rohit Arora

Promoters:
Prof. Dr. Alain J. Labro
Prof. Dr. Xaveer Van Ostade

Antwerp | November 9, 2023

Individual PhD Commission (IPC)

Prof. Dr. Dries Knapen	University of Antwerp (Chairman)
Prof. Dr. Alain J. Labro	University of Antwerp and University of Ghent (Promoter)
Prof. Dr. Xaveer Van Ostade	University of Antwerp (Promoter)
Prof. Dr. Tom Vanden Berghe	University of Antwerp (Member)

External and Internal Jury Members

Prof. Dr. Guido De Meyer	University of Antwerp (Chairman)
Prof. Dr. Alain J. Labro	University of Antwerp and University of Ghent (Promoter)
Prof. Dr. Xaveer Van Ostade	University of Antwerp (Promoter)
Prof. Dr. Francisco Ciruela	University of Barcelona (External Jury Member)
Prof. Dr. Julien Hanson	University of Liege (External Jury Member)
Prof. Dr. Ir. Yann Sterckx	University of Antwerp (Internal Jury Member)
Prof. Dr. Dries Knapen	University of Antwerp (IPC Member)

Summary

The largest family of membrane receptors, known as G protein-coupled receptors (GPCRs), are essential to cellular signaling and regulate physiological processes. Currently, ~35%–40% of US FDA-approved medications target GPCRs. A subfamily of GPCRs, Mas-related G protein-coupled receptors (MRGPRs), which belong to the δ-group of the rhodopsin-like GPCRs, was discovered two decades ago. MRGPRs are expressed by isolectin-B4-positive (IB4+) small non-myelinated sensory neurons of the dorsal root ganglia (DRG) and trigeminal ganglia (TG), mast cells, neutrophils, and macrophages and are known to regulate itch, pain, and pseudo-allergic drug reactions. In addition, MRGPRs have been identified as mediators in the renin-angiotensin system (RAS) and cardiovascular biology. Moreover, literature suggests that MRGPRs are also involved in inflammatory processes and the release of cytokines. Despite the fact that humans express eight MRGPRs (MRGPRD to G and X1-X4), information about their activation, signaling pathways, and role in inflammation is insufficient, and most of them are still classified as orphans. Since MRGPRs are involved in inflammation, which is an important physiological process, one goal of this PhD was to investigate whether β-alanine or alamandine-activated MRGPRD induces interleukin-6 (IL-6) release. To investigate that, MRGPRD-expressing HeLa cells were stimulated with either β-alanine or alamandine. Subsequently, it was observed that β-alanine activated MRGPRD-induced IL-6 release via the Gαq/Phospholipase C/NF-kB signaling pathway. Moreover, it was observed that the IL-6 release could be blocked by the Gαq inhibitor (YM-254890), the NF-kB signaling inhibitor (IKK-16), and partially by the PLC inhibitor (U-73122). Additionally, it was discovered that the MRGPRD was constitutive (ligand-independent) active, and the basal activity observed may have been caused by unidentified ligands present in the fetal bovine serum (FBS) in the culture medium. Therefore, the observation that MRGPRD mediates the release of IL-6 in vitro hints at its role as an inflammatory mediator and supports the notion that IL-6 can be used as a marker for MRGPRD activation for drug screening assays.

Recent reports suggest that amphiphilic molecules like bilirubin and bile acids (BAs) activate MRGPRX4 and contribute to cholestatic itch. However, the effect of sterols and their derivatives, i.e., BAs, on the activation of MRGPRD has not been demonstrated. Therefore, we evaluated the effect of sterol derivatives, i.e., cholesterol (CLR) and bile acids (BAs), on the activation of MRGPRD. To this end, MRGPRD-mediated IL-6 release was utilized as a screening platform. The most significant IL-6 release was observed from MRGPRD-expressing cells treated with BAs such as deoxycholic acid (DCA) and chenodeoxycholic acid (CDCA), which indicates the activation of MRGPRD. Furthermore, we found that methyl-β-cyclodextrin (MBCD), which is known to remove sterols from the plasma membrane, triggered the IL-6 release from MRGPRD-expressing HeLa cells.

Taken together, these observations point to the allosteric modulation of MRGPRD by BAs, or alternatively, modulation of plasma membrane plasticity indirectly affects the structure-function of MRGPRD.

Mechanical stimulation, which was previously underestimated, has now reemerged as an important regulator of physiological processes. Some of the GPCRs, like apelin, β2-AR, GPR68, PAR2, M3, H1R, etc., are known to be mechanosensitive and activated by shear stress, cell shrinkage, expansions, etc. Given that MRGPRD is mechanosensitive and has been implicated in dilated cardiomyopathy as well as cytokine regulation, our goal was to determine whether shear stress could activate MRGPRD, leading to the release of IL-6. In order to achieve this objective, HeLa cells expressing MRGPRD were exposed to shear stress by orbital shaking, the release of IL-6 suggested the activation of MRGPRD. The implications of these results suggest that mechanically actuated MRGPRD could regulate IL-6 release.

Furthermore, in an effort to deorphanize MRGPRs, in accordance with the involvement of cysteine proteases in the activation of some MRGPRs, an initial in silico investigation was conducted on the N-terminus sequences of MRGPRD, MRGPRE, and MRGPRF to ascertain cysteine protease cathepsin-S (CTSS) sites. The analysis revealed that both MRGPRD and MRGPRF had a consensus motif cleavage site for CTSS. The cleavage of the synthetic N-terminus peptides of MRGPRD and MRGPRF by CTSS was validated using mass spectroscopy. The calcium imaging was performed and used as a readout for CTSS-mediated MRGPRD and MRGPRF activations, which is a further step in deorphanizing the MRGPRs.

Lastly, the oligomerization of G protein-coupled receptors (GPCRs) has been known to alter ligand selectivity, receptor trafficking, promote distinct signaling, etc. Consequently, an assessment was conducted on the heteromerization of MRGPRD, MRGPRE, and MRGPRF using split-NanoLuc-based luciferase complementation (LC), bioluminescence resonance energy transfer (BRET), and co-immunoprecipitation (Co-IP) assays, and the heteromeric interactions between MRGPRE and MRGPRF were unambiguously detected with LC, BRET, and Co-IP techniques.

Overall, the result obtained in this PhD thesis was an attempt to better understand the activation mechanism of MRGPRs, the role of MRGPRs in inflammation biology, and the oligomeric interaction of MRGPRs.

Samenvatting

De grootste familie van membraanreceptoren, bekend als G proteïne-gekoppelde receptoren (GPCRs), zijn essentieel voor cellulaire signalering en reguleren fysiologische processen. Momenteel is ongeveer 35% tot 40% van de door de Amerikaanse FDA goedgekeurde medicijnen gericht op GPCR's. Een subfamilie van GPCR's, Mas-gerelateerde G-proteïne-gekoppelde receptoren (MRGPR's), die behoren tot de δ-groep van de rodopsine-achtige GPCR's, werd twintig jaar geleden ontdekt. MRGPR's worden tot expressie gebracht door isolectine-B4-positieve (IB4+) kleine niet-gemyeliniseerde sensorische neuronen van de dorsale wortelganglia (DRG) en trigeminale ganglia (TG), mestcellen, neutrofielen en macrofagen en het is bekend dat ze jeuk, pijn en ademhalingsproblemen reguleren. pseudo-allergische geneesmiddelreacties. Bovendien zijn MRGPR's geïdentificeerd als mediatoren in het renine-angiotensinesysteem (RAS) en de cardiovasculaire biologie. Bovendien suggereert de literatuur dat MRGPRs ook betrokken zijn bij ontstekingsprocessen en de afgifte van cytokines. Ondanks het feit dat mensen acht MRGPR's tot expressie brengen (MRGPRD tot G en X1-X4), is informatie over hun activering, signaalroutes en rol bij ontstekingen onvoldoende, en de meeste van hen worden nog steeds geclassificeerd als weeskinderen. Omdat MRGPRs betrokken zijn bij ontstekingen, wat een belangrijk fysiologisch proces is, was één doel van dit doctoraat om te onderzoeken of β-alanine of alamandine-geactiveerde MRGPRD de afgifte van interleukine-6 (IL-6) induceert. Om dat te onderzoeken werden HeLa-cellen die MRGPRD tot expressie brengen gestimuleerd met β-alanine of alamandine. Vervolgens werd waargenomen dat β-alanine-geactiveerde MRGPRD-geïnduceerde IL-6-afgifte via de Gaq/Phospholipase C/NF-kB-signaleringsroute. Bovendien werd waargenomen dat de afgifte van IL-6 kon worden geblokkeerd door de Gaq-remmer (YM-254890), de NF-kB-signaleringsremmer (IKK-16) en gedeeltelijk door de PLC-remmer (U-73122). Bovendien werd ontdekt dat de MRGPRD constitutief (ligand-onafhankelijk) actief was, en de waargenomen basale activiteit kan veroorzaakt zijn door niet-geïdentificeerde liganden die aanwezig zijn in het foetaal runderserum (FBS) in het kweekmedium. Daarom duidt de waarneming dat MRGPRD de afgifte van IL-6 in vitro medieert op zijn rol als ontstekingsmediator en ondersteunt het het idee dat IL-6 kan worden gebruikt als een marker voor MRGPRD-activering voor geneesmiddelenscreeningstests.

Recente rapporten suggereren dat amfifiele moleculen zoals bilirubine en galzuren (BA's) MRGPRX4 activeren en bijdragen aan cholestatische jeuk. Het effect van sterolen en hun derivaten, dat wil zeggen BA's, op de activering van MRGPRD is echter niet aangetoond. Daarom evalueerden we het effect van sterolderivaten, dat wil zeggen cholesterol (CLR) en galzuren (BA's), op de activering van MRGPRD. Voor dit doel werd MRGPRD-gemedieerde IL-6-afgifte gebruikt als een screeningplatform. De meest significante afgifte van IL-6 werd waargenomen uit cellen die MRGPRD tot expressie brengen, behandeld met BA's zoals deoxycholzuur (DCA) en chenodeoxycholzuur (CDCA), wat de activering van MRGPRD aangeeft. Bovendien ontdekten we dat methyl-β-cyclodextrine (MBCD), waarvan bekend is dat het sterolen uit het plasmamembraan verwijdert, de afgifte van IL-6 uit HeLa-cellen die MRGPRD tot expressie brengen teweegbracht. Alles bij elkaar genomen wijzen deze waarnemingen op de allosterische

modulatie van MRGPRD door BA's, of als alternatief beïnvloedt modulatie van plasmamembraanplasticiteit indirect de structuurfunctie van MRGPRD.

Mechanische stimulatie, die voorheen werd onderschat, is nu opnieuw naar voren gekomen als een belangrijke regulator van fysiologische processen. Van sommige GPCR's, zoals apelin, β2-AR, GPR68, PAR2, M3, H1R, enz., is bekend dat ze mechanosensitief zijn en worden geactiveerd door schuifspanning, celkrimp, uitzettingen, enz. Gegeven het feit dat MRGPRD mechanosensitief is en geïmpliceerd is bij zowel gedilateerde cardiomyopathie als cytokineregulatie was ons doel om te bepalen of schuifspanning MRGPRD zou kunnen activeren, wat zou leiden tot de afgifte van IL-6. Om dit doel te bereiken werden HeLa-cellen die MRGPRD tot expressie brachten blootgesteld aan schuifspanning door orbitaal schudden; de afgifte van IL-6 suggereerde de activering van MRGPRD. De implicaties van deze resultaten suggereren dat mechanisch geactiveerde MRGPRD de afgifte van IL-6 zou kunnen reguleren.

Bovendien werd, in een poging om MRGPR's te deorphaniseren, in overeenstemming met de betrokkenheid van cysteïneproteasen bij de activering van sommige MRGPR's, een eerste in silico-onderzoek uitgevoerd op de N-terminussequenties van MRGPRD, MRGPRE en MRGPRF om cysteïneprotease-cathepsine vast te stellen. S (CTSS)-sites. Uit de analyse bleek dat zowel MRGPRD als MRGPRF een consensusmotief-splitsingsplaats voor CTSS hadden. De splitsing van de synthetische N-terminuspeptiden van MRGPRD en MRGPRF door CTSS werd gevalideerd met behulp van massaspectroscopie. De calciumbeeldvorming werd uitgevoerd en gebruikt als uitlezing voor CTSS-gemedieerde MRGPRD- en MRGPRF-activeringen, wat een verdere stap is in het deorphaniseren van de MRGPR's.

Ten slotte is bekend dat de oligomerisatie van G-eiwit-gekoppelde receptoren (GPCR's) de ligandselectiviteit en het receptorverkeer verandert, duidelijke signalering bevordert, enz. Daarom werd een beoordeling uitgevoerd van de heteromerisatie van MRGPRD, MRGPRE en MRGPRF met behulp van split-NanoLuc -gebaseerde luciferase-complementatie (LC), bioluminescentie-resonantie-energieoverdracht (BRET) en co-immunoprecipitatie (Co-IP) testen, en de heteromere interacties tussen MRGPRE en MRGPRF werden ondubbelzinnig gedetecteerd met LC-, BRET- en Co-IP-technieken.

Over het geheel genomen was het resultaat van dit proefschrift een poging om het activeringsmechanisme van MRGPRs, de rol van MRGPRs in de ontstekingsbiologie en de oligomere interactie van MRGPRs beter te begrijpen.

सत्यमेव जयते
Truth alone Triumphs

~ From Mundaka Upanishad

This thesis is dedicated to my family, who stood by, supported, and encouraged me during the journey.
To all my friends who illuminated the right path.
Thank you for all the kind support.

Table of Contents

List of figures and tables

List of abbreviations

5-oxoETE	5-Oxo-eicosatetraenoic acid
7-TM	7-Transmembrane domain receptor
AT-1R	Angiotensin II receptor type I
BA	Bile acid
BAM22	Bovine adrenal medulla peptide 22
BRET	Bioluminescence resonance energy transfer
CA	Cholic acid
cAMP	Cyclic adenosine monophosphate
CCM	Cholesterol consensus motif
CDCA	Chenodeoxycholic acid
CLR	Cholesterol
CMV	Cytomegalovirus promoter
Co-IP	Co-immunoprecipitation
CPC	Ceramide phosphorylcholine
CPE	Ceramide phosphorylethanolamine
CTSD	Cathepsin-D
CTSS	Cathepsin-S
DAG	Diacylglycerol
DCA	Deoxycholic acid
DEC	Diethylstilbesterol
DMEM	Dulbecco's modified eagle medium
DMSO	Dimethylsulfoxide
DRG	Dorsal root ganglia
EC_{50}	Half maximal effective concentration
ECFP	Enhanced cyan fluorescent protein
ECL	Extracellular loop
EYFP	Enhanced yellow fluorescent protein
FBS	Fetal bovine serum

FDA	Food and drug administration
FRET	Fluorescence resonance energy transfer
FZD	Frizzled
GABA	γ-aminobutyric acid
$GABA_BR$	γ-aminobutyric acid (GABA) type B receptor
GAPs	GTPase activating proteins
GDP	Guanosine diphosphate
GEF	Guanine nucleotide exchange factor
GIP	Glucagon-dependent insulinotropic polypeptide
GLP	Glucagon-like peptide
GPCRs	G protein-coupled receptors
GTP	Guanosine triphosphate
HBSS	Hank's balanced Salt Solution
HEK-293	Human embryonic kidney 293 cells
HeLa	Cell derived from patient Henrietta Lacks
HEPES	N-2-hydroxyethylpiperazine-N-2-ethane sulfonic acid
HSVTK	Herpes simplex virus thymidine kinase promoter
HTRF	Homogeneous time resolved fluorescence
IBS	Irritable bowel syndrome
ICL	Intracellular loop
IkB	Inhibitor of nuclear factor kappa B
IKK	IkappaB kinase
IKK-16	IKK inhibitor VII
IKKα	IkappaB kinase α
IKKβ	IkappaB kinase β
IL-1β	Interleukin-1 beta
IL-6	Interleukin-6
IMPs	Integral membrane proteins
IP_1	Inositol 1-phosphate

IP_3	Inositol 1,4,5-trisphosphate
KCNQ	Potassium voltage-gated channel subfamily Q
Kir6.2	Inward-rectifier potassium channels (KCNJ11)
L-AIBA	L-aminoisobutyric acid
LC	Luciferase complementation
LCP	Lipidic cubic phase
LgBiT	Large subunit of NanoLuc Binary Technology (NanoBiT)
LPS	Lipopolysaccharides
MAPPIT	Mammalian Protein-Protein Interaction Trap
MBCD	Methyl-β-cyclodextrin
MOPS	3-(N-morpholino)propanesulfonic acid
mOrange	Monomeric orange fluorescent protein
MRGPRs	Human Mas-related G protein-coupled receptors
Mrgprs	Mice/Rats Mas-related G protein-coupled receptors
NanoBiT	NanoLuc Binary Technology
NF-kB	Nuclear factor kappa-light-chain-enhancer of activated B cells
NLuc	NanoLuc Luciferase
NO	Nitrous oxide
OPRD	δ-opioid receptor
OPRK	K-opioid receptor
OPRL	Opiate receptor-like
OPRM	μ-opioid receptor
OPRs	Opioid receptors
PA	Phosphatidic acid
PACAP	Pituitary adenylate cyclase-activating polypeptide
PAMP-12	Proadrenomedullin N-terminal 9-20 peptide
PAMs	Positive allosteric modulators
PARs	Protease-activated receptors
PBS	Phosphate-buffered saline

PC	Phosphatidylcholine
PCR	Polymerase chain reaction
PDB	Protein data bank
PE	Phosphatidylethanolamine
PI	Phosphatidylinositol
PIP	Phosphatidylinositol phosphate
PIP_2	Phosphatidylinositol bisphosphate
PIP_3	Phosphatidylinositol trisphosphate
PKA	Protein kinase A
PLC	Phospholipase C
PMPs	Peripheral membrane proteins
PPIs	Protein-protein interaction
PS	Phosphatidylserine
PUFA	Polyunsaturated fatty acids
PVDF	Polyvinylidene fluoride
RET	Resonance energy transfer
RTA	Rat thoracic aorta
SDS	Sodium dodecyl sulphate
SmBiT	Small subunit of Nanoluc Binary Technology (NanoBiT)
SMO	Smoothened
SNSRs	Sensory neuron-specific receptors
TG	Trigeminal ganglia
TMs	Transmembrane α-helices
TNF-α	Tumor necrosis factor-α
TRPA1	Transient receptor potential cation channel, subfamily A, member 1
UDCA	Ursodeoxycholic acid
VIP	Vasoactive intestinal peptide
β1-AR	β-1 adrenergic receptor

β2-AR	β-2 adrenergic receptor
β-AIBA	β-aminoisobutyric acid
β-arr1	β-arrestin-1
β-arr2	β-arrestin-2

Amino Acids

Ala	A	Alanine
Arg	R	Arginine
Asn	N	Asparagine
Asp	D	Aspartic acid
Cys	C	Cysteine
Glu	E	Glutamic acid
Gln	Q	Glutamine
Gly	G	Glycine
His	H	Histidine
Ile	I	Isoleucine
Leu	L	Leucine
Lys	K	Lysine
Met	M	Methionine
Phe	F	Phenylalanine
Pro	P	Proline
Ser	S	Serine
Thr	T	Threonine
Trp	W	Tryptophan
Tyr	Y	Tyrosine
Val	V	Valine

Chapter 1
Introduction

Chapter 1 Introduction

1.1 Background

Archaeological evidence suggests that drug use by humans may have come with the Neolithic Revolution around 10,000 BC [1]. Since the inception of civilizations, humans have been experimenting with psychoactive compounds from plants, and people were intrigued by their ability to affect the brain and treat disease. There is extensive evidence of opium use in the pre-modern medicine era [2]. The knowledge about their use in curing diseases, aiding in healing, and abuse was passed on to the next generation, but little was known about the working mechanisms and preparations of these chemicals [3, 4]. If we would consider it, the industrial revolution in the 18th century brought in an era of modern medicine, and Friedrich Sertürner invented the first modern medicine in 1804. He extracted the active chemical from opium in his laboratory, named it morphine, described the process of its isolation and crystallization and performed pharmacological and systemic studies on dogs and then on himself [5-8]. Since then, morphine has been used as an effective painkiller and continues to be so today [9]. Despite knowing the effects of a variety of plant-derived chemical substances in disease treatment or modulation, the molecular structure of chemicals and their receptive molecules in the human body were not identified until the late mid-twentieth century.

Along with the modern medicine era, it was discovered that cells are the building blocks of all living organisms. Robert Hooke first used the word "cells" in 1665 and was the first to investigate living things under a microscope. He saw honeycomb-like structures when he looked at a thin slice of cork. 200 years later, in 1895, Ernest Overton proposed the theory that lipids constitute the primary component of cell membranes, which retain the cell components. About three decades later, Evert Gorter and François Grendel discovered that the cell membrane is made of a lipid bilayer [10]. Another decade later, in 1935, Hugh Davson and James Frederic Danielli suggested that a phospholipid bilayer lies between two layers of globular proteins (Figure 1.1 A) [11]. The "Fluid Mosaic Model" of cell membrane was proposed by Seymour Singer and Garth Nicolson in 1972 as a replacement for the Davson-Danielli model, which proposed that proteins did not exist as separate layers but were buried inside the lipid bilayer that forms the cell's membrane (Figure 1.1 B) [12].

1.2 Cell membrane

The cell membrane separates and protects the interior of the cell from the outside environment. In the majority of eukaryotic cells, the membrane consists of nearly half lipids and half proteins by weight. Depending on the needs of the cells, the cell membrane's lipid, protein, and chemical composition may change. Through the expression of specialized proteins, the cell membrane is selectively permeable and

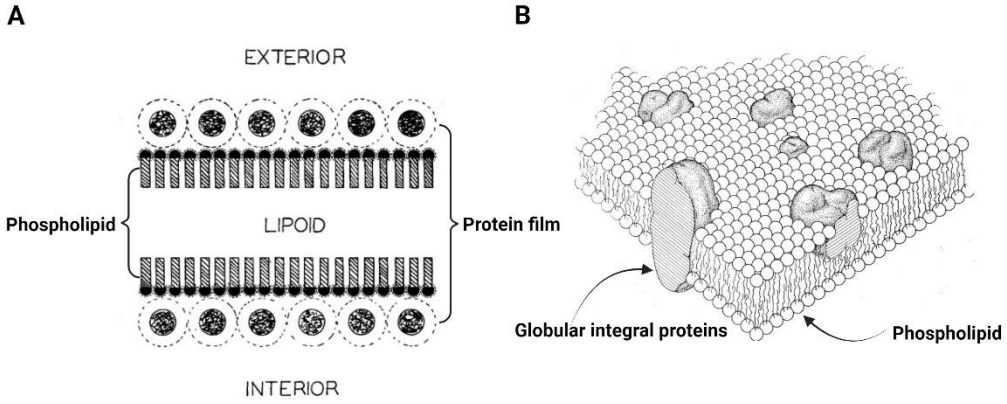

Figure 1.1: Danson-Danielli and Fluid Mosaic Model of Cell Membrane. (A) Danson-Danielli model of cell membrane displaying phospholipid bilayer (lipoid) lying between two layers of protein (exterior and interior) film. **(B)** A schematic cross-sectional view of the Fluid Mosaic Model, where proteins (globular integral proteins) are shown embedded in a phospholipid bilayer. The figures represented are modified from the original figures of Danielli and Davson et al. [11] and Singer and Nicolson et al. [12]. Figure created with BioRender.com.

regulates the flow of substances, like organic molecules or ions, into and out of the cell. The proteins within or attached to the cell membrane are involved in several biological activities, to list a few, cell adhesion, ion conductivity, and signaling and also facilitate attachment with various extracellular structures (Figure 1.2).

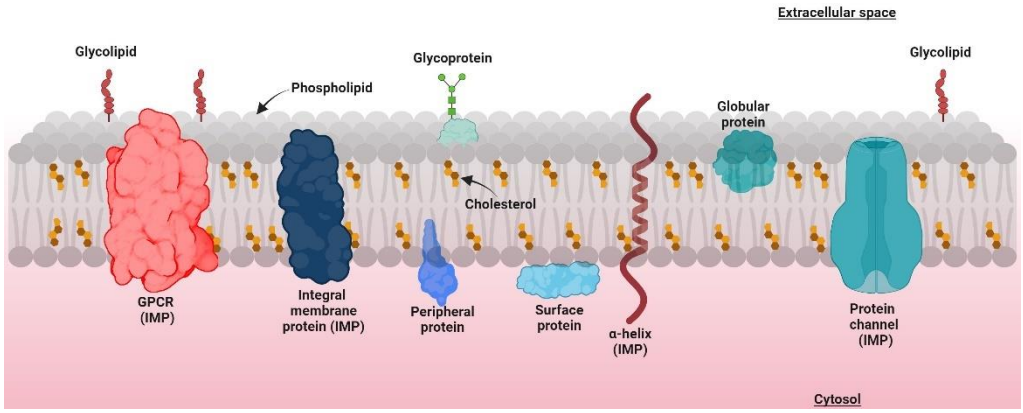

Figure 1.2: Cell membrane schematic representation. The schematic cross-sectional view of the cell membrane represents the amphipathic phospholipid bilayer; the head of the phospholipid is hydrophilic, and the tail ends are hydrophobic. The various lipids, such as glycolipids (attached) and cholesterol (CLR; embedded), are shown in between phospholipids. The membrane proteins, such as integral [G protein-coupled receptors (GPCRs), ion channel, α-helix etc.], peripheral, surface, globular, and glycoproteins, are either attached to or embedded in the phospholipid bilayer. Figure created with BioRender.com.

1.2.1 Cell membrane lipids

The amphipathic lipids, such as phospholipids and sterols (mainly cholesterol), constitute the major lipid part of the cell membrane [13]. Due to the physiochemical nature of amphipathic molecules, these lipids assemble into a lipid bilayer whereby the outsides are hydrophilic, and the core is lipophilic (i.e. hydrophobic). A phospholipid has a phosphate group (hydrophilic head) that is linked to two fatty acid chains (hydrophobic tail) via an alcohol backbone. The phospholipids are broadly categorized into glycerophospholipids and sphingolipids. The glycerophospholipids contain fatty acid chains linked by ester or alkyl ether to the C1 and C2 carbons of the glycerol backbone. Depending on the type of group attached to the phosphate, glycerophospholipids are further categorized as phosphatidylcholine (PC), phosphatidylethanolamine (PE), phosphatidylserine (PS), phosphatidic acid (PA), phosphoinositiols [phosphatidylinositol (PI); phosphatidylinositol phosphate (PIP); phosphatidylinositol bisphosphate (PIP_2); phosphatidylinositol trisphosphate (PIP_3)]. The phospholipids containing sphingoid bases are categorized as sphingolipids. The ceramide-containing sphingolipids are further subdivided such as ceramide phosphorylcholine (CPC), ceramide phosphorylethanolamine (CPE), etc.

Moreover, phospholipids interact non-covalently due to the hydrophobic effect created by their hydrophobic tail ends, which does in fact hold the cell membrane together. The fatty acid chain of phospholipids is either saturated (without double bonds in the hydrocarbon chain) or unsaturated (with double bonds in the hydrocarbon chain). The saturated fatty acid chains assist in the tight packing of the membrane, and conversely, the unsaturated fatty acid chains inhibit the tight packing of the membrane, therefore decreasing the melting temperature of the membrane and increasing fluidity.

The phospholipids comprise half of the lipids, and the rest of the plasma membrane lipids consist of cholesterol (CLR) (up to 48%) and glycolipids (2%), but CLR has the same molar amount as the phospholipids [14]. In fact, about 90% of total cell's CLR content is found in the plasma membrane [15]. As CLR positions between the hydrophobic tails of phospholipids and prevents their interaction, CLR is essential to maintain membrane biophysical properties such as fluidity, curvature, permeability, stiffening, strength, and thickness. At high temperatures, CLR reduces the fluidity of membranes, thus decreasing the permeability to molecules (organic and small molecules), and vice versa at lower temperatures. CLR is known to directly or indirectly affect the structure and function of membrane proteins and also takes part in biochemical interactions. Interestingly, the CLR percentage in cell membranes varies between cell types, tissues, organisms, and even from one individual to another.

Although only 2 percent of lipids are glycolipids, they are found on the extracellular surface of the cell membrane. The glycolipids are essentially carbohydrates (monosaccharide or oligosaccharide) attached to glycerophospholipids and sphingolipids by a glycoside covalent bond. Their function is to maintain and facilitate cell recognition in immune responses as well as provide cellular stability through the formation of interactions between cells and the extracellular matrix. Overall, phospholipids, CLR, glycoproteins, and interspersed proteins maintain appropriate membrane fluidity and biophysical properties.

1.2.2 Membrane proteins

As the lipid bilayers constitute the major structural components of the cell membrane, proteins are the other key components. Depending on how membrane proteins associate with the cell membrane, they are divided into two groups: integral membrane proteins (IMPs) and peripheral membrane proteins (PMPs). IMPs are proteins that are attached to or embedded in plasma membranes. IMPs represent approximately 20-30% of the proteins encoded by the human genome [16]. The IMPs are subdivided into monotopic and polytopic proteins. The monotopic proteins interact with the plasma membrane but do not span the lipid bilayer, whereas the polytopic (single-pass or multi-pass) proteins span the entire membrane and are also termed transmembrane proteins [17, 18]. Ion channels, receptors, transporters, linkers, enzymes, cell adhesion, and energy-accumulating and transducing proteins are examples of IMPs. Important biological functions like signaling, transport, energy transfer, and cell adhesion are carried out by IMPs. Considering that, IMPs becomes an important target for drugs to act on and are the target of 60% of clinically used drugs [19].

Proteins that are only temporarily associated with the membrane are referred to as PMPs. PMPs are loosely attached to the peripheral (inner or outer) side of the cell membrane. Their easy attachment and detachment enable them to take part in cell signaling. PMPs typically interact with ion channels and transmembrane receptors to transduce the extracellular signal and control intracellular signaling. These ancillary proteins may also function as enzymes to facilitate and control the environment of the cell. IMPs and PMPs work in conjugation to transduce the extracellular signal and regulate intracellular signaling. Overall, IMPs and PMPs function in the complex environment of the plasma membrane, where their organization and dynamics of activation are also influenced by lipids.

1.3 G protein-coupled receptors (GPCRs)

1.3.1 Receptor history and drug-interaction theories

In parallel to the development of bilipid layer theory, at the beginning of the twentieth century, John Newport Langley (1905) and Paul Ehrlich (1908) devised the notions of a "receptive substance" and a "chemoreceptor", respectively, that would mediate the drug action in cells, thus establishing the concept of the receptor in cells [20-23]. Even without knowing the existence of or seeing receptors in cells, various mathematicians, physiologists, and biophysicists advanced receptor theory and established drug-receptor interaction theories. Archibald V. Hill (1910), a mathematician turned physiologist, used mathematical and physiochemical methods to study the mode of action of nicotine and curari on the skeletal muscles of a frog, in an attempt to understand the relationship between drug-concentration and response, resulting in the first quantitative assessment of drug-concentration effect [24-26].

Alfred Joseph Clark (1933) advanced Langley and Hill's work by introducing the receptor occupancy model, to explain drug activity at receptors and quantified the relationship between drug concentration and observed biological effects [27-30]. Sir John Henry Gaddum (1937) advanced the receptor occupancy model by describing a model for the competitive binding of two ligands to a receptor [31]. The equilibrium constant for an antagonist binding to receptors was determined by Heinz Otto Schild (1947). He derived the formula to calculate the dose ratio needed to assess a drug's potency according to mass law (Figure 1.3 A). The affinity of an antagonist for a receptor was calculated using the ratio of the EC_{50} (half maximal effective concentration) of an agonist alone compared to the EC_{50} in the presence of a competitive antagonist [32-34]. Moving further, the quantitative use of drug antagonism was described by Arunlakshana and Schild in 1958 [35]. Cumulatively, Gaddam, Schild, and Arunlakshana developed the competitive inhibition model and defined the classic theory of drug antagonism, expanding the receptor-drug interaction theory. Due to the fact that the receptor-occupancy and competitive inhibition model was inherently flawed and was unable to adequately describe the concept of a partial agonist, intrinsic activity or efficacy of agonist action was established by Ariens in 1954 and Stephenson in 1956. Still, a lot of well-known scientists were skeptical of the presence of receptors in cells and thought the idea of a receptor was an abstraction, which thwarted the receptor theories from being further developed.

In spite of the fact that receptor theory came into existence in the first decade of the 20^{th} century, the presence of receptors was not identified until the 1970s [36, 37]. In the meantime, the suggestion of Davson-Danielli that proteins are located on the

membrane was picked up by some scientists, and who theorized that the receptive substance in cells might be a protein found on the membrane. Moreover, Raymond P. Ahlquist (1948) demonstrated the differential effects of adrenaline on two probable distinct receptor populations [38]. Following that, the theory of receptor-drug interaction gradually gained acceptance. The major breakthrough came due to the development of radioimmunoassay by Solomon Berson and Rosalyn Yalow in 1955, which allowed the scientific community to use it to quantify the biomolecules [39, 40]. Using a similar principle, in the 1970s, Robert Lefkowitz and associates used radioligand binding to identify distinct beta-adrenergic receptors (β-ARs) that couple to norepinephrine and the adrenergic antagonist propranolol [36, 37, 41]. Once receptors began to be recognized as specific proteins of the cell membrane, their composition and conformation were explored.

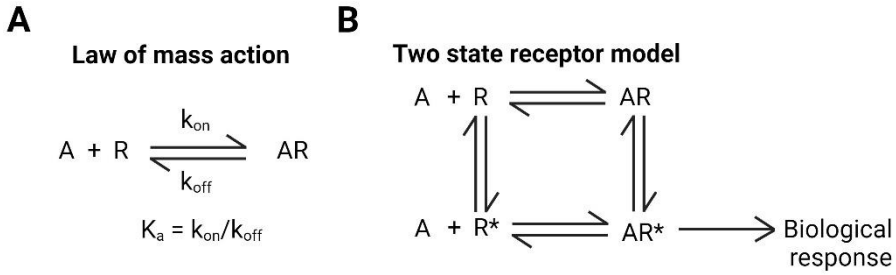

Figure 1.3: Law of mass action and two state receptor activity model. (A) The law of mass action defines that the unbound agonist (A) and receptor (R) are in equilibrium with the agonist-bound receptor (AR), where k_{on} defines the rate of binding of A to R, and k_{off} defines the rate of dissociation of A from R, K_a defines the equilibrium constant for R and A. **(B)** The two state receptor model suggests that an agonist binds primarily to the R* and subsequently to the R state receptors, changes receptor conformation, and pushes the equilibrium largely to the AR* to generate a biological response. A=agonist, R=inactive state receptor, R*=active state receptor, AR=agonist-bound receptor, AR*= agonist-bound active state receptor. Figure created with BioRender.com.

The receptor-drug interaction (occupancy and competitive inhibition) models were deemed insufficient as the receptor started to gain recognition, as well as various types of ligands for receptors (full, partial, inverse, and antagonist) were discovered. Moving further, the two-state model originally put forth by Del Castillo and Katz for ligand-gated ion channels was also applicable to receptors [42]. The receptor is believed to exist in two interchangeable states: R (inactive) and R* (active), which are in equilibrium (Figure 1.3 B). Most receptors are in the R state, which produces no or a negligible signal when there is no agonist present. The agonist in the two-state model does not activate the receptor, as is assumed in the occupation and competitive inhibition hypothesis, but instead suggests that agonist selective binding causes a

change in receptor conformation, which changes the receptor from an inactive to an active state and shifts the equilibrium towards an active state. First, the agonist (A) binds preferentially to the R* (active state receptor) and then to the R-state receptors (inactive state receptor), changes conformation, and predominantly pulls the equilibrium to the R*, and the generated response is dependent on the agonist concentration. Similarly, due to the inverse agonist's strong affinity for the R state, it can cause the opposite response and shift the balance in favor of the R state. Even at saturating doses, a partial agonist with a marginally higher affinity for R* than for R causes the equilibrium to shift towards R* and causes the submarginal response. Equilibrium is maintained when an antagonist (B) binds to R and R* with equal affinity and no reaction is triggered.

Alfred G. Gilman and Martin Rodbell's discovery of the G proteins has been of utmost significance. Due to their ability to bind guanosine triphosphate (GTP), they earned the name "G proteins" [43]. As a result, receptors that associate with G protein were called G protein-coupled receptors (GPCRs). They discovered that G proteins function as signal transducers in cells, transferring signals received via receptors, combining various signals, and then regulating essential cell functions. The expansion of receptor theory was aided by the identification of the receptor-G protein signaling mechanism. In order to describe the interaction between ligand, an active receptor, and a G protein that results in signal propagation, Andre De Lean proposed the ternary complex model (Figure 1.4 A) [44]. The extended ternary complex model was developed from the ternary model to take into account the active state receptor (R*), also known as the constitutive active receptor (Figure 1.4. B) [45]. Furthermore, in order to accommodate G proteins coupling with inactive receptors, the extended ternary model was once again expanded to the cubic ternary complex model [46].

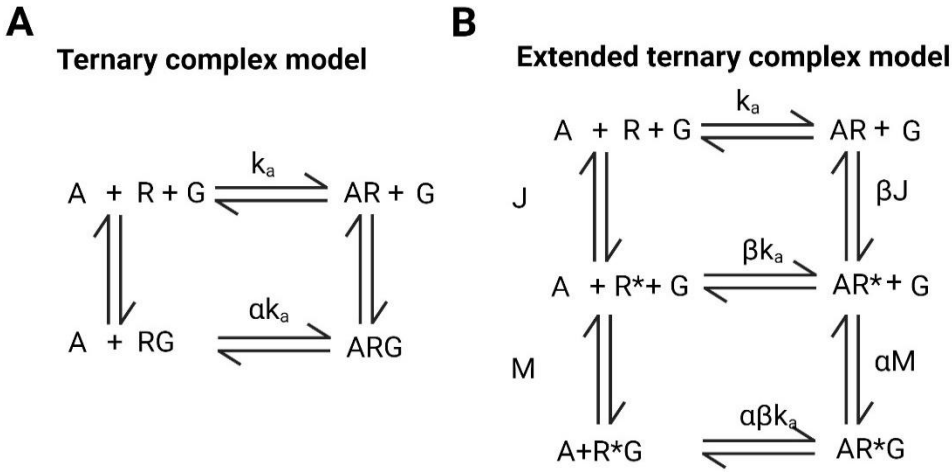

Figure 1.4: Ternary and extended ternary models for receptor activation. Biological signal

propagation is caused by the interaction of an agonist, a receptor, and a G protein (Ternary model; A). The extended ternary complex model (B) evolved from the ternary model to account for the active state receptor (R*), also known as constitutive activity. A= agonist, R=inactive state receptor, R*= active state receptor, G= G protein. The Ka defines the equilibrium constant for R and A, M is equilibrium constant for R and A, J is isomerzation constant between R and R*. α defines the cooperative factor between A and G to stabilize the ternary complex, and β defines the ability of the agonist to facilitate the transition from R to R*. Figure created with BioRender.com.

Briefly, in parallel to the development of receptor theory, the advancement in biochemical and biophysical methods and X-ray crystallography helped in determining the protein structures [47]. John Kendrew established and used the X-ray diffraction technique to determine the first 3-dimensional structure of muscle myoglobin in 1958 (Figure 1.5) [48]. Richard Henderson and Nigel Unwin were the first to structurally characterize bacteriorhodopsin, a light-harvesting membrane protein (also called purple protein) from archaeal bacteria, in 1975, with a resolution of 7 Å. Additionally, they were the first to report the presence of α-helices in membrane proteins (Figure 1.5) [49]. The first high-resolution, 3 Å structure of a membrane protein was the bacterial photosynthetic reaction center protein, which was determined by Hartmut Michel and colleagues in 1985 [50]. Since, membrane proteins have the inherent limitation of being difficult to extract, isolate, and stabilize, Euhd M Landau and his colleagues developed the lipidic cubic phase (LCP) method to facilitate the crystallization of membrane proteins in 1997 [51] and utilized the method to obtain the high-resolution structure of bacteriorhodopsin with a resolution of 2.35 Å (Protein Data Bank; PDB: 1AP9). Subsequently, LCP methods have been used to obtain the structures of multiple membrane proteins. The first crystal structure of 2.80 Å of a mammalian GPCR, bovine rhodopsin, was published in 2000 (PDB: IF88) [52]. The first X-ray crystal structure of the human β2-adrenergic receptor (β2-AR; 2.40 Å) was reported by Brian Kobilka and colleagues in 2007 (PDB: 2RH1) [53, 54]. A new chapter in GPCR research was opened in 2011 with the determination of the crystal structure of the β2AR-Gs protein complex of 3.20 Å (PDB: 3SN6; receptor-heterotrimer complex; β2AR-Gαβγ) [55]. Thereafter, several X-ray and cryo-EM structures of several GPCRs have been reported.

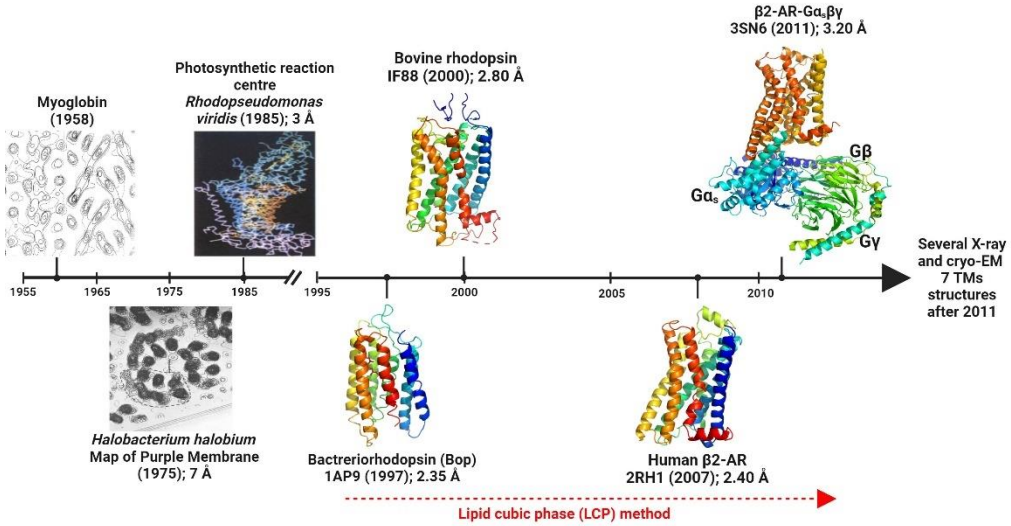

Figure 1.5: Timeline of protein structure determination. The electron density map of the muscle myoglobin molecule determined in 1958. The three-dimensional model of a light-harvesting membrane protein (purple protein) from *Halobaterium halobium* with a resolution of 7 Å was obtained in 1975 by electron microscopy is shown. A 3 Å X-ray structural analysis of well-ordered crystals of the photosynthetic reaction center *Rhodopseudomonas veridis* (1985). The high-resolution structure of bacteriorhodopsin with a resolution of 2.35 Å obtained by the LCP-based crystallization method of a membrane protein in 1997 (PBD: 1AP9). The first high-resolution crystal structures of 2.80 Å of a bovine rhodopsin (mammalian GPCR) and 2.40 Å of a human β2-AR were published in 2000 (PDB: IF88) and 2007 (PDB: 2RH1), respectively. The 3.20 Å crystal structure of β2-AR bound to GDP-bound Gs protein (PDB: 3SN6; receptor-heterotrimer complex; β2AR-Gαβγ) reported in 2011. PDB structures were visualized using PyMol (Schrödinger Inc.), and figure created using BioRender.com.

1.3.2 Classification of GPCRs

The superfamily of GPCRs is very diverse in structure and function. The human genome encodes approximately ~800 GPCRs, making them the largest group of membrane proteins in the human genome. Based on sequence homology, GPCRs are divided into six classes: class A (rhodopsin receptors), class B (secretin receptors), class C (metabotropic glutamate receptors), class D (fungal pheromone receptors), class E (cyclic AMP receptors), and class F (frizzled and smoothened receptors). Class D and E are the only ones that do not exist in vertebrates [56]. A different classification was proposed by Fredriksson in 2003, i.e., the GRAFS system, based on phylogenetic analysis using hidden Markov models, which delineated the inter-relationships among the receptors (Figure 1.6) [57, 58]. As per the GRAFS system, the vertebrate receptors were clustered into five main families, which were termed glutamate (23 members), rhodopsin (~719 members), adhesion (33 members), frizzled/taste2 (11 members),

secretin (15 members), and some proteins that could not be assigned to any family and were sectioned as "other 7-TM receptors".

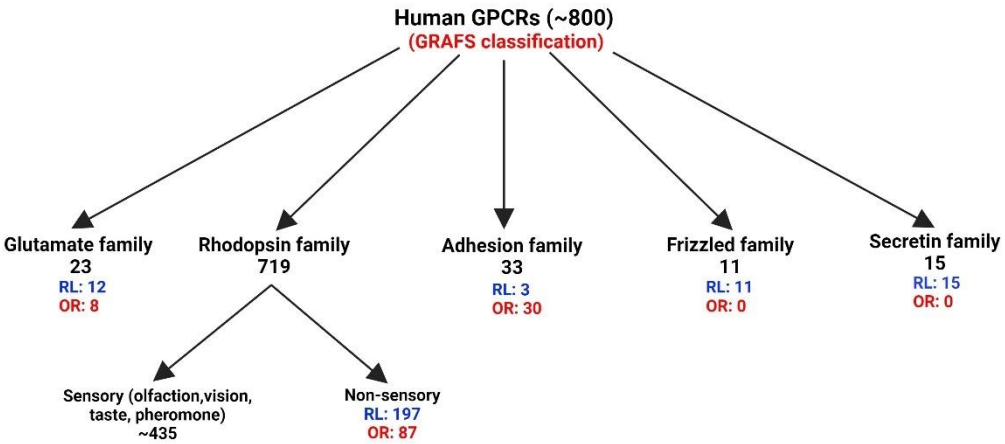

Figure 1.6: GPCRs classification based on GRAFS system. As per the GRAFS classification, GPCRs are divided into glutamate (23 members), rhodopsin (~719), adhesion (33), frizzled (11) and secretin (15) family. The rhodopsin family of GPCRs is further subdivided into sensory (~435) and non-sensory (284). The 'RL' refers to the number of receptors for which the endogenous ligand has been approved. The 'OR' refers to the number of receptors for which an endogenous ligand still has to be discovered or approved. Figure created with BioRender.com.

The rhodopsin family of GPCRs is by far the most abundant, with ~719 members, 284 of which belong to non-olfactory receptors. The rhodopsin family of GPCRs is further divided into four groups α, β, γ and δ. The δ-group of the rhodopsin family of GPCRs contains the olfactory receptors, which are the largest cluster of receptors [57]. With regards to the GRAFS classification system, the glutamate family includes metabotropic glutamate, calcium-sensing, $GABA_BR$, as well as taste type 1 receptors [59, 60]. The secretin family comprises secretin, calcitonin, parathyroid hormone-related peptides, and vasoactive intestinal peptide receptors [61, 62]. These receptors are activated by peptide hormones such as glucagon-dependent insulinotropic polypeptide (GIP), glucagon-like peptides (GLP-1 and GLP-2), secretin, vasoactive intestinal peptide (VIP), pituitary adenylate cyclase-activating polypeptide (PACAP), etc. The adhesion family receptors derive their name from their long N-terminus domains that have adhesion properties [63]. It is believed that they help cells interact with each other and with the extracellular matrix. Frizzled and smoothened family consist of one smoothened (SMO) and 10 frizzled (FZD 1-10) receptors. The FZD receptors are activated by secreted lipoglycoproteins of the WNT family [64, 65]. The SMO is activated by CLR and subsequently regulates the Hedgehog-related signaling pathway [66-68].

1.3.3 Structure-function of GPCRs

GPCRs are primarily located in the cell membrane, and their main function is to transduce extracellular signals to the interior of cells, enabling intercellular communication. GPCRs are known to maintain cellular homeostasis and are implicated in the physiology of many diseases [69, 70]. GPCRs have discrete structural features and can be divided into three regions: first, "the extracellular region," which consists of the extracellular N-terminus and three extracellular loops (ECL1-ECL3). Second, "the transmembrane region," which has seven hydrophobic transmembrane α-helices (TM1 to TM7) and third, "the intracellular cytoplasmic region," which comprises three intracellular loops (ICL1-ICL3), an α-helix (H8), and the intracellular C-terminus (Figure 1.7 A) [71].

The seven hydrophobic membrane-spanning helices organize themselves into a tertiary structure to form a barrel (Figure 1.7 B), which creates a cavity within the plasma membrane. In general, the cavity functions as a ligand-binding domain, also regarded as an orthosteric site. Upon ligand binding to the orthosteric site, or to the N-terminus or ECLs, or on the surface of the transmembrane domain, the receptor undergoes conformational rearrangements leading to the interaction with intracellular signal transducers and downstream effectors, including G proteins, beta-arrestins (β-arr), G protein-coupled receptor kinases (GRKs), etc [72]. A wide variety of agonists, including proteins, biogenic amines, photons, sterols, etc., are known to activate receptors and thereby regulate a wide range of cellular signaling [73].

The rhodopsin family is the largest group of GPCRs, and the Mas-related G protein-coupled receptors (MRGPRs) subfamily, which is the subject of this thesis, is a member of the rhodopsin family. Although the rhodopsin family of GPCRs is structurally similar, not all GPCRs respond to the same ligand [73]. Therefore, understanding the structural characteristics and activation mechanisms of individual GPCRs is of utmost significance. According to the family-wide study of the rhodopsin family of GPCRs, the residues that link the ligand-binding region to the G protein-coupling region are significantly conserved, although a universal activation mechanism has yet to be discovered [74]. The ligand-binding region of rhodopsin family GPCRs consists of motifs such as CWxP ($C^{6.47}$, $W^{6.48}$, $P^{6.50}$) and PIF ($P^{5.50}$, $I^{3.40}$, $F^{6.44}$) (Figure 1.7 D and E). Notably, the numbering of amino acid residues in GPCRs is based on the Ballesteros-Weinstein numbering scheme, which consists of two numbers, where the first denotes the helix of GPCRs and the second denotes the residue position relative to the most conserved residue [75, 76]. The $Trp^{6.48}$ residues of the CWxP motif of TM6 operate as a toggle switch when a ligand binds to the receptor, and the PIF motif, which is made up of the hydrophobic residues in TM3, TM5, and TM6, initiates a rearrangement of hydrogen-bonding connections to stabilize the active receptor conformation [72, 77]. The G

protein-binding region of the rhodopsin family of GPCRs consists of motifs such as DRY ($D^{3.49}$, $R^{3.50}$, $Y^{3.51}$) and NPxxY ($N^{7.49}$, $P^{7.50}$, $Y^{7.53}$) (Figures 1.7 F and G). The transition to the active state is regulated by the conserved $Asp^{3.49}$ of the DRY motif at the cytoplasmic end of TM3, and the nearby $Arg^{3.50}$ is essential for G protein activation [78]. Furthermore, the conserved motif NPxxY on TM7 is known to stabilize the active conformation of receptors, mediating G protein signaling and receptor internalization [79]. Additionally, the sodium-binding site is found to be moderately conserved in the rhodopsin family of GPCRs, and the key residues are $D^{2.50}$, $S^{3.39}$, $W^{6.48}$, and $N^{7.49}$, where $D^{2.50}$ controls sodium-binding and the effect of sodium on ligand binding (Figure 1.7 C).

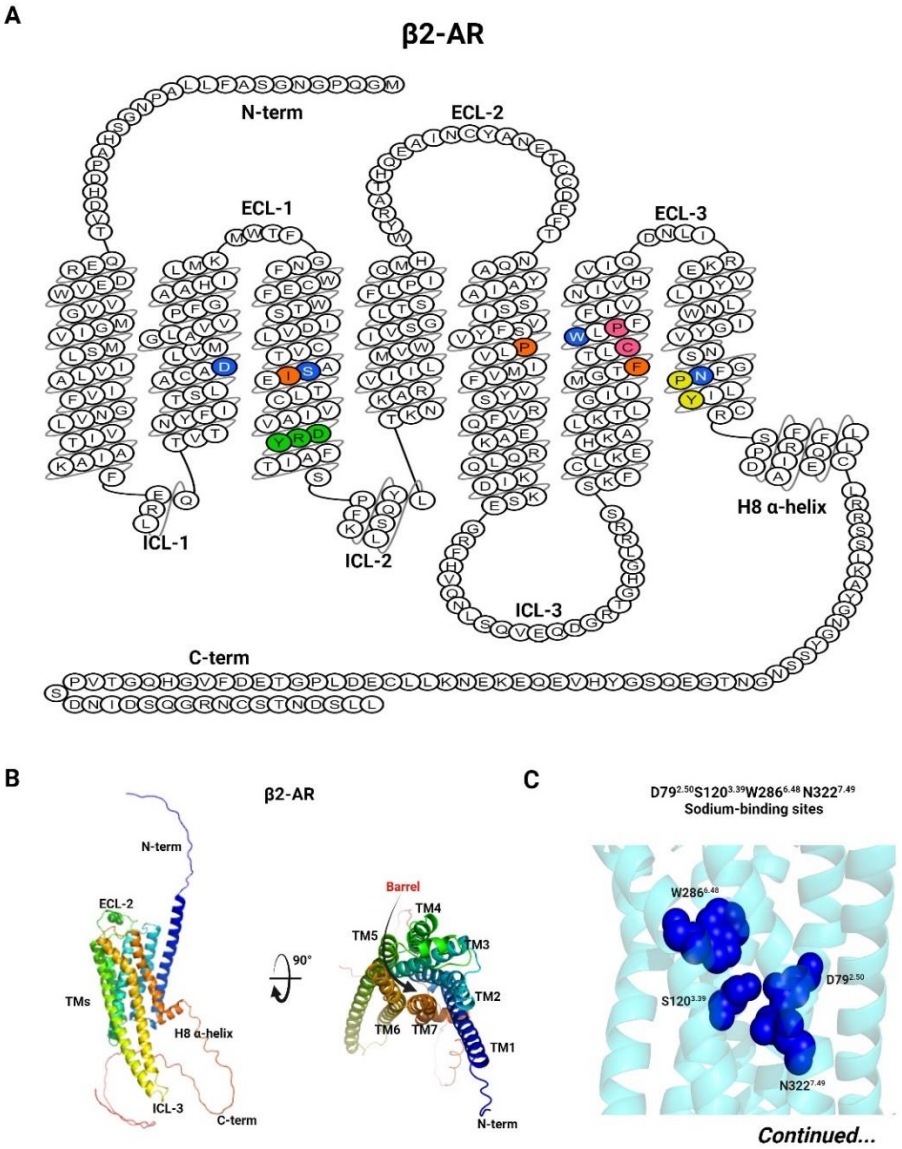

Continued...

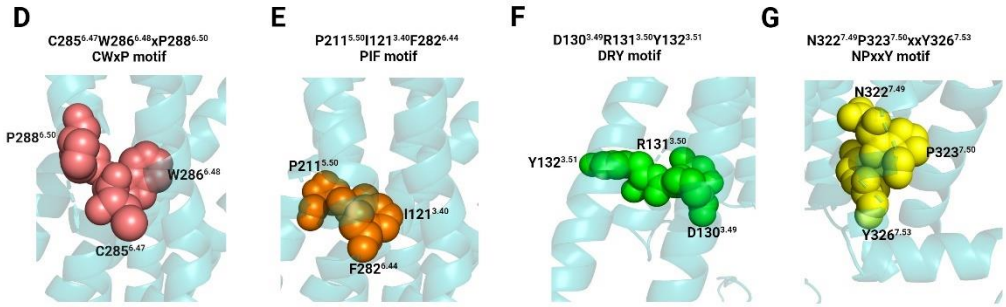

Figure 1.7: Schematic overview of 2-dimensional and 3-dimensional structures of β2-AR and evolutionary conserved motifs of the rhodopsin family of GPCRs. (A) The serpentine diagrams of β2-AR display the N-terminus, extracellular loops (ECL1-ECL-3), transmembrane α-helices (TMs), intracellular loops (ICL1-ICL3), α-helix (H8), and the intracellular C-terminus. The sodium-binding residues are colored blue, CWxP motif residues in light red, PIF motif residues in orange, DRY motif residues in green, and NPxxY residues in yellow. Note that the $W^{6.48}$ and $N^{7.49}$ residues of sodium binding sites are common between the CWxP and NPxxY motifs, respectively. (B) The AlphaFold (AF-P07550) protein structure of β2-AR displays the various parts of the receptor. The cross-sectional view of β2-AR displays a barrel-like structure formed by TMs. **(C)** The sodium-binding residues in β2-AR are shown. The evolutionary conserved motifs in β2-AR of the rhodopsin family of GPCRs, CWxP **(D)**, PIF **(E)**, DRY **(F)**, NPxxY **(G)** are represented. Serpentine diagrams were prepared using https://gpcrdb.org/; AlphaFold PDB structure was visualized and created using PyMol (Schrödinger Inc.), and BioRender.com.

1.3.4 GPCRs signal transduction

The physiological activities of living beings commence with unique signals that are received by the cell membrane, transduced, and propagated to the intracellular environment of cells. These signals are processed in microseconds-hours and transformed into a precise and unique order for maximum performance and maintaining homeostasis. Most of the time, the signals are processed by membrane proteins, of which GPCRs are one of the primary signal transducers. GPCR-mediated signaling is primarily regulated through either G protein or β-arrestin, and apart from them, various effectors and regulatory proteins work together to transmit signals [80, 81]. The ability of a receptor to differentially activate downstream signaling pathway over the other is considered biased signaling [82]. In recent times, it has been observed that the GPCR, heterotrimeric G proteins and β-arrestin could also form mega-complexes that could signaling from endosomes [83]. Altogether, the GPCR ligands, signaling pathways, and their interacting and regulatory cohorts are complex, which explains the promiscuous nature of GPCRs [84].

1.3.4.1 G protein mediated signaling

The agonist binding to a GPCR causes a conformational change in the receptor, which initiates canonical G protein-dependent signaling. In general, it is well known that the

outward displacement of transmembrane helix 6 (TM6) following ligand binding is a distinctive feature of receptor activation in the majority of the rhodopsin-like GPCRs. The rearrangements of 7-TM eliminate TM3-TM6 contacts and allow the formation of contacts between TM3-TM7 and TM5-TM6 [72, 74]. The conformational changes at the cytoplasmic end of the receptor function as a guanine nucleotide exchange factor (GEF), which facilitates the exchange of GDP for GTP in the Gα protein subunit [85]. In brief, the heterotrimeric G proteins are composed of three distinct subunits: Gα, Gβ, and Gγ. In mammals, these G proteins are encoded by at least 18 distinct α-subunit genes, 5 different β-subunit genes, and 12 different γ-subunit genes [86-88]. Gα subunit isoforms are classified into four subfamilies: Gαs (Gα stimulatory; subtypes Gαs and Gαolf), Gαi/o (Gα inhibitory; subtypes Gαi1, Gαi2, Gαi3, GαoA, GαoB, Gαt1, Gαt2, Gαg, Gαz), Gαq/11 (Subtypes Gαq, Gα11, Gα14, Gα15, Gα16) and Gα12/13 (subtype Gα12 and Gα13). This exchange causes the Gα subunit (GTP-bound) to dissociate from the Gβγ dimer and receptor. The GTP bound-Gα and Gβγ can then activate several effectors, while the receptor can activate the subsequent G protein. The active Gα-subunits then activate various effectors; for example, Gαs activate adenylyl cyclase (AC) which causes cyclic adenosine monophosphate (cAMP) upregulation, Gαi inhibits adenylyl cyclase (AC) which causes cAMP downregulation, Gαq/11 activate phospholipase C (PLC) and Gα12/13 control the actin cytoskeleton.

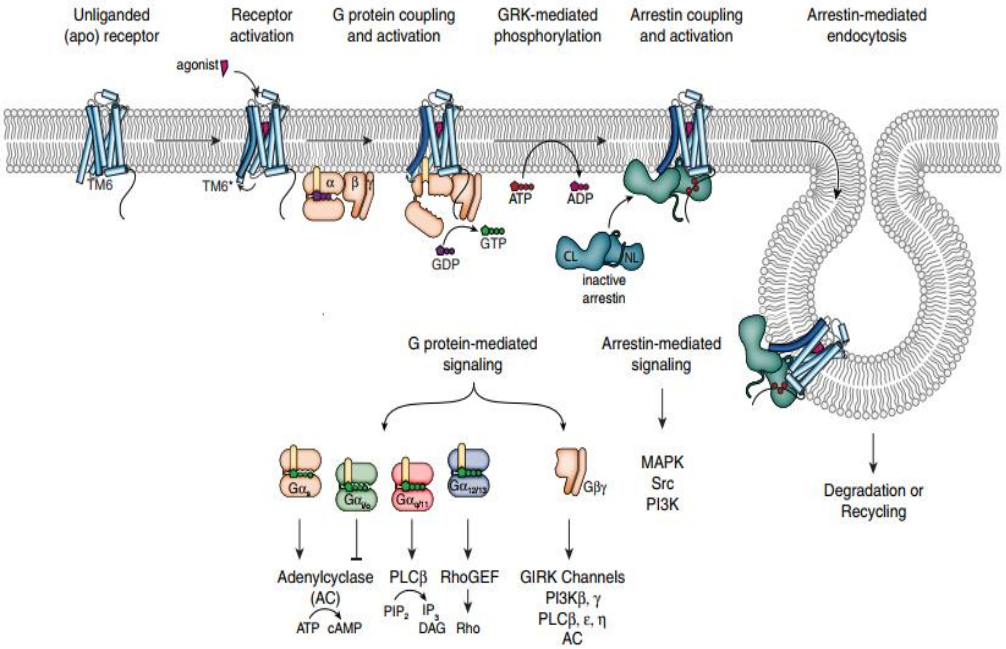

Figure 1.8 Canonical GPCRs signaling pathways. The initiation of GPCR signaling occurs when an agonist binds to the receptor, leading to conformational changes in the transmembrane domain. These modifications involve an outward displacement of the intracellular tip of transmembrane domain 6 (TM6, seen in a deeper blue shade). The activation of the receptor

facilitates the recruitment of heterotrimeric G proteins, which are composed of Gα, Gβ, and Gγ subunits. The process of G protein coupling to the receptor initiates the exchange of GDP for GTP in the Gα subunit, leading to the subsequent dissociation of the heterotrimer into the Gα and Gβγ subunits. The interaction and modulation of several downstream effectors are facilitated all the subunits. The activation or inhibition of adenylate cyclase (AC), phospholipase C (PLC), and Rho guanine exchange factor (RhoGEF) are modulated by different isoforms of Gα subunits, specifically, the Gαs isoform activates AC, the Gαi/o isoform inhibits AC, the Gαq isoform activates PLC, and the Gα12/13 isoform activates RhoGEF. Moreover, Gβγ subunits have the capability to regulate the functioning of G protein-coupled inwardly rectifying potassium (GIRK) channels, phosphatidylinositol 3-kinase (Pl3K), and phospholipase C (PLCs). The activation of G protein-coupled receptors (GPCRs) also facilitates the process of phosphorylation via the action of G protein-coupled receptor kinases (GRKs), which in turn enhance the recruitment and activation of arrestin. The process of arrestin coupling results in the desensitization of receptors and the activation of signaling pathways regulated by arrestin, including several kinases such as the mitogen-activated protein kinase (MAPK), phosphoinositide 3-kinase (PI3K), and Src kinase. The process of arrestin coupling may also elicit receptor endocytosis via clathrin-coated vesicles, subsequently leading to receptor destruction in lysosomes or recycling of the receptor back to the plasma membrane. ATP, adenosine triphosphate; PIP_2, phosphatidylinositol 4,5-bisphosphate; IP_3, inositol triphosphate; DAG, diacylglycerol *(Figure adapted from Hilger et al., 2021 [89]).*

Following this, second messengers are produced, that influence additional downstream effectors [89]. After dissociation, the Gβγ subunit can also bind to and control downstream effectors such as ion channels, GRKs etc. [90]. After some time, Gα protein siganling is terminated by hydrolysis of bound GTP to GDP. This occurs through the intrinsic GTPase activity of the Gα subunit itself or with the help of GTPase-activating proteins (GAPs) [91]. The inactive form of the Gα-subunit (Gα-GDP) is regenerated, which reassociates with the Gβγ dimer to form the "inactive" G protein complex, which can again bind to an active GPCR or constitutive receptor (Figure 1.8).

1.3.4.2 GRKs and β-arrestin mediated signaling

The Arrestin (Arr) protein family consists of four members (arrestin-1 to arrestin-4) and is critical for regulating signal transduction at GPCRs. Arrestins were first discovered as a regulatory protein of visual rhodopsin and later found to regulate the β2-adreneric receptors as well [92-94]. The initial step in receptor desensitization is the phosphorylation of serine and threonine residues in the ICL3 and C-terminus tail of the receptor by GRKs, which initiates arrestin recruitment [95]. Arrestin attachment to the receptor inhibits further Gα protein-mediated signaling. Furthermore, the interactions between the C-terminus tail of the GPCR, arrestin, and the cell membrane endocytic proteins clathrin and β2-adaptin subunit (AP-2 adaptor complex) promote the internalization of the receptor-arrestin-AP-2 complex. GPCR-arrestin vesicles are

internalized and transported either to degradative (lysosomes) or recycling pathways within the cell via the binding of arrestin to E3 ubiquitin ligases, which control receptor surface expression [96, 97]. Alternatively, it has been suggested that GPCR, Gα protein, and arrestin form super-complexes (or megacomplexes), which, when internalized can cause sustained Gα protein signaling from internalized compartments [83]. Additionally, upon internalization, arrestin is also known to interact with Raf Kinases, Akt (Protein kinase B), MEK1 (Mitogen-activated protein kinase 1), the tyrosine kinase c-Src, extracellular protein kinase (ERK)1/2, c-Jun N-terminal kinase 3 (JNK3), etc.

It is worth noting that arrestin-3 (also known as β-arrestin-2) is exclusively found in the cytoplasm, and arrestin-2 (also known as β-arrestin-1) has been shown to reside in both the cytoplasm and nucleus [98]. Moreover, it has been suggested that the rhodopsin family of GPCRs binds β-arrestin 2 higher with high affinity than β-arrestin 1 [99].

1.3.5 Role of phospholipids and sterols in GPCR function

GPCRs have been found to be activated not only by their ligands but also by various cell membrane lipids. Lipids like phospholipids (such as sphingolipids) and sterols (mainly cholesterol) are emerging as key regulators of GPCR structure and activity. All these effects are either through lipids altering membrane properties such as thickness, curvature, or surface tension or through direct binding to GPCRs. According to one study, it has been demonstrated that phosphatidylglycerol (glycerophospholipid) strongly favors agonist (isoproterenol) binding and enhances β2-AR receptor activation, whereas phosphatidylethanolamine (sphingolipids) strongly favors antagonist (alprenolol) binding and stabilizes the receptor in the inactive state [100]. In another study of β2-AR signaling, phospholipids impacted the receptor preference to interact with Gαi over Gαs because of the charge complementarity of lipid-G proteins [101]. Furthermore, phosphoinositides (PIPs) have been shown to augment an active conformation of β-arrestin and stabilize GPCR-β-arrestin complexes by encouraging a fully engaged state of the complex [102].

Cholesterol is a lipid that has been studied a lot in terms of how it changes the structure and function of GPCRs. One of the proposed mechanisms underpinning cholesterol control of GPCR activity is the specific interaction of GPCRs with membrane cholesterol. These GPCR-cholesterol interactions are frequently attributed to structural characteristics of GPCRs that may enable their preferred affinity with cholesterol. GPCR ligand binding, G protein coupling, and intracellular signaling have all been found to be affected by membrane cholesterol [103]. Cholesterol, for example, influences agonist binding to oxytocin and serotonin receptors, but its presence allows for dimerization of the NTS1 receptor [104-106].

The cell membrane has been shown to establish a microenvironment that consists of highly structured microdomains known as lipid rafts [107]. Lipid rafts are made up of very tightly packed saturated phospholipids (sphingolipids) and sterols (cholesterol). GPCRs and other signaling molecules, including heterotrimeric G proteins, key enzymes like kinases and phosphatases, trafficking proteins, and secondary messengers, are preferentially compartmented in these lipid rafts. In a recent report, it has been demonstrated that incubating HSG cells and isolated mouse submandibular acinar cells with methyl-β-cyclodextrin (MBCD), which depletes cholesterol from cell membrane and lipid rafts, reduced muscarinic receptor-mediated Ca^{2+} signaling [108]. Altogether, this evidence displays the prominent role of phospholipids and sterols in GPCR activation and functions though lipid raft or microdomains.

1.4 Orphan GPCRs

GPCRs share a common structural topology, yet not all have been found to be activated by the same ligand, indicating that GPCRs are very selective in their ligand recognition [109]. The inherent druggability of GPCRs is due to the availability of multiple binding sites for molecules to modulate the receptor activity [110, 111]. Currently, for approximately 238 receptors the endogenous ligands have been recognized, and of these, 165 are targeted by US Food and drug administration (FDA)-approved drugs (Figure 1.9 A) [112-115]. In fact, ~35-40% of the US FDA-approved drugs target GPCRs [112, 113, 116, 117]. Until an endogenous ligand is identified for a GPCR, it is regarded as an "orphan GPCR" [109]. However, molecular biology and pharmacology techniques have identified ligands for many receptors, but to date, there are still no known ligands for ~120 receptors [118]. As a result, many receptors remain orphans with poorly defined physiological functions [119]. The most targeted class is rhodopsin-like GPCRs, which account for about 94% of approved drugs for GPCRs (Figure 1.9 B). Among the approved drugs that target GPCRs, 92% and 5% are small molecules and peptides, respectively (Figure 1.9 C).

Traditionally, ligands were found first and then utilized to characterize receptors pharmacologically. In the 1980s, with the development of molecular biological techniques, researchers were able to express orphan GPCRs in cell lines and test their signal transduction using putative exogenous or endogenous ligands [120]. Concurrently, reverse pharmacology (using clinical observation to define and explore the leads through transdisciplinary approaches) aided in defining the ligands through rigorous preclinical and clinical research [121, 122]. Since it has been possible to obtain the structures of receptors, this enables us to select molecules in a clever way through structure-based in-silico screening and even design, and then utilize them for testing on receptors using high-throughput assays [123, 124]. If we are not able to find endogenous ligands in all ways, we could still utilize surrogate (nonnatural) ligands to

activate receptors [125]. This will assist in understanding receptor-related pathophysiology, and we may well be utilizing it for pharmacological purposes. Although it is worth mentioning that not all the receptors might associate with endogenous ligands, some receptors could play a role in receptor trafficking or they might need oligomerization with other receptors to function [120].

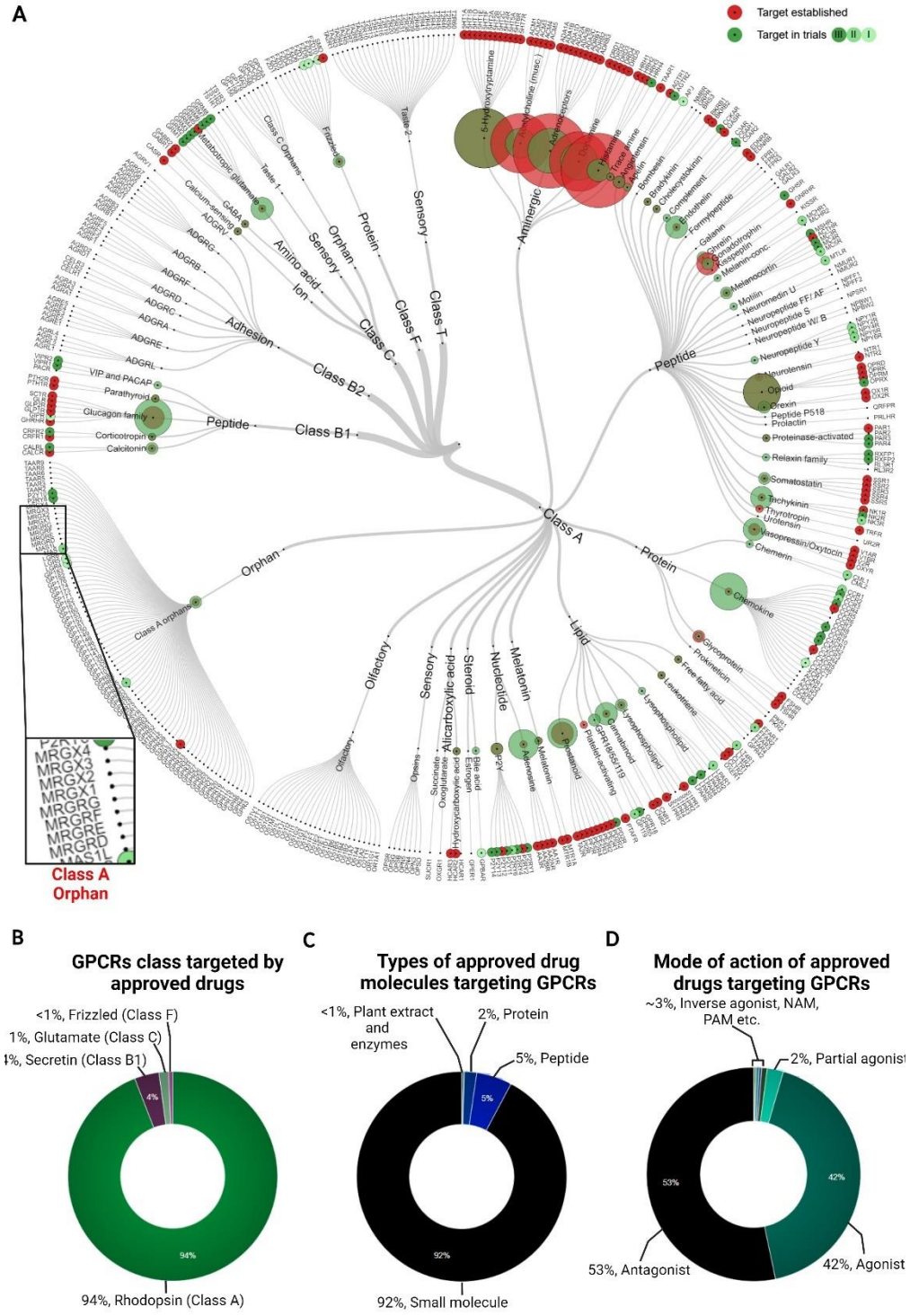

Figure 1.9: GPCRs targeted by drugs. (A) GPCRs with established targets, in the trial, and orphan receptors are shown. The orphan MRGPR family is shown in inset on the left side. **(B)** Percentage of GPCR classes targeted by approved drugs. **(C)** Various types of approved drug

molecules targeting GPCRs. **(D)** Mode of action of approved drugs on GPCRs. Figure adapted from *Hauser et al. 2017* and gpcrdb.org and created using BioRender.com.

1.5 Mas-related G protein-coupled receptors (MRGPRs)

Mas-related G protein-coupled receptors (MRGPRs) are known to mediate noxious sensations, including pain and itching. MRGPRs belong to the δ-group of the rhodopsin family of GPCRs, which includes glycoprotein receptors, purine receptors, and the olfactory receptor cluster [57]. In 1986, the first member 'MAS' receptor was found [126] and in 1990, the rat thoracic aorta (RTA) gene, which is now known as the *mrgprf* gene, was identified [127]. Notably, the name "Massey" of the individual who donated the human tumor from which the MAS gene was obtained is shortened to form the acronym MAS [126]. In the beginning of the 21st century, two distinct groups of researchers discovered a set of orphan GPCRs that were predominantly expressed in sensory neurons of the dorsal root ganglia (DRG) and trigeminal ganglia (TG) [128, 129]. Dong and his colleague discovered orphan GPCRs displaying 35% sequence identity with the Mas1 receptor [126]. Therefore, receptors were named after the MAS-receptor as Mas-related genes (Mrgs) [128]. Concurrently, Lembo and his colleagues discovered a new class of 'orphan' GPCRs and demonstrated that bovine adrenal medulla 22 peptide (BAM22) as well as its fragments bind to and activate these receptors with nanomolar affinity. Since this family of GPCRs was discovered in human and rat small sensory neurons, researchers named them sensory neuron-specific receptors (SNSRs) [129]. Later on, the HUGO Gene Nomenclature Committee referred to these proteins as MRGPRs to avoid ambiguity.

MRGPRs are a large family of receptors and are divided into nine distinct subfamilies (A-H and X) [128, 130]. MRGPR genes are located on chromosome 11 (in humans), chromosome 1 (in rats), and chromosome 7 (in mice) [128, 130-132]. In rodents, subfamilies MrgprA (subtype A1-A19), MrgprB (subtype B1-B13), and MrgprC11 are found [128, 130, 132]. The MRGPRs D to G are found in mammals, including rodents and primates [130, 132, 133]. The MrgprH is found in rodents and birds only [132]. On the other hand, MRGPRX1 (SNSR4 [129]), MRGPRX2, MRGPRX3 (SNSR1 [129]) and MRGPRX4 (SNSR6 [129]) are exclusively found in primates (humans, macaques, rhesus monkeys, etc.) [128, 132].

Initially, it was believed that all MRGPRs (except MRGPRX2) are expressed by nociceptive neurons of the trigeminal ganglia and dorsal root ganglia, which hinted at and lately proved their role in histamine-independent pruritis and pain perception [128-141]. Several reports now indicate that MRGPRs are also expressed by immune cells such as mast cells, macrophages, and neutrophils and subsequently contribute to inflammation [123, 142-158]. Although the MRGPRF was the first member of the

family, it was discovered in thoracic aortic cells, and lately, the MRGPRD has been reported in cardiovascular tissues [127, 159].

1.5.1 MRGPRs in itch and pain sensations and their modulators and activators

The noxious sensations of itch and pain cause significant suffering and impairment [160]. It has been suggested that chloroquine (an antimalarial drug) mediates the itch via MRGPRX1 [161]. Additionally, in terms of pain, activation of MRGPRX1 with bovine adrenal medulla 8-22 peptide (BAM8-22) and ML382 (positive allosteric modulators; PAMs) reduces spinal nociceptive transmission, which inhibits persistent pain in the humanized MRGPRX1 mouse model [162]. Furthermore, MRGPRX2 has been known to mediate the itch induced by various cationic drugs such as morphine, clozapine, etc. and various endogenous peptide agonists (PAMP-12, cortistatin 14) [123, 163-167]. Moreover, there is compelling evidence that MRGPRX2 mediates the neuroinflammatory pain that substance P causes [168]. Recent studies have suggested that bilirubin and bile acids activate MRGPRX4, which might contribute to cholestatic itch [169, 170]. Compound MS47134 is a strong MRGPRX4 agonist that is 47 times more selective for MRGPRX4 than the Kir6.2/SUR1 potassium channel; its role in itch and pain still needs to be discovered [171]. MRGPRs are also known to be activated by proteases, which also play a role in inducing itch [148, 151]. Recent reports suggest that MRGPRX4 interacts with receptor activity modifying protein 2, which attenuates the basal and agonist-dependent signaling of MRGPRX4 [172]. Altogether, these reports point to the involvement of MRGPRs in the pruritic-nociceptive (itch-to-pain) axis and inflammation. Considering the above-mentioned facts from various studies, MRGPR activators can be broadly classified into small molecules, peptides, and proteases (Figure 1.10). MRGPRs are still considered orphans since only a small number of endogenous ligands are known for some MRGPRs but none for MRGPRE, MRGPRF, MRGPRG, and MRGPRX3 [173, 174].

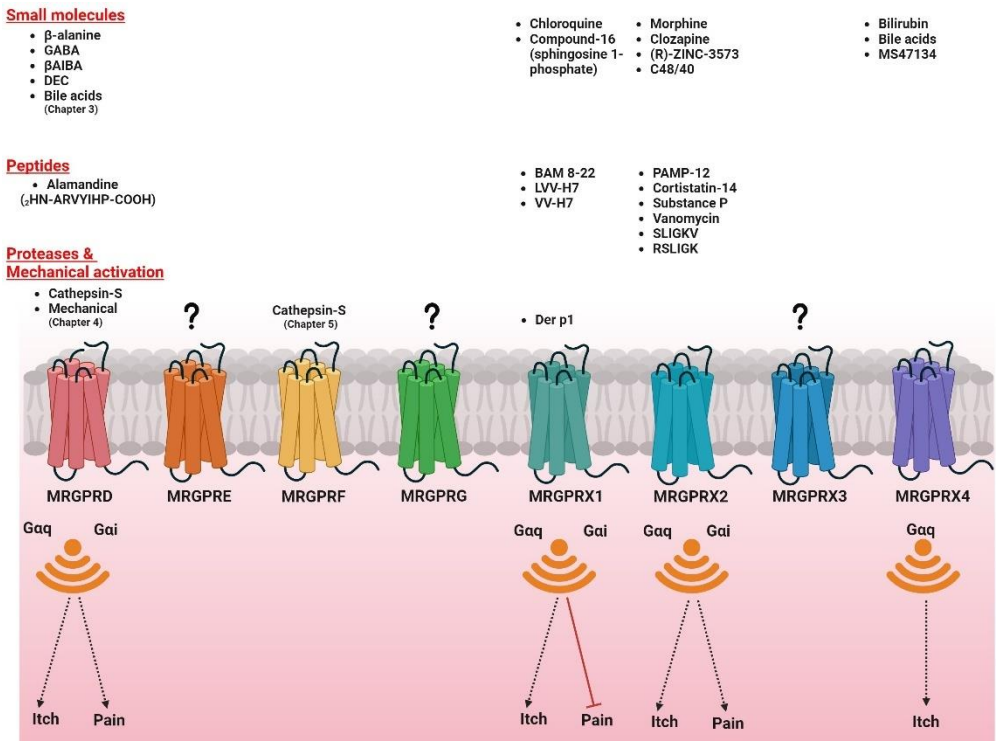

Figure 1.10: Human MRGPRs in itch and pain perception and their activators. The key activators of each MRGPR are shown, which have been reported to regulate itch and pain. The effector Gα (Gαq and Gαi) proteins that MRGPRs signal through are shown. Figure adapted from Cao, C., & Roth, B. L. (2023) and created with BioRender.com.

1.5.2 Distinct structural features of MRGPRs

Based on an evolutionary perspective, it is known that the human olfactory receptor O51E2 and the β2-AR are members of the δ-group and α-group of the rhodopsin-like GPCRs, respectively [57]. Notably, recent literature suggests that shallow ligand-binding pockets are observed in the δ-group of the rhodopsin family of GPCRs [171, 175-177]. Whereas in the β2-AR receptor, which belongs to the α-group of the rhodopsin family of receptors, the ligand-binding pocket is much deeper (Figure 1.11) [53, 178]. Moving further, in β2-AR, the calculated shortest distance between the TM6 toggle switch, i.e., $W^{6.48}$ residue and ligand (BI 167107; P0G) was 4.4 Å. Likewise, the shortest distance between the $F^{6.48}$ and the ligand (Propionate) in human O51E2 was 11.5 Å, which was substantially more than β2-AR (Figure 1.11 B and C). This affirms that, from an evolutionary point of view, the δ-group of the rhodopsin family of GPCRs not only differs on the basis of sequence from the α-group of the rhodopsin family of GPCRs, but also indicates a fundamental difference in the structural and ligand-binding properties.

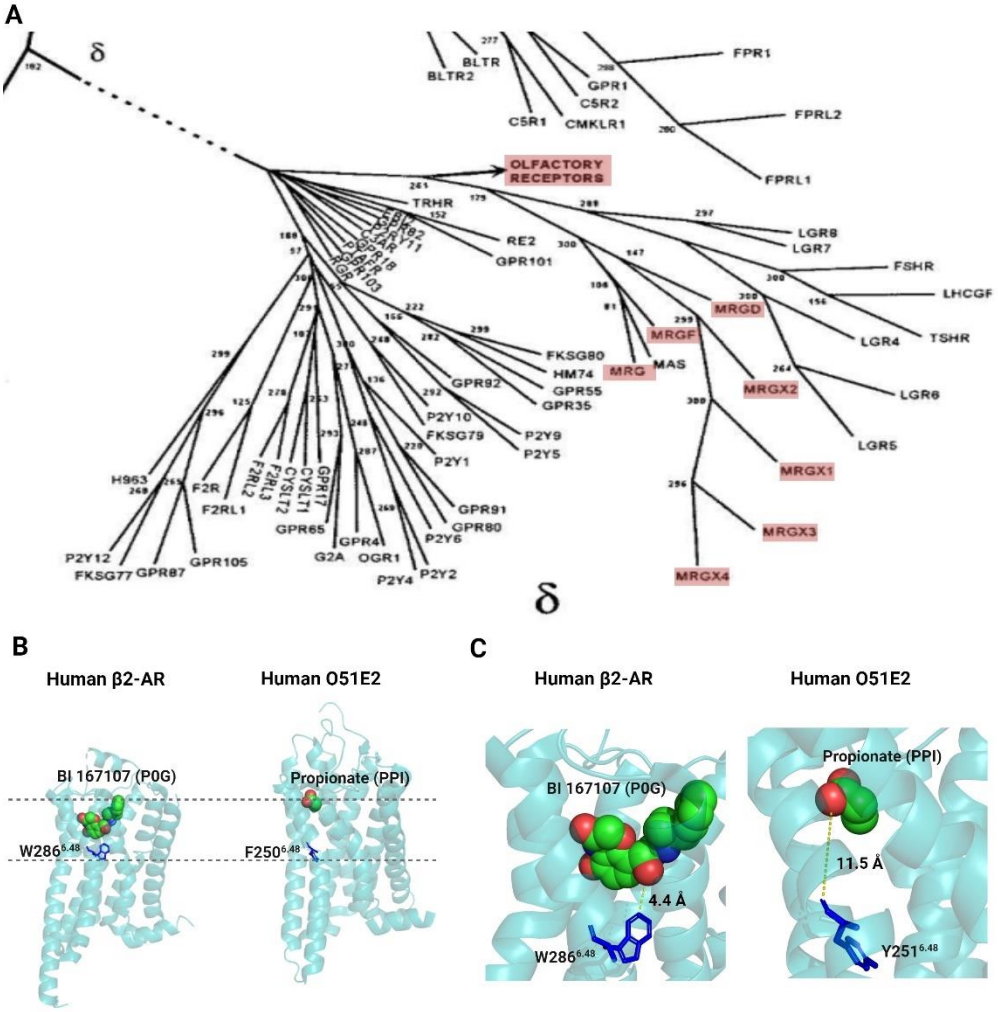

Figure 1.11: The phylogenetic tree of the δ-group of the rhodopsin family GPCRs and the shallow agonist-binding in the human odorant receptor (O51E2). (A) The phylogenetic tree representing the close relationship between MRGPRs and olfactory receptors *(figure adapted from Fredriksson et al. 2003 [57]).* **(B)** A cartoon representation of β2-AR (in cyan) BI 167107 (P0G) complex and the human odorant receptor O51E2 (in cyan) propionate complex. The human odorant receptor O51E2 has a shallow agonist-binding pocket as compared to β2-AR, which is far away from the toggle switch residue 6.48 in TM6. **(C)** The closest distance between the toggle switch residue 6.48 and bound-agonist BI167107 in β2-AR (PBD: 3SN6; 3.20 Å X-ray [179]) and propionate in O51E2 (PDB: 8F76; 3.1 Å cryo-EM [176]) are 4.4 Å and 11.5 Å, respectively. PDB structures were visualized using PyMol (Schrödinger Inc.), and figures created using BioRender.com.

Recent developments in the determination of MRGPR structures revealed distinct structural characteristics and ligand recognition properties in MRGPRs [171, 175, 177, 178]. The majority of the conventional motifs necessary for receptor activation, such

as the CWxP motif, the PIF motif, and the DRY motif, are either absent or semiconserved in MRGPRs [178]. It has been suggested that in MRGPRs, the canonical orthosteric ligand pocket is closed by this helical movement of TM6 towards TM3, thereby creating a shallow solvent-exposed ligand-binding pocket. This occurs due to the change in TM6 toggle switch residue $W^{6.48}$ (like in β2-AR) in the CWxP motif to $G^{6.48}$ (in MRGPRX1, MRGPRX2, MRGPRX4, MRGPRE, MRGPRG) or $S^{6.48}$ (MRGPRD, MRGPRF) in MRGPRs, due to which TM6 and TM3 interact more closely [175, 178]. The crucial TM3 residue $S^{3.39}$ for sodium binding is also absent from MRGPRs. Several studies have demonstrated that the sodium ion stabilizes GPCRs in an inactive state and that mutations of sodium pocket residues can increase the constitutive activity of the receptor. As a result, it has been suggested that the non-conserved sodium binding pocket may partially account for the high constitutive activity in MRGPRs [158, 178, 180]. The lack of a sodium binding site may also permit them to be triggered by a mild 'push' by ligand binding [178] or mechanical forces (chapter 5). In addition, the disulfide bond between TM3-ECL-2 which helps in stabilizing the ECL-2 on top of ligand-binding pocket and, in turn, increases the retention time and decreases the dissociation rate of agonist, does not exist in MRGPRs [178]. As suggested, this might be the reason for the low binding affinity and potencies of endogenous ligands of MRGPRs. Until now, inactive-state MRGPR structures have not been discovered.

In terms of ligand pockets, size, and charge of the ligand binding pocket, it is quite diverse in nature in the MRGPR family. In the case of MRGPRD, β-alanine carboxyl groups interact with the positively charged $R103^{3.30}$ on the TM3 and amino groups with the negatively charged $D179^{5.37}$ on the TM5 (Figure 1.12 B and 1.14 C) [175]. In MRGPRX1, the binding of the BAM8-22 agonist peptide is governed by R20 of the BAM8-22 peptide, which interacts with negatively charged $D177^{5.36}$ and $E157^{4.60}$ (Figure 1.12 D). The interaction of BAM8-22 with MRGPRX1 is further strengthened by the interaction of ML382 (a positive allosteric modulator) with BAM8-22 [177]. Cortistatin-14 binds to the negatively charged sub-pocket 1 of MRGPRX2 (Figure 1.12 F). The interaction between cortistatin-14's positively charged residues (mainly lysine and arginine) and MRGPRX2 is governed by the negatively charged residues $D184^{5.36}$ and $E164^{4.60}$[171]. Conversely, the sub-pocket 1 of MRGPR4 is inaccessible due to the ECL2 loop covering it, and the sub-pocket 2 of MRGPRX4 has an overall positive electrostatic potential surface that is accessible to MS47134 (Figure 1.12 H) [171].

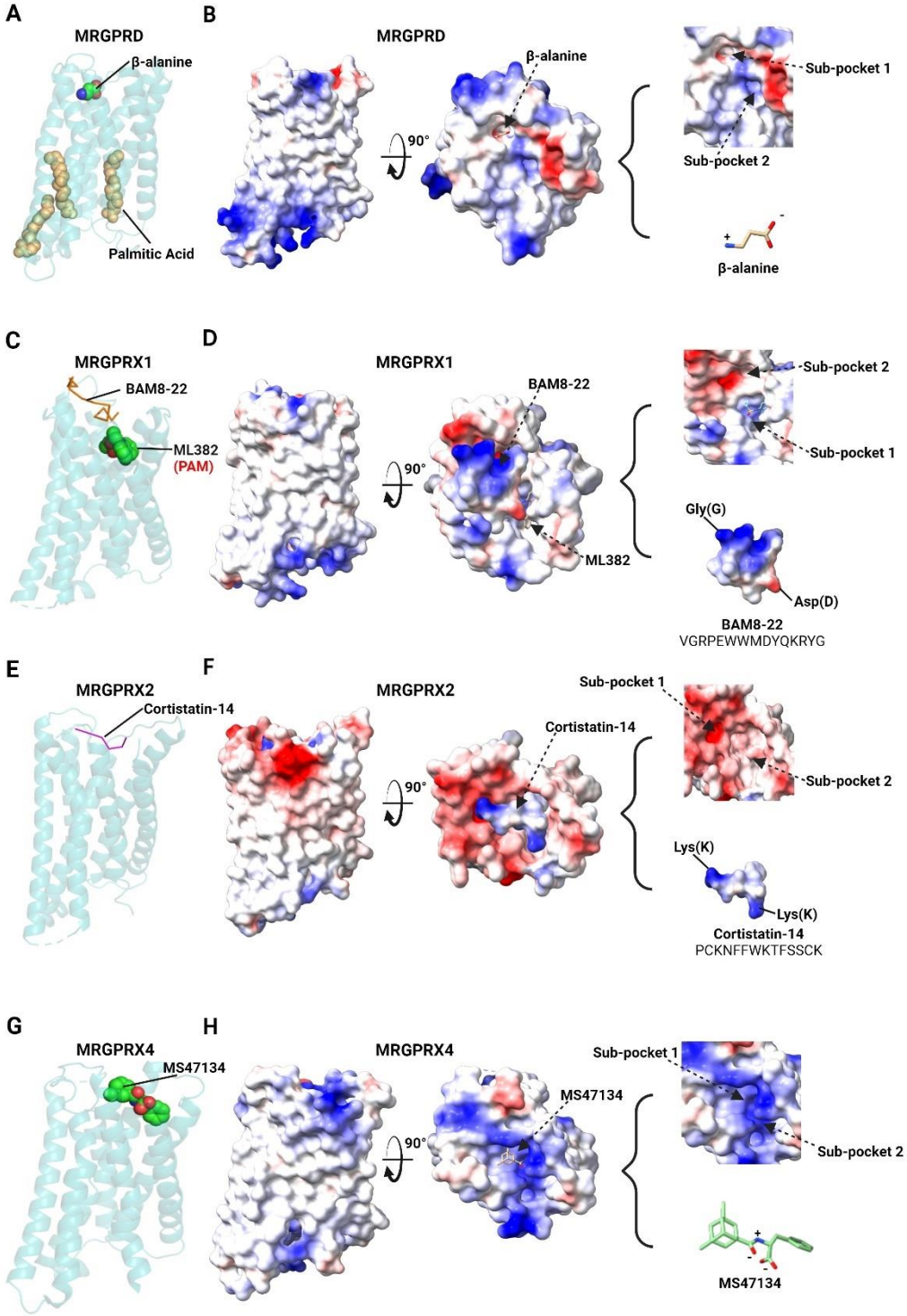

Figure 1.12: Various structures of MRGPRs. The cartoon (in cyan) representation of **(A)** MRGPRD-β-alanine complex (3.1 Å; PDB: 7Y12; cryo-EM [175]), **(C)** MRGPRX1-BAM8-22-ML382 complex (2.71 Å; PDB: 8DWG; cryo-EM [177]), **(E)** MRGPRX2-Cortistatin-14 complex (2.45 Å;

PDB: 7S8L; cryo-EM [171]), **(G)** MRGPRX4-MS47134 complex (2.6 Å; PDB: 7S8P; cryo-EM [171]). Electrostatic surface charge representation of the MRGPRD **(B)**, MRGPRX1 **(D)**, MRGPRX2 **(F),** and MRGPRX4 **(H)** generated using ChimeraX [181, 182]. The cross-sectional view of MRGPRD, MRGPRX1, MRGPRX2, and MRGPRX4 show a nice fit of β-alanine in sub-pocket 1 of MRGPRD **(B)**, BAM8-22 peptide in sub-pocket 1 and ML382 in sub-pocket 2 of MRGPRX1 **(D)**, Cortistatin-14 peptide in sub-pockets 1 and 2 **(F),** MS47134 in sub-pocket 1 of MRGPRX4 **(H),** respectively. Red and Blue colors represent negative and positive charges, respectively. PDB structures were visualized using PyMol (Schrödinger Inc.), and figures created with BioRender.com.

1.5.3 Mas-related G protein-coupled receptor D (MRGPRD)

MRGPRD is also known as MrgD and TGR7 [128, 130, 183]. The protein sequence analysis revealed 58.6% and 62.4% sequence identity between human-mouse and human-rat MRGPRD, respectively, which indicates the sequence is not highly conserved between mammals (Appendix I) [183]. MRGPRD was discovered to be expressed by the majority of isolectin-B4- positive (IB4+), small non-myelinated sensory neurons of the dorsal root ganglia (DRG) and trigeminal ganglia (TG) [128, 130, 135]. MRGPRD neurons are known to selectively innervate the superficial layers of the epidermis [135]. Later, MRGPRD expression was also discovered in mouse colonic DRG afferents [184] and lung cancer tissues [185]. Furthermore, some studies indicate that MRGPRD mRNA transcripts have been identified in aortic endothelial cells, arterial smooth muscle cells, and cardiomyocytes [159, 186, 187]. MRGPRD has also been reported to be expressed by neutrophils and macrophages [187, 188]. Another study localized the MRGPRD in osteocytes [189]. Overall, MRGPRD has been found to play a role in itch, pain, cardiovascular disease, and cancer. Elaborated functions of MRGPRD are covered in the introduction of chapters 3, 4, and 5.

It is well known that a wide range of agonists, including small molecules and peptides, can activate MRGPRD (Figure 1.10). Small molecules such as β-alanine [183] (the first discovered agonist of the MRGPRD), 3-aminoisobutyric acid (βAIBA) [190], γ-aminobutyric acid (GABA) [190, 191], diethylstilbesterol (DEC) [190], glycine [191], and 5,7-dihydroxytryptamine creatinine sulphate [191] can activate the MRGPRD receptor. The MRGPRD is also known to be activated by a polyunsaturated acid (PUFA), 5-Oxo-eicosatetraenoic acid (5-oxoETE) [184]. Additionally, the heptapeptide angiotensin 1–7 and alamandine have been reported to activate the MRGPRD receptor [192]. Of all the ligands reported above, β-alanine is the most potent and has been studied extensively. On the other hand, several compounds, such as chlorpromazine [191], thioridazine [191], (R)-propylnorapomorphine [191], PD123319 (an AT-2 receptor antagonist) [193], and the peptide D-Pro7-Ang(1-7) [194], have been reported as antagonists of MRGPRD. MU-6840, a possible anticancer drug, also exhibited antagonistic action [190].

Recently, the cryo-EM structures of the MRGPRD-Gαi complex with β-alanine and apo state (ligand independent) with a resolution of 3.1 Å (PDB: 7Y12) and 2.8 Å (PDB: 7Y15), respectively, were determined (Figure 1.13 A and B) [175]. Interestingly, it was observed that β-alanine bound shallowly to the extracellular orthosteric ligand-binding pocket. Additionally, upon ligand binding, the MRGPRD TM6 tilts substantially towards the TM3, which is opposite of what is seen in the α-group of the rhodopsin family of GPCRs. This could be attributed to the lack of conserved toggle switch residue $W^{6.48}$ which is replaced with a small residue $G^{6.48}$ in MRGPR family. This hints that MRGPRs might have a different mode of activation altogether.

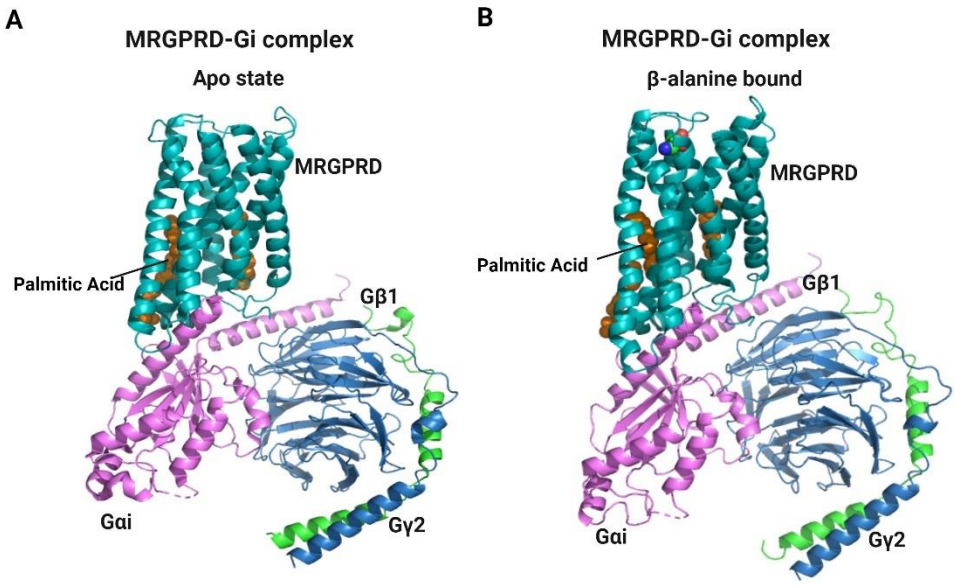

Figure 1.13: MRGPRD-Gαi complex structures. The cryo-EM structures of β-alanine bound **(A)** and apo state **(B)** MRGPRD-Gαi complex. The MRGPRD is shown in cyan, Gαi is in magenta, Gβ1 in blue and Gγ2 is in blue. Palmitic acid is in orange. PDB structures were visualized using PyMol (Schrödinger Inc.), and figures were created with BioRender.com.

According to a recent study, in the human olfactory receptor O51E2, the volatile fatty acid propionate shallowly binds to the orthosteric binding pocket. This is also observed with β-alanine's shallow binding to MRGPRD. On further analysis, it was observed that in the human olfactory receptor O51E2, the shortest distance between the toggle switch residue of TM6 $Y^{6.48}$ and the ligand propionate was 11.5 Å. Similarly, the shortest distance between toggle switch residue $S^{6.48}$ and the ligand β-alanine in human MRGPRD was 14.1 Å, which was comparable to O51E2 (Figure 1.14 A and B). The shallow binding of ligand in O51E2 and MRGPRD leads us to think that this is a classical feature of the δ-group rhodopsin family of GPCRs. If we look, there is only one amino group difference between propionate and β-alanine, which gives rise to the possibility

that MRGPRD can also be activated by volatile short-chain fatty acids such as propionate.

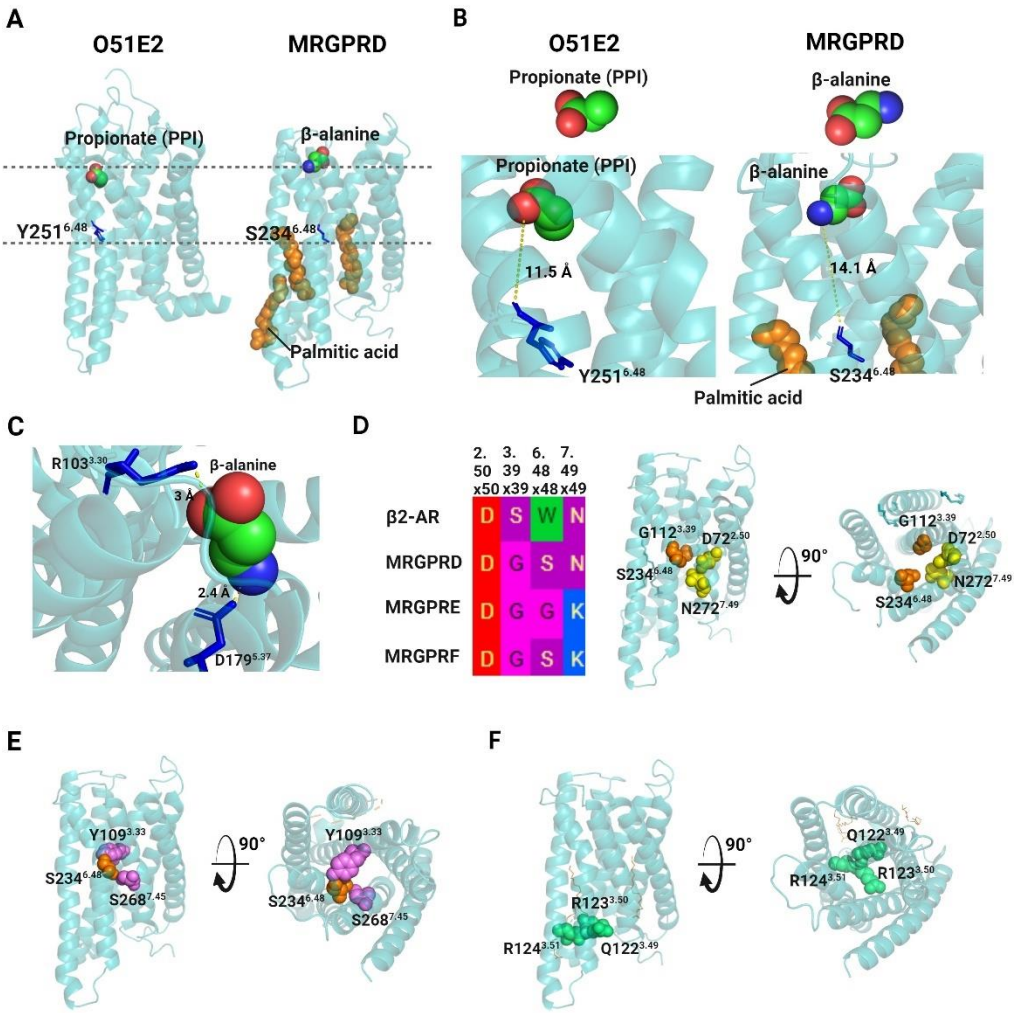

Figure 1.14: Human olfactory receptor O51E2 and MRGPRD characteristic features. (A) A cartoon representation of human olfactory receptor O51E2-Propionate (PPI) and the human MRGPRD-β-alanine complex. The human odorant receptor O51E2 has a shallow agonist-binding pocket, which is comparable to the MRGPRD. **(B)** The closest distance between the toggle switch residue 6.48 on TM6 to bound-agonist propionate in O51E2 (PDB: 8F76; 3.1 Å cryo-EM) and β-alanine in MRGPRD (PDB: 7Y12; 3.1 Å cryo-EM) are 11.5 Å and 14.5, respectively. **(C)** β-alanine carboxyl groups interact with the positively charged R103$^{3.30}$ on the TM3 and amino groups with the negatively charged D179$^{5.37}$ on the TM5. **(D)** Comparison of sodium binding residues between β2-AR, MRGPRD, MRGPRE, and MRGPRF and on the right, MRGPRD displays the lack of conserved-sodium binding residues. **(E)** Residues of hydrogen-bond network i.e., Y109$^{3.33}$, S234$^{6.48}$ and S268$^{7.45}$, which mediates constitutive activity of

MRGPRD. **(F)** Residues of D(Q)RY(C) motif of MRGPRD. PDB structures were visualized using PyMol (Schrödinger Inc.), and figure created with BioRender.com.

It has been reported that in HEK-293 cells, MRGPRD constitutively (without ligand induction) couples with the highest affinity to Gαi, Gα15, Gα13 and Gαq, respectively, and exhibits marginal coupling to β-arrestin 2 [195]. Although the mechanism behind the constitutive activity of MRGPRD has not yet been established. MRGPRD lacks the conserved sodium-binding sites ($D^{2.50}$, $S^{3.39}$, $W^{6.48}$, and $N^{7.79}$) which are known to stabilize GPCRs (Figure 1.14 D) [196]. Additionally, MRGPRD has a modification to the DRY motif (Figure 1.14 F). The $D^{3.49}$ in the DRY motif is replaced with $Q^{3.49}$ in MRGPRD, which might hinder the ionic lock formation with $R^{3.50}$. The mutation of $D^{3.49}$ has been reported to increase basal activity [78]. Also, $Y^{3.33}$, $S^{6.48}$, and $S^{7.45}$ form a network of hydrogen bonds, and Y109A and S234A mutations decreased the base activity (Figure 1.14 E) [175]. Considering the observed modifications in the MRGPRD, it would be reasonable to think that these modifications alter the conformational properties of the MRGPRD and maintain it in an active state.

1.5.4 Mas-related G protein-coupled receptor E (MRGPRE)

The MRGPRE is expressed in the dorsal root ganglia, spinal cord, and several parts of the brain [134, 197]. The protein sequence analysis showed that the human-mouse MRGPRE had 73.2% sequence identity and the human-rat MRGPRE had 72.5% sequence identity (Appendix I). It has been reported that genetic ablation of MrgprE in mice alters pain-like behavior and influences the expression of MrgprF in the spinal cord [136]. Furthermore, the rat MrgprE is reported to form a functional heterodimer with the rat MrgprD, which increases the potency of β-alanine to phosphorylate ERK1 and ERK2, as well as inhibits β-alanine-induced internalization of rMrgprD [198]. Functionally, MRGPRE has been hypothesized to be expressed in pain-related cells. Nevertheless, studying MRGPRE has been difficult due to a lack of plausible ligands for the receptor (Figure 1.15) [178].

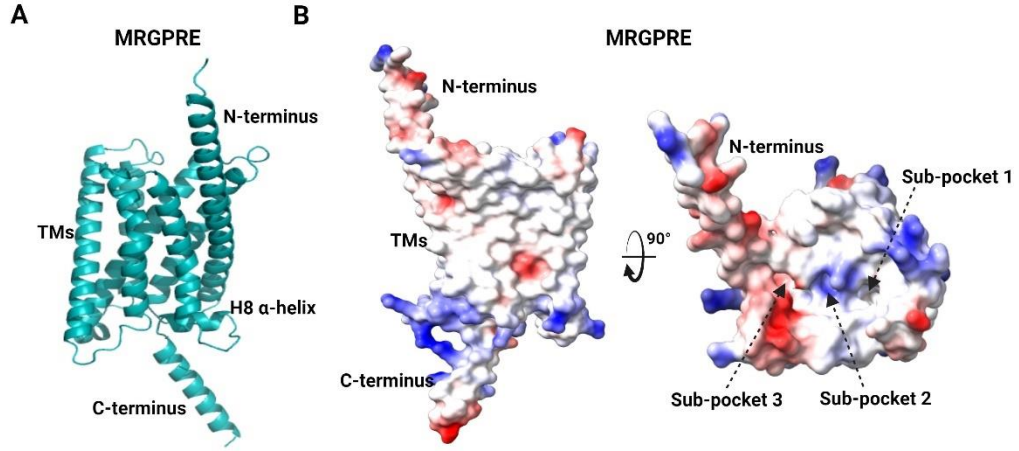

Figure 1.15: Characteristic features of human MRGPRE. (A). A cartoon representation of MRGPRE (AF_MRGPRE_Q86SM8) structure generated from the Alpha-Fold Protein Structure Database representing the N-terminus, TMs, H8-α-helix, and C-terminus of MRGPRE [199, 200]. **(B)** Electrostatic surface charge representation of the MRGPRE generated using ChimeraX [181, 182]. The cross-sectional image displays possible ligand binding pockets 1, 2 and 3. Red and Blue colors represent negative and positive charges, respectively. Figure created with BioRender.com.

1.5.5 Mas-related G protein-coupled receptor F (MRGPRF)

The rat thoracic aorta (RTA) gene, which is now known as the MRGPRF gene, was first identified in 1990 [127]. The protein sequence of the mouse and rat MRGPRF displays nearly 86% and 85.1% sequence identity to that of the human MRGPRF, respectively, which indicates that the sequence is highly conserved in mammals (Appendix I). Initially, MRGPRF was reported to be expressed in the trigeminal ganglia and dorsal root ganglia [130, 136, 197]. Nevertheless, MRGPRF expression is not limited to neurons; at the mRNA level, MRGPRF is expressed in tissues, such as the human gastrointestinal tract, smooth muscle, testis, colon, and aorta [197, 201, 202]. It has also been found that, at the mRNA level, MRGPRF is expressed by monocytes and macrophages, and the level of MRGPRF increases substantially during monocyte-to-macrophage differentiation [145]. Nevertheless, whether MRGPRF is expressed at the protein level in these cells is yet to be determined.

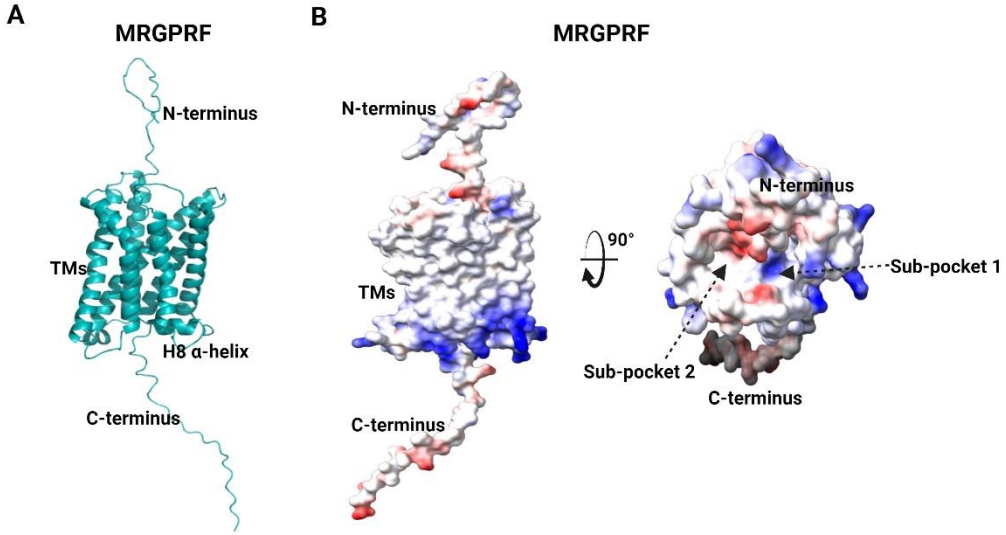

Figure 1.16: Characteristic features of human MRGPRF. (A). A cartoon representation of MRGPRF (AF_MRGPRF_Q96AM1) structure generated from the Alpha-Fold Protein Structure Database representing the N-terminus, TMs, H8-α-helix, and C-terminus of MRGPRF. **(B)** Electrostatic surface charge representation of the MRGPRF generated using ChimeraX. The cross-sectional image displays possible ligand binding pockets 1 and 2. Red and Blue colors represent negative and positive charges, respectively. Figure created with BioRender.com.

Recently, it has been demonstrated that MRGPRF plays a crucial role in inhibiting tumor cell proliferation, migration, xenograft tumor growth, and metastasis [203]. Therefore, MRGPRF is not only expressed by many cells and tissues, but it also plays a role in regulating cancer. However, so far, no endogenous ligand or activator has been identified for MRGPRF, due to which it remains orphan and understudied (Figure 1.16) [178].

Chapter 2

Aims of the study

Chapter 2 Aims of the study

MRGPRs are known to play a crucial role in itch and pain mediation and in pseudo-allergic drug reactions. In recent years, MRGPRs have begun to emerge as mediators in cardiovascular biology. Despite the fact that there is information available on some MRGPRs activation, signaling pathways, their role in inflammation is highly awaited. Furthermore, it is known that GPCRs form complex oligomers, which are known to regulate receptor activation, modulation of signaling, receptor trafficking, etc. Therefore, many physiologists and pharmacologists are trying to discover ligands for MRGPRs to define the mode of activation and associated signaling of MRGPRs. Even though many scientists have tried to understand the role of MRGPRs, progress has been limited as most MRGPRs are still orphans, and very few ligands are known to activate some MRGPRs. This limits the progress in understanding the pathophysiological role of MRGPRs. In this PhD thesis, I aimed to get a better understanding of MRGPRs by addressing three points: 1) deciphering the activation mechanism of MRGPRs; 2) the role of MRGPRs in inflammation biology; and 3) elucidating the oligomeric interaction of MRGPRs.

Chapter 3: Constitutive, basal and β-alanine-mediated activation of the human Mas-related G protein-coupled receptor D induces release of the inflammatory cytokine IL-6 and is dependent on NF-kB signaling

MRGPRs are expressed by sensory neurons, mast cells, macrophages, cardiovascular tissue, etc., and are known to regulate pruritus, nociception, and pseudo-allergic drug reactions. Some literature suggests that MRGPRs are also involved in inflammatory processes and the release of cytokines. Given the lack of evidence that MRGPRD can induce interleukin-6 (IL-6) release, we aimed to investigate if β-alanine- or alamandine-activated MRGPRD can release IL-6 and, if so, which cellular signaling pathways are involved.

Chapter 4: Bile acids-mediated activation of human Mas-related G protein-coupled receptor D induces release of the inflammatory cytokine IL-6

The majority of MRGPRs are still classified as orphan receptors since only a few endogenous or synthetic ligands for them are known. As a result, identifying and discovering the ligands like agonists, inverse agonists, allosteric modulators, and antagonists for MRGPRs is critical in order to deorphanize, recognize their associated signaling, and understand their role in pathophysiology. According to reports, amphiphilic molecules like bilirubin and bile acids (BAs) cause cholestatic itch via activating the MRGPRX4 receptor. Consequently, we aimed to investigate whether MRGPRD might also be activated by amphiphilic molecules. Therefore, we performed the counter-screening of cholesterol (CLR) and BAs against selected MRGPRs.

Chapter 5: Mas-related G protein-coupled receptor D senses fluid shear stress and induces the release of IL-6

MRGPRD has emerged as a player in the cardiovascular system, possibly regulating vascular tone and the development of dilated cardiomyopathies. Additionally, in nociceptive neurons, MRGPRD displays mechanosensitivity. Some of the GPCRs, like apelin, β2-AR, GPR68, PAR2, M3, H1R etc., are known to be activated by shear stress, cell shrinkage, and expansions. Given the significance of MRGPRD in mechanosensitivity and the regulation of cytokines, we aimed to determine if shear stress could regulate and activate MRGPRD, leading to the production of IL-6.

Chapter 6: The neglected N-terminus of human Mas-related G protein-coupled receptors: could cysteine protease cathepsin-S (CTSS) activate them?

Despite the fact that MRGPRs are known to regulate nociception, mediate drug-allergy reactions, and play a role in inflammation, the ligands and activation mechanisms that could aid in understanding receptor pathophysiology are scarce. Given that CTSS is expressed by a variety of inflammatory cell types and plays a role in the activation of primate-specific MRGPRX2 and mouse MrgprC11, the CTSS-linked activation mechanism for MRGPRD, MRGPRE, and MRGPRF was evaluated, additionally, aiming to deorphanize MRGPRE and MRGPRF.

Chapter 7: Identification of heteromeric interactions of human Mas-related G protein-coupled receptors

GPCR oligomerization can cause changes in ligand selectivity, unique coupling to signal transducers, and even receptor trafficking. This gives GPCRs a provision to fine-tune receptor-mediated signaling to regulate pathophysiological processes and opens the possibility for potential novel targets for pharmaceutical therapies. Therefore, the heteromerization of human MRGPRD, MRGPRE, and MRGPRF was evaluated, guided by the fact that rat MrgprD and MrgprE have been demonstrated to form heterodimers and regulate MrgprD trafficking and signaling.

Finally, a thorough summary of the research and findings from chapters 3 to 7 is provided in **chapter 8**, along with recommendations for further research.

Chapter 3

Constitutive, basal and β-alanine-mediated activation of the human Mas-related G protein-coupled receptor D induces release of the inflammatory cytokine IL-6 and is dependent on NF-kB signaling

Article Published in IJMS (doi: *https://doi.org/10.3390/ijms222413254)*

Rohit Arora [1,2], Kenny M. Van Theemsche [2], Samuel Van Remoortel [1], Dirk J. Snyders [2], Alain J. Labro [2,3] and Jean-Pierre Timmermans [1]

[1]Laboratory of Cell Biology and Histology, Department of Veterinary Sciences, University of Antwerp, 2610 Wilrijk, Belgium,

[2]Laboratory for Molecular, Cellular and Network Excitability, Department of Biomedical Sciences, University of Antwerp, 2610 Wilrijk, Belgium,

[3]Department of Basic and Applied Medical Sciences, Ghent University, 9000 Ghent, Belgium

Chapter 3 MRGPRD mediated release of IL-6

Abstract

GPCRs have emerged as key players in regulating (patho)physiological processes including inflammation. Members of the Mas-related G protein-coupled receptors (MRGPRs), subfamily of GPCRs are largely expressed by sensory neurons and known to modulate itch and pain. Other members of MRGPRs are also expressed in mast cells, macrophages as well as in cardiomyocytes, linking them to pseudo-allergic drug reactions and to a pivotal role in the cardiovascular system. However, involvement of Mas-related G protein-coupled receptor D (MRGPRD) in the regulation of the inflammatory mediator interleukin-6 (IL-6) has not been demonstrated to date. By stimulating human MRGPRD-expressing HeLa cells with the agonist β-alanine, we observed a release of IL-6. β-alanine-induced signaling through MRGPRD was investigated further by probing downstream signaling effectors along the Gαq/Phospholipase C (PLC), which results in a IkB kinases (IKK)-mediated canonical activation of nuclear factor kappa-B (NF-kB) and stimulation of IL-6 release. In agreement with the MRGPRD-Gαq/PLC/NF-kB/IL-6 pathway, the IL-6 release could be blocked by the Gαq inhibitor (YM-254890), the IKK (IKK-16) complex inhibitors and partly by the PLC inhibitor (U-73122). Additionally, we investigated the constitutive (ligand-independent) and basal activity of MRGPRD and conclude that the observed basal activity of MRGPRD is suggestive of hitherto unrecognized ligands in the fetal bovine serum (FBS) in the culture medium. Consequently, the dynamic range for IL-6 detection as an assay for β-alanine-mediated activation of MRGPRD is substantially increased by culturing the cells in serum free medium before treatment. Overall, the observation that MRGPRD mediates the release of IL-6 in vitro hints at a role as inflammatory mediator and supports the notion that IL-6 can be used as a marker for MRGPRD activation in in vitro drug screening assays.

Keywords: GPCRs, β-alanine; MRGPRD; Constitutive receptor; Gq inhibitor; NF-kB; Interleukin-6

Chapter 3 MRGPRD mediated release of IL-6

3.1 Introduction

The G protein-coupled receptors (GPCRs) are the largest family of membrane receptors that play a key role in cellular signaling and regulate physiological processes. Apart from the classical complement and innate immunity pathways, we now know that GPCRs significantly contribute to acute and systemic chronic inflammations [204]. In the early 2000s, a novel subfamily of rhodopsin-like GPCRs was discovered in rodents and humans, showing a substantial sequence homology with the MAS oncogene and therefore named Mas-related genes (Mrgs) [128, 130]. Initially, these Mrg receptors were thought to be mainly expressed by nociceptive neurons, where they are known to be involved in modulating itch and pain and were therefore also referred to as SNSRs [131, 132, 205]. Later on, the nomenclature Mrgs and SNSRs was replaced by Mas-related G protein-coupled receptors (MRGPRs) [118]. Recent studies demonstrated that MRGPRs are also involved in hypersensitivity [206, 207] and reported the presence of MRGPRs in other cell and tissue types, such as mast cells, macrophages and cardiovascular tissue [146, 150, 153, 154, 156, 157, 186, 208]. Several peptides and a few small molecules have been proposed as ligands for MRGPRs [123, 131, 132, 149]. However, many of these ligands activate multiple receptors and share a significant physiological overlap with other rhodopsin family GPCRs, causing the majority of MRGPRs to still be classified as orphan receptors [118]. As such, the pharmacological characterization of and insight into the physiological roles of the majority of MRGPRs remain elusive.

One member of the MRGPR family, MRGPRD, is predominantly expressed in isolectin-B4- positive (IB4+), small non-myelinated sensory neurons in dorsal root ganglia (DRG) and trigeminal ganglia (TG) of animals [128, 135]. The β-alanine-activated MRGPRD inhibits KCNQ/M K^+ currents in DRG neuronal cultures, which points to MRGPRD involvement in modulating neuronal excitability [209]. Similarly, the activation of rat MrgprD in *Xenopus* oocytes by β-alanine demonstrated the functional link between MrgprD and calcium-activated chloride channels, which was mediated via the Gq/PLC/IP_3/Ca^{2+} pathway [210]. In addition, activation of the MRGPRD receptor by β-alanine also has a regulatory impact on the transient receptor potential cation channel-A1 (TRPA1) and induces histamine-independent neuropathic itch and pain [211]. Recent study suggest that allantoin, also known as 5-ureidohydantoin or glyoxyldiureide, induces pruritus by activating MRGPRD in chronic kidney disease [212]. Moreover, in a recent publication, 5-oxoETE, a polyunsaturated fatty acid (PUFA) metabolite, has been shown to induce somatic and visceral hyperalgesia without inflammation via the MRGPRD pathway, in this way triggering noxious symptoms in constipated irritable

bowel syndrome (IBS) patients [184]. Altogether, MRGPRD seems to be involved in regulating nociception in neurons [213].

Additionally, MRGPRD has also been linked with the renin-angiotensin system (RAS) cascade of the cardiovascular system. It was found that angiotensin II (Ang II), angiotensin (1-7) and a derivative, alamandine, can activate MRGPRD and regulate signaling by Gαs/cAMP/PKA pathway [192, 214, 215]. Angiotensin II (Ang II) induces upregulation of cAMP, triggers phosphorylation of p-38 and induces fibrosis of rat vascular smooth muscle cells [216]. Intriguingly, these effects are mitigated by alamandine, which attenuates Ang II-associated hypertension and cardiac remodeling. Alamandine-activated MRGPRD also induces NO release, suggesting that MRGPRD could also be involved in cardioprotection, controlling vasodilation and fibrosis in the heart [217, 218]. Genetic ablation of MRGPRD in mice led to a reduced thermal and mechanical nociception ability of sensory neurons and caused dilated cardiomyopathy [139, 186].

MRGPRD involvement is not limited to neuron and cardiovascular tissues; high expression levels of MRGPRD have also been reported in lung cancer tissues, where it promotes cell proliferation and tumorigenicity [185]. Also, L-βAIBA, a structural analog of β-alanine and a secretory metabolite of muscle cells, promotes the survival of MRGPRD-expressing osteocytes by maintaining mitochondrial integrity, hence improving bone formation [189].

Several lines of evidence now indicate that MRGPR-mediated signaling is linked to increased production and release of inflammatory cytokines. Cells expressing MRGPRX1, another member of the MRGPR family, have been shown to release the pro-inflammatory cytokine IL-6 upon activation of the receptor through cleavage of its N-terminus by cysteine protease Der p1 [151]. In another study, alamandine-activated MRGPRD reduced the levels of the pro-inflammatory cytokines tumor necrosis factor-alpha (TNF-α) and interleukin-1 beta (IL-1β) in lipopolysaccharide (LPS)-stimulated macrophages [154]. Furthermore, a recent study hinted at MRGPRD involvement in LPS-induced inflammatory pain and activation of the NF-kB signaling pathway mediated via IkB kinases (IKKα and IKKβ) [157]. Therefore, the MRGPRD-mediated activation of NF-kB as well as the release of inflammatory cytokines (TNF-α and IL-1β), largely suggests a much broader role of MRGPRs in inflammation and immune biology than assumed so far. Given the lack of experimental proof that agonist-activated MRGPRD could mediate the release of pleiotropic cytokine IL-6, in the present study, the release of IL-6 from MRGPRD-expressing cells was analyzed.

3.2 Materials and Methods

3.2.1 Materials

DNA oligonucleotides were obtained from IDT (Leuven, Belgium). Plasmid preparations were performed using either the plasmid miniprep or maxiprep kit from Macherey-Nagel (Düren, Germany). The PCR/gel clean-up kit used to purify PCR-amplified products was from Macherey-Nagel. Agar, LB broth (high salt), SOC medium, ampicillin and kanamycin were purchased from Sigma-Aldrich (Merck; Kenilworth, NJ, USA). Restriction enzymes and T4 DNA ligase were acquired from New England Biolabs (Ipswich, MA, USA). XL2-Blue ultracompetent cells used for transformation were purchased from Stratagene (San Diego, CA, USA). Pfu DNA polymerase was obtained from Promega (Madison, WI, USA). Human MRGPRD cDNA (pENTR223.1-MRGPRD; Cat# HsCD00080297) was obtained from the DNASU [219] plasmid repository (Tempe, AZ, USA), plasmid pcDNA3.1(+)-PAR2 was a generous gift from Dr. Rithwik Ramachandran, plasmid p-NCS-Antares (Cat# 74279) coding NanoLuc (NLuc) was obtained from Addgene (Cambridge, MA, USA), and pCMV-ECFP-N1 (plasmid-cytomegalovirus promoter-Enhanced cyan fluorescent protein-N1) was from Clontech (Palo Alto, CA, USA). Dulbecco's Modified Eagle Medium (DMEM) (Cat# 41966029), FBS (Cat# 10270-106), penicillin-streptomycin, and Dulbecco's phosphate-buffered saline (DPBS; Cat# 14190169) were purchased from Gibco (Waltham, MA, USA). 100 mm cell culture dishes (CELLSTAR; Cat# 664160), 6 well cell culture plates (CELLSTAR; Cat# 657160) and 96 well black well plate (CELLSTAR; Cat# 655090) were purchased from Greiner Bio-One (Frickenhausen, Germany). β-alanine (Cat# 05160) was purchased from Sigma-Aldrich. Human PAR2 agonist (SLIGKV-NH_2; Cat# 3010) was obtained from Tocris (Abingdon, UK). The PLC inhibitor (U 73122; Cat# 1268) was purchased from Tocris, the Gαq inhibitor YM 254890 (Cat# 10-1590-0100) from Focus Biomolecules (Plymouth, PA, USA) and the IKK complex inhibitor (IKK-16; Cat# S2882) from Selleck Chemicals GmbH (Germany). Quantikine ELISA human IL-6 (Cat# D6050) was purchased from R&D Systems (Minneapolis, MN, USA). IP-One-Gq Homogeneous Time Resolved Fluorescence (HTRF), phospho-NF-kB (Ser536) cellular HTRF, Total NF-kB cellular HTRF kits and HTRF 96 well low volume white plate (Cat# 66PL96025) were acquired from Cisbio (Codolet, France). The Bradford assay kit (Cat# 23246), pierce IP lysis buffer (Cat# 87787), halt protease inhibitor cocktail (Cat# 87786), Geneticin (G418 Sulphate; Cat# 10131027) and Lipofectamine 2000 (Cat# 11668019) were obtained from Thermo Fisher Scientific (Waltham, MA, USA). The antibodies used in this study were: anti-HA rat high affinity IgG (Roche, Cat# 11867432; Sigma-Aldrich), anti-rat IgG conjugated with horseradish peroxidase (HRP) (Cat #9037; Sigma-Aldrich) and a β-actin rabbit monoclonal antibody (Cat# 4970S; Cell Signaling Technology), anti-Rabbit IgG conjugated to HRP (Cat# NBP1-75283; Novus Biologicals). NuPAGE novex 4-12% Bis-Tris gels (Cat# NP0321), NuPAGE

MOPS running buffer (Cat# NP001), NuPAGE transfer buffer (Cat# NP00061), NuPAGE LDS sample loading buffer (Cat# NP007), Restore Plus western blot stripping buffer (Cat# 46430), Pierce enhanced chemiluminescence plus western blotting substrate (Cat# 32132) and BenchMark pre-stained protein ladder (Cat# 10748010) were purchased from Thermo Fisher Scientific. Amersham Hybond-P-polyvinylidene difluoride (PVDF) membrane (Cat# RPN303F) was obtained from GE Healthcare (Boston, MA, USA).

3.2.2 Plasmid Preparation

Human MRGPRD cDNA was Polymerase chain reaction (PCR)-amplified from pENTR223.1-MRGPRD using Pfu DNA polymerase. The amplified PCR fragment was digested with the restriction enzymes HindIII/BamHI and ligated by T4 DNA ligase in pCMV-ECFP-N1 to generate the pCMV-MRGPRD-ECFP-N1 plasmid. A stop codon was introduced at the C-terminus of MRGPRD by site-directed mutagenesis to generate the pCMV-MRGPRD plasmid. Subsequently, MRGPRD was genetically tagged at its C-terminus with a human influenza hemagglutinin (HA; YPYDVPDYA) just before the stop codon to generate the pCMV-MRGPRD-HA plasmid. Similarly, human Protease-activated receptor 2 (PAR2) cDNA was PCR-amplified from pcDNA3.1(+)-PAR2 and inserted in-frame in pCMV-MRGPRD-HA (replacing MRGPRD) to generate pCMV-PAR2-HA. A blank/empty vector was generated by first introducing a XhoI restriction enzyme (RE) recognition site into pCMV-EYFP (enhanced yellow fluorescent protein)-N1 at the C-terminus end of EYFP to generate pCMV-EYFP-Xho1-N1. Subsequently, the pCMV-EYFP-XhoI-N1 plasmid was digested with NheI/XhoI and an annealed oligonucleotide was inserted to generate the pCMV-GS (pCMV-MCS-GS-MCS-GS-MCS) plasmid, having multiple cloning sites connected by a flexible linker of glycine and serine residues (2xGGGGS). The NLuc gene sequence without start codon was PCR amplified from p-NCS-Antares and inserted in-frame between BamHI/XhoI to generate pCMV-GS-NLuc plasmid. The human MRGPRD cDNA was PCR-amplified from the pCMV-MRGPRD-HA plasmid and inserted in-frame between EcoRI/SalI sites to generate the pCMV-MRGPRD-NLuc plasmid. All plasmids were verified by Sanger sequencing at the VIB Genomic core (VIB-Centre for Molecular Neurology, University of Antwerp). Plasmid are listed in Appendix II.

3.2.3 Cell culture, transfections, treatments, and IL-6 detection

HeLa cells were cultured in 100 mm dishes in a humidified incubator at 37°C with 5% CO_2 using DMEM supplemented with 10% FBS and 1% penicillin-streptomycin. For the ELISA experiments, HeLa cells were collected by trypsinization and $2.5x10^5$ cells/well were seeded in a 6 well cell culture plate. Sixteen hours post-seeding, medium was removed, and cells were washed once with 1 ml phosphate-buffered saline (PBS). Cells

were transfected with 2 µg plasmid cDNA using Lipofectamine 2000 as per the manufacturer's instructions. After 4 h, transfection medium was replaced with 2 ml DMEM supplemented with 10% FBS and 1% penicillin-streptomycin and the plates were returned to a incubator. Whenever necessary to obtain 2 µg of plasmid/well for transfection, the remaining amount was compensated with the pCMV-GS (empty) plasmid during transfection.

Twenty-four hours post-transfection, cells supernatant medium was removed. At every medium removal, cells were washed once with 1 ml PBS. Experiment timeline and treatment conditions are shown in each figure where appropriate. Two milliliters of DMEM with or without 10% FBS was added to each well containing the desired concentration of β-alanine, SLIGKV-NH_2, or FBS. The plates were returned to the incubator for another 24h before sample collection.

After the desired incubation, cell supernatant medium was collected in a 2 ml microcentrifuge tube and spun at 1,000 g for 5 min at 4°C to pellet down debris. Without disturbing the pellet, the supernatant medium was transferred into a fresh microcentrifuge tube and stored at -80°C until assayed by ELISA. For IL-6 assessment the frozen supernatant medium was thawed on ice and samples were diluted (1:200) in assay diluent buffer and IL-6 estimation was performed using an IL-6 ELISA kit as per the manufacturer's instructions. For protein sample collection, cells were first washed with 1 ml of PBS followed by addition of 300-500 µl IP-lysis buffer (supplemented with 1% protease inhibitor) to each well. Subsequently, the plates were maintained on ice for 20 min with intermittent shaking every 5 min. Lysate was collected in a microcentrifuge tube, spun at 13,000 g for 10 min at 4°C; the resulting protein supernatant was transferred into a new microcentrifuge tube and stored at -80°C for further analysis with a Bradford assay, as per the vendor's instructions. The calculated IL-6 (ng/ml) concentrations from collected supernatant medium were normalized to the protein concentrations (mg/ml) from the respective well. IL-6 release is represented in ng/mg.

3.2.4 Immunoblotting

The protein samples collected as described in section 3.3 were utilized for immunoblotting. Protein estimation was performed using Bradford reagent. Samples were prepared in IP-lysis buffer, supplemented with 5 µl of 4x NuPAGE LDS sample loading buffer and heated at 95°C for 3 min. Protein samples (20 µg) were resolved on a NuPAGE 4-12% Bis-Tris gel using NuPAGE MOPS SDS running buffer (200V for 50 min). Proteins were transferred onto PVDF membrane by wet blotting using NuPAGE transfer buffer (100V for 1 h). The blots were incubated overnight in blocking buffer (5% skimmed milk dissolved in PBS with 0.1% Tween 20) at 4°C and subsequently probed

with anti-HA rat IgG (1:1,000 in blocking buffer) for 1 h at room temperature (RT), followed by incubation with anti-rat IgG conjugated with HRP (1:2,000 in blocking buffer) for 1 h at RT. Chemiluminescence signals were detected using ECL plus substrate in an Amersham Imager 600. Subsequently, the blots were stripped using 5 ml restore plus western blot stripping buffer, washed once with PBS, and incubated overnight in blocking buffer at 4°C. On the next day, the blots were probed with anti-β-actin rabbit monoclonal antibody (1:2,000 in blocking buffer) for 1 h at RT, followed by incubation with anti-rabbit IgG conjugated to HRP (1:10,000 in blocking buffer) for 1 h at RT and the chemiluminescence signals were recorded again using ECL plus substrate in an Amersham Imager 600.

3.2.5 MRGPRD stable cell preparation and IL-6 inhibition

MRGPRD-NLuc stable cells were developed by transfecting pCMV-MRGPRD-NLuc plasmid in HeLa cells, followed by antibiotic selection of stable clones using Geneticin (1000 µg/ml).

HeLa (mock) and HeLa cells stably expressing fusion protein MRGPRD-NLuc were collected by trypsinization and $2.5x10^5$ cells/well were seeded in a 6 well cell culture plate. At 16 h post-seeding, the medium was removed, and the cells were washed once with 1 ml PBS. Subsequently, the medium was replaced by 2 ml DMEM (overnight starvation) and the plates were returned to incubator (37°C with 5% CO_2). After 24 h of serum starvation, the medium was replaced again by either with 2ml DMEM containing vehicle control (percentage of dimethyl sulfoxide; DMSO was 0.1%) or 2 ml DMEM containing the desired concentration of inhibitor (inhibitor dissolved in DMSO; 0.1%), plates were kept in incubator for 1 h. Afterwards, the cells were stimulated with vehicle (percentage of milli-Q was 0.2%) or β-alanine (dissolved in milli-Q; 0.2%). The final concentration of β-alanine was 100 µM. The plates were then returned to the incubator for another 8 h before sample collection (supernatant and protein collection, as described in section 3.3). The collected supernatant samples were thawed on ice, diluted (1:5) and IL-6 estimation was performed using the IL-6 kit as per the manufacturer's instruction. Protein estimation was done using Bradford reagent. IL-6 concentration was normalized to protein concentration, calculated to ng/mg. The relative fold change (ΔF) was derived by normalizing IL-6 (ng/mg) to that of its respective controls i.e., vehicle-treated (DMSO) or inhibitor-treated (inhibitor dissolved in DMSO, without β-alanine). The fold-change (ΔF) was further normalized to the ΔF of β-alanine-stimulated MRGPRD-expressing cells (i.e., ΔFmax) and expressed as percentage.

3.2.6 NF-kB detection and inhibition assay

HeLa (mock) and HeLa cells stably expressing fusion protein MRGPRD-NLuc were collected by trypsinization and $3x10^4$ cells/well were seeded in 96 black well plates. At 24 h post seeding, the medium was removed and replaced with 100 µl DMEM (overnight serum starvation). The next day, i.e. 48 h from seeding, the medium was replaced again with either with 50 µl DMEM containing vehicle control (percentage of DMSO was 0.1%) or 50 µl DMEM containing desired concentration of inhibitor (dissolved in DMSO; 0.1%) for 1h before stimulation with 50 µl DMEM containing vehicle control (DMSO; 0.1%) or inhibitor (dissolved in DMSO; 0.1%) with vehicle (percentage of milli-Q was 0.1%) or β-alanine (dissolved in milli-Q; 0.1%). The final concentration of β-alanine was 1 mM/well. Plates were then returned to the incubator (37°C with 5% CO_2) for another 10 min. After the desired treatment, the medium was removed and 50 µl of lysis buffer supplemented with blocking buffer was added to the wells. The plates were kept on a shaker at 100 rpm for 30 min. Then, 16 µl cell lysate was transferred to a HTRF 96-well low volume white plate (Cisbio) for phospho-NF-kB (Ser 536) and total NF-kB estimation using Cisbio HTRF kits. Briefly, 4 µl of pre-mixed donor and acceptor antibodies were added to 16 µl of cell lysate and incubated overnight at 25°C. On the next day, plates were read using an EnVision multimode plate reader. The calculated phospho-NF-kB HTRF ratios were normalized to that of total NF-kB HTRF ratios. The relative fold change (ΔF) was obtained by normalizing phospho-NF-kB/total NF-kB to that of its respective control, i.e., vehicle-treated (DMSO) or inhibitor-treated. The fold-change (ΔF) was further normalized to the ΔF of β-alanine-stimulated MRGPRD-expressing cells (i.e., ΔFmax) and expressed as percentages.

3.2.7 Data and Statistical Analysis

Data analysis was performed using Microsoft Excel and GraphPad Prism 6. The concentration-effect curve and graphs were generated using GraphPad Prism 6. The EC_{50} values were obtained by fitting the concentration-effect curve with a Hill function. To determine the dynamic range, the limit was set to EC_{10} and EC_{90}. Hereto, the EC_{10} and EC_{90} were calculated using equation 1, whereby F was set to either 10 or 90, respectively. All values are represented as the mean ± s.e.m with 'n' the number of experiments. Statistical significance was determined using one-way analysis of variance (ANOVA) and Sidak's post hoc test was applied for multiple comparisons. P values: *p≤0.05, **p≤0.01, ***p≤0.001 and ****p≤0.0001 were considered significant and p>0.05 was considered non-significant (ns).

$$\boldsymbol{LogEC50 = LogECF - \left(\frac{1}{Hillslope}\right) * Log\left(\frac{F}{100 - F}\right)} \quad (1)$$

3.3 Results

3.3.1 β-Alanine-Mediated Activation of MRGPRD Induces Release of IL-6

MRGPRD can be activated by β-alanine [183, 190], a derivative of degraded carnosine. Carnosine (β-alanyl-L-histidine) is a dipeptide molecule that is largely stored in mammalian skeletal muscles and, to some extent, in brain neurons and heart muscles [220, 221]. Carnosine, acts as a physiological buffer and scavenges reactive oxygen species to maintain cell homeostasis [222]. Carnosinase breaks down carnosine into β-alanine and L-histidine and elevates the concentration of β-alanine in plasma.

β-alanine-activated MRGPRD expressing cells predominantly upregulate inositol phosphates (IP_3/IP_1), presumably by the activation of the G protein 'Gαq', which further activates phospholipase C (PLC) that hydrolyses phosphatidylinositol 4,5-biphosphate (PIP_2) to generate diacylglycerol (DAG) and inositol 1,4,5-triphosphate (IP_3). In addition, up to a limited extent, the stimulation of MRGPRD with β-alanine also inhibits adenylyl cyclase activity and reduces cAMP production, which hence is most likely mediated by the G protein 'Gαi' [183, 209]. However, the role of the MRGPRD-activated 'Gαq' signaling cascade in regulating cytokine release has not been demonstrated. Here, we sought to determine whether β-alanine-mediated activation of MRGPRD triggers the release of IL-6. To this end, MRGPRD expressing HeLa cells were treated either with β-alanine (100 µM) or vehicle control. A significant, nearly 7-fold higher release of IL-6 was observed from MRGPRD-expressing cells treated with β-alanine, compared to β-alanine-treated control cells (transfected with empty vector; pCMV-GS). In addition, IL-6 levels of non-treated MRGPRD-expressing cells were nearly 4-fold higher than those of non-treated control cells (Figure 3.1). The difference in IL-6 release between β-alanine-treated and non-treated MRGPRD-expressing cells was 1.6-fold, which was found to be non-significant. These findings are indicative of high basal activity of MRGPRD.

Evidence from various reports suggests that IL-6 cytokines release is not limited to HeLa cells. Taking this into account, we further tested whether β-alanine mediated activation of MRGPRD expressed in another cell type, i.e., HT1080, could also induce IL-6 release [223]. To this end, HT1080 cells expressing MRGPRD were treated with either β-alanine (100 µM) or vehicle control. IL-6 release was observed from MRGPRD-expressing HT1080 cells treated with β-alanine, compared to β-alanine-treated control cells (Supplementary figure S3.1).

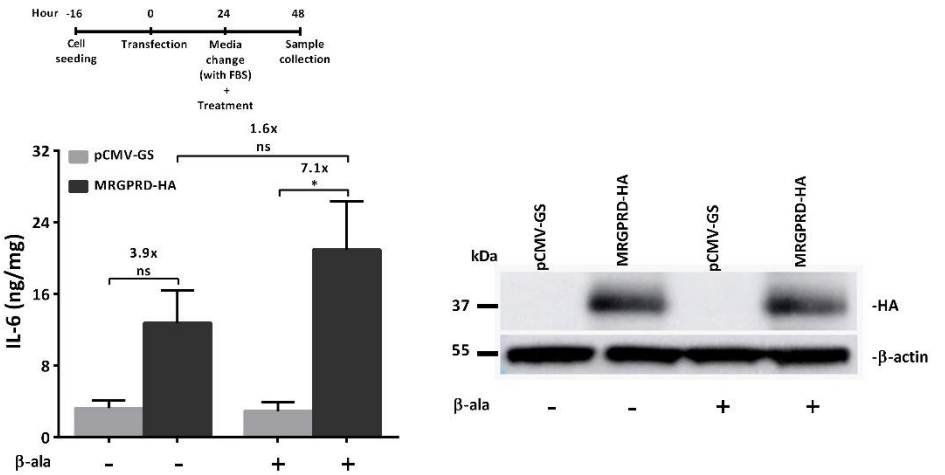

Figure 3.1. Activation of MRGPRD mediates IL-6 release. HeLa cells transiently expressing empty vector (pCMV-GS) or MRGPRD-HA were stimulated with either vehicle control or β-alanine (100 µM; final concentration/well). The normalized IL-6 release is represented in ng/mg. β-alanine- or vehicle-treated cells expressing MRGPRD released high and intermittent levels of IL-6, respectively. Whereas vehicle- or β-alanine-treated cells expressing the empty vector did not release significant amounts of IL-6 (n=3). On the right, a representative western blot of whole cell lysates from HeLa cells transiently transfected with either empty vector (pCMV-GS) or MRGPRD-HA plasmids are displayed. Expression of the MRGPRD-HA receptor (~37 kDa) was observed in both vehicle and β-alanine (100 µM)-treated MRGPRD-transfected cells, whereas cells transfected with the empty vector showed no expression (i.e., absence of a protein band of ~ 37 kDa).

3.3.2 Demonstration of Basal Activity of MRGPRD and Assay Optimization to Maximize the IL-6 Detection Window

Many GPCRs display elevated basal activity under physiological conditions, which poses challenges in terms of understanding the regulatory mechanisms of receptors and hinders drug discoveries for therapeutic purposes [195, 224, 225]. Our data indicate that MRGPRD was basally active and induced IL-6 release (Figure 3.1).

To further elucidate the IL-6 release from non-treated MRGPRD-expressing cells (Figure 3.1), i.e., basal activity of MRGPRD, we transiently transfected HeLa cells with gradually increasing amounts of plasmid cDNA per well. Our data revealed a MRGPRD expression-dependent release of IL-6 (Figure 3.2 A), which confirms the high basal activity of MRGPRD. Further stimulation of the MRGPRD expressing HeLa cells with the agonist β-alanine did not show a significant increase in IL-6 release above the basal levels. As a control, human PAR2 was utilized, to demonstrate that, in contrast to MRGPRD-

transfected cells, PAR2-transfected cells did not show a PAR2 expression-dependent release of IL-6 (Figure 3.2 B). Since it is known that the PAR2-activating peptide SLIGKV-NH_2 induces the release of IL-6 from PAR2-expressing cells [151], our experimental control consisted in treating PAR2-expressing cells with the agonist SLIGKV-NH_2, which clearly shows the PAR2 expression-dependent release of IL-6 into the medium (Figure 3.2 B).

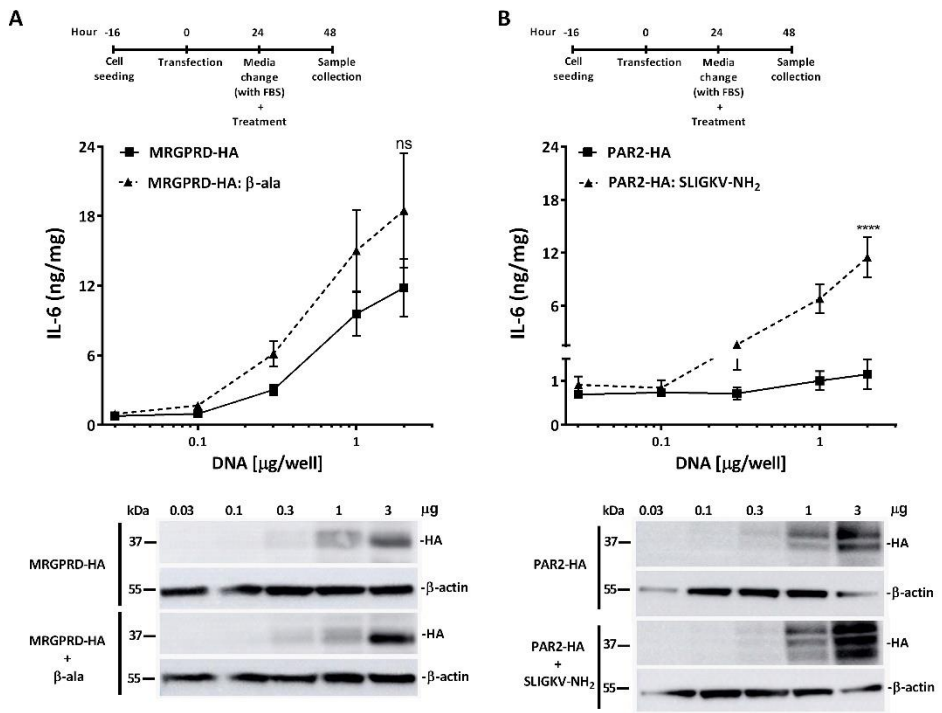

Figure 3.2. Basal activity of MRGPRD. HeLa cells expressing increasing concentration of MRGPRD-HA and PAR2-HA receptors (transfected with 0.03, 0.1, 0.3, 1 and 2 μg of cDNAs per well), when treated with vehicle control only, the MRGPRD-transfected cells did show an MRGPRD expression-dependent release of IL-6 **(A)** while the PAR2-transfected cells did not show PAR2 expression-dependent release of IL-6 **(B)**. Furthermore, when cells expressing increasing concentrations of MRGPRD-HA or PAR2-HA were treated with their respective agonists, β-alanine (100 μM) or the PAR2-agonist SLIGKV-NH_2 (100 μM), a receptor concentration-dependent gradual IL-6 release was noticed **(A, B)**. The release of IL-6 from vehicle-treated MRGPRD-HA cells points to a basal activity of the receptor (n=3). Below the graphs, representative western blot analysis of whole cell lysates from stimulated and non-stimulated HeLa cells transiently expressing increasing concentrations of MRGPRD-HA and PAR2-HA are displayed.

Having observed that MRGPRD displays high basal activity and that the effect of β-alanine stimulation on MRGPRD-expressing cells under normal physiological conditions

(i.e. in the presence of FBS) was marginal as compared to non-treated MRGPRD, we first investigated whether this activity originated from traces of unrecognized MRGPRD ligand in the FBS, which constitutes 10% of the cell culture medium [183]. Traces of ligands in FBS may keep the receptors engaged in an active state of signaling. To address this, we modified the stimulation protocol and exchanged the cell culture medium for medium without FBS after transfection. We found that MRGPRD expression was impaired when cells were cultured immediately in medium without FBS upon transfection. Therefore, in an adapted protocol we allowed the cells to express MRGPRD for 24 h before switching to medium without FBS. The first adapted protocol consisted of stimulating the MRGPRD-expressing cells with β-alanine at the time of switching to medium without FBS, i.e., 24 h post-transfection, and collecting samples for IL-6 analysis 24 h later, i.e., 48 h post-transfection (Figure 3.3 A). The fold change observed between vehicle-treated and β-alanine-treated MRGPRD-expressing cells was approximately a 2-fold, which was significantly higher as compared to the protocol using medium with FBS (displayed in Figure 3.1). Since the IL-6 readout for MRGPRD activation is very downstream of the signaling cascade, the cells most likely need to be cultured for a longer period in medium without FBS in order to reduce the high basal activity of MRGPRD. To test this, the protocol was adjusted a second time, and the cells were kept in medium without FBS (starvation) for 24 h prior to being stimulated with β-alanine. As such, the medium was replaced by medium without FBS at 24 h post-transfection and the cells were cultured for another 24 h. Subsequently, the medium was refreshed by medium without FBS and β-alanine was added. Following this protocol, stimulation of the cells was initiated at 48 h post-transfection. After another 24 h of incubation, i.e., 72 h post-transfection, the samples were collected, and IL-6 analysis was performed (Figure 3.3 B). Interestingly, the fold change observed between only vehicle-treated and β-alanine-treated MRGPRD-expressing cells increased to approximately a 5-fold, which is significantly higher and offers a good range of detection for IL-6 as an assay for activation of MRGPRD. Additionally, comparison of the two protocols revealed that the release of IL-6 from non-treated cells expressing MRGPRD was reduced by a 2.4-fold when culturing the cells for a longer period in medium without FBS (Figure 3.3 A vs. 3.3 B). These data indicate that basal activity of MRGPRD can indeed be attributed to unidentified ligands present in FBS, which is why we decided to use the adapted protocol for further experiments.

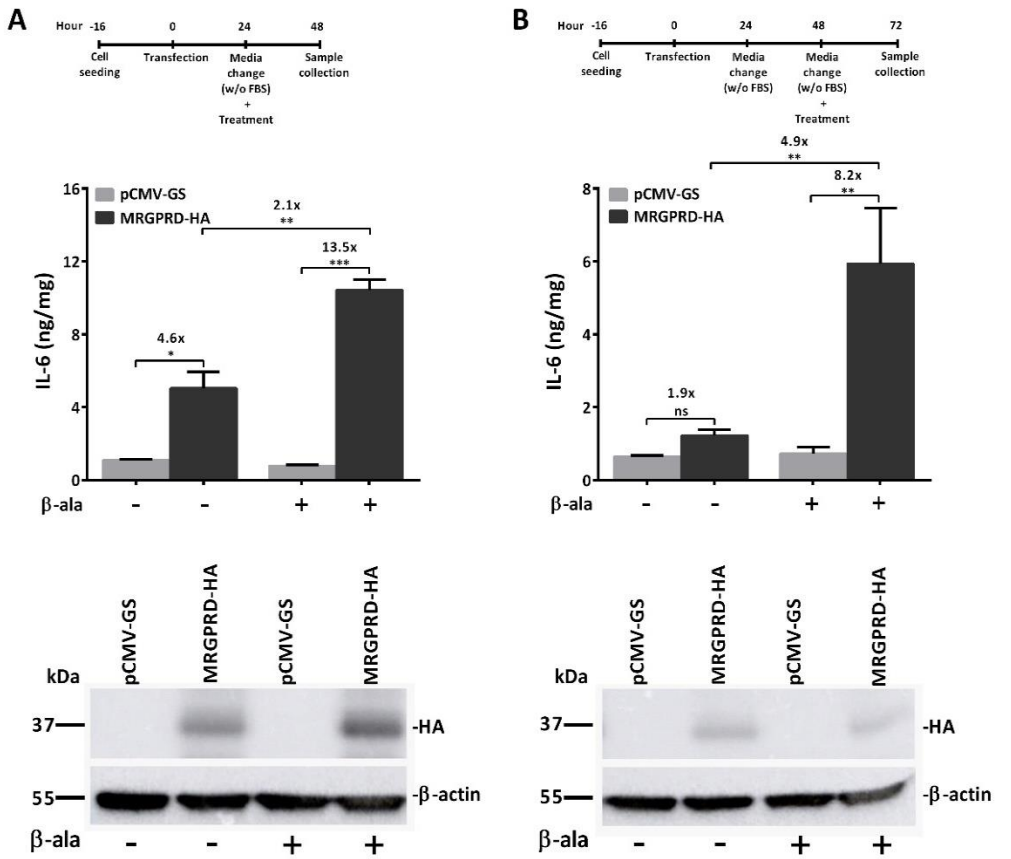

Figure 3.3. IL-6 assay optimization. To achieve a high detection window for the IL-6 assay, the experiment timeline was optimized. **(A)** At 24 h post-transfection, medium was replaced by FBS-free medium, and cells were treated with vehicle or β-alanine (100 µM). At 24 h post-treatment, i.e., at 48 h post-transfection, samples were collected for IL-6 detection. IL-6 levels from β-alanine-treated MRGPRD-HA cells were 2-fold higher when compared to those from vehicle-treated MRGPRD cells. **(B)** Similarly, at 24 h post-transfection, medium was replaced by FBS-free medium for another 24 h and at 48 h the medium was once again replaced by FBS-free medium, and cells were treated with vehicle or β-alanine (100 µM). Samples were collected for IL-6 detection after 24 h of treatment, i.e., at 72 h post-transfection. IL-6 levels from β-alanine-treated MRGPRD cells were ~5-fold higher when compared to those from only vehicle-treated MRGPRD cells, which is substantially higher than for the protocol used in **(A)**. The cells expressing empty vector (pCMV-GS), treated with β-alanine or vehicle, did not show IL-6 release above the basal level **(A, B)** (n=3). Below the graph**,** representative western blot of cell lysates from HeLa cells transiently transfected with empty vector or MRGPRD-HA plasmid, showing receptor expression in vehicle or β-alanine (100 µM)-treated MRGPRD transfected cells subjected to the experiment timeline protocols illustrated in **(A)** and **(B)**, respectively.

3.3.3 FBS is Associated with Activation of MRGPRD and Induces Release of IL-6

Having optimized the assay, we next investigated the agonistic effect of FBS on MRGPRD using the above-described protocol (Figure 3.3 B). The HeLa cells expressing MRGPRD were treated with 10%, 3% or 1% FBS-containing DMEM and FBS concentration-dependent increase in IL-6 release was observed. The MRGPRD cells stimulated with 10% and 3% FBS displayed a significant, 2.4-fold increase in IL-6 release compared to control cells (pCMV-GS transfected cells) treated with similar percentages of FBS (Figure 3.4). Cells expressing MRGPRD and treated with 1% FBS, as expected, exhibited lower IL-6 levels as compared to cells cultured in 10% and 3% FBS medium. Compared to pCMV-GS transfected control cells cultured in 1% FBS medium, the MRGPRD-expressing cells displayed a 2.1-fold higher IL-6 production. Moreover, the MRGPRD-expressing cells incubated without (0%) FBS released the lowest amount of IL-6, which was still a 1.5-fold higher than that of its respective control cells. Together these findings indicate that, in addition to being activated by FBS, MRGPRD also displays constitutive activity, which is in agreement with a recent publication [195].

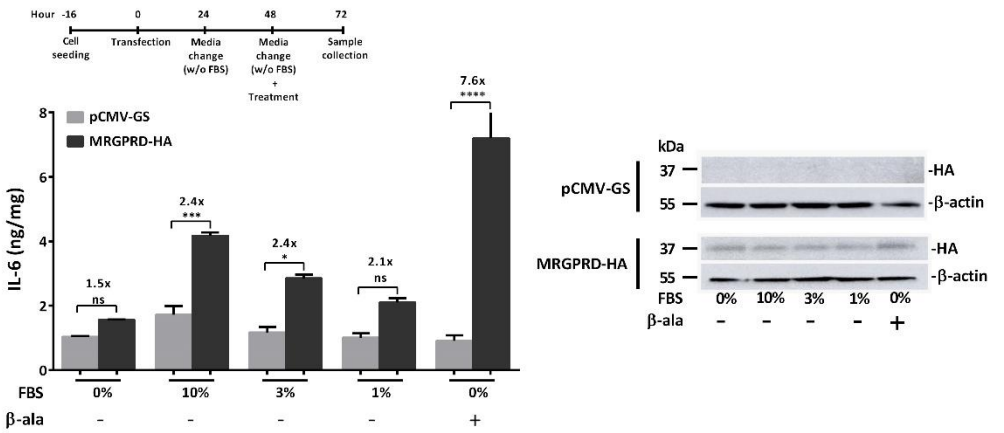

Figure 3.4. Agonistic effect of FBS and constitutive activity of MRGPRD. HeLa cells expressing MRGPRD-HA or empty vector (pCMV-GS) were challenged with medium containing 10%, 3 %, 1% FBS and FBS-free (0%) medium. Significantly increased IL-6 levels were observed with increasing concentration of FBS in cells expressing MRGPRD-HA as compared to control cells (empty vector). β-alanine (100 µM)-treated MRGPRD-HA cells served as positive control for this experiment. β-alanine- or vehicle-treated cells expressing the empty vector (pCMV-GS) did not show IL-6 release above the basal level (n=3). On the left, representative western blot of whole cell lysates from HeLa cells transiently transfected with empty vector or MRGPRD-HA plasmids, treated with vehicle or β-alanine (100 µM) under FBS (10%, 3% and 1%) or FBS-free (0%) conditions.

Having demonstrated that the high basal activity of MRGPRD is due to unidentified ligands or modulators present in FBS (Figure 3.4), we next examined whether presence or absence of FBS affects the potency of β-alanine and alters the concentration-effect curve. In all published reports of β-alanine concentration-effect curves and EC_{50} values, FBS containing medium was used to culture cells and/or the cells were starved in medium without FBS for only 1 h [190, 191, 215]. Therefore, we used our optimized timeline protocol described in Figure 3.3 B to define the EC_{50} of β-alanine for IL-6 release. Stimulation of HeLa cells expressing MRGPRD with different concentrations of β-alanine in the presence (Figure 3.5 A) or absence (Figure 3.5 B) of FBS yielded an EC_{50} of 151 ± 14 µM (n = 3) and 125 ± 10 µM (n = 4), respectively. Furthermore, no IL-6 release was observed in cells expressing empty vector (pCMV-GS) when treated with β-alanine in the presence or absence of FBS. Although MRGPRD exhibited a higher basal activity in FBS conditions compared to the FBS-free condition, the obtained EC_{50} values were comparable. However, comparison of the dynamic range by limiting the output to 10% (EC_{10}) and 90% (EC_{90}) of the maximal response revealed a higher dynamic range for IL-6 detection in FBS-free conditions. The dynamic range detected for IL-6 as an assay for MRGPRD activation with FBS and in the FBS-free condition was 2.9 and 4.6, respectively (Figure 3.5 C and 3.5 D).

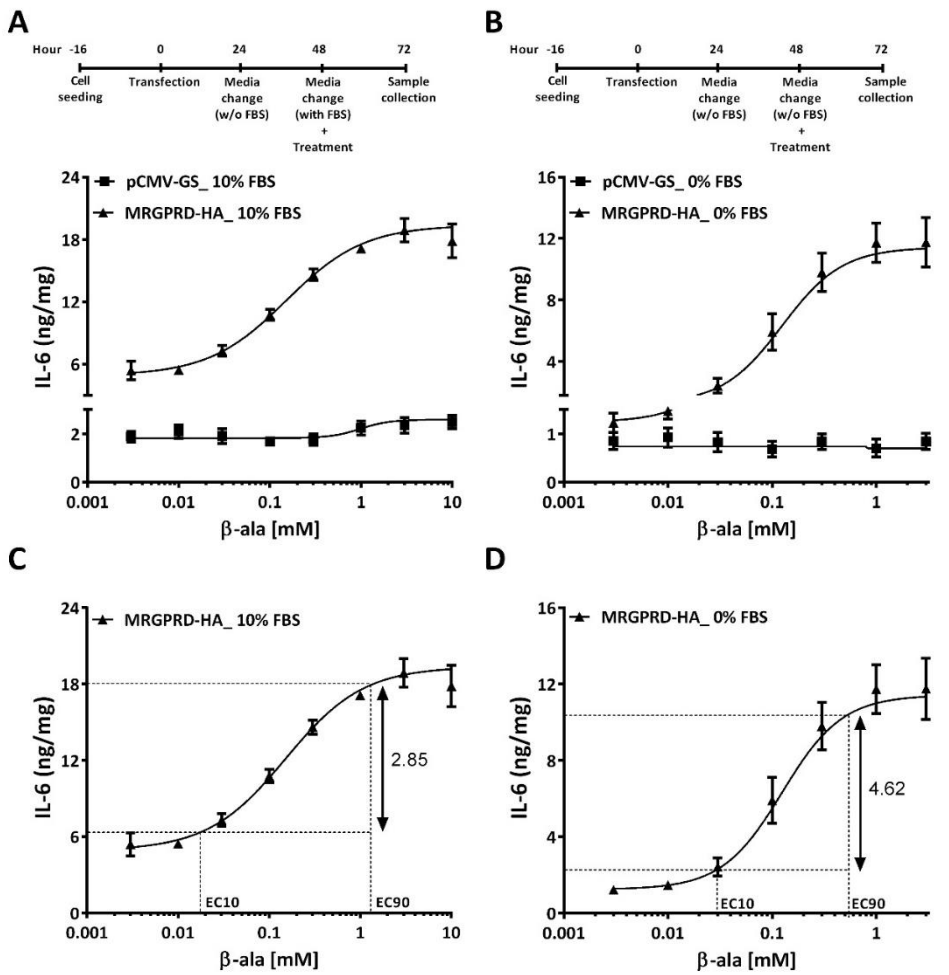

Figure 3.5. Concentration-effect curves of β-alanine obtained in the presence or absence of FBS. HeLa cells expressing the empty vector (pCMV-GS) and MRGPRD-HA were treated with increasing concentrations of β-alanine in the absence or presence of FBS. Cells expressing MRGPRD induced the release of IL-6 in a concentration-dependent manner when treated with β-alanine with FBS **(A)** or without FBS **(B)**. Higher basal activity of MRGPRD was observed in cells treated under FBS conditions as compared to non-FBS conditions. No significant IL-6 release was observed from cells expressing the empty vector (pCMV-GS) **(A, B**). The dynamic range obtained when cells were treated in FBS **(C)** conditions was 2.85, whereas it increased to 4.62 when cells were treated in FBS-free conditions **(D)**. All data represented in this figure originate from at least (n=3) experiments.

3.3.4 Inhibiting MRGPRD-Gαq/PLC/IKK/NF-kB Signaling Impedes the Release of IL-6

β-alanine-activated MRGPRD predominantly couples to Gαq protein, which upon activation stimulates PLC. Activated PLC further catalyzes the hydrolysis of PIP_2 into IP_3

and DAG. IP_3 is, subsequently, dephosphorylated to generate IP_1 (supplementary figure S3.2) [190]. In several studies, it has been demonstrated that inhibition of PLC is able to block the activation of the NF-kB signaling cascade, which regulates inflammatory gene transcriptions. In order to validate this assumption in our experimental setting, we created a HeLa cell line stably expressing MRGPRD. We first investigated whether β-alanine-mediated activation of MRGPRD could induce NF-kB phosphorylation in HeLa cells. Stimulation of the MRGPRD-expressing HeLa cells with β-alanine increased NF-kB phosphorylation, whereas no upregulation of NF-kB phosphorylation was observed in control HeLa cells (Figure 3.6 A). Before moving further, an assessment of various NF-KB pathway inhibitors was performed (supplementary figure S3.3). Furthermore, MRGPRD-expressing HeLa cells treated with a Gαq protein inhibitor (YM-254890), a pan-PLC inhibitor (U-73122) or an IKK complex inhibitor (IKK-16) [226-230] for 1 h prior to stimulation with β-alanine, blocked the phosphorylation of NF-kB as compared to vehicle-treated MRGPRD-expressing cells (Figure 3.6 A).

Likewise, we examined whether the IL-6 release resulting from the β-alanine-activated MRGPRD-Gαq/PLC/NF-kB canonical axis could be prevented by the Gαq inhibitor, the pan-PLC inhibitor or the IKK complex inhibitor. To this end, HeLa cells stably expressing MRGPRD were treated either with vehicle or with the respective inhibitors for 1 h prior to stimulation with β-alanine. The MRGPRD-expressing cells pre-incubated with Gαq protein inhibitor or IKK complex inhibitor revealed a significant decrease in IL-6 release, whereas the PLC-inhibitor equally showed a reduced but less prominent effect (Figure 3.6 B).

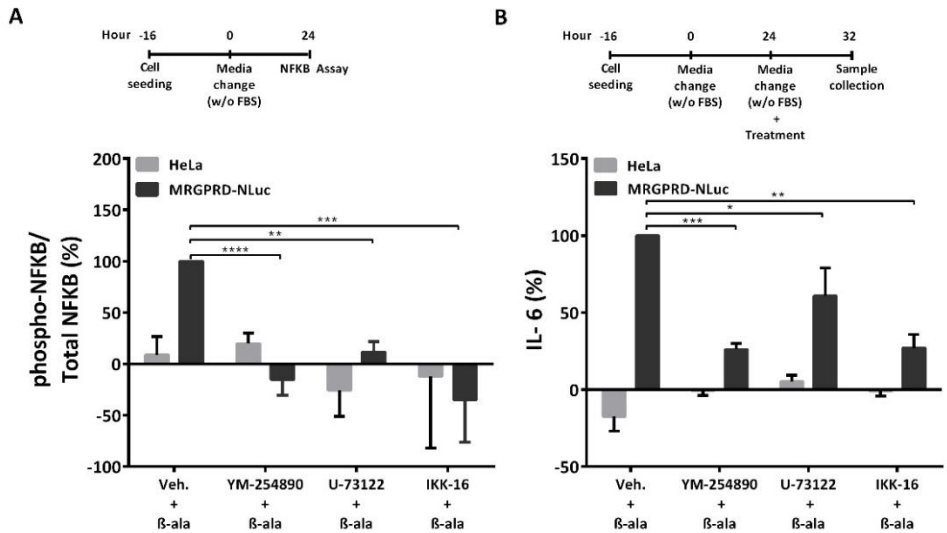

Figure 3.6. β-alanine-stimulated MRGPRD-induced IL-6 release is dependent on NF-kB activation. (A) HeLa cells stably expressing fusion protein MRGPRD-NLuc were pre-treated with either vehicle control or the Gαq inhibitor (YM-254890; 10 µM), the pan-PLC inhibitor (U-73122; 10 µM) or the IKK inhibitor (IKK-16; 5 µM) for 1 h before being stimulated with β-alanine (1mM). β-alanine-stimulated MRGPRD-expressing HeLa cells induced NF-kB phosphorylation, whereas no induction was observed in cells pre-treated with either of the three applied inhibitors. **(B)** Similarly, HeLa cells stably expressing fusion protein MRGPRD-NLuc were pre-treated with either vehicle control or Gαq (YM-254890; 10 µM) or pan-PLC (U-73122; 10 µM) or IKK (IKK-16; 5 µM) inhibitors for 1 h before being subjected to β-alanine (100 µM). MRGPRD-expressing cells upon stimulation with β-alanine showed a strongly reduced IL-6 release after being pretreated with either YM-254890 or IKK-16 and a less prominent but still significant reduced IL-6 release compared to β-alanine stimulated MRGPRD expressing cells that were not pre-exposed to the inhibitor. The data represented in this figure are from at least (n=3) experiments.

3.4 Discussion

GPCRs are capable of transducing extracellular signals into the regulation of downstream signaling pathways that control cellular responses and regulate gene expressions. As such, GPCRs have become a major target of therapeutic interventions [112]. Nevertheless, our knowledge of the GPCR-mediated inflammatory responses is still limited. In this study, we demonstrate that HeLa cells expressing MRGPRD induced the release of the pleiotropic cytokine IL-6 when activated by its agonist β-alanine (Figure 3.1).

Considering that MRGPRD has been reported as constitutively active in physiological conditions [190], we tried to further define the constitutive (ligand-independent) (Figure 3.4) and basal activity of MRGPRD (Figure 3.2 A). Our results showed that MRGPRD expressing HeLa cells in ligand-independent conditions (i.e., in the absence of agonist or FBS) release IL-6 and that IL-6 release in these cells was increased in normal physiological conditions (i.e., in the presence of FBS). The high basal activity could be attributed to the FBS, which may contain physiological concentrations of unrecognized MRGPRD-activating ligands such as β-alanine, L-βAIBA, GABA, etc. [190]. Assessment of the concentration-effect curves obtained in the medium with and without FBS did not reveal a significant difference between β-alanine EC_{50} values (Figure 3.5 A and 3.5 B), although the dynamic window for IL-6 detection increased in the medium without FBS (Figure 3.5 C and 3.5 D). Taken advantage of increased dynamic window for IL-6 detection, the assay could be utilized for screening allosteric modulators in presence and absence of ligand for the receptor.

In HeLa cells, β-alanine preferentially activates the MRGPRD-Gαq signaling pathway (IP_1 induction; supplementary Figure S3.2), which leads to IL-6 release (Figure 3.6 B). Several

studies have revealed that cytokine expression is dependent on nuclear translocation of phosphorylated NF-kB to regulate inflammatory gene transcriptions [231]. Accordingly, our results demonstrate the activation of NF-kB (Figure 3.6 A), which was blocked by a Gαq protein inhibitor, a pan-PLC inhibitor and an IKK complex inhibitor (IKKα and IKKβ inhibitor).

The IKK complex is the key regulator of the NF-kB cascade, which consists of the IKKα and IKKβ kinases, as well as of the regulatory subunit IKKγ/NEMO. Activated IKK kinases phosphorylate inhibitory IkBα (Inhibitor of NF-kB) protein, which leads to ubiquitination and degradation of IkBα to unmask the activated NF-kB to translocate to the nucleus. Our results demonstrated that IKK-16 inhibitor decreased the activation of NF-kB, which in turn reduced the IL-6 release from β-alanine-stimulated MRGPRD-expressing HeLa cells. Moreover, the observed attenuation of IL-6 release by the Gαq protein inhibitor and the intermittent inhibition of IL-6 release by the pan-PLC inhibitor (Figure 3.6 B), hint at involvement of other signaling pathways that ultimately converges into the NF-kB cascade. A contribution of for example G protein-coupled receptor kinases (GRKs), β-arrestin mediated signaling or IL-6 mediated positive feedback loops regulating in IL-6 release from MRGPRD expressing HeLa cells cannot be excluded [83, 232-234]. Altogether, our results unambiguously demonstrate the importance of MRGPRD-Gαq/PLC/NFKB signaling in the regulation of this pro-inflammatory cytokine IL-6 (Figure 3.7).

In summary, several recent studies as well as our data clearly show the regulatory role of the MRGPRD in inflammatory cytokine release. Hence, a more profound insight into the molecular mechanisms and scaffold proteins regulating the inflammation through MRGPRD might present an opportunity for further development of targeted therapeutic interventions.

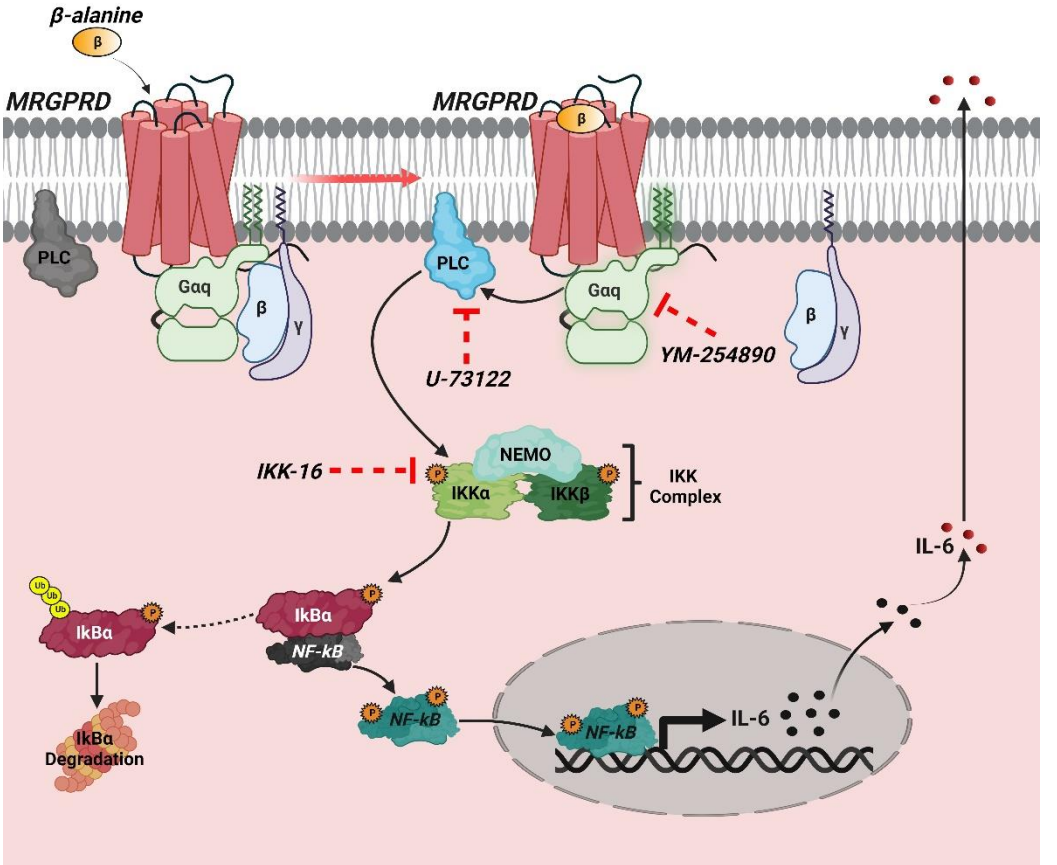

Figure 3.7. Schematic representation of β-alanine-stimulated MRGPRD-induced IL-6 release. The β-alanine activated MRGPRD-Gαq/PLC/IKK/NF-kB induces IL-6 release could be blocked using Gq (YM-254380), PLC (U-73122) and IKK/NF-kB (IKK-16) inhibitors. Figure created with BioRender.com.

3.5 Supplementary materials and figures

3.5.1 β-Alanine-Mediated Activation of MRGPRD Induces release of IL-6 from HT1080 cells

HT1080 cells were cultured in 100 mm dishes using DMEM supplemented with 10% FBS and 1% penicillin-streptomycin in incubator (37°C with 5% CO_2). HT1080 cells were trypsinised, $2.5x10^5$ cells/well were seeded in a 6 well cell culture plate. After 16 h, medium was removed, and cells were washed once with 1 ml phosphate-buffered saline (PBS). Cells were transfected with 2 µg plasmid cDNA (i.e., pCMV-GS or pCMV-MRGPRD-HA) using Lipofectamine 2000 as per the manufacturer's instructions. After 4 h, transfection medium was replaced with 2 ml DMEM supplemented with 10% FBS and 1% penicillin-streptomycin and the plate were returned to incubator. Following 24 h, medium was removed and replaced with 2 ml DMEM (overnight starvation) and plate

was returned to incubator. Next day, after 24 h, i.e., 48 h from transfection, cells were washed once with 1 ml PBS and 2 ml DMEM was added to each well containing the either vehicle control (percentage of milli-Q was 0.2%) or β-alanine (dissolved in milli-Q; 0.2%). The final concentration of β-alanine was 100 µM. After treatment plate was returned to the incubator. After incubation of 24 h, i.e., 72 h post-transfection, cell supernatant medium was collected in a 2 ml microcentrifuge tube and spun at 1,000 g for 5 min at 4°C to pellet down debris. The supernatant medium was transferred into a fresh microcentrifuge tube and stored at -80°C until assayed by ELISA. For IL-6 assessment the collected supernatant medium was thawed on ice and sample was diluted (1:100 and 1:10) in assay diluent buffer and IL-6 estimation was performed using an IL-6 ELISA kit as per the manufacturer's instructions. Interpolated IL-6 concentrations from collected supernatant medium were represented as ng/ml.

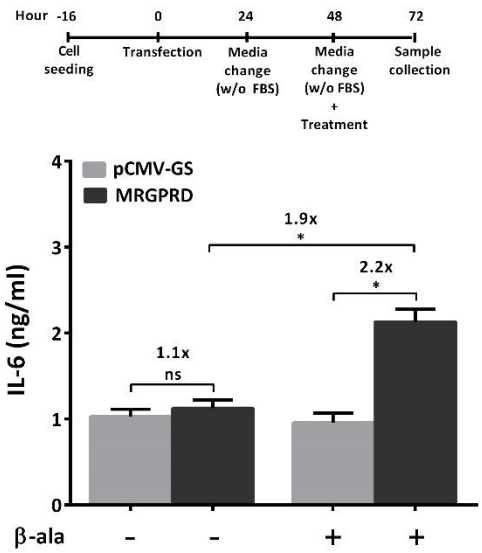

Figure S3.1. Activation of MRGPRD mediates IL-6 release in HT1080 cells. HT1080 cells transiently expressing empty vector (pCMV-GS) or MRGPRD-HA receptor were stimulated with either β-alanine (100 µM; final concentration/well) or vehicle control. A significant, 1.9-fold higher release of IL-6 was observed from MRGPRD-expressing cells treated with β-alanine as compared to vehicle-treated MRGPRD-expressing cells. Also, IL-6 levels of β-alanine treated MRGPRD-expressing cells were nearly 2.2-fold higher than those of vehicle-treated empty vector expressing control cells. The IL-6 release is represented in ng/ml (average of n=2 experiments). All values are represented as the mean ± s.e.m. Statistical significance was determined using one-way analysis of variance (ANOVA) and Sidak's post hoc test was applied for multiple comparisons.

3.5.2 β-Alanine-Mediated Activation of MRGPRD Induces IP_1 Accumulation in HeLa cells

HeLa (mock) cells and HeLa cells stably expressing fusion protein MRGPRD-NLuc (with 1000 µg/ml Geneticin) were cultured in 100 mm dishes using DMEM supplemented with 10% FBS and 1% penicillin-streptomycin in incubator (37°C with 5% CO_2). The cells were trypsinised and $2x10^4$ cells/well were seeded in 96 white, flat, opaque bottom well plate (CELLSTAR; Cat# 655083). 24 h post seeding, the medium was removed and replaced with 100 µl DMEM for overnight starvation. The next day, i.e., 48 h from seeding, the medium was replaced with 100 µl stimulation buffer (without β-alanine) containing either vehicle control (final concentration of DMSO was 0.1%) or desired concentration of inhibitor (dissolved in DMSO; 0.1%), and plate was kept in incubator for 1 h. Post-incubation, cells were stimulated with 40 µl stimulation buffer containing vehicle control (DMSO; 0.1%) or inhibitor (dissolved in DMSO; 0.1%) with vehicle control (percentage of milli-Q was 0.1%) or β-alanine (dissolved in milli-Q; 0.1%). The final concentration of β-alanine was 1 mM/well. Plate was then returned to the incubator (37°C with 5% CO_2) for 1 h. After the desired treatment, briefly, 30 µl of donor (IP_1-cryptate antibody) and 30 µl acceptor (IP_1-d2) was added to wells as per the manufacturer's instructions (Cisbio; IP-One-Gq HTRF assay). After 1 h, plate was read using an EnVision multimode plate reader. Using standard curve, HTRF ratios were interpolated to IP_1 [nM]. The relative fold change (ΔF) was obtained by normalizing IP_1 [nM] to that of its respective control i.e., vehicle-treated (DMSO) or inhibitor-treated. The fold-change (ΔF) was further normalized to the ΔF of β-alanine-stimulated MRGPRD-expressing cells (i.e., ΔFmax) and expressed as percentages.

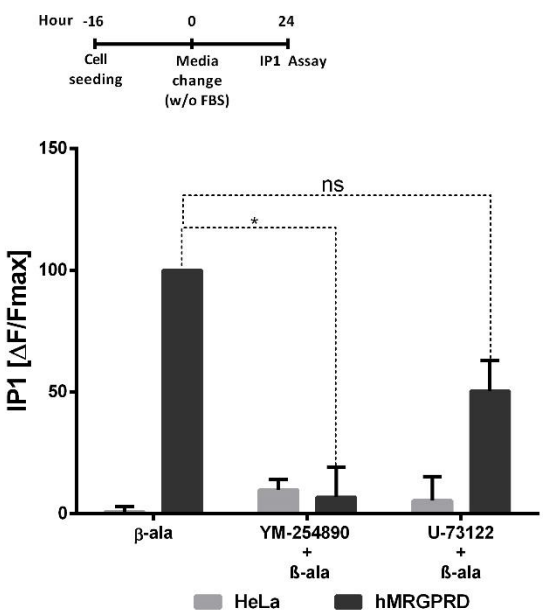

Figure S3.2. Activation of MRGPRD increased inositol monophosphate (IP_1) accumulation in HeLa cells. HeLa (mock) and Hela cells stably expressing fusion protein MRGPRD-NLuc were pre-treated with either vehicle control or the Gαq inhibitor (YM-254890; 10 µM) or the pan-PLC inhibitor (U-73122; 10 µM) for 1 h before being stimulated with β-alanine (1mM). β-alanine-stimulated MRGPRD-expressing HeLa cells induced IP_1 accumulation. No induction was observed in cells pre-treated with Gαq inhibitor, whereas partial reduction was observed for PLC inhibitor. The IP_1 accumulation is represented in percentage of ΔF/Fmax (average of n=2 experiments). All values are represented as the mean ± s.e.m. Statistical significance was determined using one-way analysis of variance (ANOVA) and Sidak's post hoc test was applied for multiple comparisons.

3.5.3 Assessment of NF-kB pathway inhibitors

We examined whether the IL-6 release resulting from the β-alanine-activated MRGPRD-Gαq/PLC/NF-kB canonical axis could be prevented by NF-kB pathway inhibitors. To this end, HeLa cells stably expressing MRGPRD were treated either with vehicle or with the respective inhibitors for 1 h prior to stimulation with β-alanine. The MRGPRD-expressing cells pre-incubated with IKK-16 i.e., IKK complex inhibitor revealed a significant decrease in IL-6 release, whereas inhibition by MG-132 and TPCA-1 was found to be non-significant (Figure S3.3). Therefore, in further studies, we decided to use IKK-16 as NF-KB pathway inhibitor.

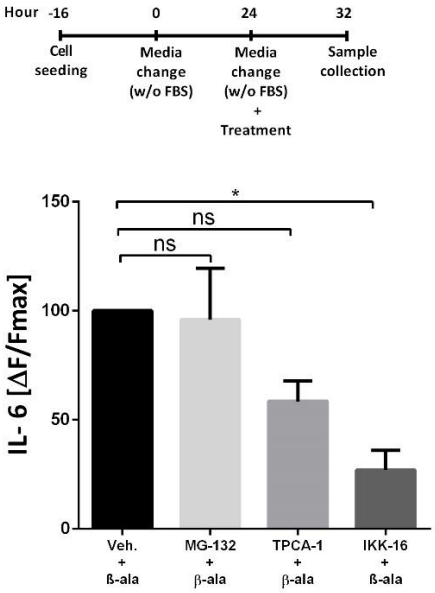

Figure S3.3. Screening of NF-KB pathway inhibitor. HeLa cells stably expressing fusion protein MRGPRD-NLuc were pre-treated with either vehicle control or the NF-kB pathway MG-132 (10 µM), TPCA-1 (10 µM) or the IKK-16 (5 µM) for 1 h before being subjected to β-alanine (100 µM). MRGPRD-expressing cells upon stimulation with β-alanine showed a strongly reduced IL-6 release after being pretreated with IKK-16 inhibitor, a less potent IL-6 reduction was observed

with TPCA-1 (non-significant) and no IL-6 reduction was observed with MG-132 (non-significant). The data represented in this figure are from at least (n=3) experiments. All values are represented as the mean ± s.e.m. Statistical significance was determined using one-way analysis of variance (ANOVA) and Sidak's post hoc test was applied for multiple comparisons.

3.5.4 Evaluation of IL-6 release from MRGPRD-expressing cells upon stimulation with alamandine

Since alamandine-mediated activation of MRGPRD induces release of NO, we also evaluated whether alamandine-mediated activation of the MRGPRD triggers the release of IL-6. To this end, Hela cells (mock, transfected with pCMV-GS) and HeLa cells transiently expressing MRGPRD were treated with either vehicle, β-alanine (100 µM), or alamandine (100 µM). The release of IL-6 was observed from β-alanine treated MRGPRD-expressing cells; however, no significant release of IL-6 was observed from alamandine-treated MRGPRD-expressing cells and HeLa (mock) cells (Figure S3.4).

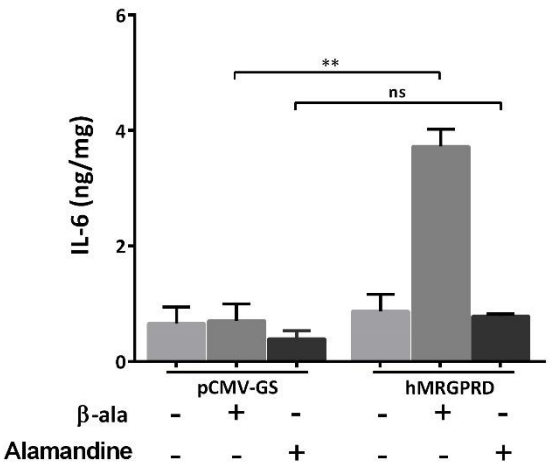

Figure S3.4. Assessment of IL-6 release from MRGPRD-expressing cells upon stimulus with alamandine. HeLa cells transiently expressing MRGPRD or transfected with empty vector (pCMV-GS) were stimulated with either vehicle, β-alanine (100 µM) or alamandine (100 µM). Substantial release of IL-6 was observed from β-alanine treated MRGPRD cells, while no significant IL-6 release was seen from alamandine-treated MRGPRD-expressing cells compared to vehicle treated. The mock transfected cells did not display IL-6 release above the basal level upon β-alanine-, alamandine- or vehicle-treatment. The data represented in this figure are from at least (n=2) experiments. All values are represented as the mean ± s.e.m. Statistical significance was determined using one-way analysis of variance (ANOVA) and Sidak's post hoc test was applied for multiple comparisons.

Author Contributions

R.A. and A.J.L. conceptualized the study plan and experimental design; R.A. constructed the plasmids and performed the ELISA, HTRF, and Western blot experiments; R.A. and

K.M.V.T. performed the IP_1 assay; R.A. and A.J.L. analyzed the data. R.A., K.M.V.T., S.V.R., D.J.S., A.J.L. and J.-P.T. interpreted data. R.A., A.J.L. and J.-P.T. wrote the paper.

Funding

This research was funded by a grant of the Flemish Foundation for Scientific Research (FWO G019314N to J.-P.T.), by grant AK814100 (to J.-P.T.), by BOF funding of Ghent University (BOF/STA/202009/013 to A.J.L.), and by a grant of the University of Antwerp, Belgium (DOCPRO1 BOF 34867 to R.A. and J.-P.T).

Acknowledgments

We would like to thank Dr. Rithwik Ramachandran (University of Western Ontario, London, Canada) for generously providing us with plasmid encoding human PAR2. We like to thank Dr. Wim Vanden Berghe (University of Antwerp, Belgium) for providing access to PerkinElmer EnVision multimode plate reader and Amersham Imager 6.

Chapter 4

Bile acids-mediated activation of human Mas-related G protein-coupled receptor D induces release of the inflammatory cytokine IL-6

Rohit Arora*[1,2], Alain J Labro*[1,3]

[1]Laboratory for Molecular, Cellular and Network Excitability, Department of Biomedical Sciences, University of Antwerp, 2610 Wilrijk, Belgium

[2]Department of Veterinary Sciences, University of Antwerp, 2610 Wilrijk, Belgium

[3]Department of Basic and Applied Medical Sciences, Ghent University, 9000 Ghent, Belgium

Chapter 4 Bile acids activate MRGPRD

Abstract

Mas-related G protein-coupled receptor D (MRGPRD) has been reported to mediate the nociceptive itch, pain, and the release of inflammatory cytokines. MRGPRD was initially found in sensory neurons of the dorsal root ganglion and has been known to regulate nociception. However, MRGPRD has emerged as a pivotal player in the regulation of the renin-angiotensin system (RAS) and dilated cardiomyopathy. The activation of MRGPRD by the ligand β-alanine and cell membrane piercing/integrating lipopolysaccharides (LPS) induces cytokine secretions. Similarly, several GPCRs are modulated and activated by plasma membrane integrating sterols and their derivatives. However, the effect of sterols and their derivatives on the activation of MRGPRD has not been demonstrated. Therefore, we evaluated the effect of sterol derivatives, i.e., cholesterol (CLR) and bile acids (BAs), in the activation of MRGPRD. To this end, HeLa cells stably expressing human MRGPRD were stimulated with CLR and BAs. The IL-6 release was observed from MRGPRD-expressing HeLa cells treated with BAs, indicating the activation of MRGPRD. Interestingly, MBCD, which is known to extract sterols from the plasma membrane, also induced the IL-6 release. Furthermore, the IL-6 release upon MRGPRD activation is mediated by the canonical nuclear factor kappa-B (NF-κB) signaling pathway. This IL-6 release could be strongly blocked by a Gαq inhibitor (YM-254890), partially blocked by an IKK complex inhibitor (IKK-16), and nominally by a PLC inhibitor (U-73122). Taken together, both the addition BAs and depletion of sterols using MBCD activates MRGPRD expressing cells and releases IL-6. These results point to the allosteric binding of BAs to MRGPRD. Alternatively, modulation of plasma membrane plasticity indirectly affects the structure-function of MRGPRD.

Keywords: GPCRs, MRGPRD, sterols, bile acids, Gq inhibitor, NF-kB, interleukin-6

Chapter 4 Bile acids activate MRGPRD

4.1 Introduction

GPCRs are one of the integral membrane proteins (IMPs), which consist of seven membrane-spanning helices that respond to various stimuli and trigger diverse cellular signaling pathways [17, 235]. In the late 1990s, it was discovered that CLR modulates the ligand binding and signal transduction abilities of GPCRs [236, 237]. Despite the fact that CLR modulates GPCR signaling, the binding of CLR to receptors remained speculative until Kobilka's lab obtained the first high-resolution human β_2-AR crystals using the cholesterol-doped monoolein cubic phase method, which helped in stabilizing the β_2-AR structure and facilitated the determination of CLR interaction with β_2-AR. Furthermore, the structure analysis of β2-AR revealed CLR binding sites on transmembrane interfaces between the two associating receptors [238-240]. Thereafter, several GPCR structures and in-silico studies provided evidence of CLR binding sites and regulation of receptors by CLR [241-245]. The cholesterol conserved motif (CCM; $W/Y^{4.50}$, $I/V/L^{4.46}$, $K/R^{4.39-4.43}$ and $Y/F/W^{2.41}$) is conserved in 21% of the rhodopsin family of GPCRs, and the first CCM was observed in β2-AR (PDB: 2RH1 and 3D4S) [239, 240]. The CCM site in β2-AR comprises $W^{4.50}$, I4.46, $R^{4.43}$, $K^{4.39}$ on TM4, and $Y^{2.41}$ on TM2, which binds to CLR as shown in (Figure 4.1 A). The aromatic Trp (W) residue at position 4.50 in TM4 of the rhodopsin family of GPCRs is the most conserved (94%) residue and appears to be involved in the most significant interaction with the cholesterol ring. Additionally, various cholesterol recognizing/interaction amino acids (CRAC/CARC; $L/V\text{-}X_{1\text{-}5}\text{-}Y\text{-}X_{1\text{-}5}\text{-}R/K$) also commonly observed on GPCR TMs [103]. Interestingly, 92% of CLR binding sites are found at 12 CLR network clusters, although there is no consensus on the location and composition of these sites [103, 246]. It has been discovered that CLR binds to TM4 and TM2 of MRGPRX1 (PDB: 7VUY; cryo-EM), indicating for presence of CCM site (Figure 4.1 B) [166].

In fact, about 90% of total cell CLR is found in the plasma membrane [15], and these high physiological levels of CLR in the plasma membrane are essential to maintain membrane biophysical properties such as fluidity, curvature, permeability, and thickness and are known to directly or indirectly affect the structure-function of IMPs, including GPCRs [247]. As a result, changes in membrane CLR causes IMPs modulation, hence regulating cellular signaling [248, 249].

It is known that, in hypercholesterolemia, CLR accumulates in macrophages, inflammatory cells, and coronary endothelial cells and promotes inflammatory responses [250]. During cholestasis the BAs flow and excretion is hampered, which increases BAs in the systemic circulation and promotes their accumulation in body tissues. The increased BAs in body tissues somehow causes the sensation of itching

[251]. The mechanism of cholestasis-mediated pruritus is not very well understood, largely due to an inadequate understanding of molecular mechanisms.

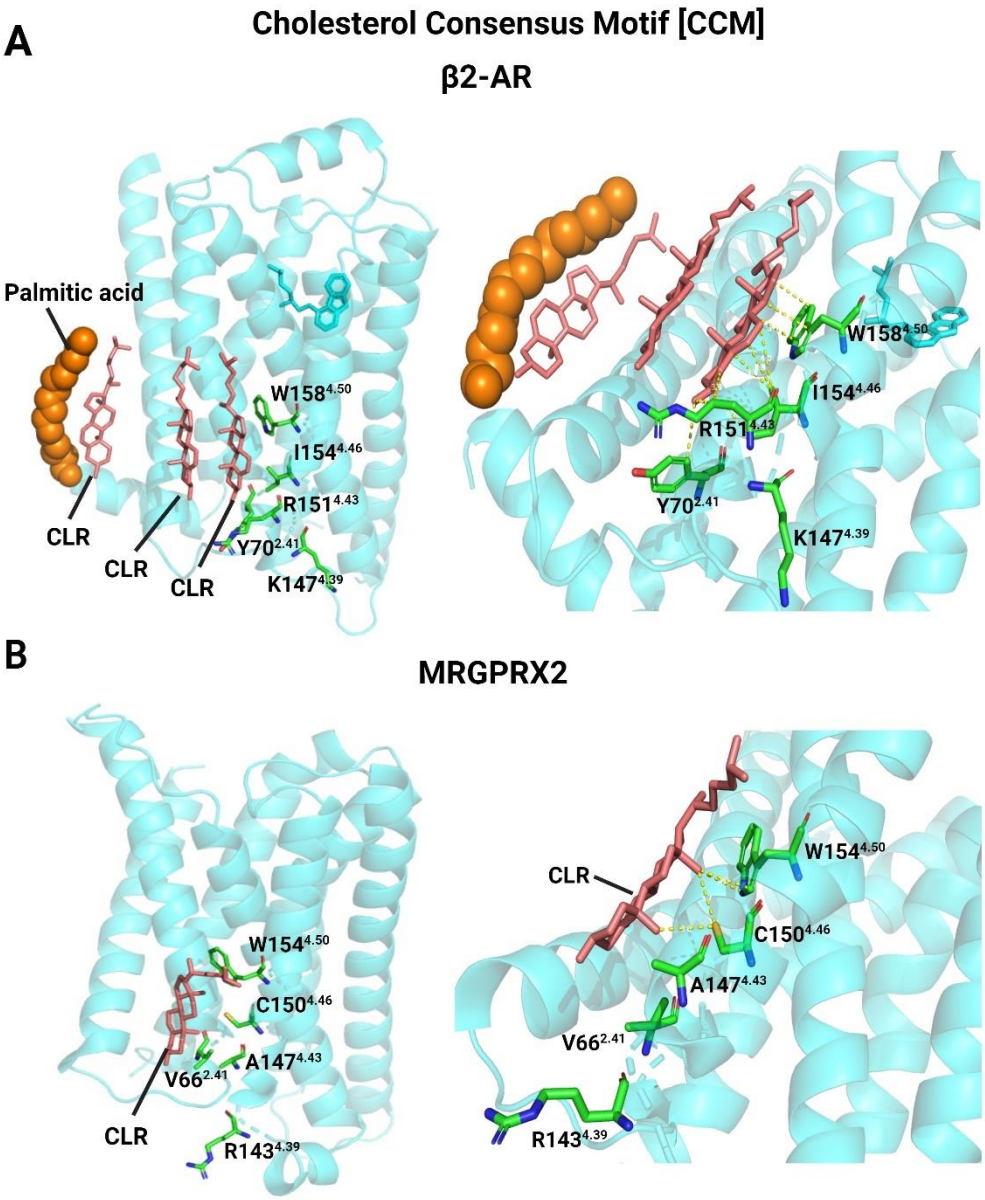

Figure 4.1: Cholesterol conserved motif in β2-AR and MRGPRX1. Specific cholesterol conserved motif in β2AR is displayed. The conserved CCM motif in β2-AR comprises $W^{4.50}$, $I^{4.46}$, $R^{4.43}$, $K^{4.39}$ on TM4 and $Y^{2.41}$ on TM2 (PDB: 2RH1; X-ray). Similarly, the cholesterol binding has been observed in MRGPRX1 (PDB: 7VUY; cryo-EM) as well, the CCM site most likely comprises of $W^{4.50}$, $C^{4.46}$, $A^{4.43}$ on TM4 and $V^{2.41}$ on TM2. Receptor represented in cyan, CLR in light red and palmitic acid in orange. PDB structures were visualized using PyMol (Schrödinger Inc.), and figures created using BioRender.com.

It is reported that Bilirubin and BAs activate the receptor MRGPRX4 and induce cholestatic itch [169, 170]. In our previous study, it was observed that the ligand β-alanine activates the MRGPRD-Gαq/PLC/NF-kB signaling cascade and induces the release of IL-6 [154, 157, 158, 175, 183]. Considering the high bioavailability of BAs (circulatory and tissues) in cholestasis conditions and MRGPRD playing a role in neuro- and cardio-pathophysiology [186, 252], we deployed an in vitro approach to identify whether BAs could activate MRGPRD and induce the release of the pleotropic cytokine IL-6.

4.2 Materials and methods

4.2.1 Materials

DMEM (Cat# 41966029), FBS (Cat# 10270-106), penicillin-streptomycin, and Dulbecco's phosphate-buffered saline (DPBS; Cat# 14190169) were purchased from Gibco (Waltham, MA, USA). 100 mm cell culture dishes (CELLSTAR; Cat# 664160), 6 well cell culture plates (CELLSTAR; Cat# 657160) were purchased from Greiner Bio-One (Frickenhausen, Germany). β-alanine (Cat# 05160), Cholesterol (CLR.; Cat# C4951), Deoxycholic acid (DCA; Cat# D2510), Chenodeoxycholic acid (CDCA; Cat# C9377), Ursodeoxycholic acid (UDCA; Cat# U5127), nateglinide (Cat# N3538) and DMSO were purchased from Sigma-Aldrich. Proadrenomedullin N-terminal 9-20 peptide (PAMP 9-12; Cat# 6551) agonist was obtained from Tocris (Abingdon, UK). The PLC inhibitor (U 73122; Cat# 1268) was purchased from Tocris, the Gq inhibitor YM 254890 (Cat# 10-1590-0100) from Focus Biomolecules (Plymouth, PA, USA) and the IKK complex inhibitor (IKK-16; Cat# S2882) from Selleck Chemicals GmbH (Germany). Human IL-6 Duoset ELISA kit (Cat# DY-206-05) was purchased from R&D Systems (Minneapolis, MN, USA). The Bradford assay kit (Cat# 23246), pierce IP lysis buffer (Cat# 87787), halt protease inhibitor cocktail (Cat# 87786), Geneticin (G418 Sulphate; Cat# 10131027) were obtained from Thermo Fisher Scientific (Waltham, MA, USA).

4.2.2 Stable cell line preparation

HeLa cells stably expressing NLuc alone and fusion protein MRGPRD-NLuc were prepared as described in chapter 3. Similarly, HeLa cells stably expressing fusion protein MRGPRX2-NLuc and MRGPRX4-NLuc were generated using the protocol described in chapter 3.

4.2.3 Cell culture, treatments, and IL-6 detection

Cells stably expressing receptors were collected by trypsinization and $2.5x10^5$ cells/well were seeded in a 6 well cell culture plate. At 16 h post-seeding, the medium was removed, and the cells were washed once with 1 ml PBS. Afterwards, the medium was replaced by 2 ml DMEM (overnight starvation), and the plates were returned to

incubator (37°C with 5% CO_2). After 24 h of serum starvation, the medium was replaced again by either with 2ml DMEM containing vehicle control (DMSO 1%) or 2 ml DMEM containing the desired concentration of compound (maintaining final DMSO concentration to 1%). For inhibition assay, prior to treatment with compounds, cells were treated with desired concentration of inhibitor for 1h. The plates were then returned to the incubator for another 8 h before sample collection (supernatant and protein collection). After the desired incubation, cell supernatant medium was collected in a 2 ml microcentrifuge tube and spun at 1,000 g for 5 min at 4°C to pellet down debris. Without disturbing the pellet, the supernatant medium was transferred into a fresh microcentrifuge tube and stored at -80°C until assayed by ELISA. For IL-6 assessment the frozen supernatant medium was thawed on ice and samples were analyzed using an IL-6 ELISA kit as per the manufacturer's instructions.

For protein sample collection, cells were first washed with 1 ml of PBS followed by addition of 300 µl IP-lysis buffer (supplemented with 1% protease inhibitor) to each well. Subsequently, the plates were maintained on ice for 20 min with intermittent shaking every 5 min. Lysate was collected in a microcentrifuge tube, spun at 13,000g for 10 min at 4°C; the resulting protein supernatant was transferred into a new microcentrifuge tube and stored at -80°C for further analysis with a Bradford assay, as per the vendor's instructions. The calculated IL-6 (ng/ml) concentrations from collected supernatant medium were normalized to the protein concentrations (mg/ml) from the respective well. IL-6 release was further extrapolated to ng/mg.

4.2.4 Data and Statistical Analysis

Data analysis and graphs were prepared using Microsoft Excel and GraphPad Prism 6. All values are represented as mean ± s.e.m. Statistical significance was determined using one-way analysis of variance (ANOVA) and multiple comparison was performed using Sidak's post hoc test. P values: *p≤0.05, **p≤0.01, ***p≤0.001 and ****p≤0.0001 were considered significant and p>0.05 was considered non-significant (ns).

4.3 Results

4.3.1 Bile acids activate MRGPRD and induce IL-6 release

The human body relies on CLR production and catabolism as an important process for preserving CLR homeostasis [253]. In the liver, the cytochrome P450 enzymes, primarily CYP7A1, catabolize CLR to BAs. The body then excretes extra BAs through feces. This mechanism prevents the accumulation of CLR and BAs in body cells and tissues. In liver function abnormalities, the catabolism of CLR is hampered, which leads to hypercholesteremia. The hypercholesteremia condition affects the formation of CLR, BAs, and triglyceride micelles, which causes a decrease in BAs excretion; therefore, the

bioavailability of circulatory BAs increases in plasma. Overall, the reduction or obstruction of bile flow is clinically called as cholestasis [254].

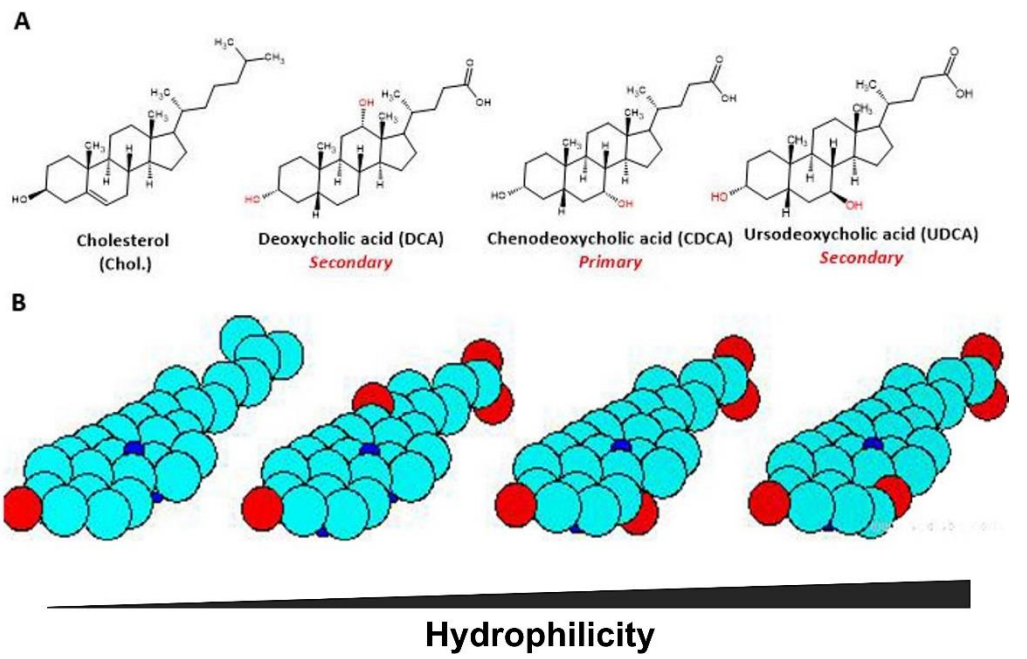

Figure 4.2. Structure of Cholesterol and Bile acids. (A). Planar structure representation of amphiphilic molecules of CLR, BAs such as deoxycholic acid (DCA), Chenodeoxycholic acid (CDCA) and Ursodeoxycholic acid (UDCA). Different hydroxyl groups (red) linked to the sterol backbone are visible in the molecular structures of BAs. DCA and UDCA are secondary BA, while CDCA is the primary BA. **(B)** 3-dimensional disk model of cholesterol, DCA, CDCA and UDCA; hydroxyl group represented in red, carbon in cyan and central hydrogen in blue. The hydrophilicity of molecules increase as follows; CLR, DCA, CDCA, UDCA. The figure was created using ChemSketch.

Itching is a frequent complaint among patients suffering from cholestasis. The evidence from the literature suggests that MRGPRs play a role in cytokine release.[151, 155, 157, 158]. Furthermore, a family member of the MRGPR family, MRGPRX4, is known to be activated by amphiphilic molecules such as bilirubin and BAs [169, 170]. Considering that we hypothesized that amphiphilic molecules such as CLR (an essential component of cell membranes), deoxycholic acid (DCA), chenodeoxycholic acid (CDCA), and ursodeoxycholic acid (UDCA) (Figure 4.2 A and 4.2 B) [255], could activate human MRGPRD, MRGPRX2, and MRGPRX4 and cause the release of IL-6. To that end, β-alanine, BAs, and nateglinide (an anti-diabetic drug that is also an agonist of MRGPRX4 [256]) were used to activate HeLa cells stably expressing MRGPRD, as measured by IL-6 release. Overall, it was discovered that DCA and CDCA significantly activated MRGPRD.

Although UDCA and nateglinide were discovered to have an effect, it was found to be non-significant as compared to DCA and CDCA (Figure 4.3 B).

PAMP-12 is a strong MRGPRX2 ligand that is known to cause the release of IL-6 when MRGPRX2 is activated [147]. When MRGPRX2-expressing stable cells were treated with PAMP-12, they released IL-6 (Figure 4.3 C). As such, no IL-6 release was detected from MRGPRX2 cells treated with BAs and nateglinide. Likewise, cells stably expressing MRGPRX4 when treated with Nateglinide, BAs, and PAMP-12 did not induce IL-6. Although nateglinide and BAs have been identified as MRGPRX4 ligands, we did not see IL-6 induction (Figure 4.3 D) [169, 170, 256]. This difference could be attributed to ligand-dependent, biased signaling [257]. Furthermore, as an experiment control, HeLa cells were also treated with BAs, nateglinide and PAMP-12 but no IL-6 release was observed (Figure 4.3 A). Intriguingly, we saw CLR crystal formation when treating the cells, since CLR is insoluble in the aqueous phase (medium). Therefore, the role of CLR in the activation of MRGPRs remains unclear or non-conclusive.

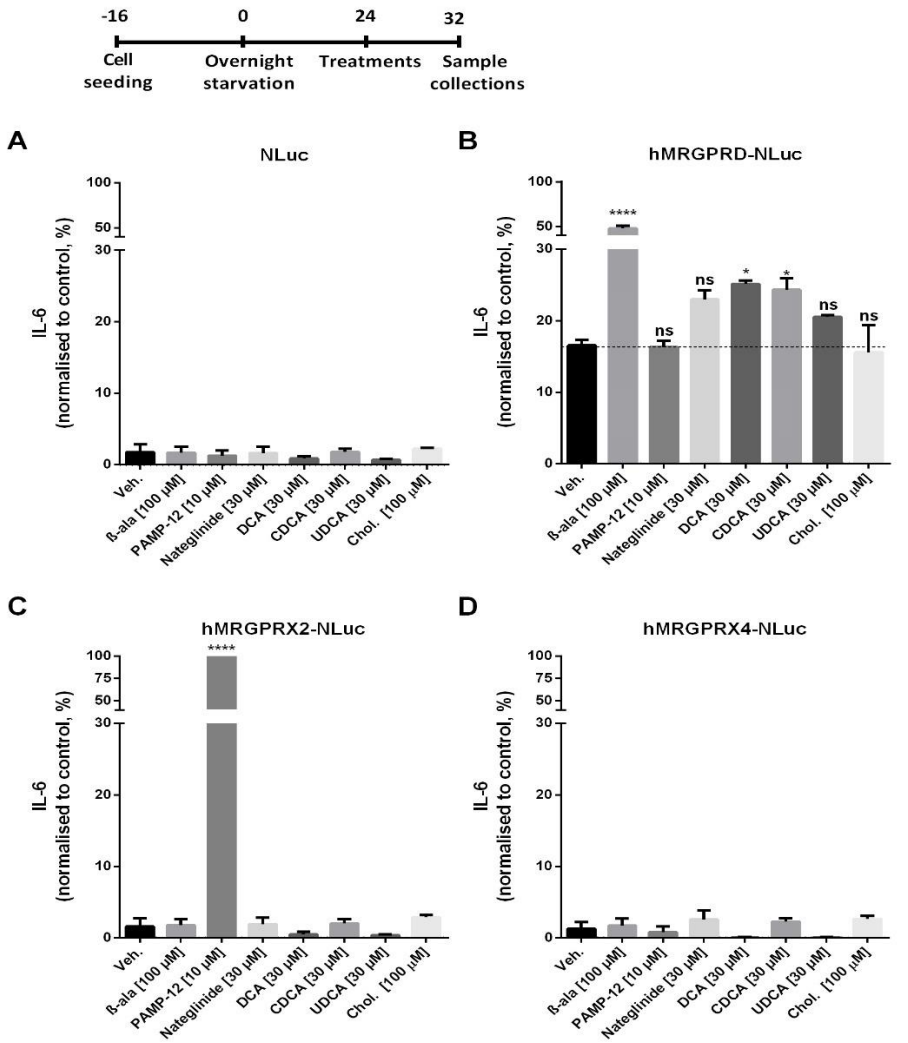

Figure 4.3. Screening of bile acids as ligand for MRGPRs activation. HeLa cells stably expressing NLuc (pCMV-NLuc) or MRGPRD-NLuc or MRGPRX2-NLuc or MRGPRX4-NLuc were stimulated with either vehicle control (DMSO; final concentration per well 1%), deoxycholic acid (DCA; 30 µM), chenodeoxycholic acid (CDCA; 30 µM), ursodeoxycholic acid (UDCA; 30 µM), CLR (Chol.; 100 µM), nateglinide (30 µM), β-alanine (100 µM) and PAMP-12 (10 µM). The normalized IL-6 release is represented in percentage of control i.e., PAMP-12 treated MRGPRX2. The graph represented in this figure originates from at least two independent experiments.

Serum cholic acid (CA) to CDCA ratios are frequently used to diagnose intrahepatic cholestasis [258]. The two principal BAs, CA and CDCA, are formed in the liver, while secondary BAs, DCA and UDCA, are created in the intestine through biotransformation by gut bacteria [259]. For the treatment of primary biliary cirrhosis and gallbladder

stones, the CDCA is frequently employed [260]. Therefore, we chose CDCA to be used in our experiments out of all BAs activating MRGPRD. First, increasing amounts of CDCA were used to activate HeLa cells that were expressing the MRGPRD (Figure 4.4). Surprisingly, we noticed cell death as the concentration increased over 30 µM; as a result, the typical concentration-response curve could not be generated. Furthermore, when HeLa (mock) cells were treated with CDCA, cells were healthy, and no IL-6 secretion was seen.

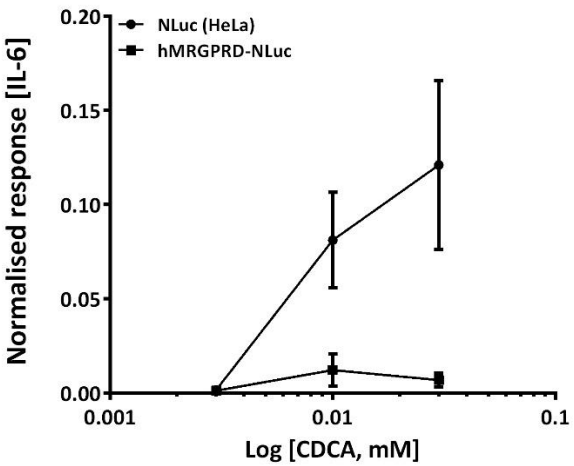

Figure 4.4. Concentration-response curve of Chenodeoxycholicacid (CDCA). HeLa cells stably expressing NLuc alone or fusion protein MRGPRD-NLuc were treated with increasing concentrations of CDCA. MRGPRD-expressing cells induced the release of IL-6 in a concentration-dependent manner when treated with CDCA. No significant IL-6 release was observed from cells expressing NLuc only. The graph represented in this figure originates from two independent experiments.

4.3.2 Cholesterol depletion from cell membrane activates MRGPRD

MBCD is a cyclic heptasaccharide generally used in the delivery of hydrophobic lipid-based molecules or drugs. MBCD is also used to dissolve CLR [261]. At higher concentrations, MBCD could deplete CLR from the cell membrane [262]. Surprisingly, we discovered that MBCD-treated MRGPRD-expressing cells induced IL-6 release in a concentration-dependent manner, whereas HeLa (mock) cells did not (Figure 4.5).

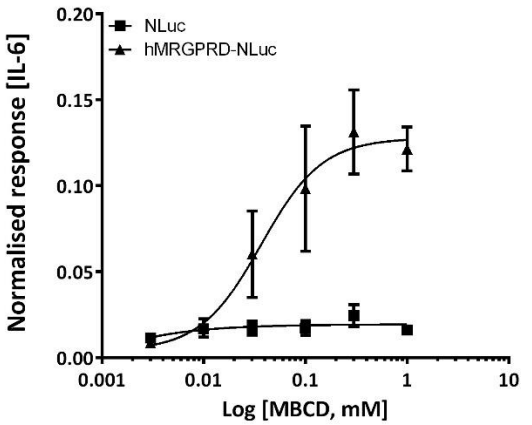

Figure 4.5. Cholesterol depletion using MBCD activates MRGPRD. HeLa cells stably expressing NLuc alone or fusion protein MRGPRD-NLuc were treated with increasing concentrations of MBCD. MRGPRD-expressing cells induced the release of IL-6 in a concentration-dependent manner. The cells that were just expressing NLuc did not release any IL-6 in a substantial amount. The graph represented in this figure is from at least two independent experiments.

4.3.3 Inhibiting MRGPRD-Gαq/IKK/NF-kB signaling cascade prevents the release of IL-6

In a previous study, we discovered that the NF-kB signaling pathway regulates IL-6 release from β-alanine-activated MRGPRD (chapter 3). Next, we examined whether CDCA-mediated activation of MRGPRD follows the Gαq/IKK/NF-kB canonical axis [157, 158]. To this end, MRGPRD-expressing cells were treated for 1 h with either a vehicle or the corresponding inhibitor before being stimulated with CDCA (Figure 4.6 A). When MRGPRD-expressing cells were pre-incubated with Gαq protein inhibitors or IKK complex inhibitors, IL-6 release was significantly reduced, while PLC inhibitors had an equivalently diminished but less pronounced effect.

As we observed that MBCD-mediated CLR depletion from the cell membrane also induced IL-6 release from MRGPRD-expressing cells, we further investigated whether the IL-6 release follows the Gαq activated NF-kB canonical pathways. When MRGPRD-expressing cells were pre-incubated with a Gαq protein inhibitor, a PLC inhibitor, or an IKK complex inhibitor, IL-6 release was significantly reduced (Figure 4.6 B). Surprisingly, the reduction in IL-6 release was found to be limited to approximately half of the MBCD-only treated cells, indicating that MBCD most likely activates the NF-kB pathway in a non-specific manner.

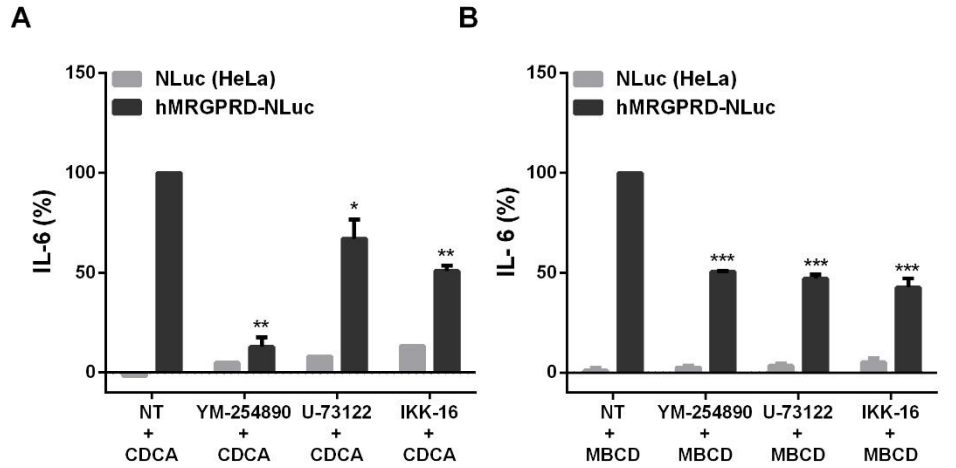

Figure 4.6. Bile acids and MBCD mediated activation of MRGPRD are dependent on Gαq activated NF-kB canonical signaling pathway. MRGPRD-expressing HeLa cells were pre-treated with either vehicle control (DMSO; 0.1%) or with the inhibitor dissolved in 0.1% DMSO, the Gαq inhibitor (YM-254890; 10 µM), the pan-PLC inhibitor (U-73122; 10 µM) or the IKK inhibitor (IKK-16; 5 µM) for 1 h before being subjected to treatments. **(A)** The cells were treated either with vehicle control (DMSO; 1%) or CDCA (30 µM; DMSO 1%). When MRGPRD-expressing cells were stimulated with CDCA, they showed a significantly reduced IL-6 release after being pretreated with either YM-254890 or IKK-16 and a less significant but still significant reduced IL-6 release from U-73122 when compared to CDCA-stimulated MRGPRD-expressing cells that had not been pre-exposed to the inhibitor. **(B)** Cell was either treated with a vehicle control (Milli-Q 1%) or with 3 mM MBCD (dissolved in Milli-Q 1%). MBCD showed a reduced IL-6 release after being pretreated with either YM-254890, U-73122, or IKK-16 as compared to only MBCD-treated cells that were not pre-exposed to the inhibitor. The data represented in this figure is from at least two independent experiments.

4.4 Discussion

In this study, we demonstrate that sterol (CLR and BAs) and the membrane CLR-depleting agent MBCD activate MRGPRD and cause the release of the pleiotropic cytokine IL-6 (Figure 4.3 and 4.5; and schematics Figure 4.8). The GPCRs constitute the largest family of IMPs and are embedded into the plasma membrane, which is comprised of a phospholipid bilayer, where CLR generally occupies the interstitial space between hydrophobic tails of phospholipids. Growing evidence from the literature suggests that various lipids, such as sterol backbone-based molecules, modulate, activate, and influence the ligand-binding on the GPCRs [169, 170, 236, 237, 245]. However, we still know very little about how sterols mediate inflammation and play a role in immunity [250].

Most of the GPCRs demonstrate co-crystallization with CLR, occupying various distinct sites among many receptors [103, 240, 246]. The plasma membrane's high physiological levels of CLR are necessary to preserve its biophysical and functional characteristics. Functionally, it has been reported that when CLR levels are low, the β2-AR couples more strongly to Gαs [263]. This suggests that CLR may play a role in regulating receptor-effector interactions [54, 243]. Depletion of CLR from the membranes of neonatal cardiac myocytes alters the signaling behavior of endogenous β2-AR [264]. In our results, we also observed the captivating biphasic behavior of MRGPRD. The depletion of membrane CLR by MBCD induced the production of IL-6 from MRGPRD-expressing cells, which was antagonized by replenishing the CLR (Figure 4.5 and Figure S4.1). This indicates that depleting membrane CLR by using MBCD could push receptors into a state of activation. This possibly indicates that i) either binding of CLR to MRGPRD, keeps receptors in an inactive state (Figure 4.7; probable CCM site on MRGPRD), or ii) the depletion of CLR from the plasma membrane, alters plasma membrane mechanics and cytoskeleton structure, thereby regulating MRGPRD-Gq signaling [265].

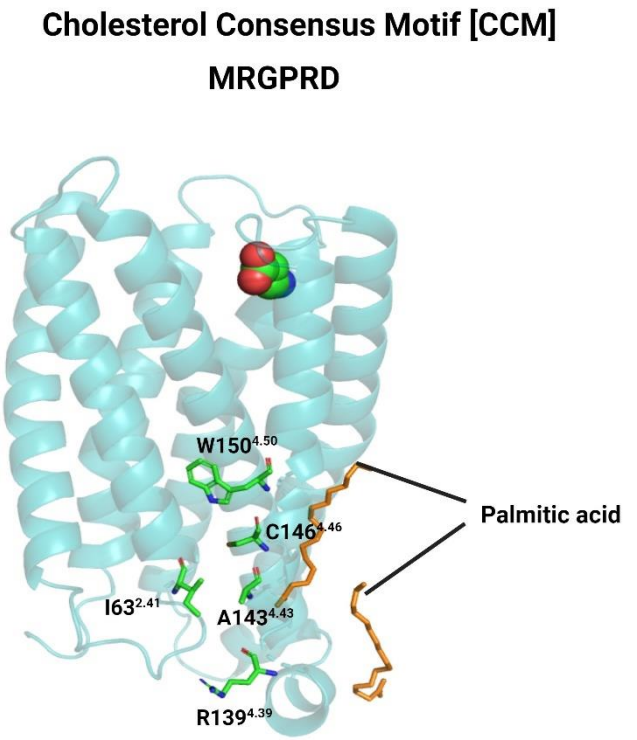

Figure 4.7: Probable CCM site in MRGPRD. Structural analysis of MRGPRD (PDB: 7Y12 [175]) reveals the conserved Try 4.450 residue on MRGPRD TM4. The observed CCM site on MRGPRD ($W^{4.50}$, $C^{4.46}$, $A^{4.43}$ on TM4 and $V^{2.41}$ on TM2) is similar to MRGPRX1. Receptor represented in cyan, CLR in light red and palmitic acid in orange. PDB structures were visualized using PyMol (Schrödinger Inc.), and figures created using BioRender.com.

BAs are amphipathic molecules, and they are synthesized from CLR catabolism in the liver. It is important to note that liver dysfunction is linked to neurological and cardiological disorders [266, 267]. An imbalance due to a metabolic disorder of the liver or an obstructive bile secretion can lead to cholestasis, which is known to cause systemic diseases like pruritus (itch) and inflammation [250, 268]. It has been observed that increased BAs in the serum cause perturbations in the plasma membrane of the RBC and lyse them, which in turn release bilirubin, thus increasing the bilirubin level in the serum[269, 270]. The recent literature suggests that bilirubin activates another member of the MRGPR family, MRGPRX4, and causes itch. Given that MRGPRD is expressed by DRG nociceptive neurons and has been linked to dilated cardiomyopathy, and after realizing that CDCA mediates activation of MRGPRD (Figure 4.3 and 4.4), investigating the role of BAs in activating MRGPRD and controlling inflammatory mediators in neurological and cardiovascular diseases has become critical.

Taken together, our findings indicate that BAs might bind allosterically to MRGPRD and activate it. The MBCD could affect membrane fluidity due to the extraction of CLR from the plasma membrane or the removal of CLR bonded to MRGPRD, resulting in MRGPRD activation. To ascertain this, additional experiments will be required to determine how relevant the association of these sterols is to MRGPRD and how depletion of these affects the packing within membrane microdomains, causing activation of MRGPRD. Altogether, these results demonstrate the importance of sterols such as BAs in regulating MRGPRD-Gαq mediated NF-kB signaling and inducing the inflammatory cytokine IL-6 (Figures 4.6 A and 4.6 B). Hence, a deeper insight into the structure and molecular mechanisms of MRGPRD activation will present a chance for further development of targeted therapeutics. It may also be able to create non-opioid painkillers and itch relievers using a structure-based drug design approach.

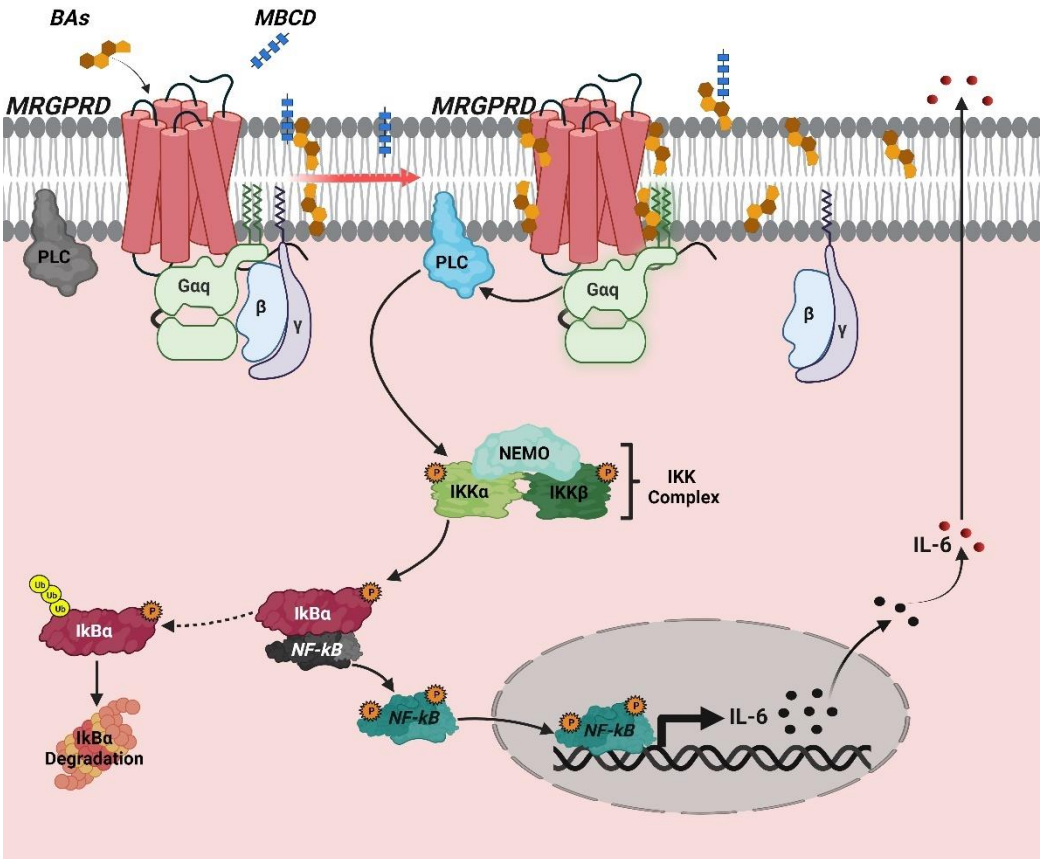

Figure 4.8. Schematic representation of MRGPRD activation by bile acids and MBCD. The BAs and MBCD activate MRGPRD-Gαq and mediate NF-kB signaling to induce the release of the inflammatory cytokine IL-6. Figure created with BioRender.com.

4.5 Supplementary Materials and figures

Since we observed that MBCD-mediated depletion of CLR from plasma membranes induced the expression of IL-6 from MRGPRD expressing cells, we further questioned whether this effect could be reversed by replenishing the CLR in plasma membranes. The MRGPRD cells were pre-treated with 3 mM MBCD for an hour and then exposed to an increasing concentration of CLR for 8 h (Figure S4.1). Interestingly, with the increasing concentration of CLR, we observed a decline in MBCD-mediated activation of MRGPRD, as measured by IL-6 release. This also indicates the MBCD treatment shifts the receptor to a high state of activation, and CLR can also work as an inverse agonist/allosteric modulator or agonist to bring the receptor into a steady state.

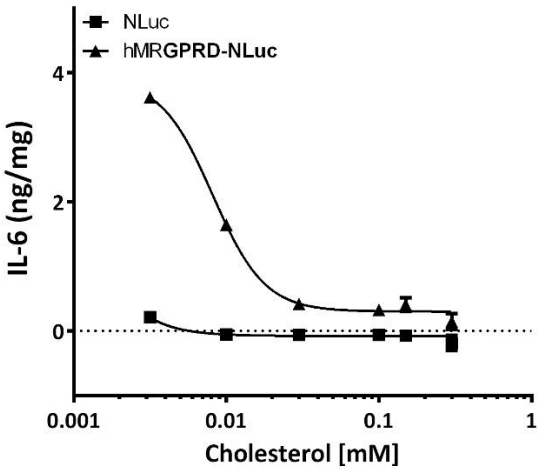

Figure S4.1. Cholesterol reduces IL-6 induction from MBCD activated MRGPRD. HeLa cells stably expressing NLuc alone or fusion protein MRGPRD-NLuc were treated for 1 h with 3 mM MBCD before being exposed to increasing concentrations of CLR (maintaining 3 mM MBCD). With the increasing concentration of CLR, the IL-6 induction from MBCD-activated MRGPRD was reduced. The cells that were just expressing NLuc did not release any IL-6. The data represented in this figure is from an experiment performed only once.

Contributions

R.A. and A.J.L. jointly conceived the idea to test cholesterol on MRGPRs. R.A. further extended studies with the bile acids utilization in consultation with A.J.L. The experiment was designed and performed by R.A.; R.A. and A.J.L. analyzed the data. R.A. wrote the chapter, A.J.L. and X.V.O. provided valuable input and edits.

Funding

This research was funded by a BOF funding of Ghent University (BOF/STA/202009/013 to A.J.L.).

Acknowledgments

We like to thank Dr. Wim Vanden Berghe (University of Antwerp, Belgium) for providing access to PerkinElmer EnVision multimode plate reader.

Chapter 5

Mas-related G protein-coupled receptor D senses fluid shear stress and induces the release of IL-6

Rohit Arora*[1], Alain J Labro*[1,2]

[1]Laboratory for Molecular, Cellular and Network Excitability, Department of Biomedical Sciences, University of Antwerp, 2610 Wilrijk, Belgium

[2]Department of Basic and Applied Medical Sciences, Ghent University, 9000 Ghent, Belgium

Chapter 5 MRGPRD activation by fluid shear stress

Abstract

GPCRs are known for their chemosensory function. Mechanical stimulation is now known to regulate cellular, biochemical, and biological processes. Unwanted cellular responses are induced when mechanical homeostasis is compromised, which is known to result in fibrosis in tissues or organs and transform them into pro-inflammatory phenotypes. During the developmental and adult stages, mechanotransduction plays an important role in neuro- and cardiovascular biology. MRGPRD plays a role in dilated cardiomyopathy and is known to be mechanosensitive. However, it is yet unclear what function a potential direct mechanical activation of MRGPRD might serve. Therefore, we sought to evaluate whether physical forces, i.e., shear stress, applied to MRGPRD could regulate the ligand-independent activation of MRGPRD and induce the release of IL-6. To this end, HeLa cells stably expressing human MRGPRD were subjected to shear stress. The IL-6 release was observed in MRGPRD-expressing HeLa exposed to shear stress, indicating the activation of MRGPRD. Overall, it was discovered that the NF-kB canonical signaling pathway was necessary for the shear stress-activated MRGPRD-related IL-6 release. These findings imply that MRGPRD is mechanosensitive, and mechanically activated MRGPRD could regulate inflammatory cytokines.

Keywords: GPCRs, MRGPRD, mechanosensory, shear stress, NF-kB, interleukin-6

Chapter 5 MRGPRD activation by fluid shear stress

5.1 Introduction

Cells and tissues sense and interpret various physical forces such as shear, tensile, and compression stress in order to perceive and integrate environmental cues [271]. Mechanotransduction is the process through which cells respond to physical forces and convert them into biochemical and biological responses [272]. The mechanism of mechanotransduction is known to be involved in numerous physiological processes, such as hearing, balance, touch, nociception, etc. However, the precise molecular mechanism involved during mechanical stimulation to elicit physiological responses has not been fully elucidated.

Primarily, it was thought that mechanosensitivity was regulated by piezo receptors [273-275]. A growing body of evidence suggests that ion channels and transporters, as well as GPCRs, are now expanding the repository of plasma membrane-associated mechanosensitive receptors [276, 277]. The GPCRs, which were largely considered to be chemosensory in function, are now known to be involved in mechanotransduction [278, 279]. The angiotensin II type 1 receptor (AT-1R) was the first reported GPCR to exhibit shear stretch-induced activation. The AT-1R is prominently expressed by cardiomyocytes, and when exposed to high pressure, it induces hypertrophy [280]. AT-1R is also known to be expressed by other cells, such as endothelial cells (ECs), when activated by stretch and shear stress-induces physiological processes including hypertension [281, 282]. Similarly, other receptors like apelin, β2AR, GPR68, PAR2, M3, H1R and many more are known to be activated by shear stress, cell shrinkage, and expansions [277, 283, 284].

Genetic ablation of Mrgprd has been reported to reduce behavioral sensitivity to noxious mechanical stimuli and cause dilated cardiomyopathy [139, 186]. Additionally, activated MRGPRD is known to release inflammatory cytokines and nitrous oxide (NO) [158, 218]. The results from our previous study hint at the possibility that modulation of the MRGPRD by CLR removal or addition of BAs is an indirect consequence of changes in the plasma membrane fluidity and flexibility (Figure 5.1 A and B). Considering the involvement of MRGPRD in neuron and cardiovascular biology and its role in regulating inflammatory cytokines, we sought to evaluate whether physical forces, i.e., shear stress, applied to MRGPRD-expressing HeLa cells could regulate the structure-function of MRGPRD and activate it to induce the release of IL-6.

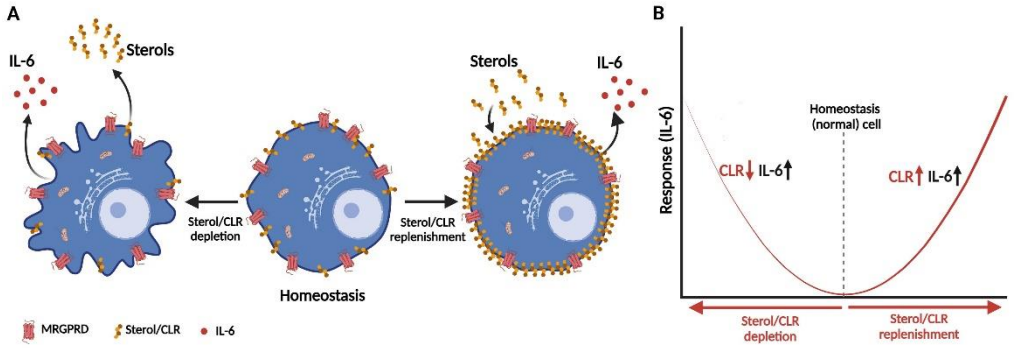

Figure 5.1. Schematic representation of proposition. (A) The sterol depletion and sterol replenishment caused the release of IL-6 from MRGPRD-expressing cells. This indicated that MRGPRD can also be activated by a change in membrane's biophysical properties, which could cause MRGPRD to adopt the active conformational state and induce the IL-6 release **(B)** IL-6 response during sterol depletion and replenishment is depicted on a predicted IL-6 response graph. Figure created with BioRender.com.

5.2 Material and methods

5.2.1 Materials and Instruments

DMEM (Cat# 41966029), FBS (Cat# 10270-106), penicillin-streptomycin, Dulbecco's phosphate-buffered saline (DPBS; Cat# 14190169), geneticin (G418 sulphate; Cat# 10131027) were purchased from Gibco (Waltham, MA, USA). 100 mm cell culture dishes (CELLSTAR; Cat# 664160) were purchased from Greiner Bio-One (Frickenhausen, Germany). The PLC inhibitor (U 73122; Cat# 1268) was purchased from Tocris, the Gq inhibitor YM-254890 (Cat# 10-1590-0100) was purchased from Focus Biomolecules (Plymouth, PA, USA), and the IKK complex inhibitor (IKK-16; Cat# S2882) from Selleck Chemicals GmbH (Germany). Duoset ELISA human IL-6 was purchased from R&D Systems (Minneapolis, MN, USA). SLA-OS-200 orbital shaker was from SciTech LabApp (Micklefield, Leeds, UK).

5.2.2 Cell culture, shear stress induction, and IL-6 detection

HeLa cells stably expressing NLuc alone and fusion protein MRGPRD-NLuc were prepared as described in Chapter 3. Cells stably expressing receptors were collected by trypsinization, and 1.0×10^6 cells/well were seeded in a 100 mm cell culture plate. At 24 h post-seeding, the medium was removed, and the cells were washed once with 2 ml PBS. Afterwards, the medium was replaced by 10 ml DMEM (overnight starvation), and the plates were returned to the incubator (37°C with 5% CO_2). After 24 h of serum starvation, the medium was replaced again with 7 ml of DMEM. The plates were then returned to the incubator (37°C with 5% CO_2), either kept stationary or on an orbital shaker at 100 rpm for 8 h before sample collection. Cell supernatant medium was

collected in a 2 ml microcentrifuge tube and spun at 1,000 g for 5 min at 4°C to pellet debris. Without disturbing the pellet, the supernatant medium was transferred into a fresh microcentrifuge tube and stored at -80°C until assayed by ELISA. For IL-6 assessment, the frozen supernatant medium was thawed on ice, and samples were analyzed using an IL-6 ELISA kit as per the manufacturer's instructions. For the inhibition assay, prior to the induction of shear stress by orbital shaking, cells were treated with the desired concentration of inhibitor for 1h (DMSO 1%). The calculated IL-6 concentrations from the collected supernatant medium were represented in pg/ml (Figure 5.2).

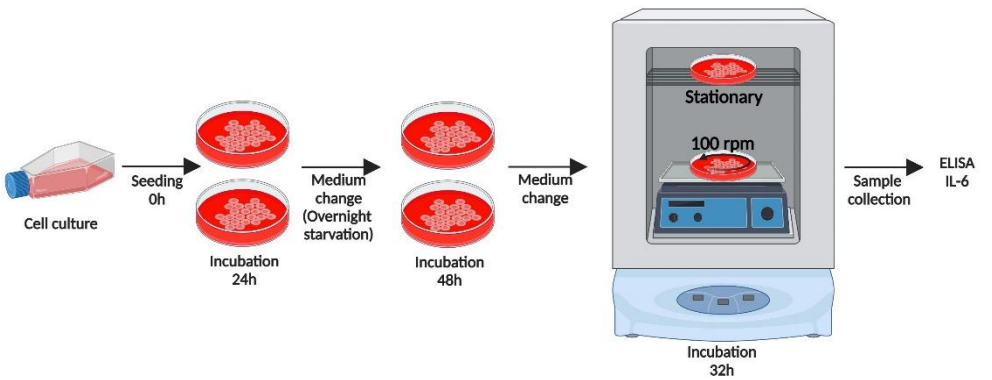

Figure 5.2. Schematics representation of the experiment procedure. Procedure to study the shear-stress induced release of IL-6 from MRGPRD-expressing cells. A detailed procedure is provided in materials and methods (section 5.2.2). Figure created with BioRender.com.

5.2.3 Data and Statistical Analysis

Data analysis and graphs were prepared using Microsoft Excel and GraphPad Prism 6. All values are represented as mean ± s.e.m. Statistical significance was determined using one-way analysis of variance (ANOVA), and multiple comparisons were performed using Sidak's post hoc test. P values of *p≤0.05, **p≤0.01, ***p≤0.001 and ****p≤0.0001 were considered significant, and p>0.05 was considered non-significant (ns).

5.3 Results

5.3.1 Shear stress activates MRGPRD and induces IL-6 release

As we observed that CLR depletion and replenishment of the plasma membrane modulated MRGPRD activity (Figure 4.5 and S4.1). We hypothesized that this effect could be a result of strain induced on the plasma membrane. In other words, pull and push-mediated structural rearrangements of the receptor could activate it. To explore this, we first tested whether shear stress might perhaps activate the MRGPRD. For that reason, MRGPRD-expressing HeLa cells were subjected to shear stress induced by orbital shaking. The shear stress induced a 1.4x higher release of IL-6 from MRGPRD-

expressing cells as compared to MRGPRD-expressing cells that were maintained stationary (Figure 5.3). Moreover, HeLa cells expressing NLuc-only did not induce IL-6 release under shear stress or stationary conditions. These findings indicate shear stress-induced activation of MRGPRD mediates IL-6 release.

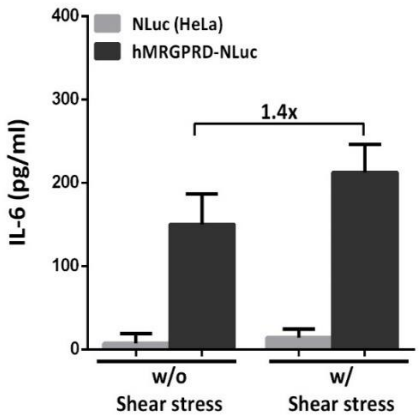

Figure 5.3. Activation of the MRGPRD by shear stress. HeLa cells stably expressing NLuc alone or fusion protein MRGPRD-NLuc were cultured in control(stationary) or under shear stress conditions induced by orbital shaking. The shear stress-induced IL-6 release was observed from MRGPRD-expressing cells, and no detectable IL-6 release was observed from cells expressing NLuc only. The cells maintained at stationary (no shear stress) did not induce IL-6 release. The graph represented in this figure is from at least two independent experiments.

5.3.2 Shear stress-activated MRGPRD-induced IL-6 release is dependent on NF-kB signaling

We previously discovered that β-alanine, BAs, and plasma membrane sterol deficiency activated the NF-kB signaling pathway, which regulated IL-6 release in MRGPRD-expressing cells. Therefore, we next examined whether IL-6 release from shear stress-induced activation of MRGPRD depends on the MRGPRD-Gαq mediated NF-kB canonical axis and can be prevented by the Gαq inhibitor, the pan-PLC inhibitor, or the IKK complex inhibitor. To this end, MRGPRD-expressing cells were treated either with vehicle or with the respective inhibitors for 1 h before being subjected to shear stress. The MRGPRD-expressing cells treated with the Gαq protein inhibitor or the IKK complex inhibitor revealed a substantial reduction in IL-6 release, whereas cells treated with the PLC inhibitor showed a marginal reduction in IL-6 release (Figure 5.4).

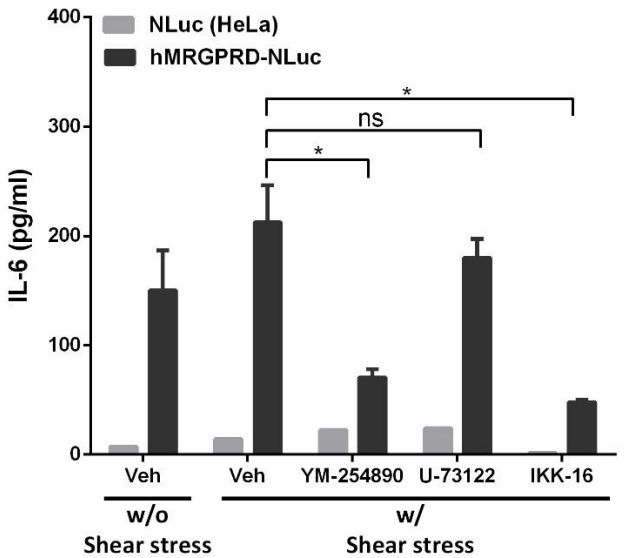

Figure 5.4. The Gαq-activated NF-kB signaling pathway is required for IL-6 release from shear stress-activated MRGPRD. HeLa cells stably expressing fusion protein MRGPRD-NLuc were pre-treated with vehicle control (DMSO; 1%) or the Gαq inhibitor (YM-254890; 1 µM), the pan-PLC inhibitor (U-73122; 10 µM) or the IKK inhibitor (IKK-16; 5 µM) for 1 h before being subjected to shear stress. Under shear stress conditions, MRGPRD-expressing cells released more IL-6 than stationary MRGPRD-expressing cells. The reduced IL-6 release was observed from MRGPRD-expressing cells pretreated with either YM-254890 or IKK-16 and a less significant reduction of IL-6 release from U-73122 when compared to shear stress-stimulated MRGPRD-expressing cells that had not been pre-exposed to the inhibitor. The data represented in this figure is from at least two independent experiments.

5.4 Discussion

One of the primary roles of the plasma membrane is to provide fluidity to several membrane-associated proteins to allow lateral diffusion, contacts, and signaling [247]. In humans, hemodynamic shear stress is one of the prominent forces that affect the membrane tension of the plasma membrane, and the shear stress applied depends on the cell's shape, size, lipid, and protein composition of the plasma membrane, thus regulating various functions and pathophysiology [278, 285, 286].

GPCRs primarily respond to a wide range of extracellular signals. Several GPCRs also show ligand-independent constitutive activity, indicating that GPCRs can spontaneously assume an active conformation [224]. Several lines of evidence now support the notion that alteration of plasma membrane characteristics by applied shear, stretch, and compression forces modulated plasma membrane properties, which in turn control the GPCRs functions. It is also well understood that GPCR interactions with lipid molecules

have a significant impact on their structure-function and modulate the GPCR's ability to adopt different conformational states [247]. Therefore, it is very apparent that GPCRs are activated by ambiguous mechanisms.

In this study, we demonstrate that HeLa cells expressing MRGPRD induce the release of IL-6 when subjected to shear stress (Figure 5.3). Having observed shear stress-induced activation of MRGPRD, we further demonstrated the IL-6 release is dependent on the NF-kB canonical signaling pathway (Figure 5.4). Altogether, our results establish the importance of MRGPRD-Gαq/NF-kB signaling in the regulation of IL-6 under shear stress. The results are suggestive of MRGPRD being mechano-sensitive.

The finding that MRGPRD is mechano-sensitive and responds to shear stress might explain its role in several pathophysiological conditions. It has been reported that disruption of a cell's mechanical homeostasis can evolve towards pro-inflammatory/pro-fibrotic phenotypes, leading to tissue or organ fibrosis [287]. If MRGPRD activation also stimulates IL-6 release in vivo, then this data might highlight MRGPRD as a regulator of the pro-inflammatory fibrotic process. However, no conclusions can be drawn yet as the exact expression of MRGPRD in cardiovascular tissue is still unknown.

Contributions

R.A. conceived the idea to test the mechanosensitivity of MRGPRs. The experiment was designed and performed by R.A. R.A. wrote the chapter, and A.J.L. and X.V.O. provided valuable input and edits.

Funding

This research was funded by a BOF funding of Ghent University (BOF/STA/202009/013 to A.J.L.).

Acknowledgment

We like to thank Dr. Wim Vanden Berghe (University of Antwerp, Belgium) for providing access to PerkinElmer Envision multimode plate reader.

Chapter 6

The neglected N-terminus of human Mas-related G protein-coupled receptors: could cysteine protease cathepsin-S activate them?

Rohit Arora[1,2], Geert Van Raemdonck[4], Jusal Quanico[4], Geert Baggerman[4], Roeland Buckinx[1], Dirk J. Snyders[2], Jean-Pierre Timmermans[1] and Alain J. Labro[1,2,3]

[1]Laboratory of Cell Biology and Histology, Department of Veterinary Sciences, University of Antwerp, 2610 Wilrijk, Belgium,

[2]Laboratory for Molecular, Cellular and Network Excitability, Department of Biomedical Sciences, University of Antwerp, 2610 Wilrijk, Belgium

[3]Department of Basic and Applied Medical Sciences, Ghent University, 9000 Ghent, Belgium

[4]Centre for Proteomics (CFP/CEPROMA), Department of Biology, Campus Groenenborger, University of Antwerp, Belgium

Chapter 6 Cathepsin-S activate MRGPRs

Abstract

Cathepsin-S(CTSS) is a thiol-containing cysteine protease found in endo-lysosomes and is known to participate in antigen processing and to mediate inflammation. The CTSS enzyme retains its activity over a broad pH range (from 2 to 9), making it a one-of-a-kind enzyme. Recent literature suggests that cysteine proteases activate PAR2 and some MRGPRs. Consistent with the prominent role of cysteine proteases in the activation of MRGPRs, we first performed an in-silico analysis of the N-terminus sequences of MRGPRD, MRGPRE, and MRGPRF. The analysis revealed that both MRGPRD and MRGPRF contain a consensus motif cleavage site for CTSS. Mass spectroscopy analysis confirmed the cleaving of synthetic N-terminus peptide of MRGPRD and MRGPRF by CTSS. To evaluate the cleavage of complete receptors expressed in HeLa cells, MRGPRD, MRGPRE, and MRGPRF were tagged at their N-terminus with Nanoluc luciferase. By assessing the bioluminescence activity of the collected supernatant after incubation with CTSS, the N-terminus cleavage of the receptors MRGPRD and MRGPRF was confirmed. In calcium imaging, receptor activation is indicated by the calcium-induced fluorescence flux in human MRGPRD and MRGPRF-transfected cells after CTSS treatment (preliminary results). These results are indicative for CTSS-linked activation mechanisms of MRGPRD and MRGPRF and are a possible step towards deorphanization of the human MRGPRF receptor.

Keywords: MRGPRs, MRGPRF, cysteine protease, cathepsin-S, calcium imaging

Chapter 6 Cathepsin-S activate MRGPRs

6.1 Introduction

Two percent of the human genome codes for proteolytic enzymes (proteases) or their inhibitors [288, 289]. Given the significant genetic investment, it is not surprising that protease are used physiologically to perform a variety of biologic functions. For example, proteases aid in food digestion and nutrient absorption. Their physiological role is further highlighted by their involvement in a variety of pathologies, including irritable bowel disease, neuropathic pain, arthritis, myocarditis, systemic muscle pain, and the healing process after surgery [290-293]. The proteases work by producing or processing molecules through proteolytic cleavage. The molecules generated or the proteolytic cleave itself can activate or deactivate effectors; in this way, proteases regulate cellular signaling in a multifaceted way [289].

It has been demonstrated that protease can activate GPCRs by cleaving the receptor's N-terminus directly or through the release of a tethered ligand peptide that is generated or unmasked by protease cleavage. In the early 1990s, it was discovered that serine proteases (such as thrombin and trypsin) activate the GPCR family member protease-activated receptor (PAR; the PAR family includes PAR1, PAR2, PAR3, and PAR4) [294, 295]. Furthermore, some adhesion family of GPCRs, known as ADGRs, are activated by a tethered ligand in a manner similar to PARs [296]. Some studies now suggest that cysteine proteases, such as cathepsins, can also activate GPCR in a similar manner to the serine proteases. For example, CTSS activates and evokes pain in a mouse model of inflammatory bowel disease via PAR2 activation [297]. Additionally, PAR2 activation by CTSS causes itch in humans [298, 299]. Similarly, CTSS activates mouse MrgprC11 and human MRGPRX2 [148] . Furthermore, Der p1, another cysteine protease and a major allergen from house dust mites, activates the human PAR2, MRGPRX1, as well as the mouse MrgprC11 [155].

The cysteine proteases contain a thiol group that has to be in the reduced form for autocatalytic activation as well as for catalytic activity. Thus, the cysteine proteases require a rather reducing environment to be physiologically active [148, 300]. The CTSS enzyme is expressed by a variety of inflammatory cell types, including lymphocytes, dendritic cells, macrophages, etc. The CTSS enzyme is stored in these cells and released when an appropriate signal is received by the inflammatory cells, this ensures site-specific release of the enzyme [301]. CTSS promotes homeostasis while also contributing to a variety of diseases, such as inflammation, lungs, cardiovascular disease, itch, and pain [302-308]. Therefore, we set out to discover cleavage sites on the N-terminus of MRGPRs in order to determine the CTSS-linked activation mechanism for MRGPRD, MRGPRE, and MRGPRF and, moreover, to deorphanize MRGPRE and MRGPRF.

6.2 Material and methods

6.2.1 Materials

DMEM (Cat# 41966029), FBS (Cat# 10270-106), penicillin-streptomycin, and Dulbecco's phosphate-buffered saline (DPBS; Cat# 14190169) were purchased from Gibco (Waltham, MA, USA). Cathepsin-S (Cat# BML-SE453-0010) was purchased from Enzo Life Sciences (NY, USA). E-64 protease inhibitor (Cat# 78432) was purchased from Thermo Fisher Scientific. 100 mm cell culture dishes (CELLSTAR; Cat# 664160) and 6 well plates were purchased from Greiner Bio-One (Frickenhausen, Germany). Nano-Glo Live cell substrate (Cat# N205A) was purchased from Promega (Madison, WI, USA). Synthetic DNA oligonucleotides were obtained from IDT (Coralville, IA, USA). Restriction enzymes were purchased from New England Biolabs (Ipswich, MA, USA). The plasmid miniprep or maxiprep kit was used to prepare the plasmids (Macherey-Nagel, Duren, Germany). The purification of PCR-amplified and gel-extracted restriction-digested products was done using a PCR/gel clean-up kit (Macherey-Nagel). Agar, LB broth (high salt), SOC medium, ampicillin and kanamycin were purchased from Sigma-Aldrich (St. Louis, MO, USA). XL2-Blue ultracompetent cells used for transformation were purchased from Stratagene (San Diego, CA, USA).

6.2.2 Preparation of NanoLuc-MRGPRs fusion cDNAs

A XhoI RE site was introduced at the C-terminus of EYFP by site-directed insertion PCR in the p-CMV/EYFP-N1 plasmid (Clontech, Palo Alto, CA, USA). The p-CMV/EYFP-XhoI-N1 plasmid was re-engineered by inserting annealed oligonucleotide (NheI-Flexi-Fwd: CTAGCAAGCTTACCGGTGGTGGTGGCAGTGAATTCAGATCTGTCGACGGTGGTGGAGGCAGT GGTGGAGGTGGCAGTGGATCCGAGCTCC, XhoI-Flexi-Rev: TCGAGGAGCTCGGATCCACT-GCCACCTCCACCACTGCCTCCACCACCGTCGACAGATCTGAATTCACTGCCACCACCACCGGTA AGCTTG) between NheI/XhoI RE sites to generate the flexi-linker plasmid p-CMV/GS, which has multiple cloning sites connected by a flexible linker of glycine and serine residues (GGGGSGGGGS). The gene sequences coding mOrange without start codon were PCR-amplified from p-mOrange-N1 (Addgene #54499) and inserted in-frame between BamHI/XhoI of pCMV-GS to generate the pCMV-GS-mOrange plasmid backbone. Subsequently, human MRGPRD (Cat# HsCD00080297), MRGPRE (Cat# HsCD00509189), MRGPRF (Cat# HsCD00509354) obtained from the DNASU plasmid repository [219] (Tempe, AZ, USA) and mouse MrgprC11 coding gene sequence were PCR-amplified using P*fu* DNA polymerase (Promega, Madison, WI, USA) were inserted in-frame between the EcoRI/SalI sites of the pCMV-GS-mOrange plasmid to generate the pCMV-MRGPRD-mOrange, pCMV-MRGPRE-mOrange, pCMV-MRGPRF-mOrange and pCMV-MrgprC11-mOrange plasmids. Furthermore, the gene sequences coding NanoLuc with start codon was PCR-amplified from p-NCS-Antares (Addgene #74279, Cambridge, MA, USA) and inserted in-frame between HindIII/EcoRI of pCMV-MRGPRD-

mOrange, pCMV-MRGPRE-mOrange, pCMV-MRGPRF-mOrange and pCMV-MrgprC11-mOrange plasmids to generate the pCMV-NLuc-MRGPRs-mOrange plasmids. All plasmid cDNA constructs were verified by Sanger sequencing. Unless stated otherwise, all products were used following the manufacturer's instructions.

6.2.3 Cell culture and NanoLuc release assay

HeLa cells were cultured in 100 mm dishes in a humidified incubator at 37°C with 5% CO_2 using DMEM supplemented with 10% FBS and 1% penicillin-streptomycin. In the 1.5 ml Eppendorf tube, 10 µg of DNA were diluted into 0.5 ml of DMEM, and in another Eppendorf tube 10 µl of Lipofectamine 2000 transfection reagent was diluted into 0.5 ml of DMEM and kept at room temperature for 5 min. Afterwards, reagents of both the tubes were mixed and incubated at room temperature for 20 min. HeLa cells were trypsinized, and 1x 10^6 cells were pelleted in a 15 ml tube by centrifugation at 300 rcf on 4°C for 5 min. The supernatant media was removed, and 1 ml of DMEM-Lipofectamine DNA mixture was added to 1.0x10^6 pelleted cells, mixed well and incubated for 20 min at room temperature with intermittent shaking. The cells were then seeded into a 100 mm cell culture plate containing 9 ml of DMEM (without serum). The media was gently removed 4 h after seeding, 10 ml of DMEM containing 10% serum was added, and the plates were returned to the incubator at 37°C with 5% CO_2. After 48 h of transfection, the cells were washed twice with PBS, scraped, and pelleted. Pelleted cells were resuspended in 300 µl PBS, and 50 µl of it was either incubated with 50 µl of PBS or 50 µl of CTSS at a final concentration 5 nM or 50 µl of CTSS (5 nM; Enzo Life Sciences Cat# BML-SE453-0010; Batch# 05011829) inactivated with 10 µM protease inhibitor E-64 or 50 µl of E-64 at final concentration of 10 µM for 15 min at 37°C. CTSS activity was stopped by adding protease inhibitor E-64 to each tube at final concentration of 20 µM. Cells were pelleted, and supernatants were collected. Bioluminescence assays were performed in triplicate with 10 µl of the supernatants according to the instructions of the manufacturer (Nano-Glo Live cell substrate; Promega, Madison, WI, USA) using IVIS imaging system.

6.2.4 Cathepsin-S digestion of the MRGPRs N-terminus peptide

The synthetic N-terminus peptides of human MRGPRs; MRGPRD (MNQTLNSSGTVESALNYSRGSTV; M.W. 2416), MRGPRE (MMEPREAGQHVGAAN; M.W. 1599) and MRGPRF (MAGNCSWEAHPGNRNKMCPGLSEAPELYSRGFLTIEQIAML; M.W. 4525) were purchased form CASLO ApS (Lyngby, Denmark). The peptides were dissolved in 50 mM Tris, pH 7.0, 0.1 M NaCl and 0.1 mM EDTA to obtain a 100 mM final concentration. 50 µl of peptide solution was incubated with 0.25 µM CTSS (Enzo Life Sciences Cat# BML-SE453-0010; Batch# 05011829) at 37°C for 15 min. The reaction

samples were analysed using MALDI-TOF MS by the Centre for Proteomics (CEPROMA), University of Antwerpen.

6.2.5 Data and Statistical Analysis

Data analysis and graphs were prepared using Microsoft Excel and GraphPad Prism 6. All values are represented as mean ± s.e.m. Statistical significance was determined using unpaired two tailed student's t-test. P values of *p≤0.05, **p≤0.01, ***p≤0.001 and ****p≤0.0001 were considered significant and p>0.05 was considered non-significant (ns).

6.3 Results

6.3.1 In-silico analysis of cathepsin-S site on N-terminus of MRGPRs

The cysteine proteases are primarily stored by the endosomes and lysosomes of immune cells and plays an important role in innate and adaptive immune responses [304, 309]. CTSS is expressed by macrophages and has been found to be upregulated in cardiovascular and inflammatory bowel disease conditions [297, 308]. Most cysteine proteases are autocatalytically activated at low pH in a reducing environment and can work in a wide pH range [310]. It has been proposed that cysteine proteases activate PAR2 and some MRGPRs [148, 155, 297, 299, 311]. The CTSS cleavage site and mechanism of CTSS-mediated activation for MRGPRD, MRGPRE, and MRGPRF are unknown. First, an in-silico analysis was performed using the MEROPS 2.0 database on the N-terminus sequences of MRGPRD, MRGPRE, and MRGPRF. As per the MEROPS database, the most preferred amino acids for cleavage by CTSS were leucine at position 2, and serine and glycine were the preferred amino acids at position 1, including but not limited to serine and glycine. Interestingly, the analysis indicated that MRGPRD and MRGPRF have consensus motifs for CTSS recognition at L5-S7 and L21-E23, respectively (Figure 6.1 A and C). The consensus motifs for CTSS recognition were not found on the MRGPRE N-terminus sequence (Figure 6.1 B).

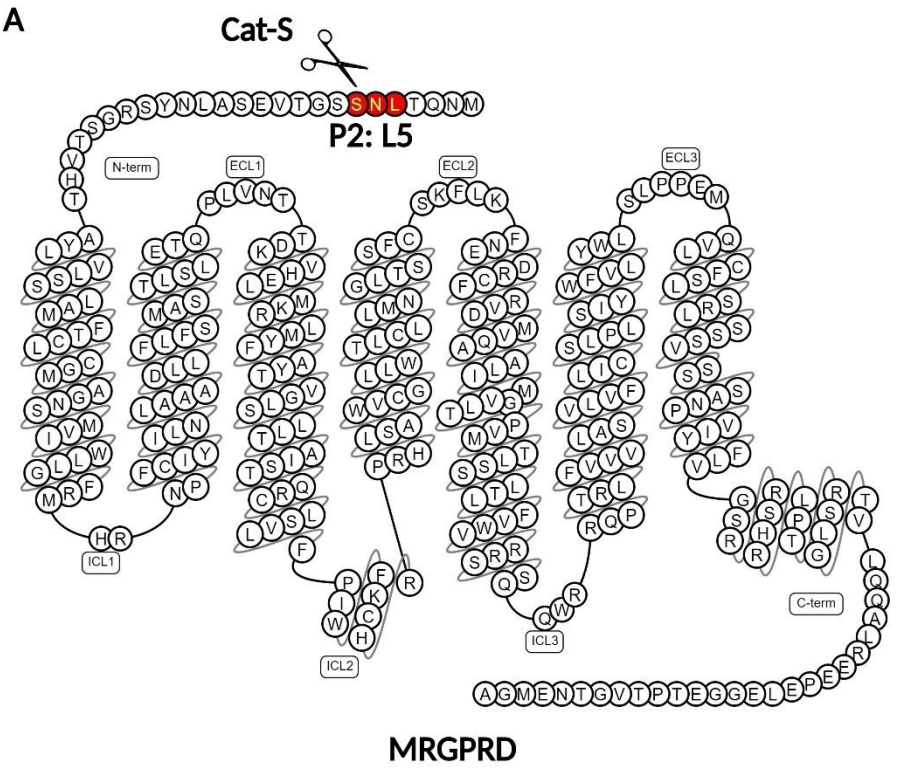
A
Cat-S
P2: L5
N-term
ECL1
ECL2
ECL3
ICL1
ICL2
ICL3
C-term
MRGPRD
B
No Cat-S cleavage site
N-term
ECL1
ECL2
ECL3
ICL1
ICL2
ICL3
C-term
MRGPRE

Continued...

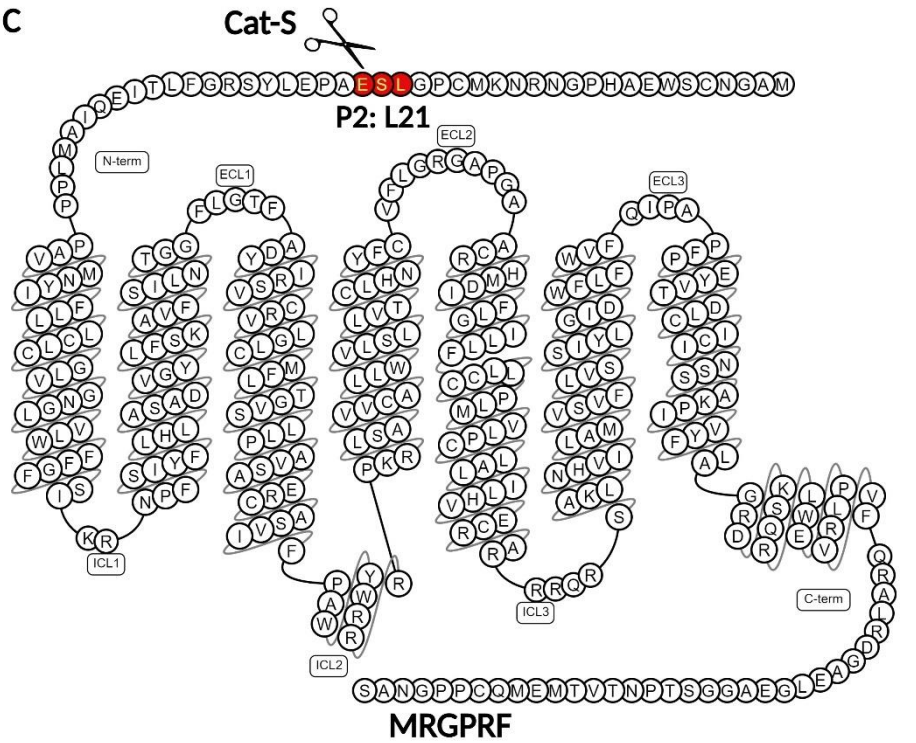

Figure 6.1. Predicated cathepsin-S cleavage site on N-terminus of MRGPRs. The N-terminus and TM1 of MRGPRD (A), MRGPRE (B), and MRGPRF (C) are represented. In-silico analysis was performed using the MEROPS 2.0 database on the N-terminus sequences of MRGPRD, MRGPRE, and MRGPRF. The putative cleavage substrate for CTSS (Cat-S) are marked in red. The N-terminus and TM1 are from serpentine diagrams obtained from https://gpcrdb.org/ and figure created with BioRender.com.

6.3.2 Cathepsin-S cleaves the N-terminus of MRGPRD and MRGPRF

Following in silico analysis, we investigated whether proteases could cleave the extracellular N-terminus of receptors in vitro. To this end, HeLa cells transiently expressing MRGPRs constructs tagged with NanoLuc at their N-terminus were treated with CTSS. The N-terminus cleavage of the receptor was assessed by measuring the luminescence level in the supernatant (Figure 6.2 A). As predicted, CTSS induced significant cleavage of the MRGPRD and MRGPRF N-terminus as determined by measurement of luminescence (Figures 6.2 B and D), whereas no cleavage of the N-terminus was observed from MRGPRE-expressing cells (Figure 6.2 C). In samples where CTSS was pretreated with the protease inhibitor E-64, no protease-mediated cleavage of the N-terminus of MRGPRD and MRGPRF was observed, confirming the role of CTSS in receptor N-terminus cleavage. The mouse MrgprC11, which has been reported to be cleaved by CTSS, did not show significant cleavage of the N-terminus (Figure 6.2 E) [148].

However this could be attributed to decreased receptor expression in human cells or receptor misfolding, resulting in receptors not being localized at the cell membrane.

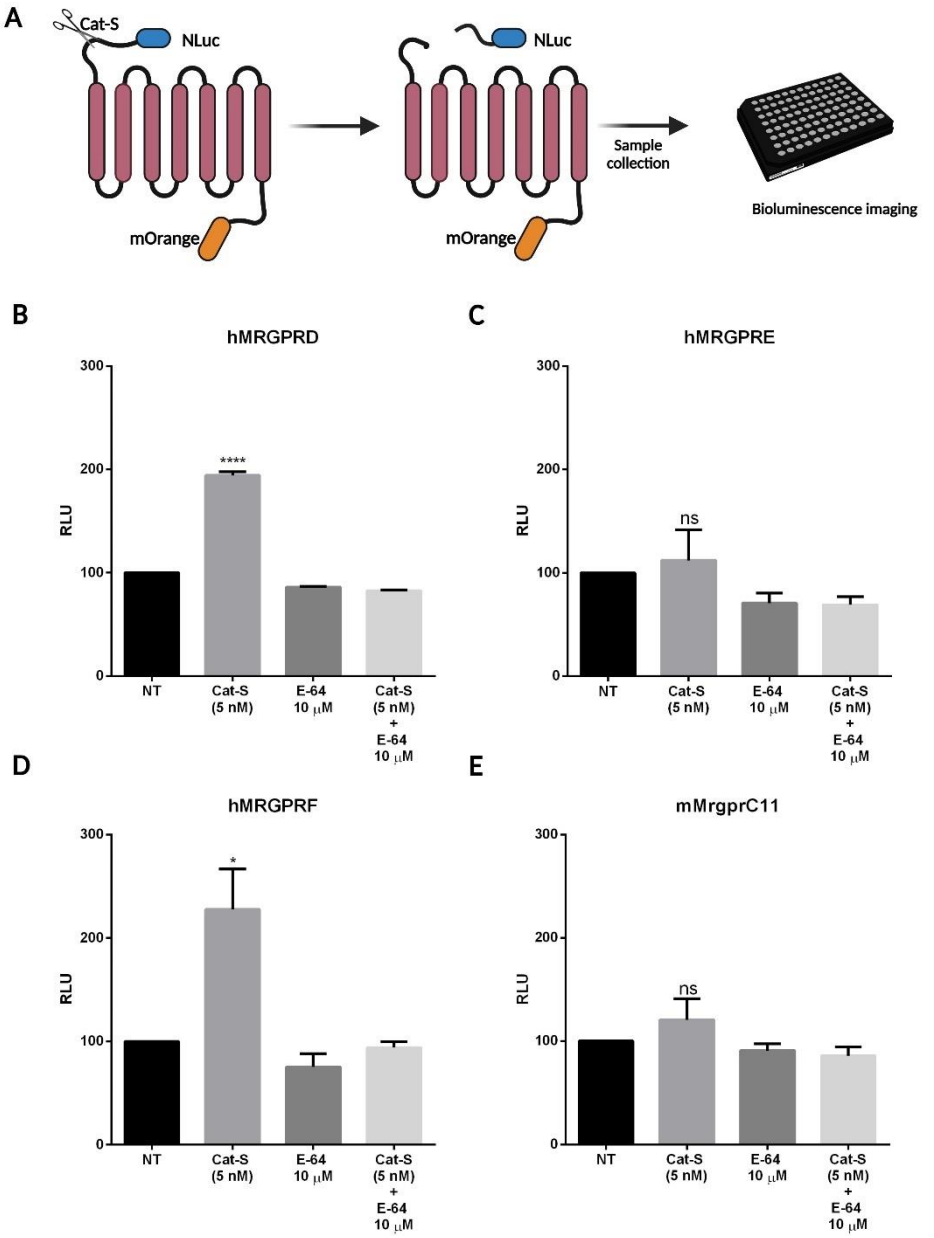

Figure 6.2. Cathepsin-S cleaves the N-terminus MRGPRs. (A) A schematic representation of the assay design. MRGPRs with NanoLuc on the N-terminus and mOrange on the C-terminus; CTSS (Cat-S) cleaves the receptor's N-terminus. BioRender.com was used to create this figure **(B)** HeLa cells transiently expressing pCMV-NLuc-MRGPRs were treated with CTSS (5 nM; Enzo Life Sciences Cat# BML-SE453-0010; Batch# 05011829). The supernatant collected after treatments was analyzed for bioluminescence. The data are presented as mean±s.e.m of three independent

experiments. P values of *p≤0.05, **p≤0.01, ***p≤0.001 and ****p≤0.0001 were considered significant and p>0.05 was considered non-significant (ns). Figure created with BioRender.com.

6.3.3 Cathepsin-S cleaves the synthetic N-terminus peptides of MRGPRs

To determine the specific protease cleavage sites, peptides corresponding to the N-terminus residues of MRGPRD (MNQTLNSSGTVESALNYSRGSTV), MRGPRE (MMEPREAGQHVGAAN) and MRGPRF (MAGNCSWEAHPGNRNKMCPGLSEAPELYSRGFL-TIEQIAML) were synthesized and subjected to CTSS. The peptides were incubated with the CTSS before being analyzed by mass spectrometry (MALDI-TOF) for peptide cleavage. For the MRGPRD N-terminus synthetic peptide, the CTSS cleaves between S7 and N6 with L5 at the P2 position. Similarly, the cleavage of MRGPRF occurred between E23 and S22, with L21 at the P2 position (Table 6.1, fragments generated are shown). There was no cleavage in the MRGPRE peptide, therefore, no new fragment was observed.

Table 6.1. MALDI-TOF mass spectroscopy data of cathepsin-S cleaved human MRGPRD and MRGPRF N-terminus peptides

MRGPRD	MRGPRF
MNQTLN	MAGNCSWEAHPGNRNKMCPGLS
NSSGTVESALNYSRGSTV	EAHPGNRNKMCPGLS
SALNYSRGSTV	WEAHPGNRNKMCPGLS
	EAPELYSRGFLT

6.4 Discussion

Cysteine cathepsins were formerly thought to be important for non-specific bulk proteolysis in the lysosomal system [304]. This perception has since sharply altered, and cathepsins are now recognized as actors in a wide range of (patho)physiological processes, including those involved in conditions like cancer, rheumatoid arthritis, and several inflammatory disorders [312, 313]. The serine proteases (trypsin and thrombin) were the main activators of PAR receptors; however, the literature now suggests that non-serine proteases are now able to activate and regulate the PARs, as well as MRGPRs [148, 155, 297, 311].

In this study, we show that CTSS cleaves the synthetic N-terminus of MRGPRD and MRGPRF receptors, but as such, no cleavage was observed for MRGPRE (Table 6.1). It was confirmed that the leucine at the P2 position is the preferred amino acid for CTSS-mediated cleavage of the N-terminus peptides, and this is consistent with the MEROPS 2.0 database (Figure 6.1). Furthermore, CTSS mediated cleavage of the N-terminus of

MRGPRD and MRGPRF receptors released the NanoLuc luciferase tagged to the N-terminus of the receptor (Figure 6.2), indicating that it may function similarly in in vivo. Although we tried to further delineate the activation of receptors using calcium imaging (Figure S6.2), after initial success and due to changes in the batch of enzyme obtained from the supplier, the results were variable, and thus we were not able to draw concrete conclusions. Additionally, we also observed cleavage of the N-terminus of β1 adrenergic receptor (β1-AR) and β2 adrenergic receptor (β2-AR) receptors by CTSS, which released the NanoLuc luciferase tagged to the N-terminus of the receptors, indicating CTSS might also activate and regulate β1-AR and β2-AR receptors (Figure S6.1).

Although no functional role could be ascribed yet, we hypothesize that cleavage of the N-terminus of MRGPRD, MRGPRF, β1-AR and β2-AR may result in conformational changes that may change the exposure of cytoplasmic domains relevant to signal transduction and regulate downstream signaling pathways. Alternatively, a peptide generated by N-terminus cleavage can itself activate the receptor or transactivate (paracrine) another receptor. Proteolytic activation of receptors is irreversible, and recent research suggests that cleavage of the N-terminus improves recycling of receptors to the membrane, or receptors are retained in endosomes, allowing them to associate with signaling partners and form "signalosomes" that generate signals in subcellular compartments [314-316].

In summary, the data indicate CTSS-mediated cleavage of the N-terminus of MRGPRD, MRGPRF, β1-AR and β2-AR, but not MRGPRE. More research is needed to determine how CTSS-mediated cleavage affects their dynamics (conformational change, internalization, and trafficking), as well as how G proteins and β-arrestin mediate cellular signaling. Consequently, these observations are a first step towards alternative mechanisms of activation for human MRGPRD, β1-AR and β2-AR and deorphanization of human MRGPRF and warrant the need for further investigations to determine whether cleavage of the extracellular N-terminus of MRGPRD, MRGPRF, β1-AR and β2-AR contributes to receptor activation or regulation, given the role of MRGPRD, β1-AR and β2-AR in cardiovascular biology [186, 218, 317]. Continuous scientific endeavors are needed to understand how these receptors are activated and subsequently control cellular signaling, as well as if they can be targeted for therapeutic purposes.

6.5 Supplementary materials and figures

6.5.1 Cathepsin-S cleaves the N-terminus of human β1-AR and β2-AR

The human β1-AR (ADRB1-Tango; Cat# 66219) and β2-AR (ADRB2-Tango; Cat# 66220) were obtained from the Addgene (Cambridge, MA, USA) [256]. The gene sequence was PCR-amplified using Pfu DNA polymerase (Promega, Madison, WI, USA) were inserted in-frame between the EcoRI/SalI sites of the pCMV-GS-mOrange plasmid to generate

the pCMV-β1-AR-mOrange and pCMV-β2-AR-mOrange plasmids. Furthermore, the gene sequences coding NanoLuc with start codon was PCR-amplified from p-NCS-Antares (Addgene #74279, Cambridge, MA, USA) and inserted in-frame between HindIII/EcoRI of pCMV-β1-AR-mOrange and pCMV-β2-AR-mOrange to generate the pCMV-NLuc-β1-AR-mOrange and pCMV-NLuc-β2-AR-mOrange plasmids. All plasmid cDNA constructs were verified by Sanger sequencing. Unless stated otherwise, all products were used following the manufacturer's instructions.

The NanoLuc release assay was performed as described in Section 6.3.2. Briefly, HeLa cells transiently expressing human β1-AR and β2-AR, tagged with NanoLuc at their N-terminus were treated with CTSS. The N-terminus cleavage of the receptor was assessed by measuring the luminescence level in the supernatant (Figure S6.1). As predicted, CTSS induced significant cleavage of the β1-AR and β2-AR [148] N-terminus as determined by measurement of luminescence. In the sample, where CTSS was pretreated with the protease inhibitor E-64, no cleavage of the N-terminus of β1-AR and β2-AR was observed, confirming the specificity of CTSS in receptor N-terminus cleavage.

A

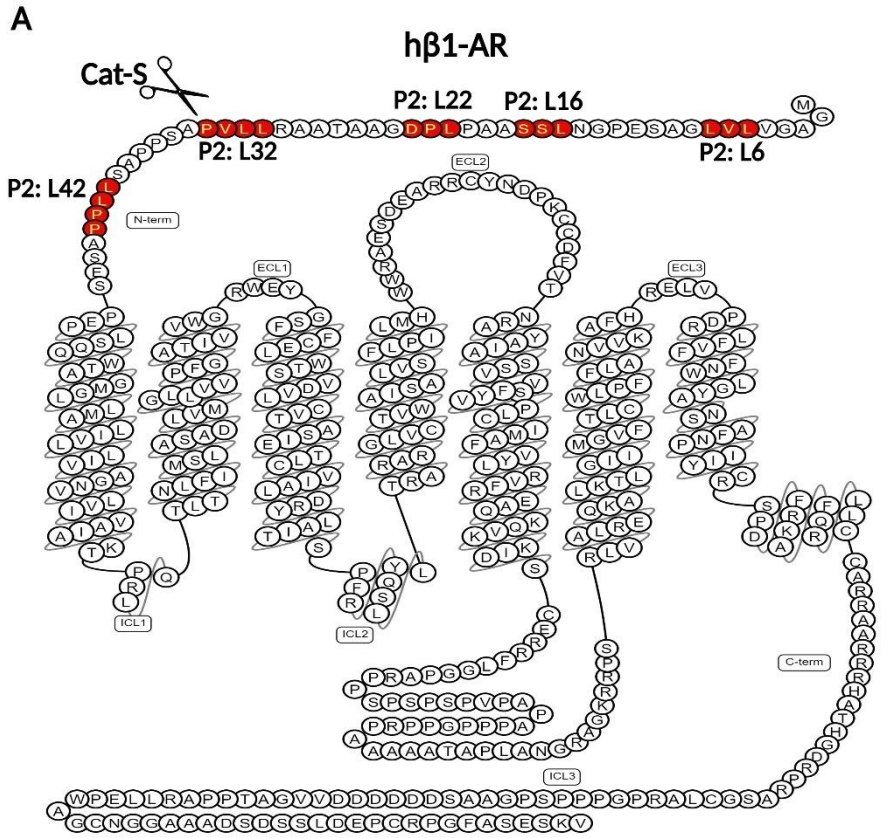

B

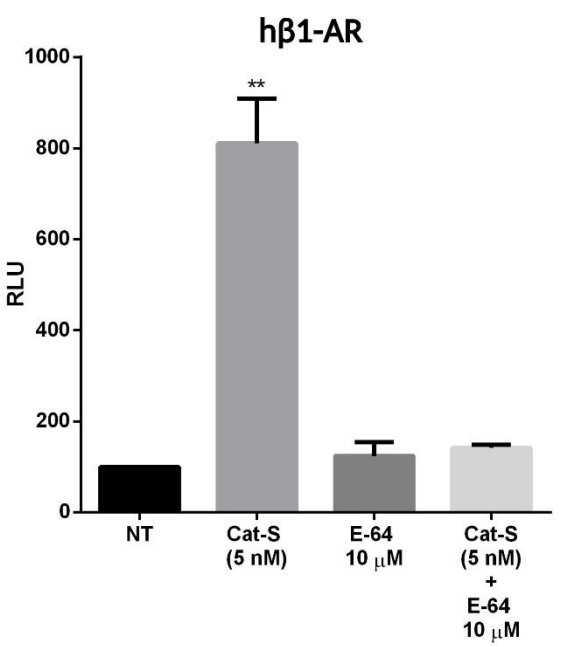

Continued...

C

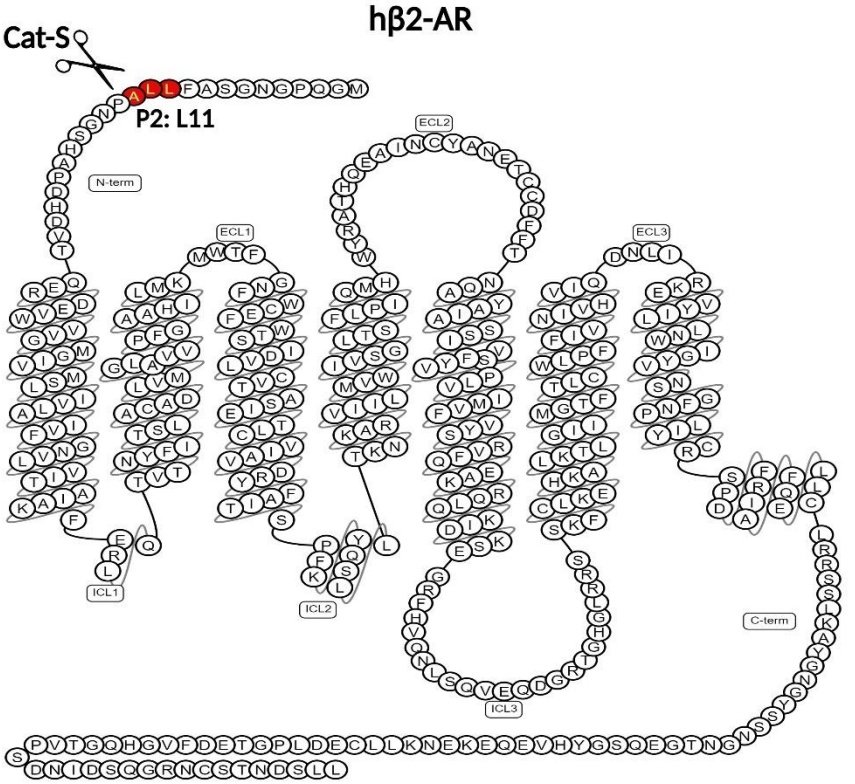
hβ2-AR
Cat-S
P2: L11
N-term
ECL1
ECL2
ECL3
ICL1
ICL2
ICL3
C-term

D

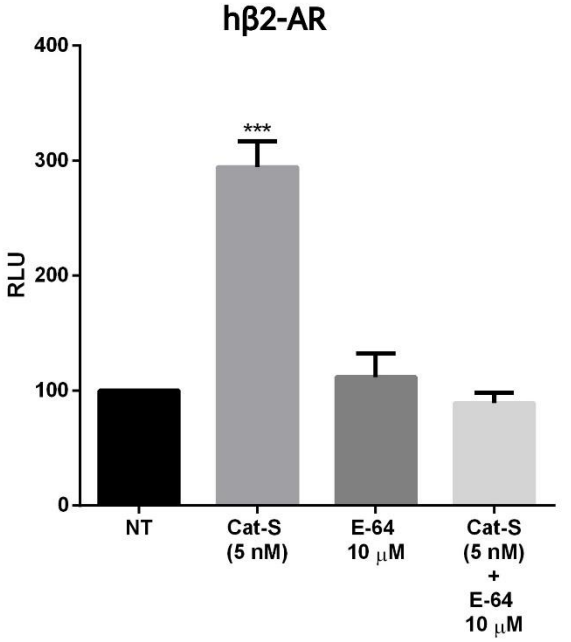
hβ2-AR
RLU
400
300
200
100
0
***
NT
Cat-S (5 nM)
E-64 10 μM
Cat-S (5 nM) + E-64 10 μM

Figure S6.1. Cleavage of the N-terminus of human β1-AR and β2-AR by cathepsin-S. Serpentine diagrams of human β1-AR (A) and β2-AR (C) are represented. In-silico analysis was performed using the MEROPS 2.0 database on the N-terminus sequences of β1-AR and β2-AR. The cleavage substrate for CTSS (Cat-S) on the β1-AR and β2-AR N-terminus is marked in red. HeLa cells transiently expressing pCMV-NLuc-β1AR-mOr and pCMV-β2-AR-mOr were treated with CTSS (5 nM; Enzo Life Sciences Cat# BML-SE453-0010; Batch# 05011829). The supernatant collected after treatments was analyzed for bioluminescence. The data are presented as mean±s.e.m of three independent experiments. P values of *p≤0.05, **p≤0.01, ***p≤0.001 and ****p≤0.0001 were considered significant and p>0.05 was considered non-significant (ns). Serpentine diagrams were prepared using https://gpcrdb.org/ and figure created with BioRender.com.

6.5.2 Cysteine protease cathepsin-S activate MRGPRs

To access the receptor activation by CTSS, live cell calcium imaging was performed. Briefly, HeLa cells were cultured in DMEM with high glucose (4.5g/L) and L-glutamine (Lonza, Basel, Switzerland) supplemented with 10% FBS (Gibco, Waltham, MA, USA) and 1% penicillin-streptomycin (Gibco), at 37°C under 5% CO_2. Cells were harvested with 0.25% trypsin-EDTA solution (Gibco) and re-seeded in a 12-well plate (Nalgene Nunc, Rochester, NY, USA) at 1.2 10^5 cells/well. Approximately 16 h after seeding, cells were transfected with 700 ng of plasmid cDNA (pCMV-MRGPRD or pCMV-MRGPRE, or p-CMV-MRGPRF) mixed with 4 µl of Lipofectamine 2000 (Invitrogen, Waltham, MA, USA) in total of 1 ml of DMEM. After 4 h, DMEM was replaced by culture medium (with 10% FBS). For co-transfections, an equal amount of plasmid cDNA was transfected (i.e., ~700 ng of pCMV-MRGPRD and ~70 ng pCMV-MRGPRF). Cells were harvested 24 h after transfection with 0.25% trypsin-EDTA solution (Gibco) and re-seeded in black 96-well plates (Cat# 655090; Greiner Bio One) at 15,000 cells/well suspended in 100 µl of culture medium. Re-seeded cells were maintained at 37°C under 5% CO_2 for 14–16 h and subsequently used for live cell calcium imaging.

The spent medium was aspirated after 16 h of seeding, and cells were washed twice with 20 mM HEPES-buffered Hank's balanced Salt Solution (HBSS) (1M HEPES, Cat# 12630080; HBSS, calcium, magnesium, no phenol red, Cat# 14025092 were from Gibco). The 100 µl of complete DMEM (with 10% FBS) containing 1 µM of Fluo-4 (an intensiometric calcium indicator; Fluo-4 AM Cat# F23917, Invitrogen) were added to each well and left at room temperature for 20 min. Following the loading of cells with Fluo-4, the medium was aspirated, the cells were washed once with 100 µl of 20 mM HEPES-buffered HBSS, and 90 µl of 20 mM HEPES buffered HBSS was added, and the cells were used immediately for calcium imaging. Calcium imaging was performed using a PerkinElmer Ultraview Vox spinning disc confocal microscope. The baseline fluorescence was recorded for 1 min before the addition of 10 µl of CTSS (final concentration of CTSS: 10 nM/well; Enzo Life Sciences Cat# BML-SE453-0010, Batch#

12011569). Images were taken every 0.5 seconds, and recordings were made for a total of 5 min. The Image J software was used for image analysis. HeLa cells transfected with MRGPRD and MRGPRF following treatment with CTSS elicit the calcium response (Figure S6.2 B and D), whereas no response was observed in MRGPRE-expressing cells (Figure S6.2 C) or non-transfected HeLa cells (Figure S6.2 A).

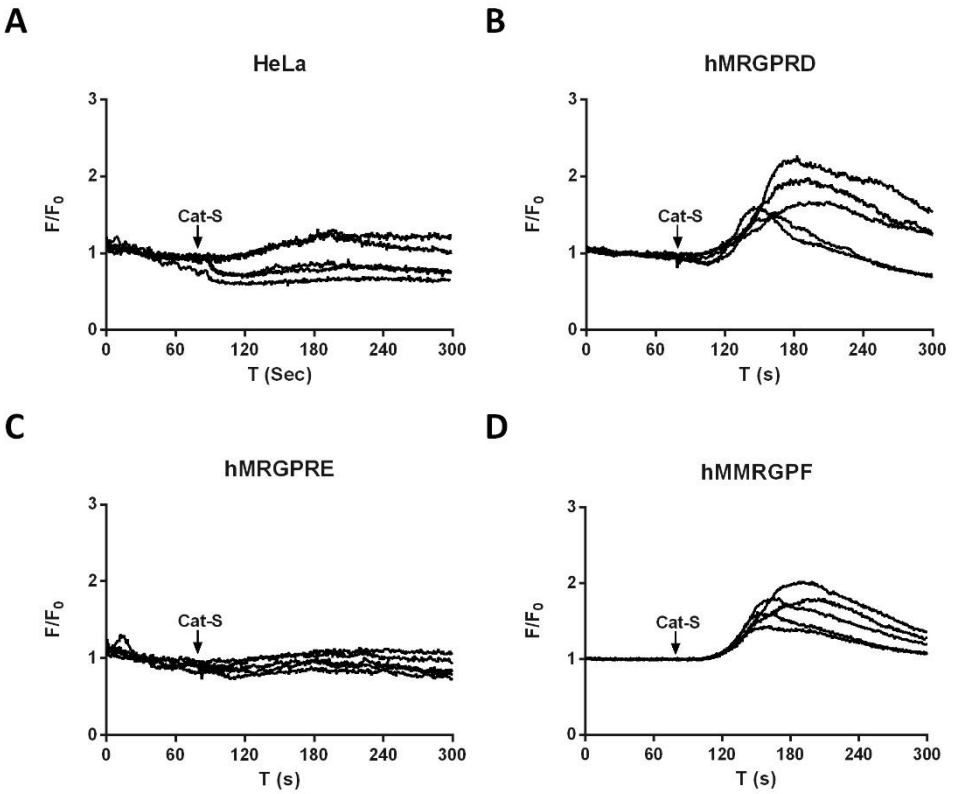

Figure S6.2. Cathepsin-S activates human MRGPRs in heterologous cells. Calcium imaging in non-transfected HeLa cells (A) and transfected with human MRGPRD (B), MRGPRE (C), and MRGPRF (D) following treatment with CTSS (Cat-S; 10 nM; Enzo Life Sciences Cat# BML-SE453-0010; Batch# 12011569). Fluo-4 based averaged fluorescence traces on CTSS treatment are shown by dashed lines. Each dashed line represents response from a single cell.

Contributions

R.A conceived the idea to deorphanize MRGPRs using cathepsin-S, proposal was approved by R.B., A.J.L. and J-P.T. The experiments were designed and performed by R.A.; R.A. analysed the data; MS data was acquired and analysed by G.V.R., J.Q. and G.B. R.A. wrote the chapter and A.J.L. and X.V.O. provided valuable input and edits.

Funding

This research was funded by a grant of the Flemish Foundation for Scientific Research (FWO G019314N to J-P.T.); and by a grant of the University of Antwerp, Belgium (DOCPRO1 BOF 34867 to R.A. and J.-P.T.); BOF funding of Ghent University (BOF/STA/202009/013 to A.J.L.).

Acknowledgments

We would like to thank the Laboratory for Microbiology, Parasitology and Hygiene (University of Antwerp, Belgium) for providing access to the PerkinElmer IVIS Spectrum.

Chapter 7

Identification of heteromeric interactions of human Mas-related G protein-coupled receptors

Rohit Arora[1,2], Samuel Van Remoortel[1], Alain J. Labro[2,3], Dirk J. Snyders[2], Roeland Buckinx[1] and Jean-Pierre Timmermans[1].

[1]Laboratory of Cell Biology and Histology, Department of Veterinary Sciences, University of Antwerp, 2610 Antwerp, Belgium.

[2]Laboratory for Molecular, Cellular and Network Excitability, University of Antwerp, 2610 Antwerp, Belgium.

[3]Department of Basic and Applied Medical Sciences, Ghent University, 9000 Ghent, Belgium

Chapter 7 MRGPRs oligomerization

Abstract

GPCRs can interact to create hetero-oligomer and homo-oligomer, or higher-order structures. Specifically, heteromerization affects how receptors function. Here we reveal hitherto undiscovered heteromeric interactions between human MRGPRs using biophysical and biochemical techniques. Split-NanoLuc-based luciferase complementation (LC), bioluminescence resonance energy transfer (BRET; NanoLuc-mOrange), and co-immunoprecipitation (Co-IP) assays were employed to screen for heteromeric interactions between human MRGPRD, MRGPRE, and MRGPRF. The results of LC and BRET suggested a heteromeric interaction between MRGPRD and MRGPRF, but Co-IP could not confirm this. While Co-IP revealed an interaction between MRGPRD and MRGPRE, neither the LC assay nor the BRET assay detected it. On the other hand, heteromeric interactions between MRGPRE and MRGPRF were unambiguously detected with LC, BRET, and Co-IP techniques. Our results demonstrate the use of a split-NanoLuc-based LC (NanoBiT) approach for GPCR oligomerization studies, which could be adapted for high-throughput screening of oligomerizations.

Keywords: GPCR, oligomerization, heteromerization, luciferase complementation, NanoBiT, BRET, Co-immunoprecipitation.

Chapter 7 MRGPRs oligomerization

7.1 Introduction

GPCRs comprise the largest, most versatile, and most dynamic superfamily of membrane receptors. They are widely involved in the transduction of various extracellular stimuli to regulate cellular signaling [235, 318]. While GPCRs have long been assumed to exist and function as monomers, several studies over the last two decades have revealed oligomerization and crosstalk between GPCRs [319-321]. It is now well accepted that the glutamate family of GPCRs, such as GABAB and metabotropic glutamate (mGlu) receptors, are obligate hetero-oligomers, which are required for receptor activation, trafficking, and modulation of intracellular signaling pathways [322, 323]. Similarly, heteromerization has been demonstrated for multiple members of the rhodopsin family of GPCRs, including β-ARs, opioid receptors, melatonin receptors, dopamine receptors, angiotensin AT1, and Bradykinin B2, each of which has a distinct pharmacological, signal transduction, and trafficking profile when compared to their monomeric receptors [321, 324, 325]. Although oligomerization has also been reported in a couple of in vivo studies correlating with the in vitro data [326-328], it should be noted that the majority of this evidence comes from studies using biochemical and biophysical tools to investigate the ectopic expression of GPCRs in heterologous cells [329-331].

The phylogenetic analysis revealed more than 75% sequence similarity between the human and rodent receptors D, E, and F, respectively. Given that rat MrgprD and MrgprE have been shown to form heterodimers and modulate MrgprD trafficking and signaling [198], and since the human MRGPRs have not been studied thus far, we set out to investigate the heteromerization of human MRGPRD, MRGPRE, and MRGPRF and, if they interact, whether that could alter the signaling profiles of the interacting receptors. To assess the heteromeric interactions of the selected MRGPRs, luciferase complementation (LC)-based NanoLuc binary technology (NanoBiT; Promega) was employed [332]. NanoBiT assay was validated by comparison with proximity-dependent assays based on resonance energy transfer (RET), such as bioluminescence resonance energy transfer (BRET) [333, 334], and lastly, the heteromerization of MRGPRs was assessed by co-immunoprecipitation [335].

7.2 Materials and methods

7.2.1 Materials

Synthetic DNA oligonucleotides were obtained from Eurogentec (Seraing, Belgium) or IDT (Coralville, IA, USA). Plasmid preparations were performed using either the plasmid miniprep or maxiprep kit (Macherey-Nagel, Duren, Germany). A PCR/gel clean-up kit was used to purify PCR-amplified and gel-extracted restriction digested products

(Macherey-Nagel). Agar, LB broth (high salt), SOC medium, ampicillin, kanamycin, and spectinomycin were purchased from Sigma-Aldrich (St. Louis, MO, USA). XL2-Blue ultracompetent cells used for transformation were purchased from Stratagene (San Diego, CA, USA). All plasmid cDNA constructs were verified by Sanger sequencing. Unless stated otherwise, all products were used following the manufacturer's instructions.

7.2.2 Cell culture and transfections

HeLa cells were cultured in DMEM with high glucose (4.5g/L) and L-glutamine (Lonza, Basel, Switzerland) supplemented with 10% FBS (Gibco, Waltham, MA, USA) and 1% Penicillin-Streptomycin (Gibco), at 37°C under 5% CO_2. For NanoBiT and NanoLuc-BRET assays, $1.2x10^5$ cells/well were seeded in a 12-well plate (Nalgene Nunc, Rochester, NY, USA) and transfected after 16h. To each well total of 1.5mg plasmid cDNA mixed with 4 ml Lipofectamine 2000 (Invitrogen, Waltham, MA, USA) in 1 ml DMEM was added, after 4h DMEM was replaced by culture medium (with 10% FBS). For co-transfections, an equal amount of plasmid cDNA was transfected (i.e., ~750ng of each receptor plasmid). When a single receptor was transfected (for example MRGPR-D-LgBiT alone), total amount of cDNA transfected was kept constant by adding 750 ng of empty p-BiT1.1-C[pHSVTK-SmBiT] (for the NanoBiT assay) or p-CMV/GS plasmids (for the NanoLuc-BRET assay) to the transfection mixture. Twenty-four hours post-transfection, cells were harvested using 0.25% trypsin-EDTA solution (Gibco) and re-seeded at 20,000 and 10,000 cells/well suspended in 100 µl of culture medium, in black 96-well plates (Cat#655090; Greiner Bio One) for the NanoBiT assay and BRET assay, respectively. Re-seeded cells were maintained at 37°C under 5% CO_2 for 14-16h and subsequently used for NanoBiT and BRET assay imaging.

7.2.3 MRGPR NanoBiT plasmid library construction and assay

MRGPRs coding gene sequences were PCR-amplified from human MRGPRD (Cat #HsCD00080297), MRGPRE (Cat# HsCD00509189) and MRGPRF (Cat# HsCD00509354) obtained from the DNASU plasmid repository (Tempe, AZ, USA)[219] using P*fu* DNA polymerase (Promega, Madison, WI, USA). The amplified PCR fragments were digested with the restriction enzymes EcoRI/XhoI (New England Biolabs, Ipswich, MA, USA) and ligated by T4 DNA ligase (New England Biolabs) in-frame into p-BiT1.1-C[pHSVTK-LgBiT] and p-BiT2.1[pHSVTK-SmBiT] (Promega), to generate the MRGPR NanoBiT plasmid library (C-terminus of MRGPR linked to the N-terminus end of LgBiT or SmBiT). To express LgBiT and SmBiT independently, a start codon was introduced at the N-terminus beginning of LgBiT and SmBiT by site-directed insertion PCR as in these plasmids (designed for creating fused proteins), the start codon was not present. The generated

plasmids were used for transfection of cells for the NanoBiT MRGPR heteromerization assay.

Using an IVIS Spectrum imaging system (PerkinElmer, Waltham, MA, USA), the cells were imaged 2 min after the addition of 50 µl substrate (1 µl Furimazine diluted in 1000 µl of culture medium). All scans were performed in luminescence mode (open lens) for 30 s and expressed as photon/sec/cm2/steradian (p/s/cm2/sr). Signal intensity was quantified by drawing regions of interest (ROIs) around each well of a 96-well plate using Living Image software (version 4.3.1). Bioluminescence intensity was normalized to the luminescence of co-transfecting LgBiT and SmBiT monomers (luminescence originating from random LgBiT-SmBiT association), and data were expressed as relative luminescence units (RLU).

7.2.4 MRGPR NanoLuc-BRET plasmid library construction and assay

A XhoI RE site was introduced at the C-terminus of EYFP by site-directed insertion PCR in the p-CMV/EYFP-N1 plasmid (Clontech, Palo Alto, CA, USA). The p-CMV/EYFP-XhoI-N1 plasmid was re-engineered by inserting an annealed oligonucleotide (IDT) between NheI/XhoI RE sites to generate the flexi-linker plasmid p-CMV-GS, which has multiple cloning sites connected by a flexible linker of glycine and serine residues (GGGGSGGGGS). The gene sequences coding for NanoLuc and mOrange with or without a start codon were PCR-amplified from p-NCS-Antares (Addgene Cat#74279, Cambridge, MA, USA) and p-mOrange-N1 (Addgene Cat#54499) and inserted in-frame between BamHI/XhoI of p-CMV-GS to generate the p-CMV-GS-NLuc (donor) and pCMV-GS-mOrange (acceptor) plasmid backbones. Subsequently, PCR-amplified MRGPRs were inserted in-frame between the EcoRI/SalI sites of the p-CMV-GS-NLuc and pCMV-GS-mOrange plasmids to generate the MRGPR NanoLuc-BRET plasmid library (C-terminus of MRGPR linked to the N-terminus of NanoLuc or mOrange). The control BRET vector was made by inserting PCR-amplified NLuc in-frame into EcoRI/SalI digested pCMV-GS-mOrange to yield pCMV-NLuc-GS-mOrange (the C-terminus of NLuc is linked to the N-terminus of mOrange). These plasmids were used for transfection of cells for the NanoLuc-BRET MRGPRs heteromerization assay as described in Section 7.2.2.

For the NanoLuc-BRET MRGPR heteromerization assay, cells were imaged immediately after addition of 50 µl substrate (1 µl Furimazine diluted in 1000 µl culture medium) by an IVIS Spectrum imaging system using appropriate donor (500 ± 20 nm) and acceptor (560 ± 20 nm) band-pass filters, with 1 s acquisition at each filter. The donor and acceptor filter signal intensities were quantified for each well using Living Image Software. The data obtained were expressed as the net BRET ratio and calculated as per equations 1 and 2 [336].

$$\text{Net BRET ratio} = \frac{BL_{\,emission}\,(Acceptor\ filter\,)}{BL_{\,emission}\,(Donor\ filter\,)} - Cf \qquad (1)$$

$$Cf = \frac{BL_{\,emission}\,(Acceptor\ filter)_{donor-only}}{BL_{\,emission}\ \ (Donor\ filter)_{donor-only}} \qquad (2)$$

As per the above equation, bioluminescence emission (BL emission) is the average radiance recorded at the acceptor and donor filters, when acceptor and donor are co-expressed (eq. 1); the correction factor 'C_f' represents the BRET signal from donor-only expressing cells (eq. 2) and hence accounts for the correction of donor-emission bleed-through in the acceptor filter. The net BRET ratios were calculated as previously described and multiplied by 1000 to give milli BRET units (mBU).

7.2.5 Co-immunoprecipitation of MRGPRs

For Co-IP experiments, the MRGPR genes were genetically tagged at their C-terminus with either a human influenza hemagglutinin (HA; YPYDVPDYA) or a c-myc (EQKLISEEDL) tag, i.e., tags were introduced just before the STOP codon. HeLa cells were cultured in 75 cm^2 culture flasks (Greiner Bio One) and transfected with ~5 µg of cmyc- and HA-tagged plasmids each (at a 1:1 molar ratio) using Lipofectamine 2000 (Invitrogen). Forty-eight hours post-transfection, cells were washed three times with ice-cold 1x Dulbecco's phosphate buffer saline (DPBS) and then scraped gently with 10 ml of ice-cold 1x DPBS using cell scrapers (Cat# 353086; BD Falcon, Franklin Lakes, NJ, USA). Collected cells were pelleted and dissolved in 250 µl ice-cold Pierce Lysis buffer (25mM Tris, 150 mM NaCl, 1 mM EDTA, 1% NP-40, 5% glycerol), supplemented with pierce protease inhibitor (Cat# 88666; Thermo Fisher Scientific, Waltham, MA, USA). Cells were lysed for 1h on ice with intermittent shaking every 15 min and afterwards centrifuged at 15,000g at 4^o C for 30 min. The collected soluble cell fraction was incubated with 3 µg of anti-cmyc antibody (Cat# C3956; Sigma-Aldrich) for 1h at 4^o C on rotor. Precipitation of the antibody-protein complex from the cell fraction was performed using Protein A/G plus agarose beads (Cat# sc-2003; Santa Cruz Biotechnology, Dallas, TX, USA). Subsequently, the protein complex was eluted by incubating the beads with 25 ml of 4x NuPAGE LDS sample buffer (Invitrogen) for 3 min at 37^o C. Next, eluted protein complexes were separated on a NuPAGE 4-12% Bis-Tris gel (Invitrogen) and transferred to a polyvinylidene difluoride (PVDF) membrane (Amersham Hybond, GE Healthcare, Chicago, IL, USA) for Western blotting. The blot was incubated in blocking buffer (5% skimmed milk dissolved in 1x DPBS with 0.1% Tween 20) overnight at room temperature. Anti-HA IgG (1:1000 in blocking buffer; Roche, Basel, Switzerland) was used to probe immunoprecipitated proteins for 2 h at room temperature, followed by incubation with anti-rat IgG conjugated with horseradish peroxidase (Cat# 1:2000 in

blocking buffer; Sigma-Aldrich) for 1 h at room temperature, and detected using enhanced chemiluminescence substrate, Pierce enhanced chemiluminescence plus western blotting substrate (Cat#32132; Thermo Fischer Scientific).

7.2.6 Data and statistical analysis: Data analysis and graphs were prepared using Microsoft Excel and GraphPad Prism 6. For statistical comparison, two-tailed unpaired student's t-test with Welch's correction was used for determining significance among test and control group. P values of *p≤0.05, **p≤0.01, ***p≤0.001 and ****p≤0.0001 were considered significant and p>0.05 was considered non-significant (ns) '*' p<0.05 was considered statistically significant.

7.3 Results

7.3.1 Assessment of human MRGPRs heteromerization using NanoLuc binary technology (NanoBiT) cell-based assay

In this study, the split-NanoLuc-based protein-fragment complementation assay was utilized for receptor heteromerization. NanoLuc is a small (19kDa) and stable luciferase protein that has been split into two subunits, namely LgBiT (18kDa) and SmBiT (1.3kDa), which were further optimized for low intrinsic subunit-subunit affinity. Unlike previously developed *Renilla* and firefly luciferase-based complementation assays, NanoBiT (LgBiT and SmBiT) low intermolecular affinity and reversible subunit association allows researchers to investigate the dynamic state of receptor-receptor and receptor-protein interactions [332, 337]. Moreover, pHSVTK-LgBiT and pHSVTK-SmBiT plasmids are driven by the herpes simplex virus thymidine kinase promotor (HSVTK), which is known to express proteins at near physiological levels [338]. Additionally, to secure flexibility between the protein of interest and reporter tags, a linker of glycine and serine repeats has been used in the NanoBiT assay system [339].

To determine the heteromerization between MRGPRs, fusion constructs linking the C-terminus of MRGPRs with either LgBiT or SmBiT were transiently co-expressed in cells (schematic representation of the principle shown in Figure. 7.1 A). Upon receptor-receptor interaction, LC-based enzymatic activity of split-luciferases (LgBiT and SmBiT) was observed after substrate (Furimazine) addition. Luminescence is dependent on the proximity of reporter subunits, therefore indicative of interaction between reporter tagged receptors [332]. The cells co-expressing MRGPRE-LgBiT/MRGPRF-SmBiT and MRGPRD-LgBiT/MRGPRF-SmBiT displayed a strong (i.e., ~19-fold higher, p<0.05) and a moderate (i.e., ~2.5-fold higher) luminescence signal, respectively, when compared to randomly interacting subunits of NanoBiT (LgBiT and SmBiT) (Figure 7.1). The cells co-transfected with MRGPRD-LgBiT/MRGPRE-SmBiT showed little or a near-background luminescent signal. Of note, the luminescence emitted from randomly interacting

NanoBiT subunits after substrate addition (evaluated by co-expressing LgBiT and SmBiT in cells) was not substantially higher than that from non-transfected cells. Furthermore, the baseline luminescence from cells expressing only a LgBiT or SmBiT tagged receptor was comparable to that of non-transfected cells, pointing to a very low background signal from split reporter subunits. Overall, these results suggest heteromeric interactions between MRGPRE and MRGPRF. As a further step, considering the intensiometric nature of the LC assays, it was decided to compare and validate the obtained results with widely used proximity-dependent RET techniques, i.e., BRET.

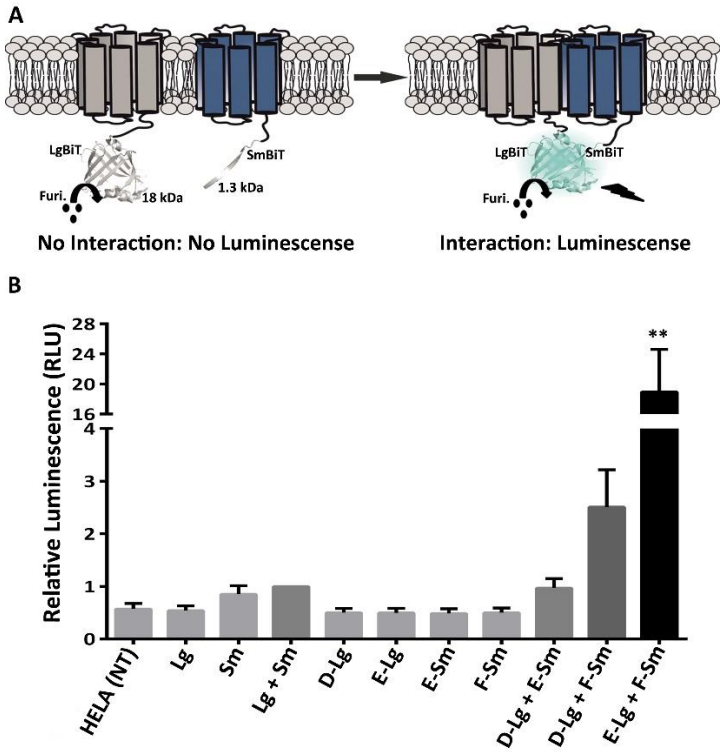

Figure 7.1: Assessment of MRGPR heteromeric interaction in living cells using NanoLuc binary technology (NanoBiT). (A) Schematic representation of the NanoBiT-based MRGPR heteromerization assay. Non-interacting receptors keep the tagged subunits of NanoBiT (LgBiT & SmBiT) apart, preventing LgBiT and SmBiT complementation and no luminescence is produced upon substrate (Furimazine) addition (left panel). When receptors interact, both NanoBiT subunits are brought in proximity allowing reconstitution of an active enzyme, which produces luminescence upon substrate addition (right panel). NanoBiT subunit representation adapted from the Protein Data Bank (PDB) 5IBO. **(B)** The MRGPRD, MRGPRE and MRGPRF tagged with LgBiT /or SmBiT are denoted as D-Lg, D-Sm, E-Lg, E-Sm, F-Lg and F-Sm, respectively. Cells co-expressing MRGPRE-LgBiT/MRGPRF-SmBiT displayed significantly higher luminescence signals. The results are expressed as relative luminescence unit (RLU) in mean ± s.e.m from three independent experiments; each experiment was performed in quadruplets.

7.3.2 Characterization of NanoLuc-BRET system

The BRET phenomenon follows Förster resonance energy transfer principles, where the donor is excited through an enzymatic reaction between the luciferase enzyme and the substrate, but not via an external excitation source as in FRET (Fluorescence resonance energy transfer). This results in improved sensitivity and a better signal-to-noise ratio in BRET compared to FRET [333, 334]. Exploiting the principle of RET, where improved quantum yield of the donor is known to increase the photon-efficiency of the BRET fusion protein, we utilized NanoLuc luciferase, which has high quantum yield compared to *Renilla* or firefly luciferases [337]. The BRET system was developed using NanoLuc (Em_{max} 460 nm) as an energy donor paired with the monomeric-fluorescent protein mOrange (mOr; 26kDa; Ex_{max}/Em_{max}: 548/562 nm) as an energy acceptor [340], providing a spectral resolution of ~105 nm between donor and acceptor emission peaks. The basic principle is schematically represented in Figure 7.3 A.

To check the efficiency of energy transfer between donor and acceptor, a BRET fusion protein linking the C-terminus of NanoLuc to the N-terminus of mOrange by means of a flexible linker composed of glycine and serine repeats was constructed. To test the NanoLuc-BRET system, cells were transiently transfected with plasmids, and the both donor and acceptor emissions were measured using 20-nm bandpass donor (490 – 510 nm) and acceptor (550 - 570 nm) filters following substrate (Furimazine) addition. The percentage photon fluxes at the donor emission filter relative to the total flux output for (1) the donor alone, (2) the donor co-expressed with the acceptor, and (3) the BRET fusion protein was 21.8 ± 0.1 %, 21.4 ± 0.1% and 17.0 ± 0.1%, respectively. Similarly, the percentage photon flux at the acceptor emission filter relative to the total flux output were 1.69 ± 0.02%, 1.66 ± 0.02% and 5.98 ± 0.14%, respectively (Figure 7.2). The decrease in donor emission and the increase in acceptor emission for the BRET fusion protein imply a non-radiative energy transfer from donor to acceptor [341]. The energy transfer efficiency between donor and acceptor is calculated as acceptor to donor emission and is expressed as the average BRET ratio (Figure 7.3 B). The average BRET ratio calculated for the BRET fusion protein was statistically higher, i.e., 0.35±0.01 ($p<0.0001$) compared to 0.08±0.00 for the donor alone (NLuc) or the donor co-expressing with the acceptor, which points to an energy transfer between donor and acceptor and hence is not a consequence of random collisions between the pairs. Thus, the average BRET ratio for the BRET fusion protein was ~4.4-fold higher than that for the donor only (NLuc), providing a sufficient dynamic range for detecting receptor-receptor, receptor-protein, or protein-protein interactions (PPIs).

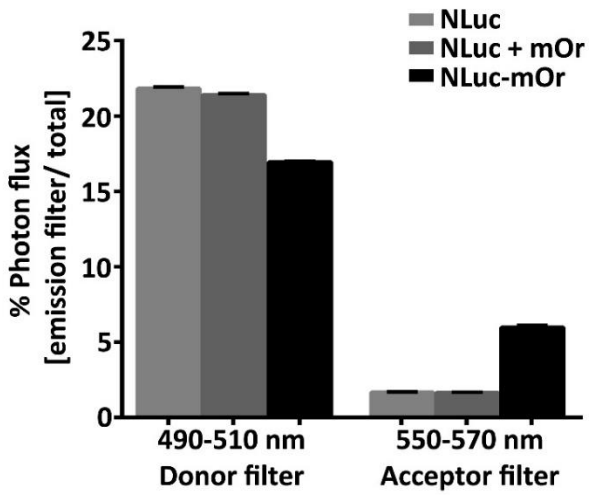

Figure 7.2: Characterization of the NanoLuc-BRET fusion construct in living cells. Percentage photon flux to total photon output from the luminescent donor (NanoLuc; NLuc); the donor co-expressed with the acceptor (mOrange; mOr) and the BRET fusion protein (NLuc-mOr; C-terminus of NLuc fused to the N-terminus of mOrange by a flexible linker of glycine and serine) at the donor (490-510 nm) and acceptor (550-570 nm) emission filters are shown. A concomitant decrease and increase were seen for NLuc-mOr in the donor and acceptor filters, respectively, indicating an energy transfer from donor to acceptor, which is not observed in uncoupled donor and acceptor. The results are expressed as mean ± s.e.m, n = 6, each experiment was performed in quadruplets.

7.3.3 Heteromeric interaction studies of MRGPRs by BRET assay

The MRGPR heteromeric interaction results, obtained from the NanoBiT assay, were further analysed with the BRET assay. The BRET assay is ratio-metric in nature and therefore not susceptible to variability in cell number, assay volume, or data acquisition time [336]. To this end, a plasmid library was generated by tagging the C-terminus of the receptors with the donor (NLuc) or acceptor (mOrange), connected by a flexible linker (composed of glycine and serine residues). Cells co-expressing MRGPRE-mOrange and MRGPRF-NLuc produced a significantly higher BRET signal (23.7 ± 2.8 mBU) compared to the other receptor combinations, confirming the heteromerization of MRGPRE and MRGPRF (Figure 7.3 C). Furthermore, MRGPRD-mOrange co-expressed with MRGPRF-NLuc or MRGPRE-NLuc also yielded moderate net BRET signals, i.e., 10.9 ± 0.9 mBU and 6.9 ± 0.4 mBU, respectively. The obtained BRET signals point to proximity between donor and acceptor chromophores, thus specifying interaction between chromophore tagged receptors.

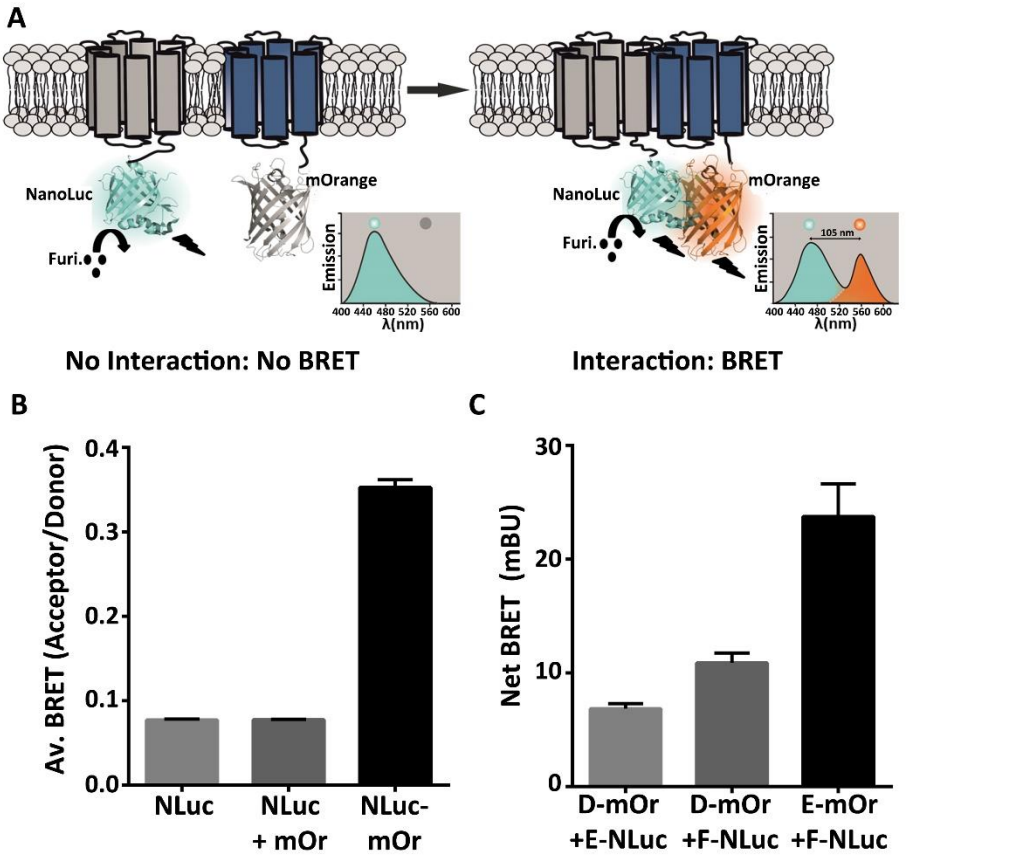

Figure 7.3: Assessment of MRGPR heteromeric interaction in living cells using NanoLuc-BRET assay. **(A)** Schematic representation of the NanoLuc-BRET-based MRGPR heteromerization assay. Non-interacting receptors keep the two chromophores at a sufficiently large distance (distance; d>10 nm) to prevent the donor (NanoLuc; NLuc)-produced resonance energy (upon substrate addition) from exciting the acceptor (mOrange; mOr) by non-radiative energy transfer (left panel). However, when the receptors interact, the two chromophores are brought in proximity (d<10 nm) and the resonance energy from the donor (NLuc) excites the acceptor (mOr) resulting in a BRET signal (right panel). Left inset: emission peak of the donor (NLuc; in blue) in the absence of BRET. Right inset reduced donor (NLuc; in blue) signal in the presence of BRET, together with an increase in the emission of the acceptor (mOr; in mOrange). Double-headed arrow represents a spectral resolution of 105 nm between donor and acceptor peak emission. The NanoLuc and mOrange structures were adapted from PDB 5IBO and 2H5O [342], respectively. **(B)** Characterization of the BRET fusion pair. Cells transiently expressing donor (NLuc) alone, donor co-expressed with acceptor (mOr) and BRET fusion (NLuc-mOr) proteins were imaged after substrate (Furimazine) addition. The average BRET ratio for NLuc-mOr was significantly higher than that for donor alone or donor co-transfected with an acceptor. The results are presented as mean ± s.e.m (n = 6, each experiment performed in quadruplets). **(C)** Determination of MRGPR heteromerization by the BRET assay. MRGPRD, MRGPRE, and MRGPRF tagged with NLuc or mOrange are denoted as D-mOr, D-NLuc, E-mOr, E-NLuc, F-mOr and F-NLuc,

respectively. The BRET signal was most prominent for the MRGPRE-mOr/MRGPRF-NLuc combination. Results in the graph are presented as mean ± s.e.m (n=3, each experiment performed in quadruplets).

7.4.4 Co-immunoprecipitation of MRGPRs

Lastly, the physical interaction between different MRGPRs was evaluated by Co-IP using a standard protocol [343]. The MRGPRE-HA was co-immunoprecipitated with MRGPRF-cmyc (Figure 7.4; lane 5), as evidenced by a ~28kDa immunoblot band of MRGPRE-HA, thus, confirming heteromeric complex formation of MRGPRE and MRGPRF. Similarly, co-immunoprecipitation of MRGPRD-HA with MRGPRE-cmyc (lane 3, ~33kDa) was observed, while co-immunoprecipitation of MRGPRD-HA with MRGPRF-cmyc (lane 4) is ambiguous. Additionally, cells expressing the dual epitope-tagged MRGPRD (HA-MRGPRD-cmyc; ~33kDa; lane 2) and lysate from cells expressing MRGPRE-HA (lane 6) were used as positive controls for immunoprecipitation and immunoblotting, respectively. It is worth noting that MRGPRE-HA at ~28 kDa corresponds to the molecular weight for MRGPRE tagged with HA, whereas HA-MRGPRD-cmyc at ~33 kDa indicates posttranslational modification of MRGPRD [198].

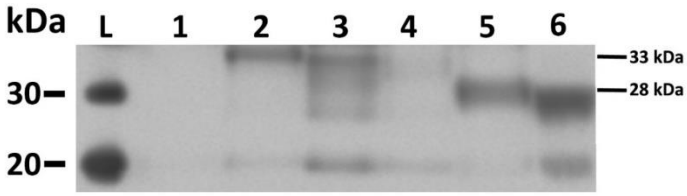

Figure 7.4: Determination of heteromerization of MRGPRs by co-immunoprecipitation. MRGPRs tagged with HA or cmyc epitopes were expressed in HeLa cells. At 48 h post-transfection, lysates from cells co-expressing MRGPRE-cmyc/MRGPRD-HA (lane 3), MRGPRF-cmyc/MRGPRD-HA (lane 4) and MRGPRF-cmyc/MRGPRE-HA (lane 5) were subjected to immunoprecipitation (IP) using anti-cmyc and further immunoblotted (IB) with anti-HA antibodies. Lysate from cells expressing the dual epitope-tagged receptor HA-MRGPR-D-cmyc (~33 kDa; lane 2) was used as positive control for IP. MRGPRE-HA (~28 kDa; lane 6) transfected cell lysates were used as control for IB. Lysates from non-transfected HeLa cells were equally subjected to IP (lane 1) to check the cross-reactivity of the anti-cmyc antibody towards endogenous cell proteins. The IB results demonstrate Co-IP of MRGPRF-cmyc-MRGPRE-HA (~28 kDa) and MRGPRE-cmyc-MRGPRD-HA, indicative of physical interaction between receptor pairs. A molecular mass marker is expressed in kDa (lane L). The immunoblot shown is representative of at least three independent experiments (n=3).

7.4 Discussion

MRGPRs are expressed in sensory neurons and have been linked to nociception, neuro-immune modulation, and mast cell activation. They have also emerged as a key player in cardiovascular biology [131, 132, 186, 198, 344, 345]. Specifically, the expression of

MRGPRD, MRGPRE and MRGPRF was detected in DRG neurons [136]. Considering the growing evidence of the functional importance of GPCR oligomerization in regulating signaling [346], the heteromeric interaction between human MRGPRD, MRGPRE, and MRGPRF was evaluated using a set of complementary techniques.

The high-throughput protein-protein interaction assay, i.e., the split-NanoLuc-based protein-fragment complementation assay (NanoBiT, Promega [332]) was applied to evaluate the heteromerization of MRGPRD, MRGPRE, and MRGPRF. Our results indicate a significantly higher luminescence for the MRGPRE-MRGPRF pair over the other combinations. It should be noted that the NanoBiT assay is a qualitative luminescence-based assay. As such, the high intensities observed with this technique point to an interaction. Heteromerization was further studied using established RET-based approaches such as BRET. Given the fact that RET relies on the proximity between donor and acceptor fluophores (distance between donor and acceptor needs to be less than 10 nm), these RET-based techniques are regarded as 'molecular yardstick' and, hence, are appropriate for the detection of similar order protein-protein proximities.

The NanoLuc-mOrange BRET pair employed revealed the highest BRET signal for heteromeric interaction between MRGPRE and MRGPRF, which is in line with the results of the NanoBiT-based assay. We also used a Co-IP approach to further demonstrate the physical association of MRGPRs. MRGPRs tagged with -HA or -cmyc epitopes subjected to Co-IP revealed the physical association of MRGPRE and MRGPRF. In contrast to the association of MRGPRE with MRGPRF, evidence for interactions between MRGPRD-MRGPRE and MRGPRD-MRGPRF was either observed in the cell imaging techniques or biochemically with Co-IP. The MRGPRD-MRGPRE pair was detected by Co-IP and is in line with the observation for the rat orthologs, suggesting rMrgprD and rMrgprE heteromerization [198]. On the other hand, data from the cell-based NanoBiT and RET based technique points towards an interaction between MRGPRD and MRGPRF, but this interaction could not be confirmed with Co-IP. Since the experimental conditions of the cell imaging techniques and Co-IP are different, several explanations can be provided for the absence or presence of interaction in either of the approaches. With NanoBiT and BRET the interaction is studied with the receptors embedded, in the membrane allowing the detection of lipid-dependent or transient receptor pairs. However, these techniques detect the proximity between reporter tags attached to receptors, thus, when the distance between the tags is greater than 10 nm or the orientation of the reporter tags is unfavorable for RET, interactions are not detected with these techniques. Conversely, Co-IP screens for physical interactions between proteins and require the receptors to be extracted from their lipid environment. Consequently, membrane-dependent receptor interactions might be lost during solubilization, and

receptor interactions are undetected. On the other hand, non-specific association due to hydrophobic domains of receptors can be promoted during solubilization [319]. Based on the limitations of the applied techniques, firm conclusions regarding the presence or absence of heteromeric interactions of MRGPRD-MRGPRE and MRGPRD-MRGPRF cannot be made.

Overall, our results demonstrate the heteromeric interaction of MRGPRE and MRGPRF in in vitro. The knocking of MrgprE influences the expression of MrgprF in the spinal cord of mice [136]. Additionally, homology analysis revealed high evolutionary conservation of MRGPRF between humans and rodents, which hints at a prominent role for MRGPRF in pathophysiology. Altogether, the observed heteromerization between MRGPRE and MRGPRF is likely to be of physiological relevance and will provide new insights when receptors are deorphanized.

In conclusion, the split-NanoLuc-based LC approach utilized for MRGPRs heteromerization studies, provides single-step real-time relative quantification of interacting receptors, high signal-to-noise ratios, and hence may be regarded as a valid alternative tool for medium- to high-throughput GPCR oligomerization screening. In addition, using this technique, the present study unequivocally revealed heteromeric interactions between MRGPRE and MRGPRF.

Author contributions

R.A./R.B./A.J.L./D.J.S./J-P.T. contributed to study conception. R.A. constructed the plasmid libraries (NanoBiT, BRET, FRET and Co-IP library, listed in Appendix II); R.A. performed the NanoBiT and BRET experiment and co-immunoprecipitation experiments; R.A. and A.J.L. wrote the original manuscript; R.B./S.V.R./R.B./A.J.L./D.J.S./J-P.T. provided valuable comments and edits.

Funding:

This study was funded by a grant of the Flemish Foundation for Scientific Research (FWO G.0193.14 to R.B. and J-P.T.).

Acknowledgement

The HeLa cell line was kindly provided by Prof. Dr. Winnok De Vos. The NanoBiT plasmids p-BiT1.1-C[pHSVTK-LgBiT] and p-BiT2.1-C[pHSVTK-SmBiT] and substrate Furimazine were gifts from Promega (Madison, WI, USA).

Chapter 8

General Discussion and Conclusions

Chapter 8 General discussion and conclusions

The seven-transmembrane (7-TM) structures in prokaryotes like halorhodopsin, proteorhodopsin, and bacteriorhodopsin are some of the oldest 7-TM. Even though these 7-TMs have changed over time, they have maintained the 7-TM structural topology and are comparable to the 7-TMs found in eukaryotes today, which are called GPCRs [51, 347, 348]. GPCRs are receptors for several external ligands, such as bitter compounds, odorants, pheromones, photons, sweets, amino acids, glycoproteins, amines, proteases, peptides, fatty acids, lipids, ions, pH changes, etc., and this list is continuously growing. Although GPCRs have evolved through lineage-specific diversifications [349], despite their great variability and complexity, it was humans who learned to exploit them for medicinal or recreational purposes, and this practice continues. MRGPRs are rhodopsin-like orphan GPCRs that only have a small number of potential ligands for their activation [131, 132, 173]. MRGPRs have been recognised to mediate histamine-independent itch, pain, and pseudo-allergic drug responses, and they have recently emerged as mediators in inflammation, cardiovascular, and cancer biology [128, 130, 136, 137, 148, 154-156, 158, 186, 344, 350, 351]. As a result, the research undertaken in this PhD focuses on elucidating the activation mechanisms of MRGPRD, MRGPRE, and MRGPRF, as well as their roles in inflammation and interactions with one another.

8.1 Conclusions, significance, and functional implication from MRGPRD studies

MRGPRD is known to regulate non-histamine-dependent neuropathic itch and pain and has demonstrated a pivotal role in the cardiovascular system [208, 211]. The results illustrated in chapter 3 demonstrate that activating MRGPRD-Gαq signaling with the ligand β-alanine causes the release of IL-6 in HeLa cells via the IKK-complex-dependent NF-kB activation [158]. To draw firm conclusions about in vivo relevance, it is necessary to study the MRGPRD-mediated IL-6 response in native cells and tissues. It is reported that IL-6 levels are increased in neuropathic pain and cardiovascular disease [352, 353]. Since MRGPRD is expressed in nociceptive neurons, aortic endothelial cells, neutrophils, and macrophages, it is tempting to speculate that what we discovered with HeLa cells could be similar in native cells and tissues, and the release of IL-6 could be a positive feedback mechanism to attract, activate, and differentiate monocytes to the site of injury or inflammation or to stimulate resident monocyte or macrophage cells for host defence or repair [354, 355]. Although the mechanism or internal cause that triggers the MRGPRD and may initiate a cascade of such reactions remains unanswered, an attempt was made to explain it with data from chapters 4 and 5.

Though several putative ligands, such as β-alanine, β-AIBA, GABA, DEC, L-AIBA, alamandine, etc., are recognised to activate MRGPRD, it was noted by the results from chapter 3 that MRGPRD was found to be basally active. This basal activity appeared to

be due to the presence of FBS in the culture medium. Therefore, it is obvious to look for an active component in FBS or human serum that can activate MRGPRD, just like it was performed for MRGPRX4 [170]. An endogenous ligand that could activate MRGPRD at submicromolar concentrations would prove beneficial in understanding the pathophysiology related to MRGPRD.

Elevated IL-6 levels are also associated with liver dysfunction [356, 357] and during cholestatic liver disease, itch has been reported as a prominent symptom [251]. Recent literature demonstrates that CLR derivatives, i.e., BAs, activate another member of the MRGPR family, MRGPRX4 (SNSR6), and cause cholestatic-mediated itch [169, 170]. Consequently, the experiment in chapter 4 illustrated that sterol derivatives, i.e., BAs such as CDCA and DCA, activate MRGPRD and induce the release of IL-6 from MRGPRD-expressing HeLa cells. We reasoned that the hepatic system and the cardiovascular system are inextricably linked, and antagonising MRGPRD improves portal hypertension in cirrhotic mice [358], as our results demonstrate that BAs can activate MRGPRD, it has become important to find out how BAs control inflammatory mediators in native tissues, where MRGPRD is expressed.

In addition, we attempted to demonstrate the activation of MRGPRD using CLR. Nonetheless, we could not draw any conclusions about the results, as it was not possible to dissolve CLR in aqueous solution (DMEM medium or even in the MBCD beyond a certain concentration) and prevent it from forming crystals again. However, our results illustrate that when MRGPRD was treated with MBCD, IL-6 release from MRGPRD-expressing HeLa cells was observed. The results may partly be explained by the fact that MBCD is known to remove CLR from cell membranes or disrupt the CLR-containing lipid rafts (microdomains), where GPCRs can be localised [107, 359]. Taken together, it allows us to speculate that CLR may bind to MRGPRD and keep it in an inactive, stable state (R), and when CLR is removed, it becomes active (R*) (please refer to Figure 4.5). Alternatively, the high activity of MRGPRD could be due to cell membrane shrinkage or a change in membrane fluidity because of CLR removal, allowing MRGPRD to interact with Gαq proteins in proximity and allowing ligand-independent MRGPRD-Gαq signaling to occur. Furthermore, our results demonstrate that MBCD-activated MRGPRD when treated with the MBCD-CLR complexes, the release of IL-6 was reduced (please refer to Figure S4.1). These results are opposite to those reported above, which reinforces the possibility that there is an interaction between MRGPRD and sterols (BAs and CLR) or that membrane fluidity is regulating the MRGPRD-Gαq interaction. As sterols activate MRGPRD and induce IL-6 release, it would be possible to assume that either sterols and β-alanine act synergistically as allosteric modulators of MRGPRD or they compete, and this feature can be exploited for drug design or delivery. Altogether, we could postulate

that this assay can also be utilized to discover the inverse agonists or negative allosteric modulator for MRGPRD. In summary, if we may speculate, during hypercholesteremia, cholestatic liver disease, or accumulation of bile acids in the body, the high level of sterols might activate MRGPRD-expressing endothelia, resident cardiac macrophages, or even DRG neurons, stimulating the release of IL-6.

Hypercholesteremia leads to plaque buildup, which is known to affect the flow of blood in the arteries [360]. It has been reported that various receptors, such as AT-1R, β2-AR etc., can be mechanically activated and are all expressed in the cells of the cardiovascular system [278, 279]. Assuming that MRGPRD is expressed in endothelial cells, cardiac resident neutrophils, or macrophages, they will face hemodynamic forces. Therefore, the preliminary results of chapter 5 shed light on the fluid shear stress-induced mechanoactivation of MRGPRD and its functional role in the production of IL-6. It is reported that binding of the meningococcal (*Neisseria meningitidis*) to the N-terminus glycans of the β2-AR enhances a mechanical stimulus, resulting in biased activation of β-arrestin-mediated signalling pathways [283]. Considering this, we could speculate that there is a possibility of N- or O-glycosylation on the N-terminus of MRGPRD (Figure 8.1 A). Therefore, it is possible that N-terminus glycosylation could help in sensing the mechanical forces, which might induce a change in receptor structure conformation, leading to receptor activation. Even though MRGPRD is nearly conserved, with ~75% sequence similarity between rodents and primates, surprisingly, the N-terminus of MRGPRD differs between gorillas and humans. In gorillas, the N-terminus of MRGPRD was extended as compared to humans (Figure 8.1 B). This raises the question of whether the N-terminus of MRGPRD as reported in humans is truncated, due to alternative splicing, differential expression of different isoforms, or a species-specific change. Seeing the extended N-terminus of gorillas, we might postulate that an extended N-terminus might provide additional traction for mechanical forces to act, which might enhance the mechanical activity of the MRGPRD receptor.

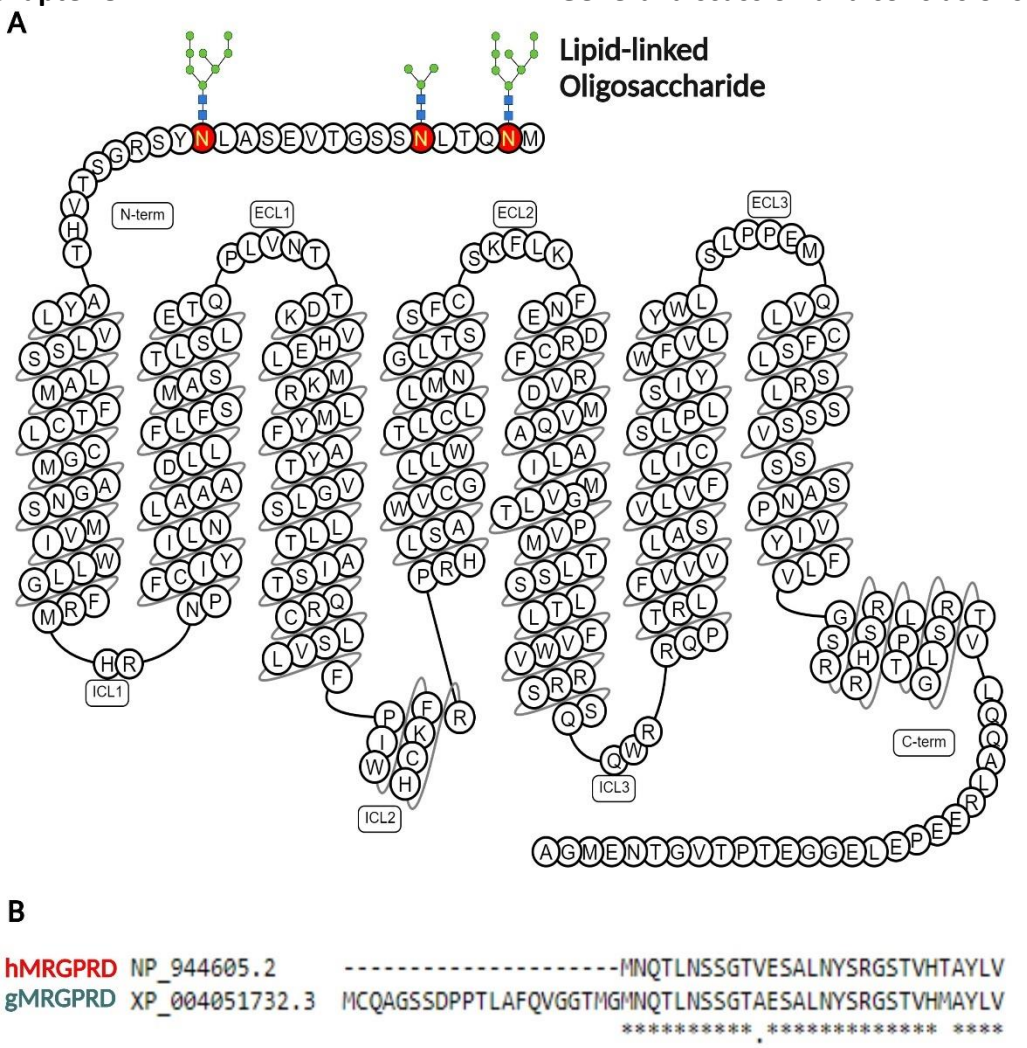

Figure 8.1. Serpentine diagram of human MRGPRD displaying the N-terminus with possible glycosylation sites and comparison of protein sequence homology between human and gorilla MRGPRD. (A) Human MRGPRD serpentine diagram with asparagine (N) highlighted in red and N-linked glycosylation. **(B)** Protein sequence alignment of the N-terminus of human MRGPRD (NP_944605.2) and gorilla(g) MRGPRD (XP_004051732.3), displaying the extended N-terminus in gorilla MRGPRD. The serpentine diagram of MRGPRD is from https://gpcrdb.org/ and figure created with BioRender.com.

Lastly, I would like to draw attention to the fact that in chapter 3, we discovered MRGPRD to be constitutively active (ligand-independent) in MRGPRD-expressing HeLa cells. However, constitutive activity could be explained in several ways: either it is dependent on CLR, which may differ from one cell types to another like for cardiomyocytes or neurons, etc.; or, in addition, the difference in membrane potential among various cell types due to the variable composition of the membrane (variability

of proteins, phospholipids, CLR etc.) might modulate receptors [361]. The resting membrane potentials of HeLa cells, neurons, and cardiomyocytes are -50 mV, -80 mV and -90 mV, respectively. Therefore, the same receptor expressed in a different cell type could behave differently and might be predisposed to a specific heterotrimeric Gα subunit and regulate different downstream signalling. Additionally, MRGPRs lack the key TM3 residue $S^{3.39}$ for sodium binding sites (loss of ionic lock, which is known to keep the receptor in inactive conformation [180]), and this might be enabling the receptor to adopt an active state when gently pushed by shear-stress or by the binding of a ligand [178].

8.2 Conclusions, significance, and functional implication from Cathepsin-S MRGPRs studies

Proteases have been known to activate GPCRs by cleaving the N-terminus of the receptor or by releasing or exposing a tethered ligand peptide by protease cleavage. It was revealed in the early 1990s that serine proteases (such as thrombin and trypsin) activate the family of PARs [289, 295]. For long time, the upregulation of cathepsins during inflammation was recognized, which were classically believed to drive the proteolytic cleavage of extracellular matrix proteins [312]. In addition, it has also been reported that the expression of cathepsins increases during neuropathic itch, pain, arthritis, myocarditis, etc. [148, 362, 363]. Nevertheless, how cathepsins regulate pathophysiology is still not very well understood [364]. Some recent research indicates that the CTSS, a member of the cathepsin family, activates MRGPRs by cleaving their N-terminus, which ultimately causes itch [148, 151]. Therefore, the results illustrated in chapter 6 demonstrate that cysteine protease CTSS can cleave the N-terminus of MRGPRD and MRGPRF. This cleavage might activate the receptor and transduce signals via G protein or β-arrestin mediated signaling. The angiotensin A_{2A} receptor (A_{2A}R)-C terminus was recently demonstrated to be a substrate of Cathepsin D (CTSD), and it has also been shown that blocking CTSD activity improves the density and cell surface expression of A_{2A}R in macrophages [365]. Similarly, considering that N-terminus cleavage of MRGPRD and MRGPRF could be a mechanism for receptor desensitization to curtail the receptor-associated signaling. Additionally, the tethered peptide generated after proteolytic cleavage of the N-terminus of the receptor can either activate the receptors themselves, activate the receptor it is interacting with (trans-activation), or even activate a remotely situated receptor. In addition, we observed that CTSS can cleave the N-terminus of β1-AR and β2-AR receptors, but what role it might play remains unanswered.

Macrophages secrete cathepsins during inflammation [366]. Considering the above-described results in chapters 3–5, activation of MRGPRD causes IL-6 secretion, and proinflammatory cytokines such as IL-6 could prime and polarise monocytes and macrophages and induces differentiation of M1-type to M2-type macrophages [355]. The M2-type macrophages are then able to control inflammation [367, 368]. This leads us to assume that CTSS secretion by M2-type macrophages might cleave the N-terminus of MRGPRs, either activating or desensitizing them, acting as a negative feedback loop, and potentially inhibiting MRGPRD-Gαq signalling (Figure 8.2). Right now, research on cathepsins is limited. Given how cathepsins work by increasing or decreasing inflammation and the role they could play in fibrosis, itch, etc., there is a need for research in this direction to understand it. In conclusion, the work performed was an attempt to elucidate the alternative mechanism of activation for MRGPRD and to deorphanize MRGPRE and MRGPRF.

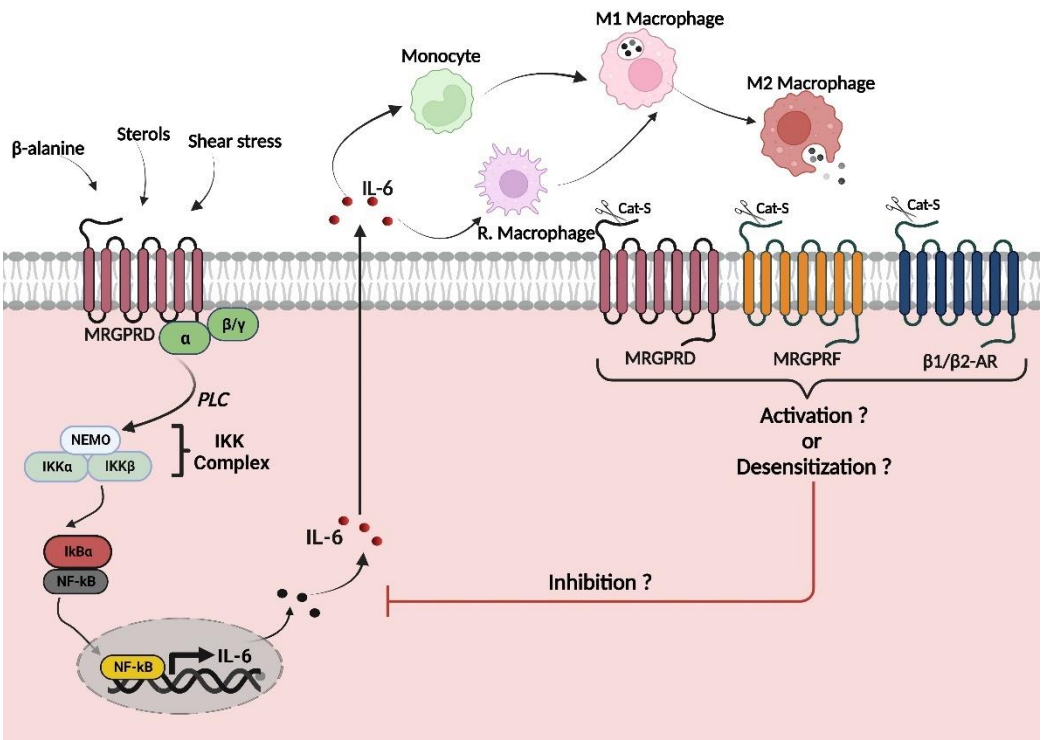

Figure 8.2. Schematic overview of the proposition for MRGPRs associated signaling. The activation of MRGPRD with its ligand β-alanine, sterols, and shear stress, induces NF-kB dependent IL-6 release. The IL-6 would most likely prime the monocytes and resident macrophages and might polarize M1 to M2 macrophages and sensitize them for cathepsin-S release. The cathepsin-S (Cat-S) could then cleave the N-terminus of MRGPRs or β1/β2-AR or even more GPCRs to activate them or desensitize to curtail the MRGPRD-associated siganling. Figure created with BioRender.com.

8.3 Conclusions, significance, and functional implication from oligomerization of MRGPRs studies

The GPCRs are not only regulated by ligand-mediated activation but are also dependent on their interacting partners. The oligomeric interactions of GPCRs have been proposed to affect receptor function and play a critical role in fine-tuning receptor-associated signaling [319, 320, 346, 369]. The co-expression of rat MrgprE with rat MrgprD enhances the potency of β-alanine induced pERK1/2 signaling while the β-alanine induced rat MrgprD internalization in presence of rat MrgprE was found to be reduced [198]. Furthermore, ablation of the orphan receptor MrgprE in mice was found to alter pain-like behaviour and influence expression of MrgprF in the spinal cord [136]. Therefore, the chapter 7 results illustrate the putative oligomeric interactions between MRGPR members MRGPRD, MRGPRE and MRGPRF. The most prominent interaction was discovered between MRGPRE-MRGPRF. Nevertheless, the findings still must be validated first by changing the orientation of tags on receptors, as well as by deploying the BRET saturation assay, competitive FRET assay etc. [370-373]. Additionally, MAmmalian Protein-Protein Interaction Trap (MAPPIT) system can be adopted for studying MRGPRs interactions [374]. Finally, the function of interaction needs to be explored in vitro and in vivo.

Literature suggests that receptor-receptor interaction is also mediated by CLR [54]. Interestingly, we observed that MRGPRD-MRGPRF interaction could be seen using NanoBiT and NanoLuc-BRET assay, but this result could not be confirmed with Co-IP. This leads us to speculate that the interactions detected in NanoBiT or NanoLuc-BRET assays, which are essentially performed in live cells, are cell-membrane dependent MRGPRD-MRGPRF interactions where CLR might be promoting the interaction, and when the membrane is solubilized by lysis for Co-IP sample preparations, the interaction was disrupted.

MRGPRs are known to regulate the itch-pain axis. It is now becoming clear that itch and pain are closely interlinked. It has also been found that itch and pain antagonize each other; for example, the reduction of pain by opioids can sometimes induce itch [375, 376]. Furthermore, deletion of MRGPRs displays prolonged mechanical and thermal pain hypersensitivity [137]. Some reports suggest that MRGPRS and opioid receptors such as MRGPRX1(SNSR-4)-δ-opioid and MrgprC11-μ-opioid form heterodimers [316, 377]. The heteromerization of MRGPRX1(SNSR-4)-δ-opioid display reduced coupling to

A

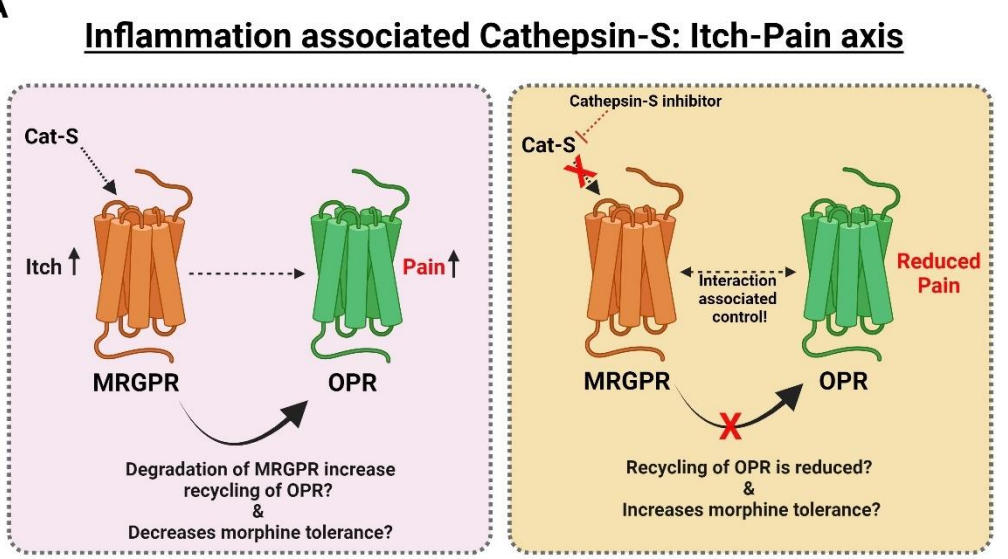

B

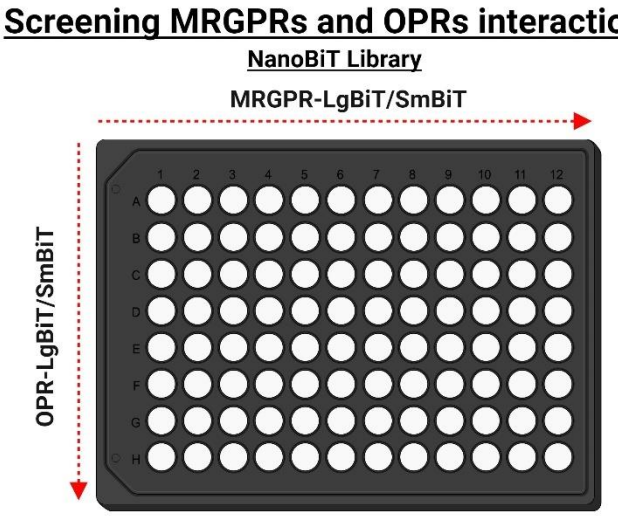

Figure 8.3. Schematic overview of the proposition for the MRGPRs-OPRs itch-pain axis. (A) The Cathepsin-S (Cat-S) associated MRGPRs activation or degradation during inflammatory condition might cause itch. The degradation of MRGPR could disrupt the possible interaction between MRGPRs and OPRs, which may increase OPR membrane retention, recycle OPRs to the cell membrane, or which may decrease opioid tolerance. Conversely, when Cathepsin-S is inhibited, the degradation of MRGPR is inhibited, which in turn could maintain the interaction between MRGPR-OPR and keep a positive feedback check on each other's signalling. **(B)** The proposed plan for screening MRGPR-OPR interactions using the NanoBiT Library (listed in Appendix II). Figure created with BioRender.com.

$G\alpha_{i/o}$ and δ-opioid antagonist naltrexone trans-inhibit SNSR-4 [377]. Furthermore, the peptide-mediated activation (BAM8-22) of MrgprC11 improved μ-opioid recycling, thus improves morphine's analgesic effects. Additionally, MrgprC11 activation reduced the coupling of μ-opioid to β-arrestin 2 and improved the morphine-dependent suppression of cAMP synthesis [316]. At the same time, we should note that pain can be relieved by inhibiting CTSS [378]. This leads us to speculate that if MRGPRs are cleaved or degraded by CTSS, this could free the opioid receptor (to signal for pain) from the MRGPR-Opioid heteromers complex, thus causing pain. In view of this, it is necessary that we now explore the heteromeric interactions between all the opioid receptors and MRGPRs (Figure 8.3).

8.4 Final comments and future prospect

The research contained in this PhD thesis provides alternative activation (BAs, CLR and mechanical mediated) mechanisms for the understudied MRGPRD and the role of the MRGPRD-Gαq/IKK/NF-kB signaling axis in regulating the inflammatory cytokine IL-6. Simultaneously, I tried to deorphanize the MRGPRE and MRGPRF and illuminate the interactions between the MRGPRD, MRGPRE, and MRGPRF. As we know, GPCR signaling is complex and regulated by multiple signal transducers and effector proteins. It will be interesting to determine the association of MRGPRD with G proteins and β-arrestin using orthogonal BRET, LC assays, etc. to ascertain the signaling pathways and its role in pathophysiology.

References

1. Merlin, M.D., *Archaeological evidence for the tradition of psychoactive plant use In the old world.* Economic Botany, 2003. **57**(3): p. 295-323.
2. Kumar, V.K., *Chapter 4 - Postclassical history*, in *Handbook on Opium*, V.K. Kumar, Editor. 2022, Academic Press. p. 39-48.
3. Touw, M., *The religious and medicinal uses of Cannabis in China, India and Tibet.* J Psychoactive Drugs, 1981. **13**(1): p. 23-34.
4. Crocq, M.A., *Historical and cultural aspects of man's relationship with addictive drugs.* Dialogues Clin Neurosci, 2007. **9**(4): p. 355-61.
5. Schmitz, R., *Friedrich Wilhelm Serturner and the discovery of morphine.* Pharm Hist, 1985. **27**(2): p. 61-74.
6. Lassner, J., *Serturner and the discovery of morphine.* Cah Anesthesiol, 1993. **41**(5): p. 549-53.
7. Klockgether-Radke, A.P., *F. W. Serturner and the discovery of morphine. 200 years of pain therapy with opioids.* Anasthesiol Intensivmed Notfallmed Schmerzther, 2002. **37**(5): p. 244-9.
8. Atanasov, A.G., et al., *Discovery and resupply of pharmacologically active plant-derived natural products: A review.* Biotechnol Adv, 2015. **33**(8): p. 1582-1614.
9. Busse, J.W., et al., *Opioids for Chronic Noncancer Pain: A Systematic Review and Meta-analysis.* JAMA, 2018. **320**(23): p. 2448-2460.
10. Gorter, E. and F. Grendel, *On Bimolecular Layers of Lipoids on the Chromocytes of the Blood.* J Exp Med, 1925. **41**(4): p. 439-43.
11. Danielli, J.F. and H. Davson, *A contribution to the theory of permeability of thin films.* Journal of cellular and comparative physiology, 1935. **5**(4): p. 495-508.
12. Singer, S.J. and G.L. Nicolson, *The fluid mosaic model of the structure of cell membranes.* Science, 1972. **175**(4023): p. 720-31.
13. Alberts, B., et al., *The lipid bilayer*, in *Molecular Biology of the Cell. 4th edition*. 2002, Garland Science.
14. Cooper, G.M., *The Cell: A Molecular Approach*, ed. 2nd. 2000, Sunderland (MA): Sinauer Associates.
15. Lange, Y., F. Echevarria, and T.L. Steck, *Movement of zymosterol, a precursor of cholesterol, among three membranes in human fibroblasts.* J Biol Chem, 1991. **266**(32): p. 21439-43.
16. Wallin, E. and G. von Heijne, *Genome-wide analysis of integral membrane proteins from eubacterial, archaean, and eukaryotic organisms.* Protein Sci, 1998. **7**(4): p. 1029-38.
17. von Heijne, G. and Y. Gavel, *Topogenic signals in integral membrane proteins.* Eur J Biochem, 1988. **174**(4): p. 671-8.
18. Entova, S., et al., *Insights into the key determinants of membrane protein topology enable the identification of new monotopic folds.* Elife, 2018. **7**.

19. Yin, H. and A.D. Flynn, *Drugging Membrane Protein Interactions.* Annu Rev Biomed Eng, 2016. **18**: p. 51-76.
20. Langley, J.N., *On the reaction of cells and of nerve-endings to certain poisons, chiefly as regards the reaction of striated muscle to nicotine and to curari.* J Physiol, 1905. **33**(4-5): p. 374-413.
21. Langley, J.N., *Croonian Lecture, 1906.—On nerve endings and on special excitable substances in cells.* Proceedings of the Royal Society of London. Series B, Containing Papers of a Biological Character, 1906. **78**(524): p. 170-194.
22. Maehle, A.H., C.R. Prull, and R.F. Halliwell, *The emergence of the drug receptor theory.* Nat Rev Drug Discov, 2002. **1**(8): p. 637-41.
23. Kenakin, T., *Principles: receptor theory in pharmacology.* Trends Pharmacol Sci, 2004. **25**(4): p. 186-92.
24. Hill, A.V., *The mode of action of nicotine and curari, determined by the form of the contraction curve and the method of temperature coefficients.* J Physiol, 1909. **39**(5): p. 361-73.
25. Hill A, V., *The possible effects of the aggregation of the molecules of hemoglobin on its dissociation curves.* J. Physiol., 1910. **40**: p. iv-vii.
26. Colquhoun, D., *The quantitative analysis of drug-receptor interactions: a short history.* Trends Pharmacol Sci, 2006. **27**(3): p. 149-57.
27. Clark, A.J., *The reaction between acetyl choline and muscle cells.* J Physiol, 1926. **61**(4): p. 530-46.
28. Clark, A.J., *The antagonism of acetyl choline by atropine.* J Physiol, 1926. **61**(4): p. 547-56.
29. Clark, A.J., *The mode of action of drugs on cells*. 1933: Edward Arnold & Co.
30. A. J. Clark, J.R., *The antagonism of acetylcholine and of quaternary ammonium salts.* Quarterly Journal of Experimental Physiology, 1937. **26**(4): p. 375-392.
31. Gaddum, J.H., *The quantitative effects of antagonistic drugs.* J. physiol, 1937. **89**(4): p. 7P-9P.
32. Schild, H.O., *pA, a new scale for the measurement of drug antagonism.* Br J Pharmacol Chemother, 1947. **2**(3): p. 189-206.
33. Schild, H.O., *pAx and competitive drug antagonism.* Br J Pharmacol Chemother, 1949. **4**(3): p. 277-80.
34. Schild, H.O., *Drug antagonism and pAx.* Pharmacol Rev, 1957. **9**(2): p. 242-6.
35. Arunlakshana, O. and H.O. Schild, *Some quantitative uses of drug antagonists.* Br J Pharmacol Chemother, 1959. **14**(1): p. 48-58.
36. Lefkowitz, R.J., et al., *ACTH receptors in the adrenal: specific binding of ACTH-125I and its relation to adenyl cyclase.* Proc Natl Acad Sci U S A, 1970. **65**(3): p. 745-52.

37. Lefkowitz, R.J., J. Roth, and I. Pastan, *Radioreceptor assay of adrenocorticotropic hormone: new approach to assay of polypeptide hormones in plasma.* Science, 1970. **170**(3958): p. 633-5.
38. Ahlquist, R.P., *A study of the adrenotropic receptors.* Am J Physiol, 1948. **153**(3): p. 586-600.
39. Berson, S.A., et al., *Insulin-I 131 metabolism in human subjects: demonstration of insulin binding globulin in the circulation of insulin treated subjects.* The Journal of clinical investigation, 1956. **35**(2): p. 170-190.
40. Berson, S.A. and R.S. Yalow, *Quantitative aspects of the reaction between insulin and insulin-binding antibody.* The Journal of clinical investigation, 1959. **38**(11): p. 1996-2016.
41. Lefkowitz, R.J. and E. Haber, *A fraction of the ventricular myocardium that has the specificity of the cardiac beta-adrenergic receptor.* Proc Natl Acad Sci U S A, 1971. **68**(8): p. 1773-7.
42. Del Castillo, J. and B. Katz, *Interaction at end-plate receptors between different choline derivatives.* Proc R Soc Lond B Biol Sci, 1957. **146**(924): p. 369-81.
43. Haga, T., et al., *Adenylate cyclase permanently uncoupled from hormone receptors in a novel variant of S49 mouse lymphoma cells.* Proceedings of the National Academy of Sciences, 1977. **74**(5): p. 2016-2020.
44. De Lean, A., J.M. Stadel, and R.J. Lefkowitz, *A ternary complex model explains the agonist-specific binding properties of the adenylate cyclase-coupled beta-adrenergic receptor.* J Biol Chem, 1980. **255**(15): p. 7108-17.
45. Samama, P., et al., *A mutation-induced activated state of the beta 2-adrenergic receptor. Extending the ternary complex model.* J Biol Chem, 1993. **268**(7): p. 4625-36.
46. Weiss, J.M., et al., *The Cubic Ternary Complex ReceptorOccupancy Model I. Model Description.* Journal of Theoretical Biology, 1996.
47. Bragg, W.L., *The structure of some crystals as indicated by their diffraction of X-rays.* Proceedings of the Royal Society of London. Series A, Containing papers of a mathematical and physical character, 1913. **89**(610): p. 248-277.
48. Kendrew, J.C., et al., *A three-dimensional model of the myoglobin molecule obtained by x-ray analysis.* Nature, 1958. **181**(4610): p. 662-6.
49. Henderson, R. and P.N. Unwin, *Three-dimensional model of purple membrane obtained by electron microscopy.* Nature, 1975. **257**(5521): p. 28-32.
50. Deisenhofer, J., et al., *Structure of the protein subunits in the photosynthetic reaction centre of Rhodopseudomonas viridis at 3Å resolution.* Nature, 1985. **318**: p. 618-624.

51. Pebay-Peyroula, E., et al., *X-ray structure of bacteriorhodopsin at 2.5 angstroms from microcrystals grown in lipidic cubic phases.* Science, 1997. **277**(5332): p. 1676-1681.
52. Palczewski, K., et al., *Crystal structure of rhodopsin: A G protein-coupled receptor.* Science, 2000. **289**(5480): p. 739-45.
53. Rasmussen, S.G., et al., *Crystal structure of the human β2 adrenergic G-protein-coupled receptor.* Nature, 2007. **450**(7168): p. 383-387.
54. Cherezov, V., et al., *High-resolution crystal structure of an engineered human β2-adrenergic G protein–coupled receptor.* science, 2007. **318**(5854): p. 1258-1265.
55. Liu, X., et al., *Structural Insights into the Process of GPCR-G Protein Complex Formation.* Cell, 2019. **177**(5): p. 1243-1251 e12.
56. Kolakowski, L.F., Jr., *GCRDb: a G-protein-coupled receptor database.* Recept Channels, 1994. **2**(1): p. 1-7.
57. Fredriksson, R., et al., *The G-protein-coupled receptors in the human genome form five main families. Phylogenetic analysis, paralogon groups, and fingerprints.* Mol Pharmacol, 2003. **63**(6): p. 1256-72.
58. Schioth, H.B. and R. Fredriksson, *The GRAFS classification system of G-protein coupled receptors in comparative perspective.* Gen Comp Endocrinol, 2005. **142**(1-2): p. 94-101.
59. Mombaerts, P., *Genes and ligands for odorant, vomeronasal and taste receptors.* Nat Rev Neurosci, 2004. **5**(4): p. 263-78.
60. Brauner-Osborne, H., P. Wellendorph, and A.A. Jensen, *Structure, pharmacology and therapeutic prospects of family C G-protein coupled receptors.* Curr Drug Targets, 2007. **8**(1): p. 169-84.
61. Hollenstein, K., et al., *Insights into the structure of class B GPCRs.* Trends Pharmacol Sci, 2014. **35**(1): p. 12-22.
62. Harmar, A.J., *Family-B G-protein-coupled receptors.* Genome Biol, 2001. **2**(12): p. REVIEWS3013.
63. Hamann, J., et al., *International Union of Basic and Clinical Pharmacology. XCIV. Adhesion G protein-coupled receptors.* Pharmacol Rev, 2015. **67**(2): p. 338-67.
64. Malbon, C.C., *Frizzleds: new members of the superfamily of G-protein-coupled receptors.* Front Biosci, 2004. **9**: p. 1048-58.
65. Huang, H.C. and P.S. Klein, *The Frizzled family: receptors for multiple signal transduction pathways.* Genome Biol, 2004. **5**(7): p. 234.
66. Blassberg, R., et al., *Reduced cholesterol levels impair Smoothened activation in Smith-Lemli-Opitz syndrome.* Hum Mol Genet, 2016. **25**(4): p. 693-705.
67. Luchetti, G., et al., *Cholesterol activates the G-protein coupled receptor Smoothened to promote Hedgehog signaling.* Elife, 2016. **5**.
68. Deshpande, I., et al., *Smoothened stimulation by membrane sterols drives Hedgehog pathway activity.* Nature, 2019. **571**(7764): p. 284-288.

69. Wang, J. and R. Xiao, *G protein-coupled receptors in energy homeostasis.* Sci China Life Sci, 2014. **57**(7): p. 672-80.
70. Heng, B.C., D. Aubel, and M. Fussenegger, *An overview of the diverse roles of G-protein coupled receptors (GPCRs) in the pathophysiology of various human diseases.* Biotechnol Adv, 2013. **31**(8): p. 1676-94.
71. Katritch, V., V. Cherezov, and R.C. Stevens, *Structure-function of the G protein-coupled receptor superfamily.*, in *Annual review of pharmacology and toxicology*. 2013. p. 531-56.
72. Hauser, A.S., et al., *GPCR activation mechanisms across classes and macro/microscales.* Nat Struct Mol Biol, 2021. **28**(11): p. 879-888.
73. Alexander, S.P., et al., *The Concise Guide to PHARMACOLOGY 2021/22: G protein-coupled receptors.* British journal of pharmacology, 2021. **178**: p. S27-S156.
74. Zhou, Q., et al., *Common activation mechanism of class A GPCRs.* Elife, 2019. **8**.
75. Ballesteros, J.A. and H. Weinstein, *[19] Integrated methods for the construction of three-dimensional models and computational probing of structure-function relations in G protein-coupled receptors*, in *Methods in neurosciences*. 1995, Elsevier. p. 366-428.
76. Isberg, V., et al., *Generic GPCR residue numbers - aligning topology maps while minding the gaps.* Trends Pharmacol Sci, 2015. **36**(1): p. 22-31.
77. Smith, S.O., *Deconstructing the transmembrane core of class A G protein-coupled receptors.* Trends Biochem Sci, 2021. **46**(12): p. 1017-1029.
78. Chung, D.A., et al., *Mutagenesis and peptide analysis of the DRY motif in the alpha2A adrenergic receptor: evidence for alternate mechanisms in G protein-coupled receptors.* Biochem Biophys Res Commun, 2002. **293**(4): p. 1233-41.
79. Schonegge, A.M., et al., *Evolutionary action and structural basis of the allosteric switch controlling beta(2)AR functional selectivity.* Nat Commun, 2017. **8**(1): p. 2169.
80. Weis, W.I. and B.K. Kobilka, *The Molecular Basis of G Protein-Coupled Receptor Activation.* Annu Rev Biochem, 2018. **87**: p. 897-919.
81. Nygaard, R., et al., *The dynamic process of beta(2)-adrenergic receptor activation.* Cell, 2013. **152**(3): p. 532-42.
82. Smith, J.S., R.J. Lefkowitz, and S. Rajagopal, *Biased signalling: from simple switches to allosteric microprocessors.* Nat Rev Drug Discov, 2018. **17**(4): p. 243-260.
83. Thomsen, A.R.B., et al., *GPCR-G Protein-beta-Arrestin Super-Complex Mediates Sustained G Protein Signaling.* Cell, 2016. **166**(4): p. 907-919.
84. Alhosaini, K., et al., *GPCRs: The most promiscuous druggable receptor of the mankind.* Saudi Pharmaceutical Journal, 2021. **29**(6): p. 539-551.

85. Rodbell, M., *The role of hormone receptors and GTP-regulatory proteins in membrane transduction.* Nature, 1980. **284**(5751): p. 17-22.
86. Hurowitz, E.H., et al., *Genomic characterization of the human heterotrimeric G protein alpha, beta, and gamma subunit genes.* DNA Res, 2000. **7**(2): p. 111-20.
87. Smrcka, A.V., *G protein betagamma subunits: central mediators of G protein-coupled receptor signaling.* Cell Mol Life Sci, 2008. **65**(14): p. 2191-214.
88. Syrovatkina, V., et al., *Regulation, Signaling, and Physiological Functions of G-Proteins.* J Mol Biol, 2016. **428**(19): p. 3850-68.
89. Hilger, D., *The role of structural dynamics in GPCR-mediated signaling.* FEBS J, 2021. **288**(8): p. 2461-2489.
90. Clapham, D.E. and E.J. Neer, *G protein beta gamma subunits.* Annu Rev Pharmacol Toxicol, 1997. **37**: p. 167-203.
91. Milligan, G. and E. Kostenis, *Heterotrimeric G-proteins: a short history.* Br J Pharmacol, 2006. **147 Suppl 1**(Suppl 1): p. S46-55.
92. Wilden, U., S.W. Hall, and H. Kuhn, *Phosphodiesterase activation by photoexcited rhodopsin is quenched when rhodopsin is phosphorylated and binds the intrinsic 48-kDa protein of rod outer segments.* Proc Natl Acad Sci U S A, 1986. **83**(5): p. 1174-8.
93. Lohse, M.J., et al., *beta-Arrestin: a protein that regulates beta-adrenergic receptor function.* Science, 1990. **248**(4962): p. 1547-50.
94. Benovic, J.L., et al., *Functional desensitization of the isolated beta-adrenergic receptor by the beta-adrenergic receptor kinase: potential role of an analog of the retinal protein arrestin (48-kDa protein).* Proc Natl Acad Sci U S A, 1987. **84**(24): p. 8879-82.
95. Gurevich, V.V. and E.V. Gurevich, *The structural basis of arrestin-mediated regulation of G-protein-coupled receptors.* Pharmacol Ther, 2006. **110**(3): p. 465-502.
96. Shenoy, S.K., et al., *Regulation of receptor fate by ubiquitination of activated beta 2-adrenergic receptor and beta-arrestin.* Science, 2001. **294**(5545): p. 1307-13.
97. Laporte, S.A., et al., *The beta2-adrenergic receptor/betaarrestin complex recruits the clathrin adaptor AP-2 during endocytosis.* Proc Natl Acad Sci U S A, 1999. **96**(7): p. 3712-7.
98. Kang, J., et al., *A nuclear function of beta-arrestin1 in GPCR signaling: regulation of histone acetylation and gene transcription.* Cell, 2005. **123**(5): p. 833-47.
99. Oakley, R.H., et al., *Differential affinities of visual arrestin, beta arrestin1, and beta arrestin2 for G protein-coupled receptors delineate two major classes of receptors.* J Biol Chem, 2000. **275**(22): p. 17201-10.
100. Dawaliby, R., et al., *Allosteric regulation of G protein-coupled receptor activity by phospholipids.* Nat Chem Biol, 2016. **12**(1): p. 35-9.

101. Thakur, N., et al., *Anionic phospholipids control mechanisms of GPCR-G protein recognition.* Nat Commun, 2023. **14**(1): p. 794.
102. Janetzko, J., et al., *Membrane phosphoinositides regulate GPCR-beta-arrestin complex assembly and dynamics.* Cell, 2022. **185**(24): p. 4560-4573 e19.
103. Sarkar, P. and A. Chattopadhyay, *Cholesterol interaction motifs in G protein-coupled receptors: Slippery hot spots?* Wiley Interdiscip Rev Syst Biol Med, 2020. **12**(4): p. e1481.
104. Gimpl, G. and F. Fahrenholz, *Cholesterol as stabilizer of the oxytocin receptor.* Biochim Biophys Acta, 2002. **1564**(2): p. 384-92.
105. Pucadyil, T.J. and A. Chattopadhyay, *Cholesterol modulates ligand binding and G-protein coupling to serotonin(1A) receptors from bovine hippocampus.* Biochim Biophys Acta, 2004. **1663**(1-2): p. 188-200.
106. Oates, J., et al., *The role of cholesterol on the activity and stability of neurotensin receptor 1.* Biochim Biophys Acta, 2012. **1818**(9): p. 2228-33.
107. Villar, V.A., et al., *Localization and signaling of GPCRs in lipid rafts.* Methods Cell Biol, 2016. **132**: p. 3-23.
108. Lee, J., et al., *Muscarinic Receptors and BK Channels Are Affected by Lipid Raft Disruption of Salivary Gland Cells.* Int J Mol Sci, 2021. **22**(9).
109. Civelli, O., et al., *Orphan GPCRs and their ligands.* Pharmacol Ther, 2006. **110**(3): p. 525-32.
110. Vidad, A.R., S. Macaspac, and H.L. Ng, *Locating ligand binding sites in G-protein coupled receptors using combined information from docking and sequence conservation.* PeerJ, 2021. **9**: p. e12219.
111. Alhosaini, K., et al., *GPCRs: The most promiscuous druggable receptor of the mankind.* Saudi Pharm J, 2021. **29**(6): p. 539-551.
112. Hauser, A.S., et al., *Trends in GPCR drug discovery: New agents, targets and indications*, in *Nature Reviews Drug Discovery*. 2017.
113. Congreve, M., et al., *Impact of GPCR Structures on Drug Discovery.* Cell, 2020. **181**(1): p. 81-91.
114. Santos, R., et al., *A comprehensive map of molecular drug targets.* Nat Rev Drug Discov, 2017. **16**(1): p. 19-34.
115. Yang, D., et al., *G protein-coupled receptors: structure- and function-based drug discovery.* Signal Transduct Target Ther, 2021. **6**(1): p. 7.
116. Tang, X.L., et al., *Orphan G protein-coupled receptors (GPCRs): biological functions and potential drug targets.* Acta Pharmacol Sin, 2012. **33**(3): p. 363-71.
117. Overington, J.P., B. Al-Lazikani, and A.L. Hopkins, *How many drug targets are there?* Nat Rev Drug Discov, 2006. **5**(12): p. 993-6.
118. Alexander, S.P., et al., *THE CONCISE GUIDE TO PHARMACOLOGY 2021/22: G protein-coupled receptors.* Br J Pharmacol, 2021. **178 Suppl 1**: p. S27-S156.

119. Diaz, C., P. Angelloz-Nicoud, and E. Pihan, *Modeling and deorphanization of orphan GPCRs.* Computational Methods for GPCR Drug Discovery, 2018: p. 413-429.
120. Civelli, O., et al., *G protein-coupled receptor deorphanizations.* Annu Rev Pharmacol Toxicol, 2013. **53**: p. 127-46.
121. Takenaka, T., *Classical vs reverse pharmacology in drug discovery.* BJU Int, 2001. **88 Suppl 2**: p. 7-10; discussion 49-50.
122. Swinney, D.C. and J. Anthony, *How were new medicines discovered?* Nat Rev Drug Discov, 2011. **10**(7): p. 507-19.
123. Lansu, K., et al., *In silico design of novel probes for the atypical opioid receptor MRGPRX2*, in *Nature Chemical Biology*. 2017, Nature Publishing Group. p. 529-536.
124. Ngo, T., et al., *Identifying ligands at orphan GPCRs: current status using structure-based approaches.* British journal of pharmacology, 2016. **173**(20): p. 2934-2951.
125. Dupuis, N., et al., *Activation of the Orphan G Protein-Coupled Receptor GPR27 by Surrogate Ligands Promotes beta-Arrestin 2 Recruitment.* Mol Pharmacol, 2017. **91**(6): p. 595-608.
126. Young, D., et al., *Isolation and characterization of a new cellular oncogene encoding a protein with multiple potential transmembrane domains.* Cell, 1986. **45**(5): p. 711-9.
127. Ross, P.C., et al., *RTA, a candidate G protein-coupled receptor: cloning, sequencing, and tissue distribution.* Proc Natl Acad Sci U S A, 1990. **87**(8): p. 3052-6.
128. Dong, X., et al., *A diverse family of GPCRs expressed in specific subsets of nociceptive sensory neurons.*, in *Cell*. 2001. p. 619-32.
129. Lembo, P.M., et al., *Proenkephalin A gene products activate a new family of sensory neuron–specific GPCRs.* Nature neuroscience, 2002. **5**(3): p. 201-209.
130. Zylka, M.J., et al., *Atypical expansion in mice of the sensory neuron-specific Mrg G protein-coupled receptor family.*, in *Proceedings of the National Academy of Sciences of the United States of America*. 2003. p. 10043-8.
131. Bader, M., et al., *MAS and its related G protein-coupled receptors, Mrgprs.*, in *Pharmacological reviews*. 2014. p. 1080-105.
132. Solinski, H.J., T. Gudermann, and A. Breit, *Pharmacology and signaling of MAS-related G protein-coupled receptors.*, in *Pharmacological reviews*. 2014. p. 570-97.
133. Liu, Q., et al., *Molecular genetic visualization of a rare subset of unmyelinated sensory neurons that may detect gentle touch.*, in *Nature neuroscience*. 2007. p. 946-8.

134. Zhang, L., et al., *Cloning and expression of MRG receptors in macaque, mouse, and human.*, in *Brain research. Molecular brain research*. 2005. p. 187-97.
135. Zylka, M.J., F.L. Rice, and D.J. Anderson, *Topographically distinct epidermal nociceptive circuits revealed by axonal tracers targeted to Mrgprd.*, in *Neuron*. 2005. p. 17-25.
136. Cox, P.J., et al., *The effect of deletion of the orphan G - protein coupled receptor (GPCR) gene MrgE on pain-like behaviours in mice.*, in *Molecular pain*. 2008. p. 2.
137. Guan, Y., et al., *Mas-related G-protein-coupled receptors inhibit pathological pain in mice.*, in *Proceedings of the National Academy of Sciences of the United States of America*. 2010. p. 15933-8.
138. Liu, Q., et al., *The Distinct Roles of Two GPCRs, MrgprC11 and PAR2, in Itch and Hyperalgesia*, in *Science Signaling*. 2011. p. ra45-ra45.
139. Cavanaugh, D.J., et al., *Distinct subsets of unmyelinated primary sensory fibers mediate behavioral responses to noxious thermal and mechanical stimuli.*, in *Proceedings of the National Academy of Sciences of the United States of America*. 2009. p. 9075-80.
140. Liu, Y., et al., *Mechanisms of compartmentalized expression of Mrg class G-protein-coupled sensory receptors.*, in *The Journal of neuroscience : the official journal of the Society for Neuroscience*. 2008. p. 125-32.
141. Meixiong, J. and X. Dong, *Mas-related G protein–coupled receptors and the biology of itch sensation.* Annual review of genetics, 2017. **51**: p. 103-121.
142. Tatemoto, K., et al., *Immunoglobulin E-independent activation of mast cell is mediated by Mrg receptors*, in *Biochemical and Biophysical Research Communications*. 2006. p. 1322-1328.
143. Lee, M.-G., et al., *Agonists of the MAS-related gene (Mrgs) orphan receptors as novel mediators of mast cell-sensory nerve interactions.*, in *Journal of immunology (Baltimore, Md. : 1950)*. 2008. p. 2251-5.
144. Liu, Q., et al., *Sensory neuron-specific GPCR Mrgprs are itch receptors mediating chloroquine-induced pruritus.*, in *Cell*. 2009, Elsevier Ltd. p. 1353-65.
145. Hohenhaus, D.M., et al., *An mRNA atlas of G protein-coupled receptor expression during primary human monocyte/macrophage differentiation and lipopolysaccharide-mediated activation identifies targetable candidate regulators of inflammation*, in *Immunobiology*. 2013, Elsevier GmbH. p. 1345-1353.
146. McNeil, B.D., et al., *Identification of a mast-cell-specific receptor crucial for pseudo-allergic drug reactions.*, in *Nature*. 2015, Nature Publishing Group. p. 237-41.

147. Kamohara, M., et al., *Identification of MrgX2 as a human G-protein-coupled receptor for proadrenomedullin N-terminal peptides.*, in *Biochemical and biophysical research communications*. 2005. p. 1146-52.
148. Reddy, V.B., et al., *Redefining the concept of protease-activated receptors: cathepsin S evokes itch via activation of Mrgprs.*, in *Nature communications*. 2015. p. 7864.
149. Karhu, T., et al., *Isolation of new ligands for orphan receptor MRGPRX1-hemorphins LVV-H7 and VV-H7.* Peptides, 2017. **96**: p. 61-66.
150. Karhu, T., et al., *Mast cell degranulation via MRGPRX2 by isolated human albumin fragments.* Biochim Biophys Acta Gen Subj, 2017. **1861**(11 Pt A): p. 2530-2534.
151. Reddy, V.B. and E.A. Lerner, *Activation of mas-related G-protein-coupled receptors by the house dust mite cysteine protease Der p1 provides a new mechanism linking allergy and inflammation.* J Biol Chem, 2017. **292**(42): p. 17399-17406.
152. Alkanfari, I., et al., *Small-Molecule Host-Defense Peptide Mimetic Antibacterial and Antifungal Agents Activate Human and Mouse Mast Cells via Mas-Related GPCRs*, in *Cells*. 2019. p. 311.
153. Arifuzzaman, M., et al., *MRGPR-mediated activation of local mast cells clears cutaneous bacterial infection and protects against reinfection*, in *Science Advances*. 2019.
154. de Carvalho Santuchi, M., et al., *Angiotensin-(1-7) and Alamandine Promote Anti-inflammatory Response in Macrophages In Vitro and In Vivo*, in *Mediators of Inflammation*. 2019. p. 1-14.
155. Serhan, N., et al., *House dust mites activate nociceptor-mast cell clusters to drive type 2 skin inflammation.* Nat Immunol, 2019. **20**(11): p. 1435-1443.
156. Elst, J., et al., *MRGPRX2 and Immediate Drug Hypersensitivity: Insights from Cultured Human Mast Cells*, in *Journal of Investigational Allergology and Clinical Immunology*. 2020. p. 1-25.
157. Lan, L., et al., *Mas-related G protein-coupled receptor D participates in inflammatory pain by promoting NF-κB activation through interaction with TAK1 and IKK complex*, in *Cellular Signalling*. 2020, Elsevier Inc. p. 109813.
158. Arora, R., et al., *Constitutive, Basal, and beta-Alanine-Mediated Activation of the Human Mas-Related G Protein-Coupled Receptor D Induces Release of the Inflammatory Cytokine IL-6 and Is Dependent on NF-kappaB Signaling.* Int J Mol Sci, 2021. **22**(24).
159. Habiyakare, B., et al., *Reduction of angiotensin A and alamandine vasoactivity in the rabbit model of atherogenesis: differential effects of alamandine and Ang(1-7).* Int J Exp Pathol, 2014. **95**(4): p. 290-5.
160. Yonova, D., *Pruritus in certain internal diseases.* Hippokratia, 2007. **11**(2): p. 67-71.

161. Liu, Q., et al., *Sensory neuron-specific GPCR Mrgprs are itch receptors mediating chloroquine-induced pruritus.* Cell, 2009. **139**(7): p. 1353-1365.
162. Li, Z., et al., *Targeting human Mas-related G protein-coupled receptor X1 to inhibit persistent pain.*, in *Proceedings of the National Academy of Sciences of the United States of America*. 2017. p. E1996-E2005.
163. McNeil, B.D., et al., *Identification of a mast-cell-specific receptor crucial for pseudo-allergic drug reactions.* Nature, 2015. **519**(7542): p. 237-241.
164. Robas, N., E. Mead, and M. Fidock, *MrgX2 is a high potency cortistatin receptor expressed in dorsal root ganglion.* Journal of Biological Chemistry, 2003. **278**(45): p. 44400-44404.
165. Wolf, K., et al., *A group of cationic amphiphilic drugs activates MRGPRX2 and induces scratching behavior in mice.* Journal of Allergy and Clinical Immunology, 2021. **148**(2): p. 506-522. e8.
166. Yang, F., et al., *Structure, function and pharmacology of human itch receptor complexes.* Nature, 2021. **600**(7887): p. 164-169.
167. Azimi, E., V.B. Reddy, and E.A. Lerner, *Brief communication: MRGPRX2, atopic dermatitis and red man syndrome.* Itch (Phila), 2017. **2**(1): p. e5.
168. Green, D.P., et al., *A mast-cell-specific receptor mediates neurogenic inflammation and pain.* Neuron, 2019. **101**(3): p. 412-420. e3.
169. Meixiong, J., et al., *MRGPRX4 is a G protein-coupled receptor activated by bile acids that may contribute to cholestatic pruritus.* Proc Natl Acad Sci U S A, 2019. **116**(21): p. 10525-10530.
170. Yu, H., et al., *MRGPRX4 is a bile acid receptor for human cholestatic itch*, in *eLife*. 2019. p. 1-27.
171. Cao, C., et al., *Structure, function and pharmacology of human itch GPCRs.* Nature, 2021. **600**(7887): p. 170-175.
172. Kotliar, I.B., et al., *Itch receptor MRGPRX4 interacts with the receptor activity-modifying proteins.* J Biol Chem, 2023. **299**(5): p. 104664.
173. Hawker, P., L. Zhang, and L. Liu, *Mas-Related G Protein-Coupled Receptors in Gastrointestinal Dysfunction and Inflammatory Bowel Disease: A Review.* British Journal of Pharmacology, 2023.
174. Alexander, S.P.H., et al., *THE CONCISE GUIDE TO PHARMACOLOGY 2019/20: G protein-coupled receptors.* Br J Pharmacol, 2019. **176 Suppl 1**: p. S21-S141.
175. Suzuki, S., et al., *Structural insight into the activation mechanism of MrgD with heterotrimeric Gi-protein revealed by cryo-EM.* Commun Biol, 2022. **5**(1): p. 707.
176. Billesbolle, C.B., et al., *Structural basis of odorant recognition by a human odorant receptor.* Nature, 2023. **615**(7953): p. 742-749.
177. Liu, Y., et al., *Ligand recognition and allosteric modulation of the human MRGPRX1 receptor.* Nat Chem Biol, 2023. **19**(4): p. 416-422.

178. Cao, C. and B.L. Roth, *The structure, function, and pharmacology of MRGPRs.* Trends in Pharmacological Sciences, 2023.
179. Rasmussen, S.G., et al., *Crystal structure of the beta2 adrenergic receptor-Gs protein complex.* Nature, 2011. **477**(7366): p. 549-55.
180. Trzaskowski, B., et al., *Action of molecular switches in GPCRs-theoretical and experimental studies.* Current medicinal chemistry, 2012. **19**(8): p. 1090-1109.
181. Goddard, T.D., et al., *UCSF ChimeraX: Meeting modern challenges in visualization and analysis.* Protein Sci, 2018. **27**(1): p. 14-25.
182. Pettersen, E.F., et al., *UCSF ChimeraX: Structure visualization for researchers, educators, and developers.* Protein Sci, 2021. **30**(1): p. 70-82.
183. Shinohara, T., et al., *Identification of a G protein-coupled receptor specifically responsive to β-alanine*, in *Journal of Biological Chemistry*. 2004. p. 23559-23564.
184. Bautzova, T., et al., *5-oxoETE triggers nociception in constipation-predominant irritable bowel syndrome through MAS-related G protein-coupled receptor D.*, in *Science signaling*. 2018.
185. Nishimura, S., et al., *MRGD, a MAS-related G-protein coupled receptor, promotes tumorigenisis and is highly expressed in lung cancer.*, in *PloS one*. 2012. p. e38618.
186. Oliveira, A.C., et al., *Genetic deletion of the alamandine receptor MRGD leads to dilated cardiomyopathy in mice*, in *American Journal of Physiology-Heart and Circulatory Physiology*. 2019. p. H123-H133.
187. Zhou, C., et al., *Expression and localization of MrgprD in mouse intestinal tract*. 2019, Cell and Tissue Research. p. 259-268.
188. Da Silva, A.R., et al., *Alamandine abrogates neutrophil degranulation in atherosclerotic mice.* Eur J Clin Invest, 2017. **47**(2): p. 117-128.
189. Kitase, Y., et al., *β-aminoisobutyric Acid, L-BAIBA, Is a Muscle-Derived Osteocyte Survival Factor*, in *Cell Reports*. 2018. p. 1531-1544.
190. Uno, M., et al., *Identification of physiologically active substances as novel ligands for MRGPRD.*, in *Journal of biomedicine & biotechnology*. 2012. p. 816159.
191. Ajit, S.K., et al., *Development of a FLIPR assay for the simultaneous identification of MrgD agonists and antagonists from a single screen.*, in *Journal of biomedicine & biotechnology*. 2010.
192. Lautner, R.Q., et al., *Discovery and characterization of alamandine: a novel component of the renin-angiotensin system.*, in *Circulation research*. 2013. p. 1104-11.
193. Blankley, C.J., et al., *Synthesis and structure-activity relationships of a novel series of non-peptide angiotensin II receptor binding inhibitors specific for the AT2 subtype.* J Med Chem, 1991. **34**(11): p. 3248-60.

194. Santos, R.A., et al., *Characterization of a new selective antagonist for angiotensin-(1-7), D-pro7-angiotensin-(1-7).* Hypertension, 2003. **41**(3 Pt 2): p. 737-43.
195. Lu, S., et al., *Constitutive G protein coupling profiles of understudied orphan GPCRs.* PLoS One, 2021. **16**(4): p. e0247743.
196. Katritch, V., et al., *Allosteric sodium in class A GPCR signaling.* Trends in biochemical sciences, 2014. **39**(5): p. 233-244.
197. Flegel, C., et al., *RNA-Seq Analysis of Human Trigeminal and Dorsal Root Ganglia with a Focus on Chemoreceptors*, in *PLOS ONE*, D.D. McKemy, Editor. 2015. p. e0128951.
198. Milasta, S., et al., *Interactions between the Mas-related receptors MrgD and MrgE alter signalling and trafficking of MrgD.*, in *Molecular pharmacology*. 2006. p. 479-91.
199. Jumper, J., et al., *Highly accurate protein structure prediction with AlphaFold.* Nature, 2021. **596**(7873): p. 583-589.
200. Varadi, M., et al., *AlphaFold Protein Structure Database: massively expanding the structural coverage of protein-sequence space with high-accuracy models.* Nucleic acids research, 2022. **50**(D1): p. D439-D444.
201. Kaur, H., et al., *Single-cell profiling reveals heterogeneity and functional patterning of GPCR expression in the vascular system*, in *Nature Communications*. 2017.
202. Uhlen, M., et al., *Proteomics. Tissue-based map of the human proteome.* Science, 2015. **347**(6220): p. 1260419.
203. Shen, Q., et al., *MrgprF acts as a tumor suppressor in cutaneous melanoma by restraining PI3K/Akt signaling.* Signal Transduct Target Ther, 2022. **7**(1): p. 147.
204. Sun, L. and R.D. Ye, *Role of G protein-coupled receptors in inflammation.* Acta Pharmacol Sin, 2012. **33**(3): p. 342-50.
205. Avula, L.R., et al., *Expression and distribution patterns of mas-related gene receptor subtypes A-H in the mouse intestine: Inflammation-induced changes*, in *Histochemistry and Cell Biology*. 2013. p. 639-658.
206. Van Remoortel, S., et al., *Mas-related G protein-coupled receptor C11 (Mrgprc11) induces visceral hypersensitivity in the mouse colon: A novel target in gut nociception?*, in *Neurogastroenterology and motility : the official journal of the European Gastrointestinal Motility Society*. 2019. p. e13623.
207. Castro, J., et al., *Activation of pruritogenic TGR5, MrgprA3, and MrgprC11 on colon-innervating afferents induces visceral hypersensitivity*, in *JCI Insight*. 2019.
208. Hrenak, J., L. Paulis, and F. Simko, *Angiotensin A/Alamandine/MrgD Axis: Another Clue to Understanding Cardiovascular Pathophysiology.*, in *International journal of molecular sciences*. 2016.

209. Crozier, R.A., et al., *MrgD activation inhibits KCNQ/M-currents and contributes to enhanced neuronal excitability.*, in *The Journal of neuroscience : the official journal of the Society for Neuroscience*. 2007. p. 4492-6.
210. Zhuo, R.G., et al., *Mas-related G protein-coupled receptor D is coupled to endogenous calcium-activated chloride channel in Xenopus oocytes.* J Physiol Biochem, 2014. **70**(1): p. 185-91.
211. Wang, C., et al., *Facilitation of MrgprD by TRP-A1 promotes neuropathic pain*. 2019.
212. Yang, Y., et al., *Allantoin induces pruritus by activating MrgprD in chronic kidney disease.* Journal of Cellular Physiology, 2023. **238**(4): p. 813-828.
213. Liu, Q., et al., *Mechanisms of itch evoked by β-alanine.*, in *The Journal of neuroscience : the official journal of the Society for Neuroscience*. 2012. p. 14532-7.
214. Villela, D.C., D.G. Passos-Silva, and R.A.S. Santos, *Alamandine: a new member of the angiotensin family.*, in *Current opinion in nephrology and hypertension*. 2014. p. 130-4.
215. Tetzner, A., et al., *G-Protein–Coupled Receptor MrgD Is a Receptor for Angiotensin-(1–7) Involving Adenylyl Cyclase, cAMP, and Phosphokinase A,* in *Hypertension*. 2016. p. 185-194.
216. Yang, C., et al., *Alamandine attenuates angiotensin II-induced vascular fibrosis via inhibiting p38 MAPK pathway.* Eur J Pharmacol, 2020. **883**: p. 173384.
217. Jesus, I.C.G., et al., *Alamandine enhances cardiomyocyte contractility in hypertensive rats through a nitric oxide-dependent activation of CaMKII.* Am J Physiol Cell Physiol, 2020. **318**(4): p. C740-C750.
218. Guedes de Jesus, I.C., et al., *Alamandine acts via MrgD to induce AMPK/NO activation against ANG II hypertrophy in cardiomyocytes*, in *American Journal of Physiology - Cell Physiology*. 2018. p. C702-C711.
219. Seiler, C.Y., et al., *DNASU plasmid and PSI:Biology-Materials repositories: resources to accelerate biological research.* Nucleic Acids Res, 2014. **42**(Database issue): p. D1253-60.
220. Schon, M., et al., *The Potential of Carnosine in Brain-Related Disorders: A Comprehensive Review of Current Evidence.* Nutrients, 2019. **11**(6).
221. Blancquaert, L., et al., *Carnosine and anserine homeostasis in skeletal muscle and heart is controlled by beta-alanine transamination.* J Physiol, 2016. **594**(17): p. 4849-63.
222. Reddy, V.P., et al., *Carnosine: a versatile antioxidant and antiglycating agent.* Sci Aging Knowledge Environ, 2005. **2005**(18): p. pe12.
223. Desai, S., et al., *Cytokine profile of conditioned medium from human tumor cell lines after acute and fractionated doses of gamma radiation*

and its effect on survival of bystander tumor cells. Cytokine, 2013. **61**(1): p. 54-62.
224. Milligan, G., *Constitutive activity and inverse agonists of G protein-coupled receptors: a current perspective.* Mol Pharmacol, 2003. **64**(6): p. 1271-6.
225. Martin, A.L., M.A. Steurer, and R.S. Aronstam, *Constitutive Activity among Orphan Class-A G Protein Coupled Receptors.* PLoS One, 2015. **10**(9): p. e0138463.
226. Taniguchi, M., et al., *YM-254890, a novel platelet aggregation inhibitor produced by Chromobacterium sp. QS3666.* J Antibiot (Tokyo), 2003. **56**(4): p. 358-63.
227. Nishimura, A., et al., *Structural basis for the specific inhibition of heterotrimeric Gq protein by a small molecule.* Proc Natl Acad Sci U S A, 2010. **107**(31): p. 13666-71.
228. Charpentier, T.H., et al., *Potent and Selective Peptide-based Inhibition of the G Protein Galphaq.* J Biol Chem, 2016. **291**(49): p. 25608-25616.
229. Bleasdale, J.E., et al., *Selective inhibition of receptor-coupled phospholipase C-dependent processes in human platelets and polymorphonuclear neutrophils.* J Pharmacol Exp Ther, 1990. **255**(2): p. 756-68.
230. Waelchli, R., et al., *Design and preparation of 2-benzamido-pyrimidines as inhibitors of IKK.* Bioorg Med Chem Lett, 2006. **16**(1): p. 108-12.
231. Oeckinghaus, A. and S. Ghosh, *The NF-kappaB family of transcription factors and its regulation.* Cold Spring Harb Perspect Biol, 2009. **1**(4): p. a000034.
232. Patil, D.N., et al., *Cryo-EM structure of human GPR158 receptor coupled to the RGS7-Gbeta5 signaling complex.* Science, 2022. **375**(6576): p. 86-91.
233. Dimri, S., et al., *Dynamic monitoring of STAT3 activation in live cells using a novel STAT3 Phospho-BRET sensor.* Am J Nucl Med Mol Imaging, 2019. **9**(6): p. 321-334.
234. D'Orazi, G., M. Cordani, and M. Cirone, *Oncogenic pathways activated by pro-inflammatory cytokines promote mutant p53 stability: clue for novel anticancer therapies.* Cell Mol Life Sci, 2021. **78**(5): p. 1853-1860.
235. Rosenbaum, D.M., S.G. Rasmussen, and B.K. Kobilka, *The structure and function of G-protein-coupled receptors.* Nature, 2009. **459**(7245): p. 356-63.
236. Pang, L., M. Graziano, and S. Wang, *Membrane cholesterol modulates galanin-GalR2 interaction.* Biochemistry, 1999. **38**(37): p. 12003-11.
237. Burger, K., G. Gimpl, and F. Fahrenholz, *Regulation of receptor function by cholesterol.* Cell Mol Life Sci, 2000. **57**(11): p. 1577-92.

238. Yao, Z. and B. Kobilka, *Using synthetic lipids to stabilize purified beta2 adrenoceptor in detergent micelles.* Anal Biochem, 2005. **343**(2): p. 344-6.
239. Cherezov, V., et al., *High-resolution crystal structure of an engineered human beta2-adrenergic G protein-coupled receptor.* Science, 2007. **318**(5854): p. 1258-65.
240. Hanson, M.A., et al., *A specific cholesterol binding site is established by the 2.8 A structure of the human beta2-adrenergic receptor.* Structure, 2008. **16**(6): p. 897-905.
241. Manna, M., et al., *Mechanism of allosteric regulation of beta2-adrenergic receptor by cholesterol.* Elife, 2016. **5**.
242. Pluhackova, K., et al., *Dynamic Cholesterol-Conditioned Dimerization of the G Protein Coupled Chemokine Receptor Type 4.* PLoS Comput Biol, 2016. **12**(11): p. e1005169.
243. Guixa-Gonzalez, R., et al., *Membrane cholesterol access into a G-protein-coupled receptor.* Nat Commun, 2017. **8**: p. 14505.
244. M. Congreve, A.B., G. Brown, R.M. Cooke, *Modeling and Design for Membrane Protein Targets*, in *Comprehensive Medicinal Chemistry III*, D.R. Samuel Chackalamannil, Simon E. Ward, Editor. 2017, Elsevier. p. 145-188.
245. Jakubik, J. and E.E. El-Fakahany, *Allosteric Modulation of GPCRs of Class A by Cholesterol.* Int J Mol Sci, 2021. **22**(4).
246. Taghon, G.J., et al., *Predictable cholesterol binding sites in GPCRs lack consensus motifs.* Structure, 2021. **29**(5): p. 499-506 e3.
247. Grouleff, J., et al., *The influence of cholesterol on membrane protein structure, function, and dynamics studied by molecular dynamics simulations.* Biochim Biophys Acta, 2015. **1848**(9): p. 1783-95.
248. van Meer, G., D.R. Voelker, and G.W. Feigenson, *Membrane lipids: where they are and how they behave.* Nat Rev Mol Cell Biol, 2008. **9**(2): p. 112-24.
249. Lee, H., et al., *Cholesterol induces cardiac hypertrophy by activating the AKT pathway.* J Steroid Biochem Mol Biol, 2013. **138**: p. 307-13.
250. Tall, A.R. and L. Yvan-Charvet, *Cholesterol, inflammation and innate immunity.* Nat Rev Immunol, 2015. **15**(2): p. 104-16.
251. Bergasa, N.V., *Pruritus of Cholestasis*, in *Itch: Mechanisms and Treatment*, E. Carstens and T. Akiyama, Editors. 2014: Boca Raton (FL).
252. Wang, H. and M.J. Zylka, *Mrgprd-expressing polymodal nociceptive neurons innervate most known classes of substantia gelatinosa neurons.*, in *The Journal of neuroscience : the official journal of the Society for Neuroscience*. 2009. p. 13202-9.
253. Li, T. and J.Y. Chiang, *Regulation of bile acid and cholesterol metabolism by PPARs.* PPAR Res, 2009. **2009**: p. 501739.

254. Dikkers, A. and U.J. Tietge, *Biliary cholesterol secretion: more than a simple ABC.* World J Gastroenterol, 2010. **16**(47): p. 5936-45.
255. di Gregorio, M.C., J. Cautela, and L. Galantini, *Physiology and physical chemistry of bile acids.* International journal of molecular sciences, 2021. **22**(4): p. 1780.
256. Kroeze, W.K., et al., *PRESTO-Tango as an open-source resource for interrogation of the druggable human GPCRome.*, in *Nature structural & molecular biology*. 2015. p. 362-9.
257. Costa-Neto, C.M., L.T. Parreiras-e-Silva, and M. Bouvier, *A pluridimensional view of biased agonism.* Molecular Pharmacology, 2016. **90**(5): p. 587-595.
258. Huang, W.M., M. Gowda, and J.G. Donnelly, *Bile acid ratio in diagnosis of intrahepatic cholestasis of pregnancy.* Am J Perinatol, 2009. **26**(4): p. 291-4.
259. Ridlon, J.M., et al., *Consequences of bile salt biotransformations by intestinal bacteria.* Gut Microbes, 2016. **7**(1): p. 22-39.
260. Polli, E.E., et al., *Treatment of radiolucent gallstones with CDCA or UDCA. A multicenter trial.* Digestion, 1981. **22**(4): p. 185-91.
261. Charlton, S.A. and J.W. Coym, *The use of methyl-β-cyclodextrin to solubilize cholesterol prior to coating onto a C18 stationary phase.* Journal of Chromatography A, 2012. **1266**: p. 69-75.
262. Mahammad, S. and I. Parmryd, *Cholesterol depletion using methyl-beta-cyclodextrin.* Methods Mol Biol, 2015. **1232**: p. 91-102.
263. Whorton, M.R., et al., *A monomeric G protein-coupled receptor isolated in a high-density lipoprotein particle efficiently activates its G protein.* Proceedings of the National Academy of Sciences, 2007. **104**(18): p. 7682-7687.
264. Xiang, Y., et al., *Caveolar localization dictates physiologic signaling of β2-adrenoceptors in neonatal cardiac myocytes.* Journal of Biological Chemistry, 2002. **277**(37): p. 34280-34286.
265. Biswas, A., et al., *Cholesterol Depletion by MbetaCD Enhances Cell Membrane Tension and Its Variations-Reducing Integrity.* Biophys J, 2019. **116**(8): p. 1456-1468.
266. Sureka, B., et al., *Neurologic Manifestations of Chronic Liver Disease and Liver Cirrhosis.* Curr Probl Diagn Radiol, 2015. **44**(5): p. 449-61.
267. Muzurovic, E., et al., *Nonalcoholic Fatty Liver Disease and Cardiovascular Disease: a Review of Shared Cardiometabolic Risk Factors.* Hypertension, 2022. **79**(7): p. 1319-1326.
268. Hegade, V.S., S.F. Kendrick, and D.E. Jones, *Drug treatment of pruritus in liver diseases.* Clinical Medicine, 2015. **15**(4): p. 351.
269. Lang, E., et al., *Bile Acid-Induced Suicidal Erythrocyte Death.* Cell Physiol Biochem, 2016. **38**(4): p. 1500-9.

270. Zhou, Y., et al., *Bile acids modulate signaling by functional perturbation of plasma membrane domains.* J Biol Chem, 2013. **288**(50): p. 35660-70.
271. Ruprecht, V., et al., *How cells respond to environmental cues - insights from bio-functionalized substrates.* J Cell Sci, 2017. **130**(1): p. 51-61.
272. Paluch, E.K., et al., *Mechanotransduction: use the force(s).* BMC Biol, 2015. **13**: p. 47.
273. Zhang, M., et al., *Mechanically Activated Piezo Channels Mediate Touch and Suppress Acute Mechanical Pain Response in Mice.* Cell Rep, 2019. **26**(6): p. 1419-1431 e4.
274. Delmas, P. and B. Coste, *Mechano-gated ion channels in sensory systems.* Cell, 2013. **155**(2): p. 278-84.
275. Honore, E., et al., *The Piezo Mechanosensitive Ion Channels: May the Force Be with You!* Rev Physiol Biochem Pharmacol, 2015. **169**: p. 25-41.
276. Wilde, C., et al., *Translating the force-mechano-sensing GPCRs.* Am J Physiol Cell Physiol, 2022. **322**(6): p. C1047-C1060.
277. Lin, H.H., et al., *Ligands and Beyond: Mechanosensitive Adhesion GPCRs.* Pharmaceuticals (Basel), 2022. **15**(2).
278. Chachisvilis, M., Y.L. Zhang, and J.A. Frangos, *G protein-coupled receptors sense fluid shear stress in endothelial cells.* Proc Natl Acad Sci U S A, 2006. **103**(42): p. 15463-8.
279. Iliff, A.J. and X.Z.S. Xu, *A Mechanosensitive GPCR that Detects the Bloody Force.* Cell, 2018. **173**(3): p. 542-544.
280. Barauna, V.G., et al., *Shear stress-induced Ang II AT1 receptor activation: G-protein dependent and independent mechanisms.* Biochem Biophys Res Commun, 2013. **434**(3): p. 647-52.
281. Ramkhelawon, B., et al., *Shear stress regulates angiotensin type 1 receptor expression in endothelial cells.* Circ Res, 2009. **105**(9): p. 869-75.
282. Zou, Y., et al., *Mechanical stress activates angiotensin II type 1 receptor without the involvement of angiotensin II.* Nature cell biology, 2004. **6**(6): p. 499-506.
283. Marullo, S., et al., *Mechanical GPCR Activation by Traction Forces Exerted on Receptor N-Glycans.* ACS Pharmacol Transl Sci, 2020. **3**(2): p. 171-178.
284. Xu, J., et al., *GPR68 Senses Flow and Is Essential for Vascular Physiology.* Cell, 2018. **173**(3): p. 762-775 e16.
285. McCormick, M.E. and E. Tzima, *Pulling on my heartstrings: mechanotransduction in cardiac development and function.* Curr Opin Hematol, 2016. **23**(3): p. 235-42.
286. Tavi, P., et al., *Cardiac mechanotransduction: from sensing to disease and treatment.* Trends Pharmacol Sci, 2001. **22**(5): p. 254-60.

287. Yeh, C.F., C. Chou, and K.C. Yang, *Mechanotransduction in fibrosis: Mechanisms and treatment targets.* Curr Top Membr, 2021. **87**: p. 279-314.
288. Puente, X.S., et al., *A genomic view of the complexity of mammalian proteolytic systems.* Biochem Soc Trans, 2005. **33**(Pt 2): p. 331-4.
289. Ramachandran, R., et al., *Proteinases, Their Extracellular Targets, and Inflammatory Signaling.*, in *Pharmacological reviews*. 2016. p. 1110-1142.
290. Esch, P.M., H. Gerngross, and A. Fabian, *Reduction of postoperative swelling. Objective measurement of swelling of the upper ankle joint in treatment with serrapeptase- a prospective study.* Fortschr Med, 1989. **107**(4): p. 67-8, 71-2.
291. Singh, R.B., et al., *Role of proteases in the pathophysiology of cardiac disease.* Mol Cell Biochem, 2004. **263**(1-2): p. 241-56.
292. Oikonomopoulou, K., et al., *Proteinases and their receptors in inflammatory arthritis: an overview.* Nat Rev Rheumatol, 2018. **14**(3): p. 170-180.
293. Xu, J., et al., *Inhibition of cathepsin S produces neuroprotective effects after traumatic brain injury in mice.* Mediators Inflamm, 2013. **2013**: p. 187873.
294. Vu, T.K., et al., *Molecular cloning of a functional thrombin receptor reveals a novel proteolytic mechanism of receptor activation.* Cell, 1991. **64**(6): p. 1057-68.
295. Hollenberg, M.D., et al., *Role of the amino- and carboxyl-terminal domains of thrombin receptor-derived polypeptides in biological activity in vascular endothelium and gastric smooth muscle: evidence for receptor subtypes.* Mol Pharmacol, 1993. **43**(6): p. 921-30.
296. Liebscher, I., et al., *New functions and signaling mechanisms for the class of adhesion G protein–coupled receptors.* Annals of the New York Academy of Sciences, 2014. **1333**(1): p. 43-64.
297. Cattaruzza, F., et al., *Cathepsin S is activated during colitis and causes visceral hyperalgesia by a PAR2-dependent mechanism in mice.* Gastroenterology, 2011. **141**(5): p. 1864-74 e1-3.
298. Zhao, P., et al., *Cathepsin S causes inflammatory pain via biased agonism of PAR2 and TRPV4.* J Biol Chem, 2014. **289**(39): p. 27215-27234.
299. Elmariah, S.B., V.B. Reddy, and E.A. Lerner, *Cathepsin S signals via PAR2 and generates a novel tethered ligand receptor agonist.*, in *PloS one*. 2014. p. e99702.
300. David Troncoso, F., D. Alberto Sanchez, and M. Lujan Ferreira, *Production of Plant Proteases and New Biotechnological Applications: An Updated Review.* ChemistryOpen, 2022. **11**(3): p. e202200017.

301. Storm van's Gravesande, K., et al., *IFN regulatory factor-1 regulates IFN-γ-dependent cathepsin S expression.* The Journal of Immunology, 2002. **168**(9): p. 4488-4494.
302. Driessen, C., et al., *Cathepsin S controls the trafficking and maturation of MHC class II molecules in dendritic cells.* J Cell Biol, 1999. **147**(4): p. 775-90.
303. Saegusa, K., et al., *Cathepsin S inhibitor prevents autoantigen presentation and autoimmunity.* J Clin Invest, 2002. **110**(3): p. 361-9.
304. Turk, V., et al., *Cysteine cathepsins: from structure, function and regulation to new frontiers.* Biochim Biophys Acta, 2012. **1824**(1): p. 68-88.
305. Jobs, E., et al., *Serum cathepsin S is associated with decreased insulin sensitivity and the development of type 2 diabetes in a community-based cohort of elderly men.* Diabetes Care, 2013. **36**(1): p. 163-5.
306. Li, X., et al., *Cathepsin S activity controls ischemia-induced neovascularization in mice.* Int J Cardiol, 2015. **183**: p. 198-208.
307. Memmert, S., et al., *Role of Cathepsin S in Periodontal Inflammation and Infection.* Mediators Inflamm, 2017. **2017**: p. 4786170.
308. Sena, B.F., J.L. Figueiredo, and E. Aikawa, *Cathepsin S As an Inhibitor of Cardiovascular Inflammation and Calcification in Chronic Kidney Disease.* Front Cardiovasc Med, 2017. **4**: p. 88.
309. Yan, X., et al., *Involvement of Cathepsins in Innate and Adaptive Immune Responses in Periodontitis.* Evid Based Complement Alternat Med, 2020. **2020**: p. 4517587.
310. Tobbell, D.A., et al., *Identification of in vitro folding conditions for procathepsin S and cathepsin S using fractional factorial screens.* Protein Expr Purif, 2002. **24**(2): p. 242-54.
311. Reddy, V.B., et al., *Cathepsin S elicits itch and signals via protease-activated receptors.* J Invest Dermatol, 2010. **130**(5): p. 1468-70.
312. Vidak, E., et al., *Cysteine Cathepsins and their Extracellular Roles: Shaping the Microenvironment.* Cells, 2019. **8**(3).
313. Vizovišek, M., M. Fonović, and B. Turk, *Cysteine cathepsins in extracellular matrix remodeling: Extracellular matrix degradation and beyond.* Matrix Biology, 2019. **75**: p. 141-159.
314. Stoeber, M., et al., *A Genetically Encoded Biosensor Reveals Location Bias of Opioid Drug Action.* Neuron, 2018. **98**(5): p. 963-976 e5.
315. Geppetti, P., et al., *G Protein-Coupled Receptors: Dynamic Machines for Signaling Pain and Itch*, in *Neuron*. 2015.
316. He, S.-Q., et al., *Oligomerization of MrgC11 and μ-opioid receptors in sensory neurons enhances morphine analgesia.*, in *Science signaling*. 2018. p. 1-16.

317. Lohse, M.J., S. Engelhardt, and T. Eschenhagen, *What is the role of β-adrenergic signaling in heart failure?* Circulation research, 2003. **93**(10): p. 896-906.
318. Pierce, K.L., R.T. Premont, and R.J. Lefkowitz, *Seven-transmembrane receptors.* Nat Rev Mol Cell Biol, 2002. **3**(9): p. 639-50.
319. Bouvier, M., *Oligomerization of G-protein-coupled transmitter receptors.* Nat Rev Neurosci, 2001. **2**(4): p. 274-86.
320. Ferre, S. and R. Franco, *Oligomerization of G-protein-coupled receptors: a reality.* Curr Opin Pharmacol, 2010. **10**(1): p. 1-5.
321. Wang, W., Y. Qiao, and Z. Li, *New Insights into Modes of GPCR Activation.* Trends Pharmacol Sci, 2018. **39**(4): p. 367-386.
322. Tateyama, M., et al., *Ligand-induced rearrangement of the dimeric metabotropic glutamate receptor 1alpha.* Nat Struct Mol Biol, 2004. **11**(7): p. 637-42.
323. Kniazeff, J., et al., *Closed state of both binding domains of homodimeric mGlu receptors is required for full activity.* Nat Struct Mol Biol, 2004. **11**(8): p. 706-13.
324. Gaitonde, S.A. and J. Gonzalez-Maeso, *Contribution of heteromerization to G protein-coupled receptor function.* Curr Opin Pharmacol, 2017. **32**: p. 23-31.
325. Milligan, G., *G protein-coupled receptor dimerisation: molecular basis and relevance to function.* Biochimica et Biophysica Acta (BBA)-Biomembranes, 2007. **1768**(4): p. 825-835.
326. Albizu, L., et al., *Time-resolved FRET between GPCR ligands reveals oligomers in native tissues.* Nat Chem Biol, 2010. **6**(8): p. 587-94.
327. Kern, A., et al., *Apo-ghrelin receptor forms heteromers with DRD2 in hypothalamic neurons and is essential for anorexigenic effects of DRD2 agonism.* Neuron, 2012. **73**(2): p. 317-32.
328. Fernandez-Duenas, V., et al., *Untangling dopamine-adenosine receptor-receptor assembly in experimental parkinsonism in rats.* Dis Model Mech, 2015. **8**(1): p. 57-63.
329. Jordan, B.A. and L.A. Devi, *G-protein-coupled receptor heterodimerization modulates receptor function.* Nature, 1999. **399**(6737): p. 697-700.
330. Angers, S., et al., *Detection of beta 2-adrenergic receptor dimerization in living cells using bioluminescence resonance energy transfer (BRET).* Proc Natl Acad Sci U S A, 2000. **97**(7): p. 3684-9.
331. Lavoie, C., et al., *Beta 1/beta 2-adrenergic receptor heterodimerization regulates beta 2-adrenergic receptor internalization and ERK signaling efficacy.* J Biol Chem, 2002. **277**(38): p. 35402-10.
332. Dixon, A.S., et al., *NanoLuc Complementation Reporter Optimized for Accurate Measurement of Protein Interactions in Cells.* ACS Chem Biol, 2016. **11**(2): p. 400-8.

333. Förster, T., *Zwischenmolekulare Energiewanderung und Fluoreszenz.* 1948(437): p. 55-75.
334. Xu, Y., D.W. Piston, and C.H. Johnson, *A bioluminescence resonance energy transfer (BRET) system: application to interacting circadian clock proteins.* Proc Natl Acad Sci U S A, 1999. **96**(1): p. 151-6.
335. Sambrook, J. and D.W. Russell, *Identification of associated proteins by coimmunoprecipitation.* CSH Protoc, 2006. **2006**(1).
336. De, A., et al., *Evolution of BRET Biosensors from Live Cell to Tissue-Scale In vivo Imaging.* Front Endocrinol (Lausanne), 2013. **4**: p. 131.
337. Hall, M.P., et al., *Engineered luciferase reporter from a deep sea shrimp utilizing a novel imidazopyrazinone substrate.* ACS Chem Biol, 2012. **7**(11): p. 1848-57.
338. Damdindorj, L., et al., *A comparative analysis of constitutive promoters located in adeno-associated viral vectors.* PLoS One, 2014. **9**(8): p. e106472.
339. Evers, T.H., et al., *Quantitative understanding of the energy transfer between fluorescent proteins connected via flexible peptide linkers.* Biochemistry, 2006. **45**(44): p. 13183-92.
340. Shaner, N.C., et al., *Improved monomeric red, orange and yellow fluorescent proteins derived from Discosoma sp. red fluorescent protein.* Nat Biotechnol, 2004. **22**(12): p. 1567-72.
341. De, A., et al., *BRET3: a red-shifted bioluminescence resonance energy transfer (BRET)-based integrated platform for imaging protein-protein interactions from single live cells and living animals.* FASEB J, 2009. **23**(8): p. 2702-9.
342. Shu, X., et al., *Novel chromophores and buried charges control color in mFruits.* Biochemistry, 2006. **45**(32): p. 9639-47.
343. Jamieson, C., et al., *Rac1 augments Wnt signaling by stimulating beta-catenin-lymphoid enhancer factor-1 complex assembly independent of beta-catenin nuclear import.* J Cell Sci, 2015. **128**(21): p. 3933-46.
344. Jesus, I.C.G., et al., *An Overview of Alamadine/MrgD Signaling and Its Role in Cardiomyocytes.* Am J Physiol Cell Physiol, 2022.
345. Grazzini, E., et al., *Sensory neuron-specific receptor activation elicits central and peripheral nociceptive effects in rats*, in *Proceedings of the National Academy of Sciences*. 2004. p. 7175-7180.
346. Sleno, R. and T.E. Hebert, *The Dynamics of GPCR Oligomerization and Their Functional Consequences.* Int Rev Cell Mol Biol, 2018. **338**: p. 141-171.
347. Shalaeva, D.N., M.Y. Galperin, and A.Y. Mulkidjanian, *Eukaryotic G protein-coupled receptors as descendants of prokaryotic sodium-translocating rhodopsins.* Biol Direct, 2015. **10**: p. 63.
348. Strotmann, R., et al., *Evolution of GPCR: change and continuity.* Mol Cell Endocrinol, 2011. **331**(2): p. 170-8.

349. de Mendoza, A., A. Sebe-Pedros, and I. Ruiz-Trillo, *The evolution of the GPCR signaling system in eukaryotes: modularity, conservation, and the transition to metazoan multicellularity.* Genome Biol Evol, 2014. **6**(3): p. 606-19.
350. Carey, R.M., *Newly discovered components and actions of the renin-angiotensin system.*, in *Hypertension (Dallas, Tex. : 1979)*. 2013. p. 818-22.
351. Shen, Q., et al., *MrgprF acts as a tumor suppressor in cutaneous melanoma by restraining PI3K/Akt signaling.* Signal Transduction and Targeted Therapy, 2022. **7**(1): p. 147.
352. Serizawa, K., et al., *Interleukin-6: evolving role in the management of neuropathic pain in neuroimmunological disorders.* Inflammation and Regeneration, 2021. **41**(1): p. 1-11.
353. Kanda, T. and T. Takahashi, *Interleukin-6 and cardiovascular diseases.* Jpn Heart J, 2004. **45**(2): p. 183-93.
354. Gabay, C., *Interleukin-6 and chronic inflammation.* Arthritis research & therapy, 2006. **8**(2): p. 1-6.
355. Mitani, H., et al., *Activity of interleukin 6 in the differentiation of monocytes to macrophages and dendritic cells.* British journal of haematology, 2000. **109**(2): p. 288-295.
356. Kreiner, F.F., et al., *Interleukin 6 in diabetes, chronic kidney disease, and cardiovascular disease: mechanisms and therapeutic perspectives.* Expert Rev Clin Immunol, 2022. **18**(4): p. 377-389.
357. Ali, A.L., N.P. Nailwal, and G.M. Doshi, *Emerging role of interleukins for the assessment and treatment of liver diseases.* Endocrine, Metabolic & Immune Disorders-Drug Targets (Formerly Current Drug Targets-Immune, Endocrine & Metabolic Disorders), 2022. **22**(4): p. 371-382.
358. Gunarathne, L.S., et al., *Mas-related G protein-coupled receptor type D antagonism improves portal hypertension in cirrhotic rats.* Hepatology Communications, 2022. **6**(9): p. 2523-2537.
359. Allen, J.A., R.A. Halverson-Tamboli, and M.M. Rasenick, *Lipid raft microdomains and neurotransmitter signalling.* Nat Rev Neurosci, 2007. **8**(2): p. 128-40.
360. Larosa, J.C., *Understanding risk in hypercholesterolemia.* Clinical Cardiology: An International Indexed and Peer-Reviewed Journal for Advances in the Treatment of Cardiovascular Disease, 2003. **26**(S1): p. 3-6.
361. Vickery, O.N., J.P. Machtens, and U. Zachariae, *Membrane potentials regulating GPCRs: insights from experiments and molecular dynamics simulations.* Curr Opin Pharmacol, 2016. **30**: p. 44-50.
362. Clark, A.K., et al., *Inhibition of spinal microglial cathepsin S for the reversal of neuropathic pain.*, in *Proceedings of the National Academy of Sciences of the United States of America*. 2007. p. 10655-60.

363. Wang, Y., et al., *Cathepsin B aggravates coxsackievirus B3-induced myocarditis through activating the inflammasome and promoting pyroptosis.* PLoS pathogens, 2018. **14**(1): p. e1006872.
364. Yadati, T., et al., *The ins and outs of cathepsins: Physiological function and role in disease management.* Cells, 2020. **9**(7): p. 1679.
365. Skopál, A., et al., *Cathepsin D interacts with adenosine A2A receptors in mouse macrophages to modulate cell surface localization and inflammatory signaling.* Journal of Biological Chemistry, 2022. **298**(5).
366. Liuzzo, J.P., et al., *Inflammatory mediators regulate cathepsin S in macrophages and microglia: A role in attenuating heparan sulfate interactions.* Mol Med, 1999. **5**(5): p. 320-33.
367. Fernando, M.R., et al., *The pro-inflammatory cytokine, interleukin-6, enhances the polarization of alternatively activated macrophages.* PLoS One, 2014. **9**(4): p. e94188.
368. Sanmarco, L.M., et al., *IL-6 promotes M2 macrophage polarization by modulating purinergic signaling and regulates the lethal release of nitric oxide during Trypanosoma cruzi infection.* Biochimica et Biophysica Acta (BBA)-Molecular Basis of Disease, 2017. **1863**(4): p. 857-869.
369. Ferre, S., et al., *Oligomerization of G protein-coupled receptors: Still doubted?* Prog Mol Biol Transl Sci, 2020. **169**: p. 297-321.
370. De, A., R. Arora, and A. Jasani, *Engineering Aspects of Bioluminescence Resonance Energy Transfer Systems*, in *Engineering in Translational Medicine*, W. Cai, Editor. 2014, Springer London: London. p. 257-300.
371. Angers, S., et al., *Detection of β2-adrenergic receptor dimerization in living cells using bioluminescence resonance energy transfer (BRET).* Proceedings of the National Academy of Sciences, 2000. **97**(7): p. 3684-3689.
372. Ciruela, F., J.-P. Vilardaga, and V. Fernández-Dueñas, *Lighting up multiprotein complexes: lessons from GPCR oligomerization.* Trends in biotechnology, 2010. **28**(8): p. 407-415.
373. Canals, M., et al., *Homodimerization of adenosine A2A receptors: qualitative and quantitative assessment by fluorescence and bioluminescence energy transfer.* Journal of neurochemistry, 2004. **88**(3): p. 726-734.
374. Tavernier, J., et al., *MAPPIT: a cytokine receptor-based two-hybrid method in mammalian cells.* Clin Exp Allergy, 2002. **32**(10): p. 1397-404.
375. Atanassoff, P.G., et al., *Enhancement of experimental pruritus and mechanically evoked dysesthesiae with local anesthesia.* Somatosens Mot Res, 1999. **16**(4): p. 291-8.
376. Kumar, K. and S.I. Singh, *Neuraxial opioid-induced pruritus: An update.* J Anaesthesiol Clin Pharmacol, 2013. **29**(3): p. 303-7.
377. Breit, A., et al., *Simultaneous activation of the delta opioid receptor (deltaOR)/sensory neuron-specific receptor-4 (SNSR-4) hetero-oligomer*

by the mixed bivalent agonist bovine adrenal medulla peptide 22 activates SNSR-4 but inhibits deltaOR signaling. Mol Pharmacol, 2006. **70**(2): p. 686-96.

378. Clark, A.K., et al., *Inhibition of spinal microglial cathepsin S for the reversal of neuropathic pain.* Proc Natl Acad Sci U S A, 2007. **104**(25): p. 10655-60.

Appendix I: Protein sequence analysis

Protein sequence analysis of mouse, rat, and human MRGPRD, MRGPRE and MRGPRF

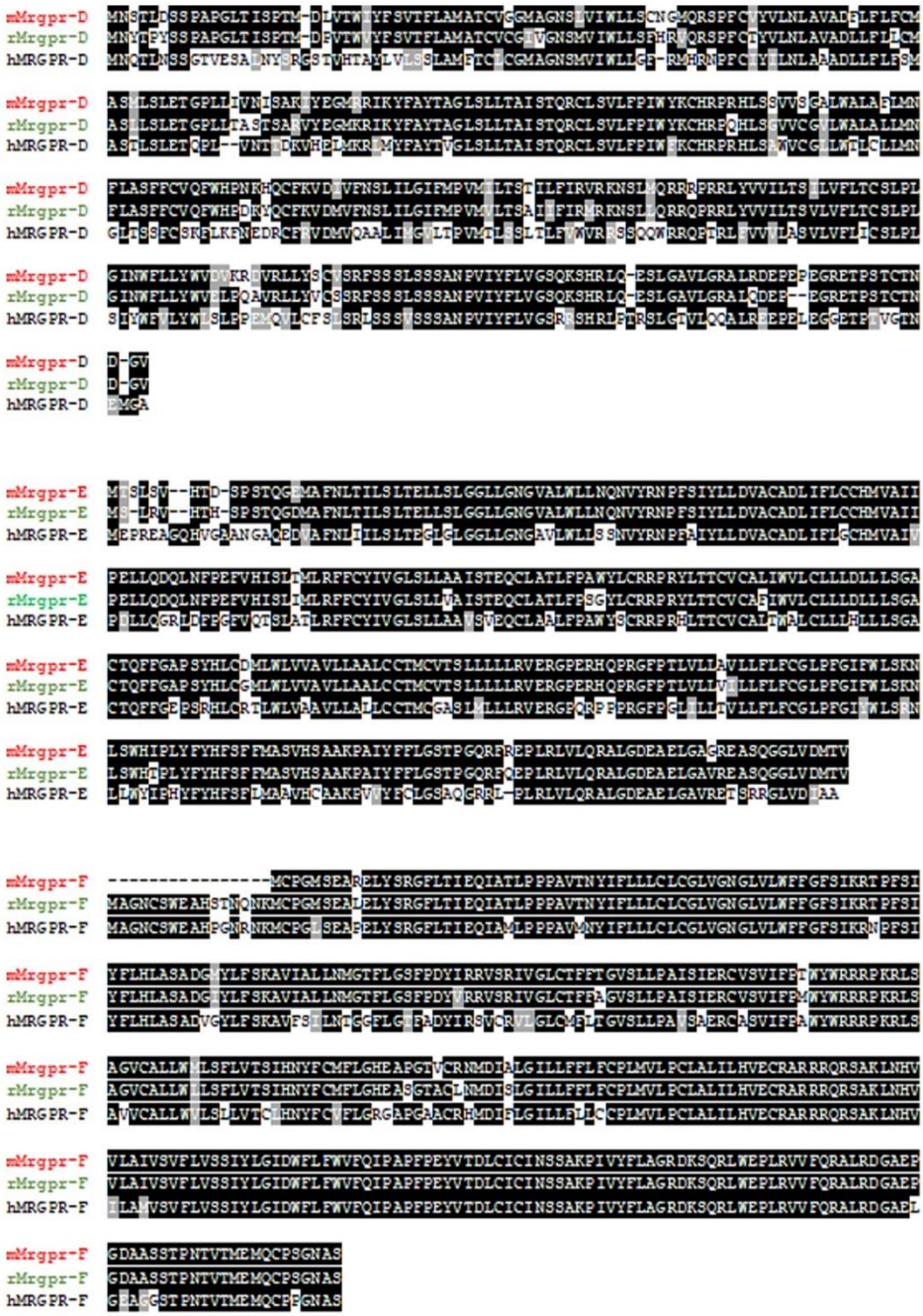

Figure A.1: Protein sequence analysis of MRGPRD, MRGPRE, and MRGPRF. Protein sequence alignments of mouse, rat, and human MRGPRD, MRGPRE and MRGPRF. Identical residues were shaded in black, while similar residues were shaded in grey. Multiple sequence alignments of protein sequences were performed using the T-Coffee1 program and further shaded by BOXSHADE (https://embnet.vital-it.ch/software/BOX_form.html).

Appendix II: Plasmid Libraries Prepared

NanoBiT Plasmid Library

NanoBiT plasmid backbones	
1. pHSVTK-MCS-LgBiT *(Gift from Promega to RA)*	2. pHSVTK-MCS-SmBiT *(Gift from Promega to RA)*
NanoBiT plasmid with start codon	
3. pHSVTK-MCS-**s**LgBiT	4. pHSVTK-MCS-**s**SmBiT
Mas-related G protein-coupled receptors (MRGPRs)-NanoBiT plasmids	
5. pHSVTK-**MRGPRD**-LgBiT	6. pHSVTK-**MRGPRD**-SmBiT
7. pHSVTK-**MRGPRE**-LgBiT	8. pHSVTK-**MRGPRE**-SmBiT
9. pHSVTK-**MRGPRF**-LgBiT	10. pHSVTK-**MRGPRF**-SmBiT
11. pHSVTK-**MRGPRG**-LgBiT	12. pHSVTK-**MRGPRG**-SmBiT
13. pHSVTK-**MRGPRX1**-LgBiT	14. pHSVTK-**MRGPRX1**-SmBiT
15. pHSVTK-**MRGPRX2**-LgBiT	16. pHSVTK-**MRGPRX2**-SmBiT
17. pHSVTK-**MRGPRX3**-LgBiT	18. pHSVTK-**MRGPRX3**-SmBiT
19. pHSVTK-**MRGPRX4**-LgBiT	20. pHSVTK-**MRGPRX4**-SmBiT
Opioids Receptors (OPRs)-NanoBiT plasmids	
21. pHSVTK-**OPRD1**-LgBiT	22. pHSVTK-**OPRD1**-SmBiT
23. pHSVTK-**OPRK1**-LgBiT	24. pHSVTK-**OPRK1**-SmBiT
25. pHSVTK-**OPRL1**-LgBiT	26. pHSVTK-**OPRL1**-SmBiT
27. pHSVTK-**OPRM1**-LgBiT	28. pHSVTK-**OPRM1**-SmBiT
29. pHSVTK-**OPRΔM1**-LgBiT	30. pHSVTK-**OPRΔM1**-SmBiT

β-adrenergic receptors (β2-ARs or ADRBs)-NanoBiT plasmids	
31. pHSVTK-**ADRB1**-LgBiT	32 pHSVTK-**ADRB1**-SmBiT
33. pHSVTK-**ADRB2**-LgBiT	34. pHSVTK-**ADRB2**-SmBiT
Protease-activated receptor (PAR)- NanoBiT plasmids	
35. pHSVTK-**PAR2**-LgBiT	36. pHSVTK-**PAR2**-SmBiT

BRET Plasmid Library

BRET plasmid backbone (empty vector)	
1. pCMV-GS (MCS-GS Flexi Linker) ***(Prepared in lab)***	
BRET plasmid backbones (NLuc and mOrange)	
2. pCMV-MCS-NLuc	3. pCMV-MCS-mOrange
BRET control plasmids (NLuc and mOrange backbones with start codon and NLuc-mOrange fusion plasmid)	
4. pCMV-MCS-**s**NLuc	5. pCMV-MCS-**s**mOrange
6. pCMV-**s**NLuc-mOrange	
Mas-related G protein-coupled receptors (MRGPRs)-BRET plasmids	
7. pCMV-**MRGPRD**-NLuc	8. pCMV-**MRGPRD**-mOrange
9. pCMV-**MRGPRE**-NLuc	10. pCMV-**MRGPRE**-mOrange
11. pCMV-**MRGPRF**-NLuc	12. pCMV-**MRGPRF**-mOrange
13. pCMV-**MRGPRX1**-NLuc	14. pCMV-**MRGPRX1**-mOrange
15. pCMV-**MRGPRX2**-NLuc	16. pCMV-**MRGPRX2**-mOrange
17. pCMV-**MRGPRX4**-NLuc	18. pCMV-**MRGPRX4**-mOrange
β-adrenergic receptors (β-ARs or ADRBs)- BRET plasmids	
19. pCMV-**ADRB1**-NLuc	20. pCMV-**ADRB1**-mOrange
21. pCMV-**ADRB2**-NLuc	22. pCMV-**ADRB2**-mOrange

Mouse Mas-related G protein-coupled receptor (Mrgpr) - BRET plasmids	
23. pCMV-**MrgprC11**-NLuc	24. pCMV-**MrgprC11**-mOrange

FRET Plasmid Library

FRET plasmid backbones (empty vector)	
1. pCMV-ECFP-N1	2. pCMV-EYFP-N1
Mas-related G protein-coupled receptors (MRGPRs)-FRET plasmids	
3. pCMV-**MRGPRD**-ECFP	4. pCMV-**MRGPRD**-EYFP

5. pCMV-**MRGPRE**-ECFP	6. pCMV-**MRGPRE**-EYFP
7. pCMV-**MRGPRF**-ECFP	8. pCMV-**MRGPRF**-EYFP
9. pCMV-**MRGPRX1**-ECFP	10. pCMV-**MRGPRX1**-EYFP
11. pCMV-**MRGPRX2**-ECFP	12. pCMV-**MRGPRX2**-EYFP
β-adrenergic receptors (β-ARs or ADRBs)- FRET plasmids	
13. pCMV-**ADRB1**-ECFP	
14. pCMV-**ADRB2**-ECFP	15. pCMV-**ADRB2**-EYFP
Protease-activated receptor (PAR)- FRET plasmids	
16. pCMV-**PAR2**-ECFP	17. pCMV-**PAR2**-EYFP

Mouse Mas-related G protein-coupled receptor (Mrgpr) - FRET plasmids	
18. pCMV-**MrgprC11**-ECFP	19. pCMV-**MrgprC11**-EYFP

FRET Plasmid Library (monomeric fluorescent protein)

FRET plasmid backbones (empty vector)	
20. pCMV-**m**CFP-N1	21. pCMV-**m**YFP-N1
Mas-related G protein-coupled receptors (MRGPRs)-FRET plasmids	
22. pCMV-**MRGPRD**- **m**CFP-N1	23. pCMV-**MRGPRD**- **m**YFP-N1
24. pCMV-**MRGPRE**- **m**CFP-N1	25. pCMV-**MRGPRE**- **m**YFP-N1
26. pCMV-**MRGPRF**- **m**CFP-N1	27. pCMV-**MRGPRF**- **m**YFP-N1

Small 's' denotes the start codon. Small 'm' denotes monomeric. NanoLuc and mOrange are nanoluciferases (Promega), and monomeric Orange is a fluorescent protein, respectively.

Co-Immunoprecipitation Plasmid Library

HA-tagged plasmids
1. pCMV-HA-**MRGPRD**-ECFP
2. pCMV-HA-**MRGPRD**-EYFP
3. pCMV-**MRGPRD**-HA
4. pCMV-**MRGPRE**-HA
5. pCMV-**MRGPRF**-HA
6. pCMV-**PAR2**-HA
7. pCMV-HA-**MRGPRD**
cmyc-tagged plasmids
8. pCMV-**MRGPRD**-cmyc
9. pCMV-**MRGPRE**-cmyc
10. pCMV-**MRGPRF**-cmyc
11. pCMV-cmyc-**MRGPRE**
12. pCMV-cmyc-**MRGPRF**
13. pCMV-cmyc-**MRGPRD**-HA

Plasmid Library: NanoLuc Tagged on the N-terminus of the Gene

NanoLuc-tagged on the N-terminus of Mas-related G protein-coupled receptors (MRGPRs) [pCMV-MCS (GS Flexi linker) backbone plasmid]	
1. pCMV-NLuc-**MRGPRD**-mOrange	2. pCMV-NLuc-**MRGPRE**-mOrange
3. pCMV-NLuc-**MRGPRF**-mOrange	4. pCMV-NLuc-**MRGPRX1**-mOrange
5. pCMV-NLuc-**MRGPRX2**-mOrange	
NanoLuc-tagged on the N-terminus of β-adrenergic receptors (β-ARs or ADRBs) [pCMV-MCS (GS Flexi linker) backbone plasmid]	
6. pCMV-NLuc-**ADRB1**-mOrange	7. pCMV-NLuc-**ADRB2**-mOrange

NanoLuc-tagged on the N-terminus of Mouse Mas-related G protein-coupled receptor (Mrgpr) [pCMV-MCS (GS Flexi linker) backbone plasmid]	
8. pCMV-NLuc-**MrgprC11**-mOrange	

NanoLuc-tagged on the N-terminus of Mas-related G protein-coupled receptors (MRGPRs) [pCMV-EYFP-N1 backbone plasmid]	
9. pCMV-NLuc-**MRGPRD**-EYFP	10. pCMV-NLuc-**MRGPRE**-EYFP
11. pCMV-NLuc-**MRGPRF**-EYFP	

Miscellaneous Plasmids

pCMV-MCS (GS Flexi linker) plasmid backbone
1. pCMV-MRGPRX1
2. pCMV-MRGPRX2
3. pCMV-MRGPRX4
4. pCMV-ADRB2
5. pCMV-MRGPRD(E12H)-mOrange
pCMV-ECFP-N1 or -EYFP-N1 (FRET) plasmid backbone
6. pCMV-MRGPRD
7. pCMV-MRGPRE
8. pCMV-MRGPRF
9. pCMV-ADRB2
10. pCMV-PAR2
11. pCMV-MRGPRD(E12H)-EYFP
11. pCMV-MRGPRD(E12H)-EYFP

Curriculum Vitae

ROHIT ARORA

Email: rohit0288@gmail.com
ORCID: 0000-0002-4670-4447

Education

Doctoral Student: Department of Veterinary Sciences (2014-Present)
University of Antwerp, Belgium
PhD Thesis:
Mas-related G protein-coupled receptors: activations, interactions, and their role in inflammation
Under supervision:
Prof. dr. Alain J Labro and Prof. dr. Xaveer Van Ostade

Master of Technology (Integrated) in Biotechnology (2007-2012)
Dr. D.Y. Patil Biotechnology and Bioinformatics Institute, Pune, India
Master's Thesis **(2011-2012)**:
Expanding the bioluminescence resonance energy transfer (BRET)-based color palette and biosensor development for in vitro to *in vivo* deep-tissue imaging (SRET).
Under supervision:
Dr. Abhijit De, Scientist G, Advanced Centre for Treatment Research & Education in Cancer, Tata Memorial Centre, Navi-Mumbai, India

Certifications

Federation of European Laboratory Animals Sciences Association (FELASA) – Scientist Category 'C', 2015.

Employment

Research Associate (2012-2014)
Molecular Functional Imaging Laboratory (Dr. DE Lab)
Advanced Centre for Treatment Research & Education in Cancer, Tata Memorial Centre, Navi-Mumbai, India
Projects:

1. Designed and developed NanoLuc Luciferase based Bioluminescence Resonance Energy Transfer (NanoLuc-BRET) biosensor
2. Developed Firefly Luciferase (FLuc) based FLuc-BRET system
3. Design and development of Sequential Resonance Energy Transfer (SRET) systems

Scientific Skills

In vitro and In vivo assay/imaging:
BRET based tool and assay development for in vitro (High Throughput Screening assays), drug screening, luciferase assays, protein-protein interactions, Homogenous Time-Resolved Fluorescence (HTRF) assays, In vivo imaging (bioluminescence and BRET).

Biochemistry:
Enzymatic assay, protein isolation, protein purification, SDS-PAGE, western blotting, co-immunoprecipitation, Immunohistochemistry, Immunofluorescence

Cell biology:
Cell culture, cell viability assays, transfection, stable cell lines preparations (episomal and viral), flow cytometry

Molecular biology:
Restriction digestion, agarose gel electrophoresis, PCR based cloning (designing PCR primer, in-silico cloning planning), Site directed mutagenesis, plasmid & genomic DNA Isolation, RNA isolation, RT-PCR

Microbiology:
Bacterial culture

Microscopy:
Confocal microscopy, FRET, functional calcium imaging

Instruments/software:
Multiwell-Plate reader utilization, calibration and maintenance (FLUOstar BMG Labtech, EnVision PerkinElmer, GloMax Promega, Varioskan LUX), Spectrophotometers, Mass-spectrometry (LC-MS), IVIS Imaging systems, GraphPad, PyMol, Schrodinger Suite (Molecular docking, simulations), Photoshop and CorelDraw

Publications

Work of 2011-2014

- Abhijit De, **Rohit Arora** and Akshi Jasani.
  Engineering aspects of Bioluminescence Resonance Energy Transfer Systems.
  Engineering in Translational Medicine. Editor: Weibo Cai. Springer Publication.
  DOI: 10.1007/978-1-4471-4372-7_10. Citations 10

- Abhijit De, Akshi Jasani, **Rohit Arora** and Sanjiv S. Gambhir. September 23, 2013.
  Evolution of BRET biosensors from live cell to tissue-scale in vivo imaging.
  Frontiers in Endocrinology: Molecular and Structural Endocrinolgy.
  DOI:10.3389/fendo.2013.00131. Citations 58

- Shalini Dimri, **Rohit Arora**, Akshi Jasani and Abhijit De.
  Dynamic monitoring of STAT3 activation in live cells using a novel STAT3 Phospho-BRET sensor.
  Am J Nucl Med Mol Imaging 2019;9(6):321-334
  URL: https://www.ncbi.nlm.nih.gov/pubmed/31976162. Citations 7

Work of 2019-2021

- **Rohit Arora**, Kenny M Van Theemsche, Samuel Van Remoortel, Dirk J Snyders, Alain J Labro, Jean-Pierre Timmermans. December 9, 2021.
  Constitutive, Basal, and β-Alanine-Mediated Activation of the Human Mas-Related G Protein-Coupled Receptor D Induces Release of the Inflammatory Cytokine IL-6 and Is Dependent on NF-kB Signaling.
  International Journal of Molecular Sciences. 2021, 22(24), 13254
  DOI: **https://doi.org/10.3390/ijms222413254**. Citations 7

Manuscripts Awaiting Submission

Work of 2020-2022

- **Rohit Arora,** Alain J Labro
  Bile acids-mediated activation of human Mas-related G protein-coupled receptor D induces release of the inflammatory cytokine IL-6

- **Rohit Arora**, Alain J Labro
  Mas-related G protein-coupled receptor D senses fluid shear stress and induces the release of IL-6

Manuscript Awaiting Major Revision

Work of 2014-2018

- **Rohit Arora**, Samuel Van Remoortel, Alain J. Labro, Erik Fransen, Dirk J. Snyders, Roeland Buckinx and Jean-Pierre Timmermans
  Identification of heteromeric interactions of human Mas-related G protein-coupled receptors D, E and F
  (Submitted to Scientific Reports. Rejected, asked for major correction. August 2018)

Abstracts

Oral Presentations

- **Rohit Arora**, Samuel Van Remoortel, Alain J. Labro, Erik Fransen, Dirk J. Snyders, Roeland Buckinx and Jean-Pierre Timmermans
  Elucidating homo- and heteromeric interaction of human Mas-related G protein-coupled receptors using high-throughput luciferase complementation screening (NanoBiT).
  Discover Glo European Tour, April 2017, Ghent, Belgium.

- **Rohit Arora**, S.V. Remoortel, G.V. Raemdonck, G. Baggerman, R. Buckinx, D.J. Snyders, A.J Labro, J.P. Timmermans.
  Cathepsin S-mediated activation of human Mas-related G protein-coupled receptor F: a story of an underrated role for cysteine protease(s) in inflammatory bowel condition?
  31st Belgium week of Gastroenterology, February 2019, Antwerp, Belgium.

- **Rohit Arora**, Joni Heymans, Nikola Papovic, Alain J Labro
  Role of macro-molecules in activating human Mas-related G protein-coupled receptor D: allosteric/orthosteric ligand or mechano-sensitive?
  PhysPhar-Belgium. Belgian Society of Physiology and Pharmacology. April 2022

Poster Presentations

- **Rohit Arora,** Samuel Van Remoortel, Omnia Mohey-Elsaeed, Alain J. Labro, Dirk J. Snyders, Roeland Buckinx and Jean-Pierre Timmermans
  Screening for oligomeric interactions of human Mas-related G protein-coupled receptors: a comparative analysis of biophysical and biochemical techniques
  18th GPCR Retreat, October 2017, Ottawa, Canada.

- **Rohit Arora,** S.V. Remoortel, A.J. Labro, D.J. Snyders, R. Buckinx and J.P. Timmermans.

Unravelling homo- and heteromeric interactions of Mas-related G protein-coupled receptors: a gut perspective.
Neuro-gastroenterology and Motility, August 2018, Vol. 30, Issue S1. doi: https://doi.org/10.1111/nmo.13423.

- **Rohit Arora,** Samuel Van Remoortel, Geert Van Raemdonck, Geert Baggerman, Roeland Buckinx, Dirk J. Snyders, Alain J. Labro and Jean-Pierre Timmermans
  Mas-related G protein-coupled receptor F (hMRGPRF) N-terminal proteolytic cleavage detection by NanoLuc
  Discover Glo European Tour, May 2019, Brussels, Belgium

- **Rohit Arora**, S.V. Remoortel, D.J. Snyders, A.J. Labro, J.P. Timmermans.
  Activation of human Mas-related G protein-coupled receptor D induces release of IL-6, indicating a possible role of MRGPRD in the regulation of inflammatory mediators.
  20th GPCR Retreat, September 2019, Bromont, Canada.

Acknowledgement

Firstly, I would like to thank my promoter, **Prof. Dr. Alain J. Labro**, who helped in multiple ways to make me able to defend this thesis. I still remember we first met in 2014 to discuss the project, where you began as a collaborator. We immediately connected well, as we both had an interest in developing biophysical tools and using them for our line of research. In some days, I began working on plasmid cloning work in your lab (although technically Prof. Dirk Snyders Lab), and you, being a wonderful host, always provided all the resources. Within some months, we saw the positive results of MRGPRs oligomerization using NanoBiT systems, and you, being passionate about science, immediately accepted my proposal to further expand the studies with BRET systems, as they had some edge over the FRET. As per the project and time demanded, you became my co-promoter, and lastly, when things went bad, you took over the job of promoter as well. I can't even count how many brainstorming sessions we had over coffee, and we always had more ideas to work on, but limitations of resources didn't allow us to pursue them. Although sometimes we had some differences of opinion, eventually we picked the best option for further developing the project. I really wanted to thank you for buying the HTRF filters from your funds, which I was able to install in one of the only available multiplate reader within our reach. Moreover, you also bought NF-kB HTRF kits for testing the idea we had for the MRGPRD IL-6 story, and it worked, and we were able to publish the first article, which allowed me to be able to defend this thesis. There are countless things that I can't even write about here; just in short "If you were not there, I would not have reached graduation for sure". I thank you for all your support and standing by me, and yes, especially thank you for arranging to pay me for a few months when no one else has paid me for years.

I would also like to thank **Prof. Dr. Xaveer Van Ostade** for becoming my promoter. As Prof. Alain's job contract came to an end with the university, there was a situation where my PhD would come to an end without defence. But your acceptance to become the promoter gave me survival. I would also like to thank you for your very valuable input on my thesis, which helped me improve it. I would really like to thank you for all the selfless help you have provided.

I would like to express my gratitude to the esteemed members of my jury, **Prof. Dr. Francisco Ciruela**, **Prof. Dr. Julien Hanson**, and **Prof. Dr. Ir. Yann Sterckx**, for showing interest in my thesis. I express my gratitude for your valuable feedback and am eagerly waiting to discuss the subject matter of my thesis with you. I would also like to thank Prof. Dr. Guido De Meyer for being the chairman of my jury committee and managing and moderating the thesis defence procedure.

I want to thank **Abbi Van Tilborg** for helping me with a lot of different lab procedures. There are many good things about working with you. I could always count on you to get

lab supplies, help with molecular work, and do cell culture work. We both liked talking about our lives over lunch and sharing our cooking recipes. I also saw you being stressed as your job contract was about to end because the lab was closing, but you found a new job on the T2 floor, which made you smile again.

I also want to thank **Evy Mayeur**. We never worked on the same projects, but I liked having you in the same office, and talking about things other than science. I also appreciated your advice to be patient with my PhD. It really helped me get through the hard times.

I also want to thank **Dieter Van De Sande** for being a great coworker. At first, we didn't talk much because we were both busy with our own projects. But when we started going to course work together, we started to get to know each other and found that we were both funny and witty. I saw how passionate and committed you were to the work, which was truly impressive, and you were always there to help when anyone needed it. I want to thank you very much for bringing me food and medicine when I was very sick with chicken pox.

I would like to thank you, **Laura Coonen**, for being a wonderful colleague. I have never seen a person like you who is so calm, composed, and diligent in handling projects. We had a good number of failures while doing microscopy, but within minutes you used to decide to refine the protocol and start over it all again. I have also seen your multiple western blot failures, and within minutes you had a new plan in hand to start all over...and your famous words "let's start again" that too with a big smile. I hope you continue to do so; this will surely lead you to attain good heights.

I want to thank **Joke Robijns** for being the coolest colleague. Although in the beginning we had very little interaction, as we got to know that we both had an inclination for playing musical instruments, we became friends. I am always thankful that you invited me to your musical concerts. I am also thankful that you introduced me to Belgian folk dance and taught me some dance steps. Although I was terrible at learning, you never gave up on teaching.

I'll always be grateful to **Kenny Van Theemsche**, **Samuel Van Remoortel**, **Jeroen Stas**, **Glenn Regnier**, **Chloe Bars**, **Aleksandra Nijak**, and everyone else I've worked with. Thanks a lot for being a great coworker.

I will always be grateful to my friends **Aman Paul**, **Priyanka Malik**, **Pooja Tajpara**, **Parul Gupta**, **Sandeep**, and everyone else who helped me with my PhD. You were always there for me when I needed help.

I also want to thank **Michel Bouvier**, **Brian Kobilka**, **Rithwik Ramachandran**, and everyone else in the GPCR community who helped me by giving good ideas that saved my PhD in the end.

I will always be grateful to my parents and brother for being there for me and giving me all the help and finances, I needed to finish my PhD.

A special thanks to my master's thesis supervisor, **Prof. Dr. Abhijit De**, for bestowing me with a scientific temper. If I hadn't trained under you, this PhD would not have been possible at all.